Quantitative Measurements of Brønsted Acidity in Zeolites by Ammonia IRMS-TPD Method

アンモニア IRMS-TPD 法によるゼオライト内 Brønsted 酸性質の定量的測定

January 2009

Graduate School of Engineering, Tottori University

Department of Materials Science

鳥取大学大学院工学研究科

物質生産工学専攻

Katsuki SUZUKI

鈴木 克生

Faculty Advisors

Professor Miki Niwa
Associate Professor Naonobu Katada
Assistant Professor Kazu Okumura

Preface

This study has been carried out during 2004-2009 under the direction of Professor Miki Niwa at the Department of Chemistry and Biotechnology, Graduate School of Engineering, Tottori University. The present study has been partially supported by the Japan Society for the Promotion of Science (JSPS) research fellowship from 2007 to 2009.

This thesis presents the new characterization method named IRMS-TPD (infrared spectroscopy/ mass spectroscopy-temperature programmed desorption) for quantitative measurement of solid acidity. The analysis approach for quantitative evaluation of heterogeneous Brønsted acid sites in zeolite by IRMS-TPD method, the relationship between the Brønsted acid strength and the paraffin cracking activity, and the quantum chemical approach for investigation of the physicochemical property of zeolite will be mentioned.

I sincerely appreciate supervisor, Professor Miki Niwa for his kind educational suggestions. I also deeply appreciate Associate Professor Naonobu Katada and Assistant Professor Kazu Okumura.

I deeply thank Dr. German Sastre in the Instituto Tecnologia Quimica for his collaboration and helpful encouragement.

I would like to express my heartfelt gratitude to co-workers, Dr. Takashi Atoguchi and Dr. Tomonori Kanougi in the UBE Industries, Ltd., and Professor Akira Miyamoto, Professor Momoji Kubo and Dr. Mohamed Elanany in Tohoku university, and Professor Ryong Ryoo and Dr. Minkee Choi in the Korea Advanced Institute of Science and Technology for their collaborations and helpful discussions.

I sincerely thank Dr. Akinobu Shiga in the LUMMOX Research Laboratory for his interesting and beneficial discussions.

I thank all co-workers, predecessors and good friends in the Niwa Laboratory. Especially, I wish to thank Dr. Ryosuke Yoshimoto, Mr. Shinji Nishikawa, Ms. Kazuyo Isamoto, Mr. Daisuke Hayashi, Mr. Takuya Tsubaki, Mr. Takeshi Kato, Ms. Yukari Aoyagi, Mr. Takuma Nishio, Mr. Takayuki Noda, Mr. Tatsuya Torikai, Ms. Mariko Mori, Mr. Hiroyasu Tamagawa and Mr. Wataru Miyatani. My study has been strongly supported by precious and important knowledge obtained from their works.

Finally, I would like to especially thank my grandfather, grandmother, father and mother for their encouragements and supports.

Katsuki Suzuki

鈴木 克生

Contents

Chapter 1.

General Introduction

The crystalline aluminosilicate so-called zeolite which has regular micro-pore systems (with diameters < 2 nm) is one of the functionally materials, and it is commercially utilized in petrochemical processes as solid acid catalyst[1].

The single TO_4 tetrahedra (T = Si or Al) is primary building unit (PBU) in zeolite framework, and three-dimensional topologies of zeolite materials are built up from corner-shared TO_4 units. Figure 1-1 shows the first and second layers around a central tetrahedron where all the T atoms are tetra-coordinated. The maximum number of T atoms in second layer is 12. The stereoscopic conformation of zeolite is built by those coordination sequences. Additionally, zeolite-like materials which include transition metals (*e.g.* Ga, Fe, B, Ge, Ti, Zn, Mn) in the tetrahedral positions have been synthesized[2~8].

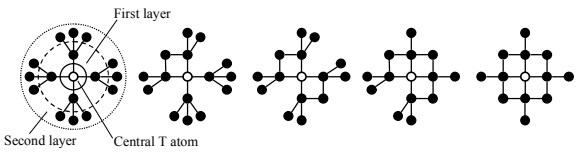

Figure 1-1. Concentric clusters of zeolite.

The framework types of zeolite have been summarized in "ATLAS OF ZEOLITE FRAMEWORK TYPES" published by Elsevier[9]. Each zeolite framework type is categorized by specific IUPAC three-letter codes. For example, framework type code (FTC) of Y-type zeolite which is most important material in petrochemical process is FAU. 23 kinds of secondary building units (SBU) and 36 kinds of composite building units (CBU) have been presented, and zeolite structures are categorized according to combination between those basic building units.

Figure 1-2 shows three types of zeolite framework structures. FAU structure consists of sodalite (SOD) cages which are connected with double six rings (D6Rs); on the other hand, LTA structure is built by combination between sodalite cage and double four rings (D4Rs). The unique large cage systems (supercage and α-cage) are built from basic units such as SOD, D6Rs and D4Rs. The

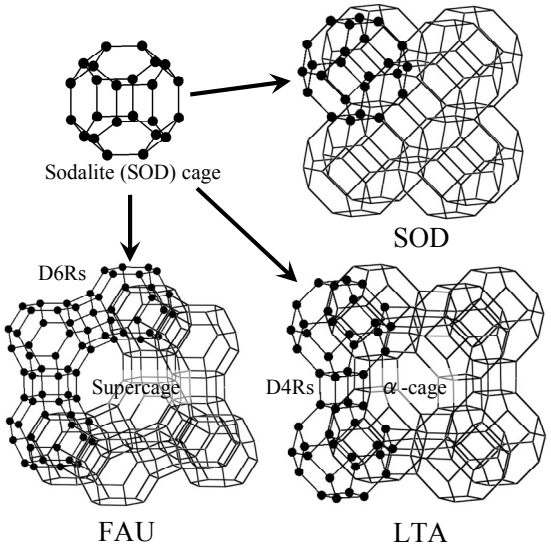

Figure 1-2. The zeolite framework structures consisted SOD unit. Only the positions of tetrahedral (T) sites are illustrated.

synthesis of new framework type has been frequently attempted by advanced synthetic methods, and currently, 176 kinds of zeolite framework types have been approved (in 2007).

In this chapter, several abilities and catalytic activities of zeolites will be briefly summarized.

Ion-exchanging Ability and Solid Acidity

The ion-exchanging ability of zeolite is generated from isomorphous substitution of Si^{4+} by Al^{3+} located in the tetrahedral site. A lack of positive charge caused by replacement of Si^{4+} by Al^{3+} in neutral silicate network is balanced by adding positively charged cations such as Na^+, K^+, NH_4^+, H^+.[10] A proton bonds to O atom in the ≡Si-O-Al$^-$≡ linkage, and this generated OH group works as proton donor, so-called Brønsted acid site (Figure 1-3 (b)). Generally, H-formed zeolite is obtained by a thermal activation of NH_4-formed zeolite (Figure 1-3 (a)). Almost all NH_3 molecules are removed by a thermal treatment at *ca.* 773 K; as a result, H-formed zeolite is obtained[11]. Similarly, the acidic OH groups are generated by replacement of other trivalent transition metals such as Ga, Fe and B atoms. For example, MFI- and MWW-type metalosilicates have been synthesized, and those physicochemical properties have been studied by many researchers[12-16].

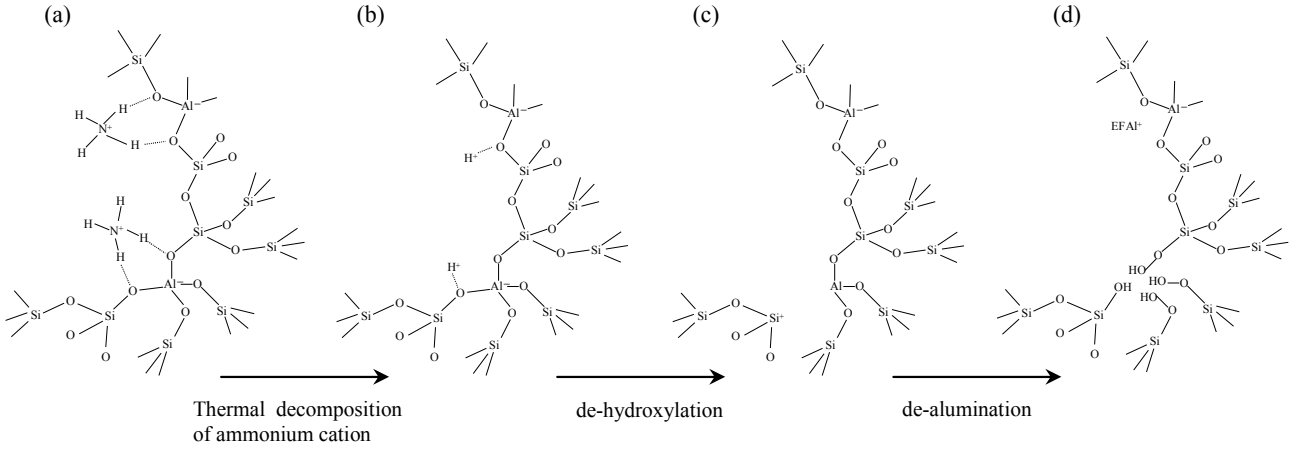

Figure 1-3. Generating mechanism of surface hydroxyl groups in zeolite.

On the other hand, an electron acceptor (Lewis acid site) is generated by thermal de-hydroxylation of acidic OH group. The de-hydroxylation in zeolite is induced by calcination above *ca.* 773 K. Ward studied the relationship between the calcination temperature and the concentration of Brønsted and Lewis acid sites in H-Y by IR measurement using pyridine as a probe molecule[11]. The classical structure of Lewis acid site in zeolite is tri-coordinated Al atom (Figure 1-3 (c)). However, in ^{27}Al NMR measurement, the identified Al species in zeolite are tetra-, penta- and hexa- coordinated species, and the signal assigned to tri-coordinated species is not presented. Thus, the tri-coordinated Al species can be considered as unstable species (shown in Figure 1-3 (c)), and it is reasonably deduced that the tri-coordinated Al species are removed from the framework. The removed Al species is stabilized as extra-framework Al (EFAL) species such as $Al(OH)^{2+}$ and AlO^+ in the framework, and it can be identified as the realistic Lewis acid site. As a result, hydroxyl nest ($[\equiv Si(OH)]_4$) is generated in the defective position caused by de-alumination (Figure 1-3(d))[12].

Generally, the distinction of types of acid sites (Brønsted or Lewis) is performed by infrared adsorption experiments using basic probe molecules such as pyridine, ammonia, acetonitrile; and quantitative estimation of

acid sites is calculated according to the extinction coefficients for adsorbed species based on the Lambert-Beer equation. The frequencies and reported extinction coefficients assigned to adsorbed species on acid sites are summarized in Table 1-1.

Table 1-1. Frequencies and extinction coefficients of IR absorption bands assigned to adsorbed typical probe molecules on acid sites.

	Frequency IR mode extinction coefficient (ε)	
	Lewis	Brønsted
Pyridine (C_5H_5N)	1450 ring stretch (Py) 2.37[a] (m^2 mol^{-1})[b] 2.22[c] (cm μmol^{-1})[d]	1540 ring stretch (PyH^+) 0.72[a] m^2 mol^{-1} 1.67[c] cm μmol^{-11}
Ammonia (NH_3)	1620 $\delta(NH_3)_{asym.}$ 2.2[e] m^2 mol^{-1}	1460 $\delta(NH_4^+)_{asym.}$ 14.7[e] m^2 mol^{-1} 13.0[f] cm μmol^{-1}
D_3-acetonitrile (CD_3CN)	2325, 2310 $\nu(C\equiv N)$-$L_{strong,\ weak}$ 3.60[g] cm μmol^{-1}	2297 $\nu(C\equiv N)$-B 2.05[g] cm μmol^{-1}

[a] ref. 13, [b] Obtained from band height (m^2 mol^{-1}), [c] ref. 14, [d] Obtained from integrated band area (cm μmol^{-1}), [e] ref. 15, [f] ref. 16, [g] ref. 17

Several experimental and theoretical studies on the local structures and the physicochemical properties of Lewis acid site have been performed[18-20]. Among them, the analysis of synergism between Brønsted and Lewis acid sites derived by EFAL species in ultra-stable Y (USY) zeolites would be one of the most important subjects. Several researchers have suggested that one of the origins of high catalytic performance of USY is enhancement of the acid strength[21, 22]. Corma *et al.*[23] proposed the mechanism of synergism between acidic OH and EFAL species, as described in scheme 1-1. In that case, EFAL species directly interact to the acidic OH group, and the electron density of around acidic OH group is delocalized. As a result, the polarizability of acidic OH group is increased. Recently, Li *et al.*[24] studied the effect of EFAL species on enhancement of Brønsted acidity in USY by means of a combined technique of solid state NMR and density functional calculation. They concluded that the neutral and cationic EFAL species ($Al(OH)_3$ and $Al(OH)^{2+}$) were preferable Lewis acid sites in the supercage and the sodalite cage, respectively; and those EFAL species indirectly interacted to the Brønsted acid sites.

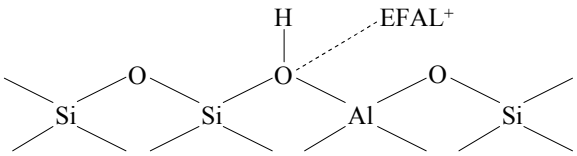

Scheme 1-1

Among the zeolite-like materials, silicoalumino-phosphate (SAPO) molecular-sieve is one of the most important materials as industrial catalyst[25-28]. The topologies of SAPO molecular sieves are similar to alumino-silicate (zeolites), and those frameworks are built from corner-shared tetrahedral networks of AlO_4, PO_4 and SiO_4 units[29]. The Brønsted acid site in SAPO material is generated by isomorphous substitution of P^{5+} in the neutral alumino-phosphate ($AlPO_4$) structure by Si^{4+} and H^+. On the other hand, neutral Si-O-Si linkage is generated by substitutions of neighboring Al^{3+} and P^{5+} atoms by two Si^{4+} atoms; *i.e.*, the Brønsted acidity is not generated in that case. The several kinds of Si substitution mechanisms into AlPO frameworks have been studied by many researchers, and several topological environments of acid sites in SAPO frameworks have been

proposed[30-32]. In petrochemical processes, CHA-type SAPO molecular sieve (SAPO-34) is known as an excellent catalyst for the conversion of methanol to ethylene and propylene in the so-called MTO (methanol to olefin) process[25-28]. The small-pore systems (8MR, 3.8 × 3.8) in CHA structure show shape selectivity for molecular size of light-olefins. Additionally, the selectivity of olefin is improved by transition metals such as Co[33], Ni[34], Mn[35] and Cr[36] atoms insertions into the SAPO-34 framework.

Shape Selectivity

Shape selectivity in zeolite originates from the regular micropore systems[37-41]. The shape selectivity is categorized into three types: (I) reactant, (II) product and (III) transition state (Figure 1-4).

(I) Reactant selectivity is caused by steric hindrance imposed on a reactant by a pore entrance which has appropriate size similar or smaller to molecule.

(II) Product selectivity occurs when some of the products formed within the pores are too bulky to diffuse out as observed products. *p*-xylene synthesis by alkylation of toluene with methanol is based on product selectivity. Industrial process of selective formation of *p*-xylene by means of MFI-type molecular sieves (10 MR, 5.5 × 5.1 and 5.6 × 5.3) was commercialized by Mobil Corporation in 1975. The improvement of the shape-selectivity has been attempted by the narrowing of the pore entrance size and the deactivation of the external acidity. In control of the pore entrance size, ion-exchanged method and chemical vapor deposition (CVD) of silica have been frequently performed.

(III) Restricted transition state selectivity occurs when certain reactions are prevented because the corresponding transition state would require more space than available in the cavities. Neither reactant nor potential product molecules are prevented from diffusing through the pores. Reactions requiring smaller transition states proceed unhindered.

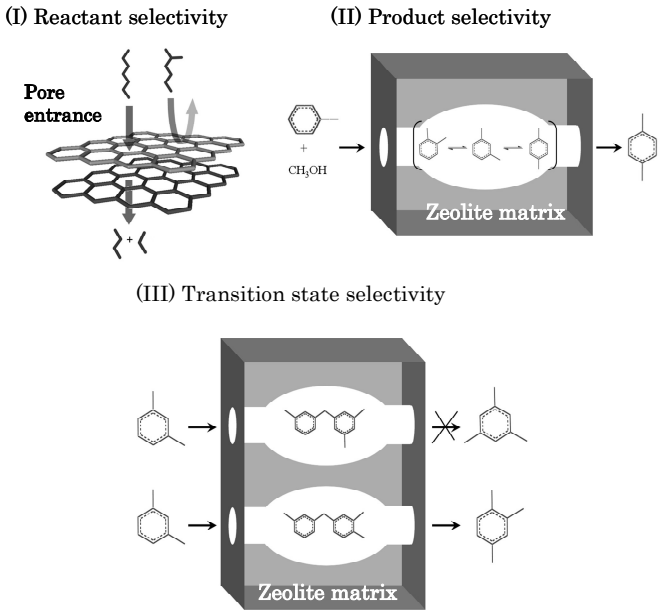

Figure 1-4. Schematic illustrations of shape selectivity effects in zeolite.

Metal Cation-Exchanged Zeolite

Hydrothermal stability of zeolite framework and distribution of active species can be controlled by ion exchange treatments[42, 43]. In addition, exchanged metal cations act as Lewis acid sites; and those show several characteristic adsorptive properties. Those Lewis acid strengths are influenced by the physicochemical properties of cations and zeolites[44, 45]. For example, lithium exchanged FAU and CHA zeolits have effective nitrogen sorption characteristics, and this property is useful in the separation of oxygen and nitrogen from air[46]. The location of cations in zeolite structures is known to affect their adsorptive properties, and those are

determined by X-ray and neutron diffractions and solid-state NMR measurement[47-49]. Figure 1-5 shows cation sites in FAU and CHA structures. CHA-type zeolite has four kinds of cation locations. Site I locates in inside the D6Rs, and site II locates in 6MR of D6Rs. Sites III and III' locate within the 8MR window. In FAU structure, sites I and I' locate within the D6Rs and the sodalite cage, respectively. Sites II and II' locate within the sodalite cage and super cage, and sites III and III' locates within the super cage. Rear-earth metal trivalent cation and/or alkali earth divalent metal cation exchanged Y zeolites have been utilized as FCC (fluid catalytic cracking) catalyst in the initial stage[50, 51]. The polarizing power of polyvalent metal cation dissociates adsorbed water, producing the hydrated metal cation and Brønsted acid site. Ward explained that the high catalytic activity of polyvalent metal cation exchanged Y zeolite was caused by the high electrostatic potential of polyvalent cation[52]. Vayssilov *et al.* studied the inductive effect on acidic O1H group located in the supercage by means of first-principle calculation based on density functional theory (DFT), and they reported that the more effective enhancement of Brønsted acidity was caused by presence of Ca^{2+} in Site II[53].

Atoguchi and Kanougi reported that the BEA zeolite showed high catalytic performance for phenol oxidation into catechol and hydroquinone with hydrogen peroxide as oxidant[54, 55]. BEA zeolite has three-dimensional large pore system and mild acidity, and those properties are suitable for the oxidation process which is de-activated by coking. Additionally, the products selectivity was improved by the ion exchange of alkali earth divalent cations (Mg^{2+}, Ca^{2+}, Sr^{2+} and Ba^{2+}), and CaH-BEA was the most effective catalyst among them. The reason of enhancement of selectivity by ion exchange treatment has been considered as the reducing of amount of very strong acid sites located in the defective position. In that case, exchanged divalent cations perform as Lewis acid sites.

Zeolite-based catalysts and adsorbents are considered as useful materials for the removal of harmful substances. Cu exchanged ZSM-5 is known as effective catalyst of selective catalytic reduction (SCR) of NO_x using hydrocarbon reductant[56]. However, Al atom in tetrahedral position is eliminated from the framework when zeolite is used in the presence of water vapor at high temperature[57]. On the other hand, over-exchanged Fe-ZSM-5 has relatively high hydrothermal stability, but the activation temperature is too high[58]. In the viewpoint of commercialization, catalytic performances of zeolite-base catalysts in NO_x reduction reaction are not yet enough. On the other hand, H-MOR, H-Y[59] and Ag-loaded MFI zeolites[60] are known as effective adsorbents of unburned hydrocarbons within initial stage of car exhaust so-called cold-start emission.

In recent year, Chassaing *et al.* studied the catalytic performance of Cu(I)-exchanged zeolites at azide-alkyne Huisgen

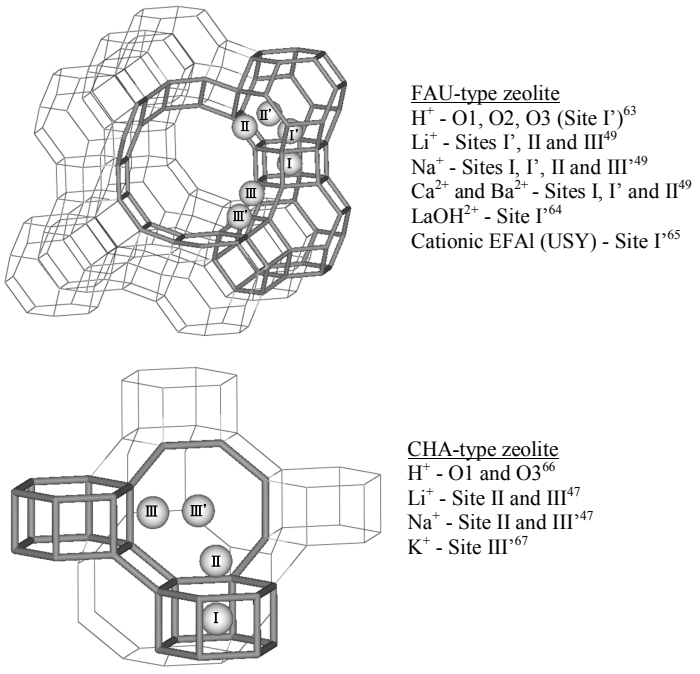

FAU-type zeolite
H^+ - O1, O2, O3 (Site I')[63]
Li^+ - Sites I', II and III[49]
Na^+ - Sites I, I', II and III'[49]
Ca^{2+} and Ba^{2+} - Sites I, I' and II[49]
$LaOH^{2+}$ - Site I'[64]
Cationic EFAl (USY) - Site I'[65]

CHA-type zeolite
H^+ - O1 and O3[66]
Li^+ - Site II and III[47]
Na^+ - Site II and III'[47]
K^+ - Site III'[67]

Figure 1-5. Cation positions in FAU- and CHA-type zeolites.

cycloaddition[61]. This Cu(I)-catalyzed organic synthetic route is typical reaction in so-called "click chemistry" introduced by Sharpless[62], and this concept is known as a fantastic methodology in synthesis of high-polymer materials and medical products. Chassaing's work[61] is probably the first attempt of a utilization of zeolite-based catalysts for Huisgen cycloaddition, and this approach is interesting.

New Class of Micro- and Meso-Porous Materials

The syntheses of new classes of micro- and meso-porous materials have been frequently carried out, and those novel materials show interesting functional properties. For example, it is known that transition metals in zeolite framework act as active sites which show unique catalytic activity. MFI-type titanosilicate (TS-1) would be one of the most graceful successes of synthesis of highly active catalyst[68]. TS-1 is known as excellent catalyst for oxidation using hydroperoxide as oxidant, and it has been commercialized as industrial catalyst. In recent years, Tatsumi's group has successfully synthesized the Ti-MWW zeolite which has higher catalytic performance than that of TS-1 on alkene epoxidation[69-71]. Additionally, Ti-doped mesoporous silica molecular sieves such as Ti-MCM-41 and Ti-MCM-48 are known as highly active catalyst on oxidation of bulky molecules[72]. On the other hand, Corma's group reported that the Sn atom in the tetrahedral position of Sn-beta zeolite directly works as effective active Lewis acid site for Baeyer-Villiger reactions[73].

Generally, zeolites are hydrothermally synthesized at high-temperature and high-pressure conditions (hydrothermal synthesis). The selections of organic SDA (structure directing agent) molecule, contained anion and cation are important components in synthesis of the zeolite structure. For example, it has been known that the introduction of F^- anion leads to the formation of zeolites with high crystallinity[74, 75]. In addition, substitution of Si in the tetrahedral position by Ge is effective technique for creating D4Rs unit. Corma's group has created the new zeolite materials such as ITQ-13[76], ITQ-21[77], ITQ-22[78] and ITQ-24[79] by the Ge insertion method in a fluoride media. Structure of ITQ-13 has three-dimensional channel systems containing medium 9- and 10-MRs. This material shows higher catalytic activity and propylene yield compared with a USY in vacuum gas-oil (VGO) cracking reaction, thus it will be hopeful catalysts in petrochemical processes[80].

Recently, in order to improve the performance in catalyzing bulky molecule, the synthesis of zeolite/mesoporouos molecular sieve composites (ZMC) using zeolites as silica-aluminua source has been performed[81]. This material has mesopore systems and strong acid sites originated from zeolite crystal structure, and it shows a high catalytic activity for paraffin cracking. On the other hand, Jacobsen *et al.* synthesized the mesoporous zeolites by means of using large carbon particle as the template molecule[82]. The synthesis of "mesoporous-zeolites" is frequently performed, but the characterizations of the solid acidity and the catalytic performance have not been performed enough. However, this concept would be hopeful approach of synthesis of functional porous materials.

In synthesis of the other new material, organic-inorganic hybrid microporous materials have been successfully synthesized by Yamamoto *et al.*[83] The novel type of materials denoted as ZOL (zeolite with organic groups as lattice) contains hydrophobic Si-(CH_2)-Si linkages in the framework. In the viewpoint of catalytic performance, design and preparation of organic-inorganic materials are effective approaches for improvement of liquid phase catalytic performance. In addition, Inagaki *et al.*[84] have synthesized organo-silica hybrid mesoporous materials. Because Chemical, electrical and optical functionalities are integrated within the

frameworks, the hybrid materials is one of the promising catalysts.

Zeolite as Catalyst

As described above, the catalytic activity of zeolites depends on the solid acidity, shape selectivity and ion exchanging ability. Table 1-2 shows the typical zeolite-based catalysts[85]. Zeolite-based catalysts have been mainly used in petrochemical industrial processes. In recent years, application of zeolite-based heterogeneous catalyst into fine chemical industry has been attempted. The understanding of the reaction mechanism is key step for the design and synthesis of better catalysts. Therefore, development of *in situ* characterization methodology of reaction mechanism is important subject. The structures and dynamics of surface atoms on catalyst strongly attribute to the catalytic activity. In the viewpoint of analysis of active site structure, *in situ* EXAFS measurement is one of the most effective methodologies[86]. More advanced information would be obtained by means of the application of developed techniques such as Quick XAFS (QXAFS)[87], Dispersive XAFS (DXAFS)[88] and the combined technique of XAFS and XRD[89].

Table 1-2. Summary of zeolite-based catalysts

	FTC	Process
ultra-stabilized Y-type zeolite (USY)	FAU	Fluid Catalytic Cracking (FCC) of VGO and fuel oil
Pt-Pd-HY		hydrocracking of VGO
Fe-H-USY		hydrocracking of fuel oil
H-mordenite	MOR	aromatics trans-alkylation, dimethylamine synthesis
Pt-H-mordenite		hydroisomerization of light gasoline, xylene isomerization
H-beta	BEA	benzene alkylation, aromatics acylation
Pt-K-L-type zeolite	LTL	hexane aromatization
H-ZSM-5	MFI	toluene disproportionation, MTG, xylene isomerization, hydration of cyclohexene, dewaxing,
Silicalite-1		Beckmann rearrangement
GaMFI		Synthesis of BTX from LPG
Pb-ZSM-5		Synthesis of pyridine bases from aldehydes and NH_3
FeZSM-5		Selective oxidation of benzene to phenol with N_2O
TS-1		oxidation using peroxide
H-MCM-22	MWW	benzene alkylation
Pt-SAPO-11	AEL	paraffin hydroisomerization
H-ferrierite	FER	light olefin (C4, 5) skeletal isomerization
Ni-erionite	ERI	increasing octane number of light gasoline
H-SAPO-34	CHA	MTO
H-chabazite		dimethylamine synthesis
H-rho	RHO	dimethylamine synthesis

Characterization Methodologies of Solid Acidity

Important industrial processes such as FCC, MTG and MTO are promoted by the Brønsted acid sites in zeolites. Therefore, the accurate measurement of solid acidities of zeolites is one of the important subjects in order to analyze those catalytic performances. For this reason, many experimental and theoretical studies of solid acidity of zeolites have been carried out. In the following section, typical characterization methodologies of solid acidities will be summarized.

Infrared Spectroscopy

Weakly basic probe

Generally, the acid strength (or polarizability) and concentration of acidic OH groups are evaluated by using basic molecules which protonated or not-protonated by the Brønsted acid sites. Acid (AH)-base (B) reaction is presented in following scheme;

$$AH + B \rightleftharpoons AH\cdots B$$

The IR spectral shape of AH···B complex is changed by the strength of interaction between them. The unperturbed AH group in zeolite is characterized by three kinds of IR modes. One is the AH stretching mode (νAH), and the others are the in- and out-of-plane bending vibrations denoted as δ and γ, respectively. In the OH stretching region (3800 to 2500 cm^{-1}) of zeolites, the absorption bands assigned to the Si-OH and Al-OH groups are generally observed at *ca.* 3745 and 3666 cm^{-1}, respectively. Those hydroxyl groups are located in the boundaries of the zeolite crystal or in the surface of non-crystalline domain. Then, absorption bands assigned to acidic SiO(H)Al groups are observed in the range of 3650 to 3500 cm^{-1}. On the other hand, δ and γ modes are observed at *ca.* 1100 and 350 cm^{-1}, respectively (Scheme 1-2)[90, 91].

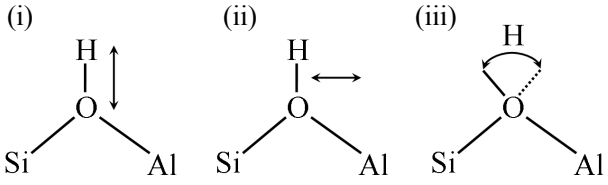

Unperturbed SiO(H)Al group
(i) Stretching vibration (ν) ··· *ca.* 3610 cm^{-1}
(ii) in-plane bending vibration (δ) ··· *ca.* 1100 cm^{-1}
(iii) out-of-plane bending vibration (γ) ··· *ca.* 350 cm^{-1}

Scheme 1-2

When N_2 is adsorbed on H-zeolites, two kinds of absorption bands assigned to N≡N stretching modes are observed at 2335 and 2352 cm^{-1}.[92] Those absorption bands have been identified to the adsorbed N_2 molecules on the Lewis and Brønsted acid sites, respectively. Lewis acid site acts as acceptor of lone pair of N_2 molecule; in other words, the donative bond is formed between them. Therefore, the stretching mode of N≡N bond is shifted to larger frequency (blue-shift). Similarly, νN≡N mode is perturbed by the electrostatic interaction with the positively charged hydrogen atom.

On the other hand, with the increase of the N_2 pressure, the intensity of absorption band assigned to OH stretching mode is decreased; in contrast, new broad absorption band assigned to perturbed OH groups by N_2 molecules is developed at lower frequency. This shift to lower frequency (red-shift) of OH band is caused by a forming hydrogen bond with N_2 molecules. The degree of red-shift ($\Delta_{\nu OH}$) shows strength of hydrogen bonds between them; *i.e.,* it indicates the magnitude of polarizability of OH groups.

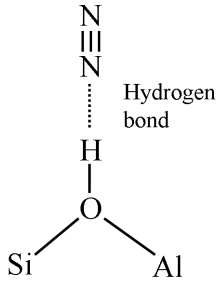

Perturbed SiO(H)Al group
(i) Stretching vibration (ν) → red-shift
(ii) in-plane bending vibration (δ) → blue-shift
(iii) out-of-plane bending vibration (γ) → blue-shift
(iv) Stretching vibration (ν) → blue-shift

IR absorption intensity and band width → increase

Scheme 1-3

The degree of red-shift of OH band depends not only on the acid strength of OH group but also proton affinity (PA) of probe molecule, and the interaction with more strongly basic probe molecule leads larger shift. The PAs of gas phase molecules are summarized in ref. 91. The PA of N_2 (494.5 kJ mol^{-1}) is much smaller than those of typical strong base molecules such as ammonia (853.5 kJ mol^{-1}) and pyridine (924 kJ mol^{-1}). Similarly, IR absorption bands assigned to OH groups are red-shifted by forming hydrogen bond with weakly basic molecules such as CO, H_2, hydrocarbons, and aromatic compounds. Then, the absorption intensity of perturbed OH groups increases with increase of the degree of red-shift of νOH ($\Delta_{\nu OH}$). Makarova *et al.* reported the linear relationship between the $\Delta_{\nu OH}$ caused by hydrogen bonds with several base molecules and the broadened OH band

areas (and the full width at half-maximum, fwhm)[93].

Among the several basic molecules, acetonitrile (AN) has been frequently used as a probe molecule in order to measure the solid acidity[94]. The proton affinity of AN is relatively strong (792 kJ mol^{-1}), but it is not protonated by Brønsted acid site in zeolite. Distinction of type of acid sites (Brønsted or Lewis-type) is carried out by observation of CN stretching band (at *ca.* 2400-2200 cm^{-1}). However, spectral shape in CN stretching region is strongly complicated by the Fermi resonance between the νCN band and the combination band between the δCH_3 and νCC modes. In general, this problem has been overcome by using a deutrated acetonitrile (d_3-AN). The absorption bands at 2332-2323, 2300 and 2278 cm^{-1} have been identified as adsorbed species on the Lewis acid site, the acidic SiO(H)Al groups and the terminal SiOH groups, respectively. On the other hand, the perturbed OH group by d_3-AN adsorption shows three characteristic broad absorption bands so-called ABC pattern at *ca.* 2800, 2400 and 1600 cm^{-1}. The splitting of the shifted νOH band into the components A and B is caused by a Fermi resonance between a broadened OH band and the overtone of the in-plane bending OH band (2δOH). Additionally, component C is originated from Fermi resonance between a stretching band of perturbed OH groups and the overtone of the ont-of-plane bending OH band (2γOH).

Strongly basic probe

When the PA of basic molecule approaches 836 kJ mol^{-1} (200 kcal mol^{-1}), the basic molecule is protonated by Brønsted acid site as described in following scheme.[91]

$$AH + B \rightleftharpoons A^{-}\cdots HB^{+}$$

Ammonia (PA = 853.5 kJ mol^{-1}) and pyridine (PA = 924 kJ mol^{-1}) are known as typical strongly basic molecules, and those spectral properties are useful for quantitative estimation of the concentration and strength of acid sites.

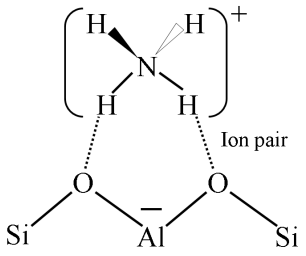

Scheme 1-4

The kinetic diameter of ammonia based on the Lennard-Jones relationship is 2.6 Å, and the diameters of 6MR of sodalite cage and 12MR of supercage in FAU structure are 2.6 and 7.4 Å, respectively. Because the kinetic diameter is small, an ammonia molecule reaches almost all acid sites in zeolites. The protonated ammonia (ammonium cation, scheme 1-4) shows absorption bands at *ca.* 1450 and 3300 cm^{-1}, and coordinated ammonia shows absorption bands at *ca.* 1250, 1630 and 3300 cm^{-1}. The absorption band at 1450 cm^{-1} is assigned to asymmetric bending mode of ammonium cation, and the adsorption bands at 1250 and 1630 cm^{-1} are assigned to symmetric and asymmetric bending modes of ammonia. The broad absorption band assigned to NH stretching vibration is observed at *ca.* 3400-2000 cm^{-1}.[95] This spectral shape is very complex because that depends on the adsorption configuration such as mono-, bi-, tri-, and tetra-dentate.

The ring stretching vibration (mode 19b denoted by Wilson[96]) of protonated pyridine (pyridinium cation) and coordinated pyridine are observed at *ca.* 1540 and 1450 cm^{-1}, respectively. The detail of spectral assignments of adsorbed pyridine species are described in ref. 97 and 98. The kinetic diameter of pyridine is relatively large (5.85 Å), thus it can not reach the acid sites located in the small pore. The accessibility of pyridine as bulky molecule to acid site would be effective information in the identification of acid sites in large pore. As an

example, spectra of pyridine adsorbed *in situ* prepared H-Y zeolite are presented in Figure 1-6.[11] In the spectrum of activated H-Y zeolite at 723 K (spectrum a), three kinds of absorption bands assigned to the external Si-OH groups, the SiO(H)Al groups located in the supercage and the narrow cages are observed at 3742, 3643 (HF, high frequency) and 3540 (low frequency) cm^{-1}, respectively. By an adsorption of excess pyridine (spectrum b), the absorption bands of Si-OH and OH_{HF} are completely disappeared. On the other hand, the decreasing of band intensity of OH_{LF} is not completely carried out. Then, only the absorption band of OH_{LF} is completely restored by evacuation at 473K (spectrum c). As shown in Scheme 1-5, the 6MR of sodalite cage is too small for pyridine penetration, but the OH groups located in the sodalite cage is pulled out to the super cage by forming a hydrogen bond between strongly basic molecules like a pyridine. In that case, the broad absorption band assigned to perturbed OH_{LF} groups by pyridine adsorption is observed at 3300-2750 cm^{-1}. But those weakly adsorbed species are removed at low temperature[97]. On the other hand, the intensity of absorption band assigned to pyridinium caiton (1540 cm^{-1}) linearly increases with decreasing of OH_{HF} band; *i.e.,* those spectral changes indicate that a pyridinium ion can be formed only on the OH_{HF} group. Khabtou *et al.* determined the extinction coefficients of OH_{HF} and OH_{LF} groups and pyridinium cation based on the difference of accessibility of pyridine molecule to the OH_{HF} and OH_{LF} groups[97].

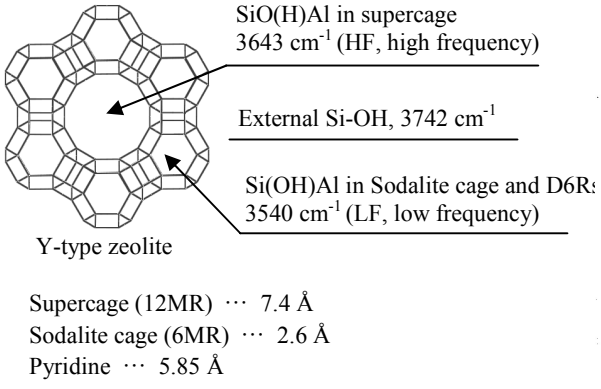

Scheme 1-5

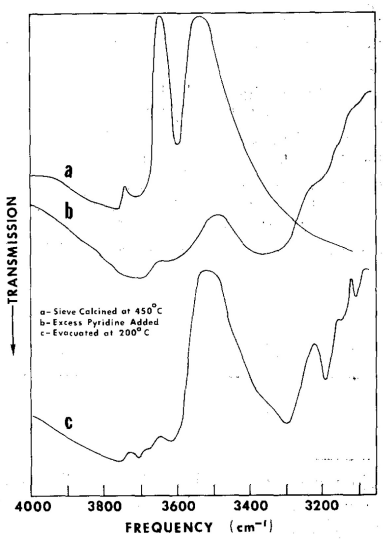

Figure 1-6. FTIR spectra of pyridine adsorbed *in-situ* prepared H-Y zeolite. (a) activated NH_4-Y at 723 K, (b) excess pyridine added, (c) evacuated at 473 K. Reproduced from ref. 11.

^{1}H MAS NMR

The electronic properties of protons can be observed by ^{1}H MAS NMR measurement. The shielding effect of more positively charged protons to the external magnetic field is lower. Therefore, the signal assigned to acidic OH group which has higher proton donor ability is observed at low magnetic field. Thus, the chemical shift is estimated as scale of the Brønsted acid strength.

Brunner has found the linear relationship between the chemical shift of proton (δH) and the frequency of the OH stretching vibration (νOH)[99]. As an example, Figure 1-7 shows IR and ^{1}H MAS NMR spectra of H-BEA zeolite[100]. In IR spectrum (Figure 1-7 (a)), the adsorption bands at 3745 cm^{-1} is assigned to internal and/or external Si-OH groups, and band at 3610 cm^{-1} is assigned to the acidic SiO(H)Al groups located in main channel. Then, the broad adsorption band in the region 3600 to 3200 cm^{-1} is assigned to the H-bonded acidic SiO(H)Al

groups to the neighboring oxygen atoms and H-bonded silanol groups located in defective position. On the other hand, in ^{1}H MAS NMR spectrum (Figure 1-7 (b)), the signals at 1.8 and 4.4 ppm are assigned to protons of silanols and acidic OH groups, respectively. Additionally, the broad signal in the region 3 to 7 ppm is assigned to H-bonded silanol groups and/or acidic SiO(H)Al groups. As shown in Figures 1-7, a nearly mirror image relation is obtained between the shapes of IR and NMR spectra. However, whereas the relative intensity of IR absorption bands of each component is dependent on those extinction coefficients, that of NMR signals shows the actual proportion of protons.

In *ab initio* quantum chemical calculation, Civalleri *et al.* reported the linear relationship between the de-protonation energy ΔE_{DP} and the δH[101]. Additionally, Pint *et al.* have suggested the relationship between the δH and the adsorption heat of ammonia obtained by TPD measurement[102].

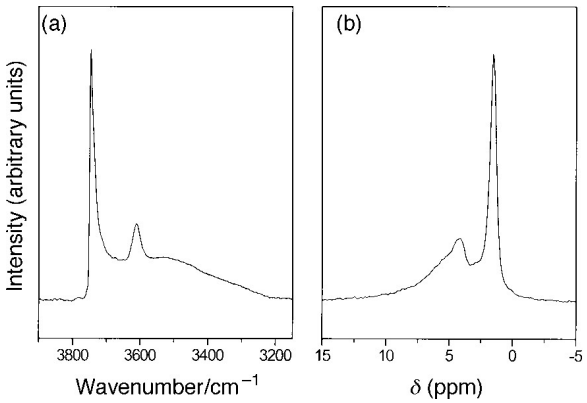

Figure 1-7. FTIR (a) and ^{1}H MAS NMR (b) spectra of H-BEA zeolite. Reproduced from ref. 100.

Calorimetric Measurement of Differential Adsorption Heat

Generally, microcalorimetry measurement is performed by using strong base probe molecules such as pyridine and amine[103, 104]. The adsorption amount and heat mean the acid amount and strength, respectively. However, microcalorimetric and volumetric measurements do not discriminate between Brønsted and Lewis acid sites. The shape of the calorimetric curve is divided into three regions, and those assignments of adsorbed species are assumed as described below;

Initial region (at low coverage) ⋯ Strongly adsorbed species on EFAL species (Lewis acid sites).

Second region (plateau region) ⋯ Adsorbed species on the Brønsted acid sites.

Third region (at high coverage) ⋯ Weakly physisorbed species.

A constant heat at the plateau region is strongly dependent on the framework structure, and the adsorption amount at the end of plateau region is almost similar to the content of tetrahedral Al atoms. However, the temporal cost for measurement is very high; in addition, distinction between the chemi- and physisorbed species is difficult.

Neutron Diffraction Study

The X-ray beam is mainly scattered by the electrons around the ion and molecule, thus the determination of location of light atoms coexistent with heavy atoms is impossible. In contrast, the atomic scattering factor in neutron beam is almost same regardless of the weight of atoms. Therefore, the neutron diffraction study is useful methodology of the direct determination of proton location in H-zeolites. Generally, neutron diffraction measurement is performed using deutrated zeolite as a sample. The accurate topologies of several kinds of zeolites such as D-Y[63], D-SSZ-13[66], D-SAPO-34[105], D-MOR[106] and D-FER[107] have been analyzed.

Temperature Programmed Desorption (TPD) of Ammonia

The kinetic diameter of ammonia is small (2.6 Å) enough to reach almost all acid sites located in zeolite pore. Therefore, temperature programmed desorption (TPD) of ammonia is frequently used for the accurate quantitative measurement of solid acidity. The Ammonia TPD method has been established as effective and convenient methodology, thus we have performed the characterization of acid properties of several kinds of solid acids by means of this methodology[108,109].

The TPD spectrum of ammonia which was measured under conventional conditions (*W/F* (weight of sample/volumetric flow rate of carrier) ratio was *ca.* 13 kg m^{-3} s) shows two desorption peaks at low and high temperatures (Figure 1-8 (a)). The *h*-peak (high temperature peak) was assigned to the chemisorbed ammonia species on the acid sites; on the other hand, the *l*-peak (low temperature peak) contains considerable amounts of ammonia physically adsorbed on NH_4^+ cations. Therefore, counting a low-temperature peak as an acid site mistakenly leads to overestimation of the number of acid sites. We have improved the method of ammonia TPD in order to overcome the disadvantage; a water vapor treatment method to remove ammonia hydrogen-bonded to ammonium cation which had been adsorbed on acid site was established (Figure 1-8 (b)-(d)).

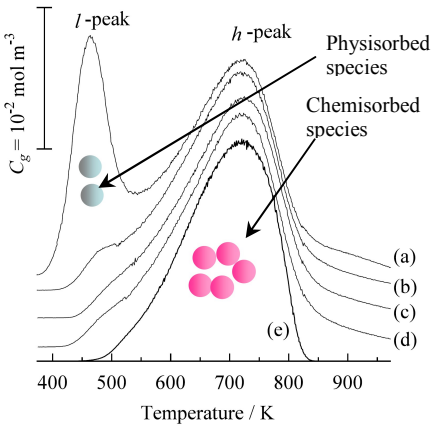

Figure 1-8. TPD spectra of H-MOR (NH_4-exchanged JRC-Z-M15, Si/Al_2 = 15.0, Na/Al = 0.04) measured by conventional method (a) and water vapor treatment method with 1 (b), 2 (c) and 4 (d) times of repetition of introduction of water and evacuation, and simulated curve (e).

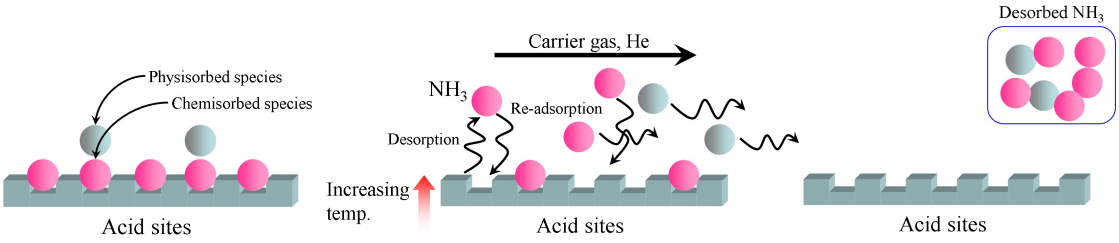

Figure 1-9. Ammonia TPD process under the conventional conditions.

The ammonia TPD process under the conventional conditions was illustrated in Figure 1-9. When the TPD is measured under normal conditions, it is controlled by the free re-adsorption of ammonia, and thus the peak maximum temperature is influenced not only by the acid strength but also the by the *W/F*. Therefore, temperature for ammonia desorption does not simply correlate with the strength of acid sites. The apparent desorption rate under the equilibrium condition is related to the thermodynamic parameters (*i.e.*, ΔS and ΔH, entropy and enthalpy changes with respect to the desorption) according to the theoretical equation of TPD[108]. Using the theoretical equation, we can determine the ammonia adsorption heat as an index of acid strength. The adsorption heat of ammonia is dependent on the zeolite structure and is not related with the chemical composition; *i.e.,* this result indicates that the acid strength is strongly dependent on the crystal structure[109].

Density Functional Theory Calculation

The Kohn-Sham density functional theory (DFT) calculation[110] has rapidly developed in recent years, and been utilized as effective methodology for physicochemical analysis of zeolites. The advantages of DFT calculation are low computational cost and high calculation precision. Therefore, the calculations within periodic boundary condition by using a large zeolite unit cell have been frequently performed. In the study of zeolite acidity, adsorption energy of base molecule, de-protonation energy (or proton affinity), frequency of OH stretching vibration, chemical shift of ^{1}H MAS NMR have been calculated as scale of the acid strength[111, 112].

General Understanding of Brønsted Acidity and Catalytic Activity

Brønsted acidity and catalytic activity of zeolite have been studied by many researchers using several methodologies. General understanding of those subjects will be briefly summarized in the following section.

Strength of Acidic SiO(H)Al Group

The considerable factor which controls Brønsted acid strength of zeolite can be categorized into three components; (i) chemical property, (ii) physical property, and (iii) chemical/physical combination property.

(i) Chemical property

The IR absorption band of stretching vibration assigned to acidic SiO(H)Al group shifts to low frequency according to decreasing of tetrahedral Al atoms in the framework[128]. In other words, this spectral change means that the polarizability of O-H bond increases with increase of the Si/Al_2 ratio. Jacobs *et al.* explained this phenomenon was caused by change of the framework electronegativity based on Sanderson's model[113, 114]. The intermediate electronegativity is based on the Sanderson's opinion "When two or more atoms initially different in electronegativity combine chemistry, they adjust to have the same intermediate electronegativity within the compound". The intermediate electronegativity (S_{int}) and the partial charge (q) of compound $P_pQ_qR_r$ are obtained from the Sanderson's equation (1).

$$S_{int} = (S_P^{\,p} \cdot S_Q^{\,q} \cdot S_R^{\,r})^{1/(p+q+r)}$$
$$q_Q = (S_{int} - S_Q)/[2.08 \times S_Q^{\,0.5}]$$

Where S_Q is the electronegativity of atom Q. The Sanderson's electronegativities Si, Al, O, H and Na atoms as principal components of zeolites are 2.84, 2.22, 5.21, 3.55 and 0.70, respectively. For example, the intermediate electronegativity of Al_2O_3 is given as:

$$S_{Al2O3} = (2.22^2 \times 5.21^3)^{1/5} = 3.70$$

and the partial charges of Al and O atom (q_{Al} and q_O) are given as:

$$q_{Al} = (3.70 - 2.22)/[2.08(2.22)^{0.5}] = 0.48$$
$$q_O = (3.70 - 5.21)/[2.08(5.21)^{0.5}] = -0.32$$

The electoronegativity of Si (2.84) is higher than Al (2.22), therefore the framework electronegativity of zeolite is

increased according to increasing the Si/Al_2 ratio. As a result, the partial charge of H atom is positively enhanced; *i.e.*, the strength of Brønsted acid site is enhanced. This explanation has been successfully accepted by many researchers. However, the distribution of Brønsted acid strength in the identical zeolite framework cannot be fully explained by this concept.

(ii) Physical property

The strongly dependence of acid strength on the crystal structure of zeolite has been positively accepted as the common concept, because the reason of weaker acidity of silica-alumina compared with zeolite which has the same composition must be difference of the crystal structure.

In the investigations of electronic properties of constituent atoms of zeolite, solid state NMR measurement would be suitable experimental method. The most tetrahedral Si atoms in zeolite framework locate in the $Si(O\text{-}Al)_n(O\text{-}Si)_{4-n}$ environments (n = 0 ~ 4). The ^{29}Si NMR chemical shift assigned to Si(nAl) (n = 0 ~ 4) is shifted to low magnetic field at regular intervals (*ca.* 5 ppm) with increasing of number of the nearest neighboring Al atoms. Then, the chemical shift assigned to isolated Si atom (n = 0) depends on the framework structure. For example, the Si(0Al) signals in FAU[115], CHA[116] and MOR[117] type zeolites are observed at -105.8, -110.0 and -112.2 ~ -115.0 ppm, respectively. Additionally, it has been discovered that the ^{29}Si NMR chemical shift is affected by either distances between neighboring T atoms or T-O-T bond angles[118-121]. ^{29}Si NMR chemical shift is shifted to high magnetic field with increasing the T-O-T bond angle; in other words, this NMR-based empirical rule means that the Si atom of Si-O-T linkage in larger angle is more positively charged.[101] And then, Lippmaa *et al.* suggested that the ^{27}Al NMR chemical shifts closely parallel those of ^{29}Si.[121] Additionally, Pingel *et al.* reported that the ^{17}O chemical shift assigned to O atom in the Si-O-T linkage shifts to higher magnetic field with increasing the Si-O-T bond angle[122]. The empirical relationships between the solid state NMR chemical shifts and the T-O-T bond angles are summarized in Scheme 1-6.

Empirical relationships between NMR Chemical shift and T-O-T bond angle (θ)

- ^{17}O
  δ O (ppm) = -0.71 θ + 143.7 … ref. 122
- ^{27}Al
  δ Al (ppm) = -0.5 θ + 132 … ref. 121
- ^{29}Si
  δ Si (ppm) = -0.5793 θ – 25.44 … ref. 118

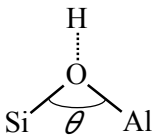

Oxygen hybrid orbital in SiO(H)Al linkage

s-character of oxygen hybrid orbital (ρ)
= cos θ /(cos θ -1) … ref. 140

- ^{17}O
  δ O (ppm) = -214 ρ + 136 … ref. 140

Increasing of Si-O(H)-Al bond angle (θ)
→
T-O bond → *s*-character is increased
→ bond length is shortened
O-H bond → *p*-character is increased
→ bond strength is weakened

Scheme 1-6. Summary of relationships between electronic property and local structure of SiO(H)Al linkage.

As mentioned above, the electronic property of SiO(H)Al group is affected by the local geometric property. In addition, the effect of geometric property to the acidity of OH group has been studied by theoretical methodology. In the initial stage of theoretical study, various simple relationships between the local geometric property and the acidity of OH group were suggested. For example, theoretical studies have suggested that a larger bond angle of the Si-O(H)-Al linkage leads to an increase of the Brønsted acidity[123,124]. This is explained by changing of the hybrid orbital of the O atom in Si-O(H)-Al linkage. When the Si-O-Al bond angle is increased, *s*-character of the T-O bonds are increased (T-O bond length is shortened). In that case, the

p-character of the O-H bond is increased (O-H bond length is lengthened), *i.e.,* strength of the O-H bond is weakened and the proton donation becomes easily. These local geometrical factors controlling the Brønsted acid strength can be categorized as a short-range factor.

(iii) Chemical/physical combination property

The field of computational chemistry is rapidly advancing, and the computational precision is remarkably enhancing. The recently computational studies have suggested that the calculated frequencies of acidic OH groups are not always determined by the local structures such as the T-O-T angle and T-O bond length. On the other hand, the good relationship between the gradient norm of the electrostatic potential at the proton and the OH stretching frequencies has been reported by Sastre *et al.*[125, 126]. The effect of long-range Coulombic interaction between the anionic zeolite framework and proton is therefore considered one of the controlling factors of the acid strength. However, detail of the long-range effect has not been clarified yet.

Hydrocarbon Cracking Activity of Zeolites

In the catalytic reaction using Brønsted acid site as the active center, the catalytic performance is affected by the concentration and the strength[127]. If acid concentration is too high, the product selectivity would be decreased by the developing of consecutive reaction. Similarly, too strong acid strength leads the rapidly formation of byproduct.

Hydrocarbon cracking by using zeolite catalysts is the most important reaction in petrochemical processes. The reaction mechanism is categorized into two routes. One is the bimolecular process with a tri-coordinated carbenium ion chain reaction (β scission) carried out by hydride transfer, and the other is monomolecular process[128-130]. The bimolecular process begins under the high alkane partial pressure condition. On the other hand, when the alkane partial pressure is low, the reaction temperature is high and the coverage is low, hydrocarbon cracking begins with a monomolecular initiation step. This reaction mechanism following first-order kinetics can be described in follow equations.

$$\mathrm{RH\ (gas\ phase)} \rightleftharpoons \mathrm{RH\cdots H^{+}\text{-}Zeolite} \qquad (1)$$

$$\mathrm{RH\cdots H^{+}\text{-}Zeolite} \rightleftharpoons [\mathrm{RH_2^{+}\text{-}Zeolite}] \Rightarrow \mathrm{Cracked\ products} \qquad (2)$$

Where RH is the gas phase reactant alkane, H^+-Zeolite is proton-formed zeolite and RH_2^+ is the penta-coordinated carbonium ion[131]. At first step (Equation (1)), the pysisorbed alkane is in equilibrium with the gas phase. At second step (Equation (2)), the phsisorbed alkane is protonated by acidic SiO(H)Al group; as a result, carbonium ion is formed as the transition state species. Then, the unstable carbonium ion is dissociated to the cracked products. In this case, the apparent reaction rate (R_{app}) is shown in follow equation;

$$R_{app} = k_{int} K_{Eq} P_{RH} \qquad (3)$$

Where k_{int} is the intrinsic reaction rate constant for step (2), K_{Eq} is the equilibrium adsorption constant for step (1), and P_{RH} is partial pressure of alkane. In other words, this reaction is first order in P_{RH}. This reaction mechanism is supported by our previous study about hydrocarbon cracking activity of H-ZSM-5[132]. In step (2),

therefore, the intrinsic activation energy (E_{int}) should be related to the apparent activation energy (E_{app}) obtained by Arrhenius equation and the adsorption heat of alkane (ΔH_{ads}). As summarized in the Equation (4), the E_{int} has been generally assigned to the sum of the E_{app} and ΔH_{ads}.

$$E_{int} = E_{app} - \Delta H_{ads} \quad (4)$$

Naturally, E_{app} strongly depends on the zeolite structure. USY, BEA, ZSM-5 and MCM-22 are typical zeolites which show high catalytic activity for hydrocarbon cracking. On the other hand, differential heats of alkane adsorptions (ΔH_{ads}) have been measured by several researchers, and those parameters strongly depend on the zeolite structures (pore diameter and/or framework density)[133, 134]. In addition, the ΔH_{ads} decrease with increasing of chain length of hydrocarbon[134].

Interestingly, many researchers have suggested that intrinsic activation energies of several zeolites are same[129,130]; additionally, it is constant regardless of the chain length of hydrocarbon[135]. If this proposition is true, it can be concluded that the activation energy of hydrocarbon cracking is dependent on the framework structure and is not correlated with the Brønsted acid strength. However, the strength of Brønsted acid site in zeolite is considered as an important factor which characterizes the catalytic performance in several reactions[127, 136]. By means of quantum chemical calculations, van Santen *et al* suggested the linear relationship between the activation energy of ethane cracking and the deprotonation energy of the acidic OH group as active site[137]. In other words, this relationship means that the empirical Brønsted-Polanyi rule can be applied to the hydrocarbon cracking reaction[138,139]. As described above, difference of opinion about origin of catalytic activity of hydrocarbon cracking exists among each researcher.

Objective and Outline of This Thesis

The author believes that the accurate quantitative measurement of zeolite acidity is the most important approach for understanding the hydrocarbon cracking activity. However, the quantitative evaluation of relationship between the acid strength and the hydrocarbon cracking activity has never been fully performed. The difficulty of quantitative measurement of acid strength is considered the crucial stumbling block in this discussion. Therefore, the development of effective methodology for quantitative characterization of solid acidity is important subject.

Our laboratory has proposed the new characterization method named infrared-mass spectroscopy/ temperature-programmed desorption (IRMS-TPD) of ammonia. This method is combined technique of usual ammonia TPD measurements and *in situ* infrared spectroscopy measurements. By the *in situ* FT-IR spectroscopic analysis on solid acid surface during the ammonia TPD process, the quantitative measurements of solid acidity and the identification of the structure of acid site (Brønsted or Lewis types) can be carried out simultaneously. Additionally, Kohn-Sham DFT calculation with sufficient-accuracy and low-computational is effective methodology for supporting the experimental results. In order to quantify the Brønsted acidity of zeolites, the author will investigate the physicochemical property of zeolites by means of the combined approach of the IRMS-TPD measurement and DFT calculation.

The objective of this study can be divided into following four subjects.

(i) Optimization of the experimental conditions of ammonia IRMS-TPD measurement.

(ii) Experimental evaluation of physicochemical property of Brønsted acidity of zeolite based on systematic measurements of solid acidities of various zeolites.

(iii) Clarification of the relationship between the paraffin cracking activity and the Brønsted acid strength.

(iv) Theoretical analysis of Brønsted acid strength based on experimental knowledge.

In Chapter 2, the Brønsted acidities obtained by ammonia IRMS-TPD method and the paraffin cracking activities of several zeolites are summarized. In Chapter 2-1, Brønsted acidities and octane cracking activities of partially ion exchanged NaH-MOR zeolites are mentioned. Identification of two kinds of acidic OH groups located in the 12 and 8MRs framework systems are carried out. In addition, optimized experimental condition of IRMS-TPD measurement and the analysis method are summarized. In Chapter 2-2, the identification and the quantitative measurement of the catalytic active sites in Na_2H_2-EDTA treated USY zeolite are carried out. In Chapter 2-3, quantitative measurements on four kinds of acidic OH groups in H-Y zeolite assigned to the non-equivalent framework oxygen sites are carried out. In Chapter 2-4, the relationship between the paraffin cracking activities of typical zeolites (MOR, FAU, MFI, FER, MWW, BEA and modified Y zeolites) and those Brønsted acid strengths is discussed. In addition, the spectral and thermodynamic parameters of Brønsted acid sites in zeolites are summarized. The extinction coefficient of asymmetric bending vibration of NH_4^+ species on Brønsted acid sites is determined.

In Chapter 3, the combined studies of ammonia IRMS-TPD measurement and density functional calculation on Brønsted acid strength are summarized. In Chapter 3-1, adsorption energies of ammonia on Brønsted acid sites in typical zeolites are evaluated by embedded cluster DFT calculations, and those calculated values are compared with the corresponding experimental values. In Chapter 3-2, the Brønsted acidities of four kinds of nonequivalent acidic OH groups in H-CHA zeolite are quantitatively evaluated by means of ammonia IRMS-TPD measurements and periodic DFT calculations.

In Chapter 4, from viewpoint of difference of Brønsted acidities, the hydrocarbon cracking activities of normal and mesoporous ZSM-5 materials, Al-MCM-41 and silica-alumina are discussed. In addition, the acid strengths of Brønsted acid sites located in defective positions are evaluated by embedded DFT calculations.

In Chapter 5, the Brønsted acid strengths of divalent metal cation exchanged Y zeolites and USY are evaluated by periodic DFT calculations, and the enhancement mechanism of Brønsted acid strength is discussed.

General conclusions of this thesis and future prospects will be summarized in Chapter 6.

References

1. A. Corma, *Chem. Rev.,* **95**, 559 (1995).
2. M. Wallau, R. Spichitinger, K.K. Unger, A. Tissler and R. Thome, *US Pat.,* 5466432.
3. V. Nair and R. Szostak, *US Pat.,* 5077026.
4. M.K. Rubin, *US Pat.,* 5063037.
5. A. Corma, F. Rey, S. Valencia, J.L. Jordá and J Rius, *Nat. Mater.* **2**, 493 (2003).
6. W. Fan, P. Wu, S. Namba and T. Tatsumi, *J. Catal*., **243**, 183 (2006).
7. P. Mcanespie, A. Dyer and B. Mehta, *US Pat.,* 4329328.
8. H.G. Manyer, G.S. Chaure and A Kumar, *Green Chem*., **8**, 344 (2006).

9. Ch. Baerlocher, L.B. McCusker and D.H. Olson: Atlas of Zeolite Framework Types, 6th edition, Elsevier, Amsterdam, 2007.
10. S.E. Tung and E. McIninch, *J. Catal*., **10**, 166 (1968).
11. J.W. Ward, *J. Catal*., **9**, 225 (1967).
12. J.M. Chezeau, L. Delmotte, J.L. Guth, *Zeolites*, **11**, 598 (1991).
13. L. Kubelková, S. Beran, A. Malecka and V.M. Mastikhin, *Zeolites*, **9**, 12 (1989).
14. C.A. Emeis, *J. Catal,*. **141**, 347 (1993).
15. J. Datka, B. Gil and A. Kubacka, *Zeolites*, **15**, 501 (1995).
16. K.M. Dontsova, L.D. Norton and C.T. Johnston, *Soil Sci. Soc. Am.J.,* **69**, 1225 (2005).
17. B. Wichterlová, Z. Tvarůžková, Z. Sobalík and P. Sarv, *Micropor. Mesopor. Mater*., **24**, 223 (1998).
18. M. Elanany, M. Koyama, K. Momoji, E. Broclawik and A. Miyamoto, *Appl. Surf. Sci*., **246**, 96 (2005).
19. G.D. Chukin, A.S. Kulikov and S.A. Sergienko, *React. Kinet. Catal. Lett.,* **27**, 287 (1985).
20. L. Benco, T. Demuth, J. Hafner, F. Hutschka and H. Toulhoat, *J. Catal.*, **209**, 480 (2002).
21. F. Lónyi and J.H. Lunsford, *J. Catal.*, **136**, 566 (1992).
22. A.W. Peters and C.C. Wu, *Catal. Lett.,* **30**, 171 (1995).
23. A. Corma, V. Fornés and F. Ray, *Appl. Catal*., **59**, 267 (1990).
24. S. Li, A. Zheng, Y. Su, H. Zhang, L. Chen, J. Yang, C. Ye and F. Deng, *J. Am. Chem. Soc.,* **129**, 11161 (2003).
25. W. Song, J.F. Haw, J.B. Nicholas and C.S. Heneghan, *J. Am. Chem. Soc.,* **122**, 10726 (2000).
26. B. Arstad and S. Kolboe, *J. Am. Chem. Soc.,* **123**, 8137 (2001).
27. W. Wang, Y.J. Jiang and M. Hunger, *Catal. Tpday,* **113**, 102 (2006).
28. M. Hunger, *Micropor. Mesopor. Mater*., **82**, 241 (2005).
29. D. Barthomeuf, *Zeolites*, **14**, 394 (1994).
30. G. Sastre, D.W. Lewis and C.R.A. Catlow, *J. Phys. Chem.* B, **101**, 5249 (1997).
31. G. Sastre and D.W. Lewis, *J. Chem. Soc. Faraday Trans*., **94**, 3049 (1998).
32. G. Sastre, D.W. Lewis and A. Corma, *Phys. Chem. Chem. Phys*., **2**, 177 (2000).
33. S.H. Jhung, J.-H. Lee, J.W. Yoon, J.-S Hwang, S.-E. Park and J.-S. Chang, *Micropor. Mesopor. Mater*., **80**, 147 (2005).
34. M.-A. Djieugoue, A.M. Prakash and L. Kevan, *J. Phys. Chem.* B, **103**, 804 (1999).
35. N. Rajic, *J. Serb. Chem. Soc.,* **70**, 371 (2005).
36. S. Hočevar and J. Jevec, *J. Catal.* **135**, 518 (1992).
37. S.M. Csicsery, *Zeolites*, **4**, 202 (1984).
38. D.S. Santilli and S.I. Zones, *Catal. Lett.* **7**, 383 (1990).
39. H. Takashi, M. Niwa and Y. Murakami, *J. Catal.,* **128**, 551 (1991).
40. K. Tominaga, S. Maruoka, M. Gotoh, N. Katada and M. Niwa, *Micropor. Mesopor. Materials*, in press.
41. R. Brzozowski and W. Skupiński, *J. Catal.,* **210**, 313 (2002).
42. P. Chu, *US Pat.,* 4845063.
43. M. Niwa, K. Suzuki, N. Katada, T. Kanougi and T. Atoguchi, *J. Phys. Chem.* B, **109**, 18749 (2005).
44. R. Yoshimoto, K. Hara, K. Okumura, N. Katada and M. Niwa, *J. Phys. Chem.* C, **111**, 1474 (2007).

45. R.C. Deka and K. Hirao, *J. Mol. Catal. A: Chem.,* **181**, 275 (2002).
46. T.R. Gaffney, *Curr. Opin. Solid State and Mater. Sci.* **1**, 69 (1996).
47. L.J. Smith, H. Eckert and A. K. Cheetham, *J. Am. Chem. Soc.***122**, 1700 (2000).
48. M. Feuerstein, G. Engelhardt, P.L. McDaniel, J.E. MacDougall and T.R. Gaffney, *Micropor. Mesopor. Mater*., **26**, 27 (1998).
49. T. Frising and P. Leflaive, *Micropor. Mesopor. Mater*., **114**, 27 (2008).
50. P.B. Venuto, L.A. Hamilton, P.S. Landis and J.J. Wise, *J. Catal*., **4**, 81 (1966).
51. V.J. Frilette, P.B. Weisz and R.L. Golden, *J. Catal.,* **1**, 301 (1962).
52. J.W. Ward, *J. Catal*., **10**, 34 (1968).
53. G.N. Vayssilov, N. Rosch, *J. Phys. Chem.* B., **105**, 4277 (2001).
54. T. Atoguchi, T. Kanougi, T. Yamamoto and S. Yao, *J. Mol. Catal. A: Chem.,* **220**, 183 (2004).
55. T. Atoguchi and T. Kanougi, *J. Mol. Catal. A: Chem.,* **222**, 253 (2004).
56. H. Yahiro and M. Iwamoto, *Appl. Catal.* A*,* **222**, 163 (2001),
57. A. Ali, C.J. Loughran and D.E, Resasco, *Appl. Catal.,* B, **4**, 13 (1997).
58. X. Feng, W.K. Hall, *Catal. Lett.,* **41**, 45 (1996).
59. Toyota auto body co. ltd., J-tokkyo, 2-135126.
60. Idemitsu kosan and Nissan motor, J-tokkyo, 4-278617.
61. S. Chassaing, M. Kumarraja, A.S.S. Sido, P. Pale and J. Sommer, *Org. Lett.,* **9**, 883 (2007).
62. H.C. Kolb, M.G. Finn and B. Sharpless, *Angew. Chem. Int. Ed.* **40**, 2004 (2001).
63. M. Czejck, H. Jobic, A.N. Fitch and T. Vogt, *J. Phys. Chem.* **96**, 1535 (1992).
64. A.K. Cheetham, M.M. Eddy and J.M. Thomas, *J. Chem. Soc. Chem. Commun,* 1337 (1984).
65. A. Gola, B. Rebours, E. Milazzo, J. Lynch, E. Benazzi, S. Lacombe, L. Delevoye and C. Fernendez, *Micropor. Mesopor. Mater*., **40**, 73 (2000).
66. L.J. Smith, A. Davidson and A.K. Cheetham, *Catal. Lett.* **49**, 143 (1997).
67. L.J. Smith, H. Eckert and A.K. Cheetham, *Chem. Mater.,* **13**, 385 (2001).
68. G. Bellussi and M.S. Rigutto, *Stud. Surf. Sci. Catal.*, **145**, 151 (1994).
69. W. Fan, P. Wu, S. Namba and T. Tatsumi, *Angew. Chem. Int. Ed*., **43**, 236 (2004).
70. P. Wu, D. Nuntasri, J. Ruan, Y. Liu, M. He, W. Fan, O. Terasaki and T. Tatsumi, *J. Phys. Chem*. B, **108**, 19126 (2004).
71. W. Fan, P. Wu, S. Namba and T. Tatsumi, *J. Catal*., **243**, 183 (2006).
72. N. Igarashi, K. Hashimoto and T. Tatsumi, *Micropor. Mesopor. Mater.,* **104**, 269 (2007).
73. A. Corma, L.T. Nemeth, M. Renz and S. Valencia, *Nature*, **412**, 423 (2001).
74. R. Mostowicz, F. Crea and J.B-. Nagy, *Zeolites*, **13**, 678 (1993).
75. E.M. Flanigen and R.L. Patton, *US Pat*., 4073865.
76. A. Corma, M. Puche, F. Rey, G. Sankar and S.J. Teat, *Angew. Chem. Int. Ed*., **42**, 1156 (2003).
77. A. Corma, M.J.D-Cabaňas, J.M-Triguero, A. Rey and J. Rius, *Nature*, **418**, 514 (2002).
78. Q. Li, A. Navrotsky, F. Rey and A. Corma, *Micropor. Mesopor. Mater.,* **74**, 87 (2004).
79. R. Castaňeda, A. Corma, V. Fornés, F. Rey and J. Rius, *J. Am. Chem. Soc.*, **125**, 7820 (2003).
80. R. Castaňeda, A. Corma, V. Fornés, J. M-Triquero and S. Valencia, J. Catal., **238**, 79 (2006).

81. Y. Goto, Y. Fukushima, P. Ratu, Y. Imada, Y. Kubota, Y. Sugi, M. Ogura and M. Matsukata, *J. Porous Mater*., **9**, 43 (2002).
82. C.J.H. Jacobsen, C. Madsen, J. Houzvicka, I. Schmidt and A. Carlsson, *J. Am. Chem. Soc.*, **122**, 7116 (2000).
83. K. Yamamoto, Y Sakata, Y, Nohara, Y. Takahashi nad T. Tatsumi, *Science,* **300**, 470 (2003).
84. S. Inagaki, S. Guan, T. Ohsuna and O. Terasaki, *Nature*, **416**, 304 (2002).
85. T. Tatsumi and Y. Nishimura, "Recent Development of Zeolite Catalysts" (2004).
86. K. Bando, T. Saito, K. Sato, T. Tanaka, F. Dumeigil, M. Imamura, N. Matsubayashi and H. Shimada, *Topic. in Catal*., **18**, 59 (2002).
87. K. Okumura, K. Kato, T. Sanada and M. Niwa, *J. Phys. Chem.* C, 111, 14426 (2007).
88. K. Okumura, R. Yoshimoto, S. Yokota, K. Kato, H. Tanida, T. Uruga and M. Niwa, *Physica. Scripta*., **T115**, 816 (2005).
89. W. Vogel, H. Knözinger, B.T. Carvill, W.M.H. Sachtler and Z.C. Zhang, *J. Phys. Chem.* B, **102**, 1750 (1998).
90. W.P.J.H. Jacobs, H. Jobic, J.H.M.C. van Wolput and R.A. van Santen, *Zeolites*, **12**, 315 (1992).
91. C. Paze, S. Bordiga, C. Lamberti, M. Salvalaggio, A. Zecchina and G. Bellussi, *J. Phys. Chem.* B, **101**, 4740 (1997).
92. F. Wakabayashi and K. Domen, *Catalysis Surveys from Japan*, **1**, 181 (1997).
93. M.A. Makarova, A.F. Ojo, K. Karim, M. Hunger and J. Dwyer, *J. Phys. Chem.,* **98**, 3619 (1994).
94. F. T.-Starzyk, A. Travert, J. Saussey and J.-C. Lavalley, *Topic. in Catal.*, **6**, 111 (1998).
95. J.A. Lercher, C. Crűndling and G. E.-Mirth, *Catal. Today*, **27**, 353 (1996).
96. E.B. Wilson, *Physical, Review*, **45**, 706 (1934).
97. S. Khabtou, T. Chevreau and J.C. Lavalley, *Micropor. Mater.*, **3**, 133 (1994).
98. R. Buzzoni, S. Bordiga, G. Ricchiardi, C. Lamberti and A. Zecchina, *Langmuir*, **12**, 930 (1996).
99. E. Brunner, *J. Mol. Str.* **355**, 61 (1995).
100. C. Pazè, A. Zecchina, S. Spera, A. Corma, E. Merlo, G. Spanò and G. Girotti, *Phys. Chem. Chem. Phys*., **1**, 2627 (1999).
101. B. Civalleri, E. Garrone and P. Ugliengo, *Chem. Phys. Lett*., **299**, 443 (1999).
102. R.R. Pinto, P. Borges, M.A.N.D.A. Lemos, F. Lemos, J.C. Vedrine, E.G. Derouane, F.R. Riberio, *Appl. Catal., A: Gen*., **39**, 284 (2005).
103. D.J. Parrillo and R.J. Gorte, *Catal. Lett.*, **16**, 17 (1992).
104. A. Auroux, *Topics in Catal*., **19**, 205 (2002).
105. L. Smith, A. K. Cheetham, L. Marchese, J. M. Thomas, P. A. Wright and J. Chen, *Catal. Lett*., **41**, 13 (1996).
106. A. Martucci, G. Cruciani, A. Alberti, C. Ritter, P. Ciambelli and M. Rapacciuolo, *Micropor. Mesopor. Mater*., **35-36**, 405 (2000).
107. A. Martucci, A. Alberti, G. Cruciani, P. Radaelli, P. Ciambelli and M. Rapacciulo, *Micropor. Mesopor. Mater.* **30**, 95 (1999).
108. M. Niwa, N. Katada, M. Sawa and Y. Murakami, *J. Phys. Chem.,* **99**, 8812 (1995).

109. N. Katada, H. Igi, J.H. Kim and M. Niwa, *J. Phys. Chem.* B, **101**, 5969 (1997).
110. W. Kohn, *Novel Lectures in Chemistry 1996-2000*, 213 (2003).
111. M. Brändle and J. Sauer, *J. Am. Chem. Soc.,* **120**, 1556 (1998).
112. U. Eichler, M. Brändle and J. Sauer, *J. Phys. Chem.* B, **101**, 10035 (1997).
113. W.J. Mortier, *J. Catal.,* **55**, 138 (1978).
114. P.A. Jacobs and W.J. Mortier, *Zeolites*, **2**, 226 (1982).
115. N. Katada, Y. Kageyama, K. Takahara, T. Kanai, H.A. Begum and M. Niwa, *J. Mol. Catal., A: Chem.,* **211***,* 119 (2004).
116. K. Suzuki, G. Sastre, N. Katada and M. Niwa, *Phys. Chem. Chem. Phys.*, **9**, 5980 (2007).
117. N. Katada, T. Kanai and M. Niwa, *Micropor. Mesopor. Mater*., 75, 61 (2004).
118. C.A. Fyfe, Y. Feng and H. Groudey, *Micropor. Mater.*, **1**, 393 (1993).
119. J.M. Thomas, J. Klinowski, S. Ramdas, B.K. Hunter and D.T.B. Tennakoon, *Chem. Phys. Lett*., 102, **158** (1983).
120. G. Engelhardt and R. Radeglia, *Chem. Phys. Lett.,* **108**, 271 (1984).
121. S. Ramdas and J. Klinowski, *Nature*, **308**, 521 (1984).
122. E. Lippmaa, A. Samoson and M. Mägi, *J. Am. Chem. Soc*., **108**, 1730 (1986).
123. A. Redondo and P.J. Hay, *J. Phys. Chem.*, **97**, 11754 (1993).
124. J.B. Nicholas, R.E. Winans, R.J. Harrison, L.E. Iton, L.A. Curtiss and A. J. Hopfinger, *J. Phys. Chem*., **96**, 10247 (1992).
125. D.W. Lewis and G. Sastre, *Chem. Commun*., 349 (1999).
126. G. Sastre, V. Fornes and A. Corma, *J. Phys. Chem.* B, 104, 4349 (2000).
127. For example, F. Lónyi, A. Kovács and J. Valyon, *J. Phys. Chem.* B, **110**, 1711 (2006).
128. W.O. Haag and R.M. Dessau, Proc. 8th Intern. Conger. Catal. Berlin, **2**, p. 305 (1984).
129. S.M. Babitz, B.A. Williams, J.T. Miller, R.Q. Snurr, W.O. Haag and H.H. Kung, *Appl. Catal. A; Gen.,* **179**, 71 (1999).
130. J. A. van Bokhoven, B.A. Williams, W. Ji, D.C. Koningsberger, H.H. Kung and J.T. Miller, *J. Catal.*, **224**, 50 (2004).
131. G. Olah, *J. Am. Chem. Soc*., **94**, 808 (1972).
132. T. Hashiba, D. Hayashi, N. Katada and M. Niwa, *Catal. Today*, **97**, 35 (2004).
133. F. Eder and J.A. Lercher, *J. Phys. Chem.* B, **101**, 1273 (1997).
134. F. Eder, M. Stockenhuber and J.A. Lercher, *J. Phys. Chem. B*, **101**, 5414 (1997).
135. T.F. Narbeshuber, H. Vinek and J.A. Lercher, *J. Catal*., **157**, 388 (1995).
136. P. Borges, R.R. Pinto, M.A.N.D.A. Lemos, F. Lemos, J.C. Védrine, E.G. Derouane and F.R. Ribeiro, *J. Mol. Catl. A: Chem.,* **229**, 127 (2005).
137. M.V. Frash and R.A. van Santen, *Topics in Catal.*, **9**, 191 (1999).
138. N. Brønsted, *Chem. Rev.* **5**, 231 (1928).
139. M.G. Evans and N.P. Polanyi, *Trans. Faraday Soc.*, **34**, 11 (1938).
140. D. Freude, T. Loeser, D. Michel, U. Pingel and D Prochnow, *Solid State Nucl. Magn. Reson.* **20**, 46 (**2001)**.

Chapter 2.

Ammonia IRMS-TPD Measurements of Solid Acidity of Zeolites

2-1. Ammonia IRMS-TPD study on the Distribution of Acid Sites in Mordenite

Synopsis

Using an IRMS-TPD (temperature programmed desorption) of ammonia, we studied the nature, strength, crystallographic location, and distribution of acid sites of mordenite. In this method, infrared spectroscopy (IR) and mass spectroscopy (MS) work together to follow the thermal behavior of adsorbed and desorbed ammonia, respectively; therefore, adsorbed species were identified, and their thermal behavior was directly connected with the desorption of ammonia during an elevation of temperature. IR-measured TPD of the NH_4^+ cation was similar to MS-measured TPD, thus showing the nature of Brønsted acidity. From the behavior of OH bands, it was found that the Brønsted acid sites consisted of two kinds of OH bands at high and low wavenumbers, ascribable to OH bands situated on 12- and 8-member rings (MR) of mordenite structure, respectively. The amount and strength of these Brønsted hydroxyls were measured quantitatively based on a theoretical equation using a curve fitting method. Up to ca. 30% of the exchange degree, NH_4^+ was exchanged with Na^+ on the 12-MR to arrive at saturation; therefore, in this region, the Brønsted acid site was situated on the large pore of 12-MR. The NH_4^+ cation was then exchanged with Na^+ on 8-MR, and finally exceeded the amount on 12-MR. In the 99% NH_4-mordenite, Brønsted acid sites were located predominantly on the 8-MR more than on the 12-MR. Irrespective of the NH_4^+ exchange degree, the strengths ΔH of Brønsted OH were 145 and 153 kJ mol^{-1} on the 12- and 8-MR, respectively; that is, the strength of Brønsted acid site on the 8-MR was larger than that on the 12-MR. A density functional theory (DFT) calculation supported the difference in the strengths of the acid sites. Catalytic cracking activity of the Brønsted acid sites on the 8-MR declined rapidly, while that on the 12-MR was remarkably kept. The difference in strength and/or steric capacity may cause such a difference in the life of a catalyst.

Introduction

Brønsted acidity in the framework of zeolites is a matter of importance for fundamental and industrial investigations. It is known that the acid site (H^+) of a zeolite is generated by the isomorphous substitution of Si_4^+ in the silicate framework by Al^{3+}. Many techniques, for example, ammonia TPD (temperature-programmed desorption) using MS (mass spectroscopy),[1,2] confirmed that the number of acid sites was principally equal to that of aluminum atoms inside the zeolite framework. Quantitative agreement between the numbers of acid sites and the framework aluminum was, in the early stage of this investigation, limited to siliceous zeolites with less than 1.5 mol/ kg of acid site; however, after a precise study using NH_4-type zeolites, it was extended to Y-type zeolites with a high concentration of acid sites[3]. NH_4-type zeolites retain the structure, and after removing ammonia, an in situ prepared H-type zeolite shows the number of acid sites equal to the aluminum cation in the framework, as long as it is kept unexposed to the outside humidity[4].

Also, the strength of acid sites of zeolites is important to interpret their catalytic property. It has been clarified that the average strength of a zeolite is dependent on its crystal structure. It is possible to study the zeolite acidity from the quantum chemical calculation[5-7]. With the help of these advanced techniques, global understanding on solid acidity is now in progress. For a complete understanding of zeolite acidity, the acid strength of each crystallographically specific site should be determined experimentally.

It has been known previously that mordenite has a very strong acid site. Its ammonia adsorption heat, *ca.* 150 kJ mol^{-1}, measured by ammonia TPD is greater than that of any other studied zeolites[1,2]. Mordenite looks like a zeolite that has acid sites with relatively homogeneous strength; however, the distribution of the acidity has been investigated. There are four kinds of T sites, named T1-T4, as shown in Figure 2-1-1; four oxygen atoms bond with the Al in each T site and hydroxyls direct toward 8- or 12-member rings. As mentioned below, however, OH positioned in the small side pockets of four and five-member rings is unknown. Totally, 10 kinds of oxygen exist in the framework of mordenite and therefore 10 kinds of Brønsted acid sites are structurally possible. The location of Al in the mordenite was studied by Alberti,[8,9] and the distribution of Brønsted acid sites has been studied by IR (infrared) spectroscopy using NH_3,[10] pyridine,[11] N_2,[12] and CO[13] as probes, individually or comprehensively[14].

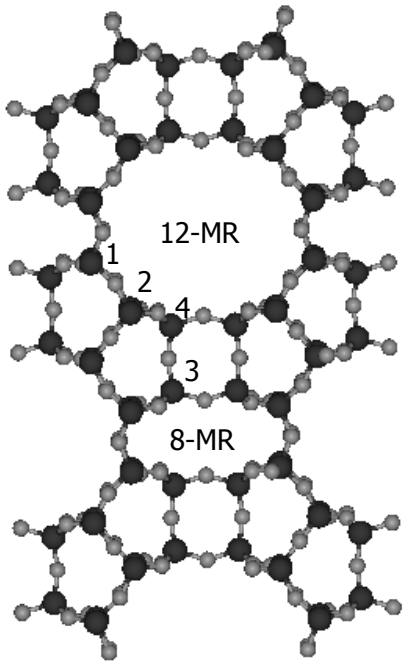

Figure 2-1-1. Four kinds of nonequivalent tetrahedral sites in MOR structure.

In this subchapter, we study the acidic property of mordenite using IRMS-TPD of ammonia, a new technique for characterization in which IR and MS work together and the site and strength of Brønsted OH bands are clearly revealed[15]. From the comparison of MS-TPD with IR-TPD, the thermal behavior of ammonia adsorbed on each OH group can be observed. Thus, with this method, we can get an insight into the nature of Brønsted acid sites in detail.

Experimental Section

IRMS-TPD of Ammonia

IR (Perkin-Elmer Spectrum-One) and MS (Pfeiffer QME200) were connected with a vacuum line to which helium was allowed to flow as a carrier (Figure 2-1-2). The experimental apparatus is described elsewhere in detail[15]. To avoid a delay in the desorbed ammonia arriving at the MS, we selected a rapid flow rate (vide infra); at the selected standard conditions, helium was allowed to flow into the line kept at 25 Torr (1 Torr = 0.133 kPa) with 125 ml min^{-1}. An IR beam was transmitted to the self-compressed disk (about 8 mg and 10 mm in diameter). After evacuation of the sample at 813 K, IR spectra were recorded before and after ammonia adsorption, shown as N(*T*) and A(*T*) (*T*, temperature in K), respectively, during the elevation of temperature from 373 to 873 K in a ramp rate of 10 K min^{-1}. The difference spectra, A(*T*) - N(*T*), were calculated to identify the adsorbed species and the OH band interacted with the species. A differential change in the absorption intensity with respect to the measured temperature, -d{A(*T*) - N(*T*)}/d*T*, was calculated at the selected wavenumber (hereafter, called IR-TPD) to compare with TPD measured by MS operating at *m*/*e*, 16.

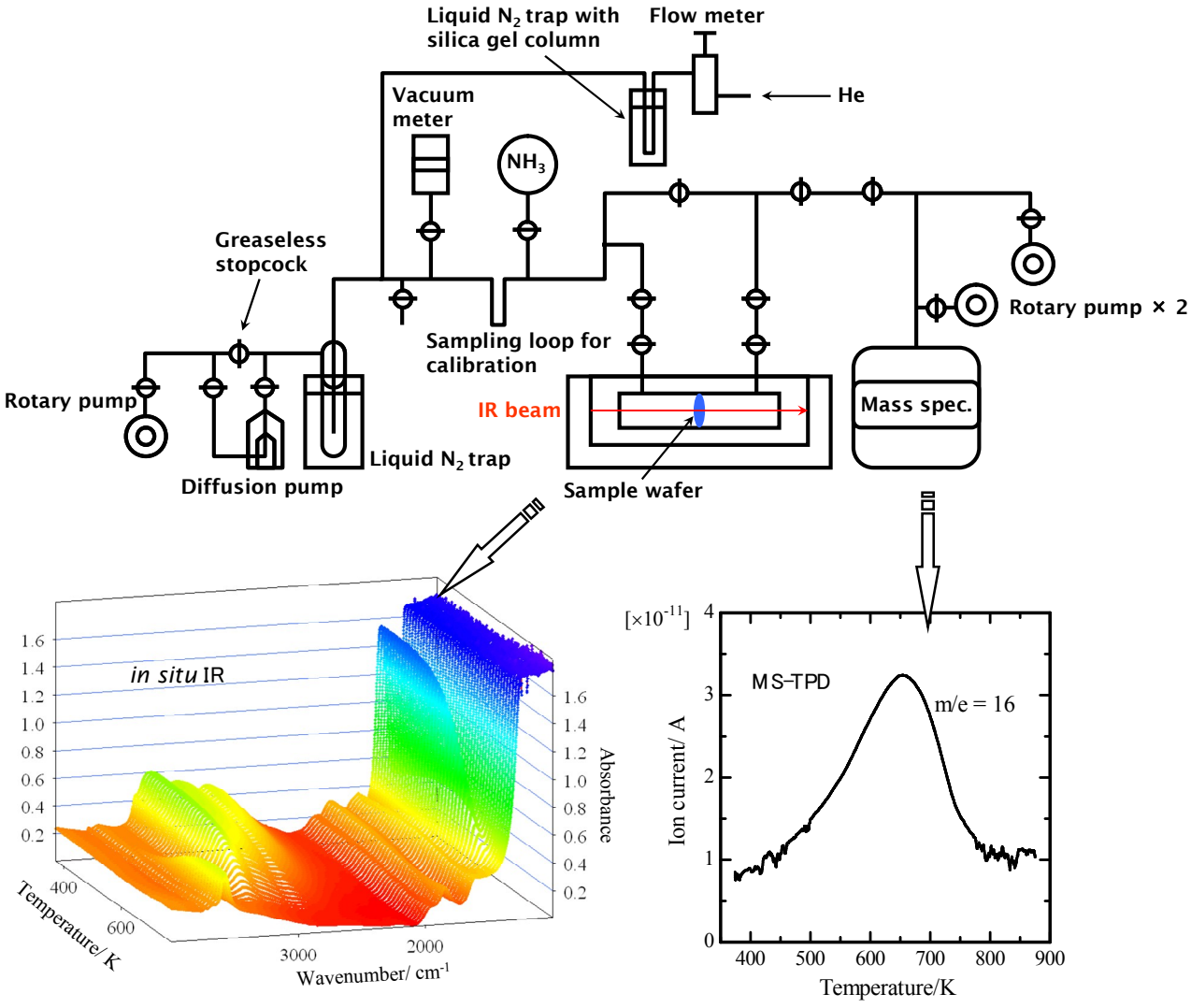

Figure 2-1-2. Experimental arrangement of the IRMS-TPD

Materials

Na-form mordenite with Si/Al_2 = 15 (Reference Catalyst, Catalyst Society of Japan, JRC-Z-M15) was ion-exchanged with NH_4NO_3 and evacuated in the IR cell at 813 K as above. Five species of mordenite with various exchange degrees of NH_4^+ were prepared, and the composition was measured by ICP (inductively coupled plasma) spectroscopy after digestion in HF. Because the ammonium-type zeolite retains the finest conditions of solid acid sites, it was evacuated in the IR cell and the in situ prepared HNaM-15 was used for the IRMS-TPD measurement throughout the present study.

Catalytic Reaction

The cracking of octane was measured by a continuous flow method. Octane vapor mixed with nitrogen carrier gas (partial pressure of octane, 14 Torr) was allowed to low into a Pyrex glass reactor heated at 673 K. A zeolite sample (0.03 g) was activated at 813 K in a dried N_2 flow for 1 h before the reaction. The products and reactant were fed into a gas chromatograph directly through a six-way valve and analyzed using a silicone capillary column and flame ionization detector.

Density Functional Theory (DFT) Calculation

DFT calculations were carried out, for all periodic models before and after NH_3 adsorption, by solving Kohn Sham equation self-consistently[16] as implemented in DMol^3 software[17]. The one-electron Schrödinger equations were solved only at the k = 0 wave-vector point of the Brillouin zone. Basis sets were represented by the numerical type atomic orbitals, and in this study double numerical with polarization (DNP) basis sets were employed. The Vosko-Wilk-Nusair (VWN) local correlation functional[18] was used in order to optimize geometries. The SCF (self-consistent field) convergence criterion was set to 10^{-5} Ha, and the gradient convergence criterion was set to 10^{-3} Ha/ Bohr.

Results

Experimental Conditions for IRMS-TPD of Ammonia

When ammonia TPD is measured under conventional experimental conditions, it is controlled under the equilibrium between ammonia molecules in the gas phase and adsorbed on the sample[1,2]. The theory for TPD experiments controlled by the equilibrium between gaseous and adsorbed ammonia molecules predicts a linear relation between these parameters.

$$C_g = -\frac{\beta A_0 W}{F}\frac{d\theta}{dT} = \frac{\theta}{1-\theta}\frac{P^\circ}{RT}e^{-\frac{\Delta H}{RT}}e^{\frac{\Delta S}{R}} \qquad (1)$$

Where Cg is the concentration of ammonia in gas phase (mol m^{-3}), β is the heating rate of temperature (K s^{-1}), A_0 is the desorption amount (mol kg^{-1}), W is the amount of sample (kg), F is the flow rate of carrier gas (m^3 s^{-1}), θ is the extent of coverage of adsorption sites by ammonia, T is temperature (K), P^0 is the pressure at thermodynamic standard conditions (1.013 × 10^5 Pa), R is the gas constant (8.314 J K^{-1} mol^{-1}), ΔH and ΔS are

enthalpy (J mol^{-1}) and entropy (J K^{-1} mol^{-1}) change by ammonia desorption, respectively.

At the peak maximum of TPD spectrum (T_m), differential change of Cg with respect to temperature becomes zero. Thus the eq (1) can be converted to the following equation.

$$\ln T_m = -\ln \frac{A_0 W}{F} = \frac{\Delta H}{\Delta T_m} + \frac{\beta(1-\theta_m)^2(\Delta H - RT_m)}{P^0 \exp(\Delta S / R)} \qquad (2)$$

Because the second term of the right-hand side is practically a constant, plots of the value in the left-hand side against $1/T_m$ gives a straight line of slope ΔH/R, from which ΔH (enthalpy change by ammonia desorption, namely the heat of ammonia adsorption) is measured[19].

We have measured ammonia TPD for the characterization of acid sites under the following standard conditions[2]; 0.1 g of the sample, 60 ml min^{-1} of the carrier gas flow rate and 100 Torr of the pressure inside the cell. However, the conditions were not appropriate for the present experiment of IRMS-TPD, because, due to the large volume and complex shape of *in-situ* IR cell, desorbed ammonia was delayed in arriving at the mass spectrometer; thus, an accurate comparison between TPD spectra measured by IR and MS was difficult. Therefore, a rapid flow rate of helium carrier gas was required to measure the profiles of ammonia adsorbed and desorbed correctly. However, too fast a flow rate (too large mass amount per time) of the carrier gas made the concentration of desorbed ammonia low, resulting in the difficulty in detecting ammonia by MS. After the TPD profiles were examined under various conditions, finally, the most suitable conditions were chosen (120 ml min^{-1} of the carrier gas, 25 Torr of inside pressure, and *ca.* 0.008 g of the sample). In other words, TPD in the present study was measured with a contact time of 1/100 of that in our previous measurements.

Because the contact time of carrier gas was much shorter than that in previous experiments, the conditions must be examined to know whether ammonia molecules are in equilibrium. To do so, we examined a dependence of the temperature of desorbed peak (T_m) on the contact time of the carrier gas. Ammonia TPD was measured on the *in-situ* prepared HM-15 by varying not only the flow rate of helium carrier gas but also the pressure inside the IR cell with the weight of the sample being kept 0.008 g. The peak temperature of ammonia desorption, measured by MS, shifted higher when increasing the contact time W/F, as shown in Figure 2-1-3. Figure 2-1-4 shows the relationship between the parameters derived from the theoretical equation (2). A linear correlation was observed at the smaller values of $1/T_m$, that is, at larger contact times, but it did not extend to the conditions (120 ml min^{-1} of the flow rate and 25 Torr of the pressure inside the cell) that were chosen in the present study. This means that the TPD experiment in the present study was incompletely controlled by the equilibrium.

ΔH on the *in situ* prepared HM-15 was determined using a linear portion of the plot in Figure 2-1-4 on the basis of a theoretical equation (2), and it was determined as 153 kJ mol^{-1}, which was in agreement with the value reported previously[1,2]. ΔS (entropy change by ammonia desorption) could be calculated from the determined ΔH based on the theoretical equation. ΔS consists of ΔS upon phase transformation (*i.e.*, desorption) and ΔS upon physical mixing with carrier gas helium. ΔS upon desorption was regarded as being almost the same as ΔS upon the vaporization of liquid ammonia, that is, 95 J K^{-1} mol^{-1} [1]. Therefore, ΔS upon physical mixing was determined to be 47 J K^{-1} mol^{-1}. Thus, the determined value of ΔS is used in the present study (vide infra) to calculate the

ΔH by the simulation of IR-TPD spectrum.

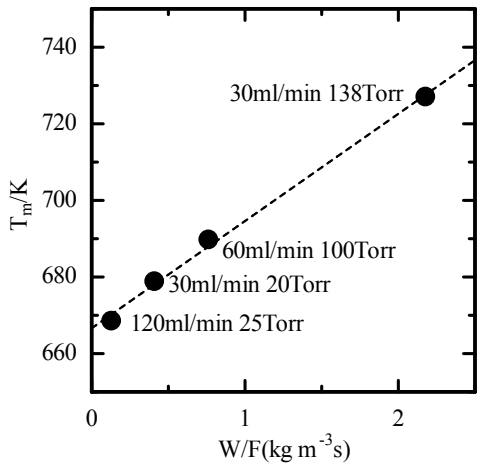

Figure 2-1-3. Dependence of peak maximum temperature on the experimental conditions (W/F).

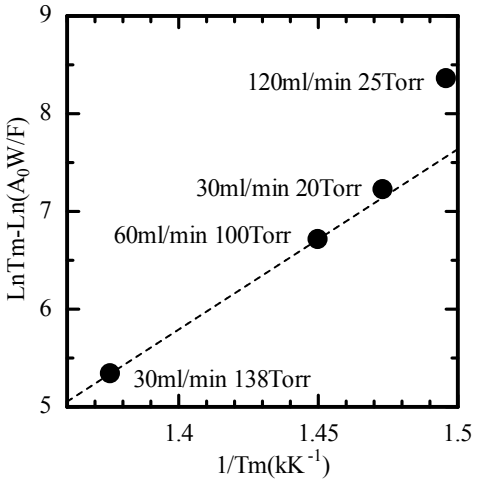

Figure 2-1-4. Plots for confirmation of TPD experiments controlled by the equilibrium between ammonia molecules in the gas phase and adsorbed on the solid.

Temperature Effect for OH Absorption Band

To analyze the change in position, shape and intensity of the OH band by heating, before the adsorption of ammonia, we measured the IR spectra of *in situ* prepared HM-15 in a helium flow with increasing and decreasing the temperature. It was confirmed that the position, shape, and intensity of IR absorption of the OH band changed reversibly with the temperature. By raising the temperature, the peak shifted to the low wavenumber, and the absorbance decreased; and these changes occurred reversibly, as shown in Figure 2-1-5. Therefore, these changes should be corrected to analyze the difference spectra quantitatively. As shown in Figure 2-1-5, a linear relationship between the band position and measurement temperature was observed. From the slope of linear relationship, the change of band position with respect to difference in temperature was described as

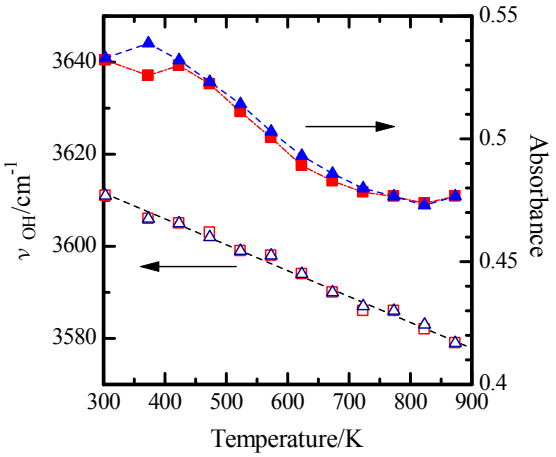

Figure 2-1-5. Change of OH band position and absorbance with the temperature on *in situ* prepared HM-15 in which the temperature was increased (□, ■) or decreased (△, ▲).

$$\frac{\Delta \nu}{\Delta T} = -0.056 \text{ cm}^{-1}\text{ K}^{-1} \qquad (3)$$

where $\Delta\nu$ and ΔT are differences in wavenumber and temperature, respectively. The wavenumbers of difference

spectra are therefore corrected into the values which should be observed at 373 K using eq (3). After the correction, the change in shape of the OH band with the measurement temperature became small enough to neglect (vide infra).

However, the change of absorbance in Figure 2-1-5 from 500 to 700 K could be described by a following equation, when ΔA denoted the difference in absorbances

$$\frac{\Delta A}{\Delta T} = -2 \times 10^{-4}\ \mathrm{K}^{-1} \qquad (4)$$

However, the rate of recovery of OH band intensity by increasing the temperature, (-d{A(T) - N(T)}/dT, i.e., IR-TPD) was *ca.* $4 \times 10^{-3}\ \mathrm{K}^{-1}$ at the peak maximum and therefore considerably higher than the temperature dependence in eq (4) (vide infra). In the IRMS-TPD, furthermore, not an absolute value of absorbance but the difference in absorbances before and after ammonia adsorption is utilized for the analysis. Therefore, the temperature effect on the absorbance is, more or less, canceled. The absorbance is thereby used without correction.

IRMS-TPD on the In situ HM-15 (NH_4^+, 99% Exchange Level)

Figure 2-1-6 shows the difference spectra of ammonia on the *in situ* prepared HM-15. After the adsorption of ammonia, at 373 K, a strong absorption ascribable to the bending vibration of the NH^{4+} cation was observed at 1430 cm^{-1}. NH stretching vibration was characteristically observed in the broad range of 3400-2500 cm^{-1}.[20] However, a negative change of the peak intensity was observed in the OH region; obviously, this is because the NH_4^+ cation was formed on the Brønsted OH. Elevating the temperature reduced the intensities of positive bands of the adsorbed species and recovered the OH bands.

We calculated IR-TPD from changes in the intensities of these bands while increasing the temperature. IR-TPD for the NH_4^+ band intensity (Figure 2-1-7) was almost analogous to the MS measured ammonia TPD, thus proving that the acid sites were predominantly Brønsted type. However, the recovery behavior of the negative OH band during the elevation of temperature showed a shift of the band. As shown in Figure 2-1-8 (a), a negative absorption was observed at 3603 cm^{-1} at 373 K, but the position shifted gradually to a lower wavenumber, 3574 cm^{-1} at 773 K.

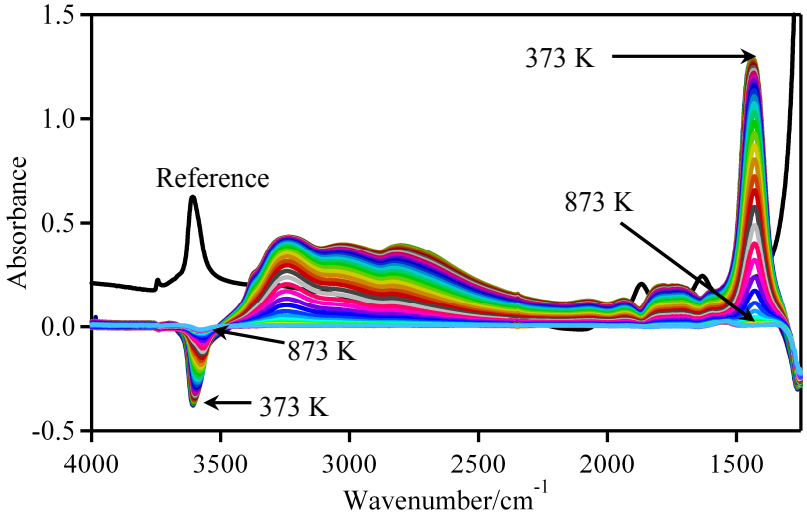

Figure 2-1-6. Difference spectra of ammonia on the in situ prepared HM-15 during the elevation of temperature from 373 to 873 K. Reference spectrum was obtained at 373 K before the adsorption of ammonia.

The shift of the negative OH band was confirmed in Figure 2-1-8 (b), that is, wavenumber corrected spectra, showing that ammonia was adsorbed on different types of OH with different strengths. Obviously, the weaker Brønsted acid site is located at the OH showing the band at a high wavenumber, and the stronger one at the low wavenumber. From the corrected spectra in Figure 2-1-8 (b), one kind of the OH band ascribable to the stronger Brønsted acid site was identified at 3585 cm^{-1}. However, another weaker OH band was identified at 3616 cm^{-1}; the band position was clearly identified on NH_4NaM (NH_4 exchange degree, 31%) on which only the weaker OH exists (vide infra).

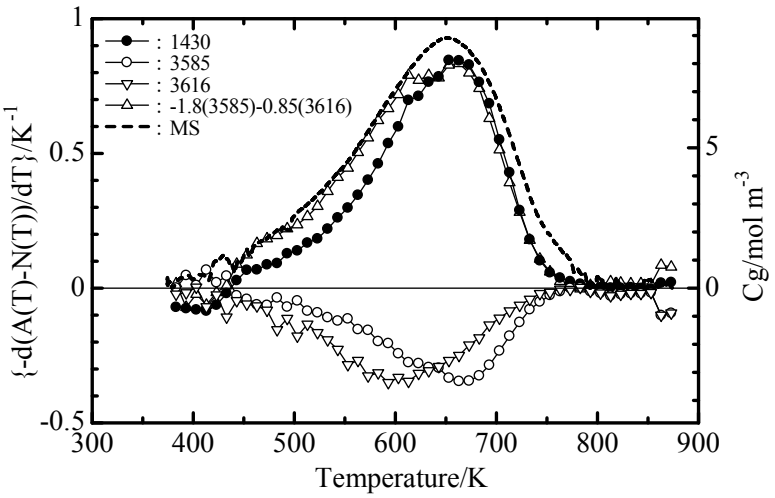

Figure 2-1-7. IR-TPD of ammonia on the in situ prepared HM-15 for the NH_4^+ and OH bands shown in the corner and MS-TPD (change of desorbed ammonia concentration, Cg) for a comparison.

Furthermore, the shape of OH band in the corrected spectra did not depend on the measurement temperature, as shown in Figure 2-1-8 (b). Therefore, IR-TPDs for two kinds of OH were calculated at the positions of 3585 and 3616 cm^{-1}, as shown in Figure 2-1-7. The sum of the two spectra of IR-TPD of OH was similar to MS-TPD, after these were multiplied by appropriate coefficients, that is, 1.8 and 0.85 for IR-TPD of OH at 3585 and 3616 cm^{-1}, respectively. Thus, it was found that not only IR-TPD of NH_4^+ but also MS-TPD was related to the two kinds of OH band. In other words, two kinds of Brønsted OH exist in mordenite, on which ammonia is adsorbed as NH_4^+. The reciprocal of adopted coefficient corresponds to extinction coefficient of OH bands, and the relative ratio, 1/1.8 : 1/0.85, almost agrees with ratio of the reported values[11], 1.55 and 3.50 cm μmol^{-1} for OH at 3584 and 3602 cm^{-1}, respectively.

In previous literature, OH bands of mordenite are identified at 3612 and 3575 cm^{-1} as those located in the 12- and 8-MRs of the mordenite structure, respectively[10-12]. Therefore, based on the above finding, it is concluded that the Brønsted acid site on 8-MR is stronger than that on 12-MR. Furthermore, it is recognized that the Brønsted acid site is located at the 8-MR, mainly because the MS-TPD and IR-TPD of NH_4^+ have a relation closer to the

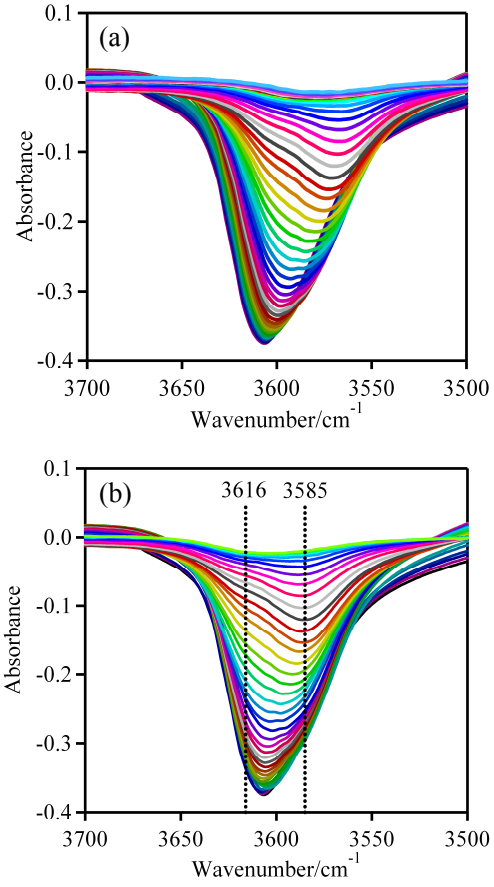

Figure 2-1-8. Enlarged portion of OH band in Figure 2-1-6 ((a), upper) and the corrected spectra using the eq (3) ((b), lower).

IR-TPD of the OH band on the 8-MR at 3585 cm^{-1}; this is quantified more exactly in the following.

In the present study, the amount and strength of the Brønsted acid site were measured quantitatively. To do so, we simulated[2] IR-TPD spectra of two kinds of OH bands on the basis of the theoretical equation. As described above, ΔS of 47 J K^{-1} mol^{-1} upon desorption of ammonia (phase transformation) was assumed as a parameter required for the simulation. Furthermore, it was defined that two kinds of Brønsted OH at 3616 and 3585 cm^{-1} are the sites with different strengths ΔH and amounts A_0, respectively; and the sum of the simulated TPD should be fitted to the IR-TPD of NH_4^+ as well as to MS-TPD. As shown in Figure 2-1-9, the simulated IR-TPD spectra of OH bands were fitted to the experimentally observed ones, and the sum of them fitted to MS-TPD, satisfactorily. Thus, the amounts and strengths of the two kinds of Brønsted acid sites were determined for in situ prepared HM-15 (99% of exchange level), as summarized in Table 2-1-1. It was found, therefore, that the Brønsted acid sites were located in 8-MR more than in 12-MR, and the strength of the Brønsted acid site in the 8-MR was larger than that of the site located in the 12-MR.

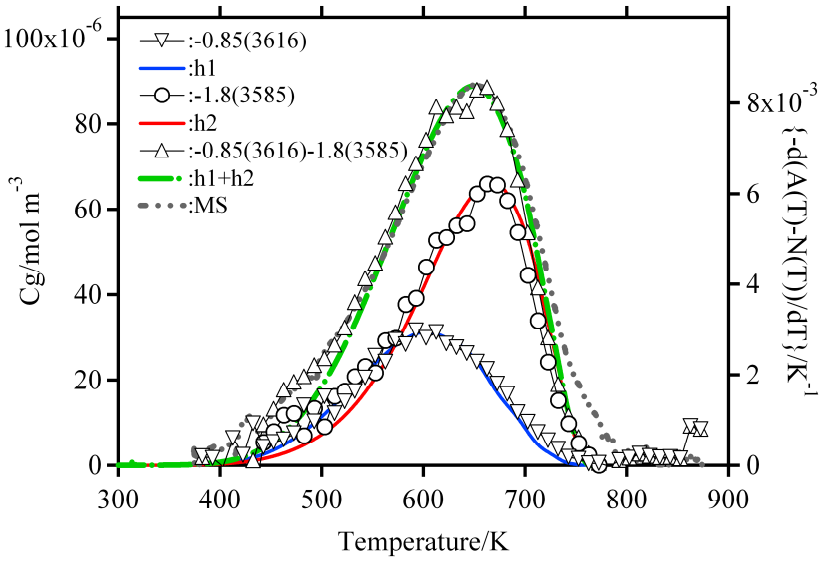

Figure 2-1-9. Comparison of the simulated spectra of IR-TPD with the experimentally observed IR-TPD at 3616 and 3585 cm^{-1}. $-0.85I_{3616}$ and $-1.8I_{3585}$ are fitted to the simulated ones (h1 and h2), respectively, and sum of those IR-TPD and sum simulated ones (h1+h2) are fitted to the MS-TPD.

Table 2-1-1. Amount and strength of Brønsted acid OH on mordenite with different NH_4^+ exchange levels.

	OH in 12-MR		OH in 8-MR		
NH_4^+ / %	A_0 / mol kg^{-1}	ΔH^a / kJ mol^{-1}	A_0 / mol kg^{-1}	ΔH^a / kJ mol^{-1}	A_0 total / mol kg^{-1}
99	0.42	147(9)	0.77	155(8)	1.19
64	0.4	146(8)	0.42	150(7)	0.82
47	0.41	145(8)	0.1	153(8)	0.51
31	0.37	143(7)	0		0.37
7	0.15	142(8)	0		0.15

[a] Value in parentheses shows standard deviation of the acid strength ΔH in kJ mol^{-1}.

IRMS-TPD on the Partially Ion-Exchanged Mordenites

The technique of IRMS-TPD was then applied to the $NaNH_4$-mordenites with exchange degrees of NH_4^+, 64 to 7%. The bending vibration of NH_4^+ was observed at 1430 to 1440 cm^{-1} throughout the samples. As decreasing the exchange level of the NH_4^+ cation, the OH band not only changed the intensity but also shifted the band position (Figure 2-1-10). OH bands were, like in the 99% NH_4-mordenite, analyzed by dividing them into two absorption bands, except for the 31 and 7% NH_4-mordenites, because in these cases only one kind of OH band was observed.

As a typical experimental result, the corrected difference spectra of the OH band on the $NaNH_4$-mordenite (NH_4^+ exchange degree, 31%) were shown in Figure 2-1-11. It was found that only one kind of OH existed at 3616 cm^{-1}, and the shape of the OH was independent of the measurement temperature above 473 K. The broad OH band below 473 K was caused by the so-called *l*-peak ammonia, described below. The OH band at 3616 cm^{-1} was identified as OH located in 12 MR, and the change of intensity was analyzed, as shown in Figure 2-1-12. IRTPD of NH_4^+ bending was almost similar to MS-TPD, and it was also related with corrected IR-TPD of OH bands; therefore, the above conclusions were applicable to these partially cation exchanged mordenites.

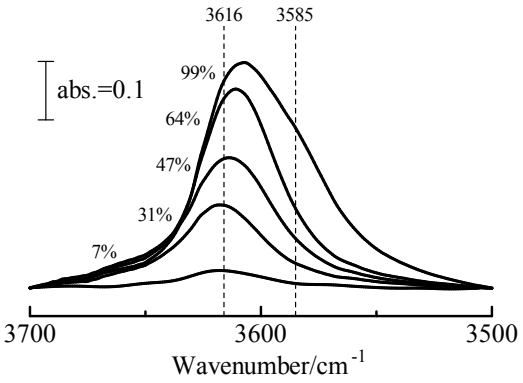

Figure 2-1-10. OH bands measured at 373 K before the adsorption of ammonia, N(373 K), with varying degrees of NH_4^+ exchange shown in the Figure.

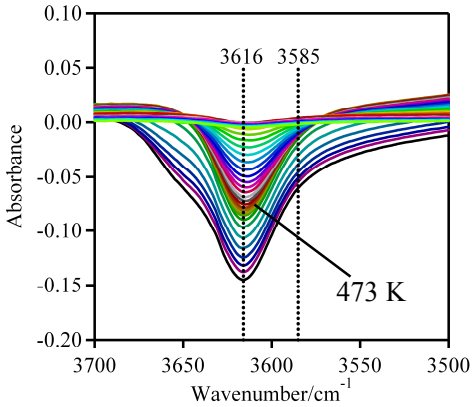

Figure 2-1-11. Corrected difference spectra using eq (3) observed on $NaNH_4$-mordenite (exchange degree of NH_4^+, 31 %).

MS-TPD on the highly Na-containing mordenite showed desorption of ammonia at *ca.* 410 K, as shown in Figure 2-1-12, which was named *l*-peak and regarded as ammonia adsorbed on the Na cation; the intensity of the *l*-peak increased with an increase in the concentration of Na cations. As shown in Figure 2-1-12, the *l*-peak could be related to the IR-TPD of OH band at 3616 cm^{-1} because desorption of ammonia at *ca.* 410 K recovered the intensity of this band. A

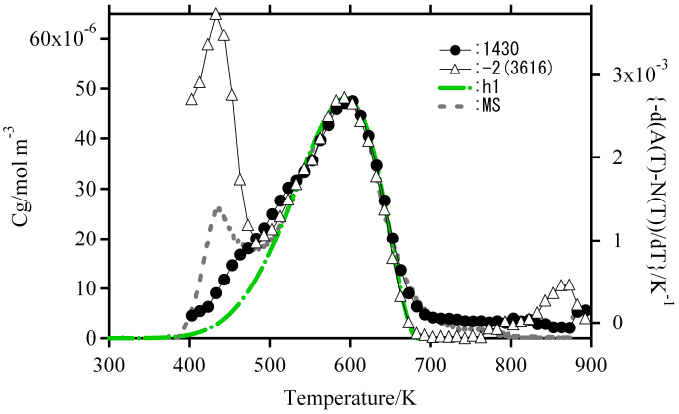

Figure 2-1-12. Comparison between MS-TPD, simulated spectrum of ammonia TPD (h1), IR-TPD of NH_4^+ at 1430 cm^{-1}, and IR-TPD of OH at 3616 cm^{-1} multiplied by −2.

sharp absorption at 1650 cm^{-1} was observed in the reference spectrum, N (373 K), and the band intensity changed upon adsorption and desorption of the *l*-peak ammonia. It was therefore considered that ammonia was adsorbed on Na^+ and simultaneously interacted with OH. This type of ammonia is thereby considered not directly related with the Brønsted acidity, and therefore, the TPD profiles ascribable to the *l*-peak desorption were disregarded for the simulation.

By simulation procedures, we calculated the strength and amount of Brønsted OH, as shown in Table 2-1-1. The strength of the acid site, ΔH, was almost constant, independent of the degree of NH_4^+ cation exchange, and averaged values were 153 and 145 kJ mol^{-1} for Brønsted acid sites situated on 8-MR and 12-MR, respectively. A simple conclusion should be noted that the smaller wavenumber is due to the stronger acidity of the Brønsted OH groups, consistent with the weaker OH bond that should induce the stronger protonation ability.

However, the amount and distribution of acid sites depended strongly on the exchange degree, as shown in Figure 2-1-13. With increasing the degree of NH_4^+ exchange, acid sites increased preferentially in the 12-MR, and saturated at more than 30% of the exchange degree. Acid sites situated on the 8-MR were observed only at exchange degrees higher than 30%, and the amount exceeded that on the 12-MR at more than 70%.

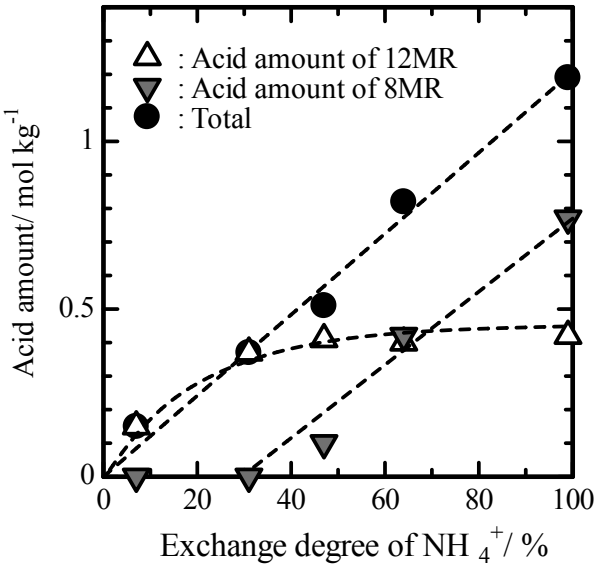

Figure 2-1-13. Amounts of acid site situated on 8- and 12-menmber rings against the degree of NH_4^+ exchange.

Extinction Coefficient for Bending Vibration of NH_4^+

According to the Lambert-Beer equation, the absorbance, *A*, for adsorbed NH_4^+ can be described as

$$A = \varepsilon \cdot cl = \varepsilon \frac{W}{S} c_w \qquad (5)$$

where *c* and *l* are concentrations of the measured species and thickness of the sample, respectively. Because we measure the species adsorbed on a solid, *c* is replaced by ($c_w d$), (c_w, weight based concentration in mol kg^{-1} and *d*, density), and *l* is replaced by *w*/ (*Sd*) (*w*, weight of the sample and *S*, cross sectional area). The absorbances, *A*, for the bending vibration of NH_4^+ measured at 373 K on five kinds of NH_4Na-mordenite were therefore plotted against wc_wS^{-1} in Figure 13, and

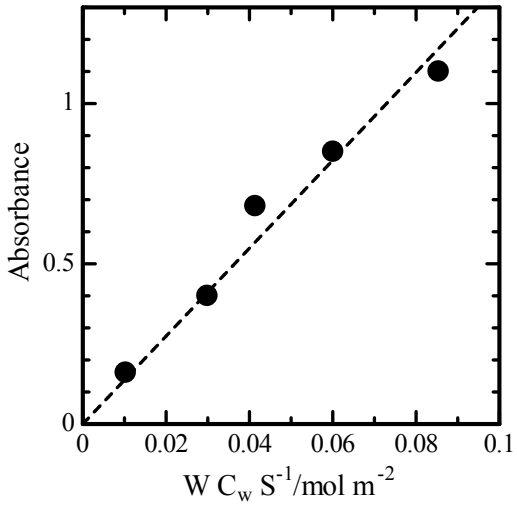

Figure 2-1-14. Determination of extinction coefficient of the NH_4^+ bending vibration band.

ε was determined 13.7 m^2 mol^{-1} from the linear relation. Thus, the obtained value of extinction coefficient almost agrees with that reported on mordenite[21] (14.7 m^2 mol^{-1}).

Catalytic Activity for Cracking of Octane

Figure 2-1-15 shows the catalytic activity for octane cracking on *in situ* prepared NaH-mordenites measured 1 min after the start of the continuous flow reaction. The catalytic activity measured in the early stage increased almost proportionally with the exchange degree of NH_4^+.

However, activities declined rapidly as shown in Figure 2-1-16. Deactivation of the catalytic activity was fast on the mordenites with high degrees of NH_4^+ exchange but became small on 31% of the exchange degree. The activity on 7% NH_4-mordenite was clearly different from others, because it did not decline for 300 min at all. At 300 min after the reaction, activities on 31 and 7% NH_4-exchanged mordenites were higher than those on other mordenites. Therefore, the deactivation behavior correlated well with the distribution of acid sites; on the catalysts with slow deactivation behavior (31 and 7% NH_4-exchanged mordenites), acid sites were preferentially located on the 12-MR, as shown above. In summary, the acid sites on the 8-MR possessed higher activity on the initial stage of the reaction, whereas the sites on the 12-MR were relatively inactive, but hardly declined by time on stream. A higher catalytic activity for hexane cracking on the acid sites located on the 8-MR of mordenite was also reported by Lukyanov *et al*[22].

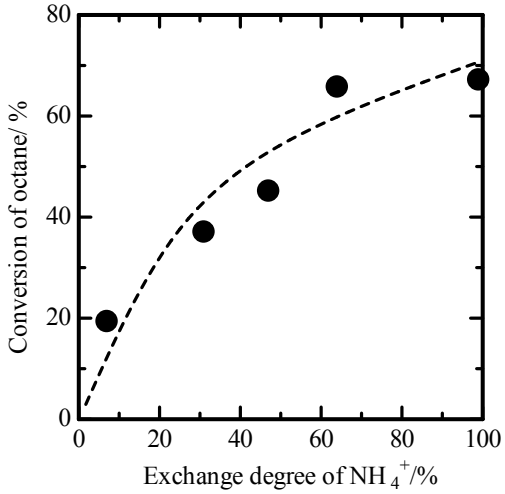

Figure 2-1-15. Conversion of octane 1 min after the reaction against the exchange degree of NH_4^+.

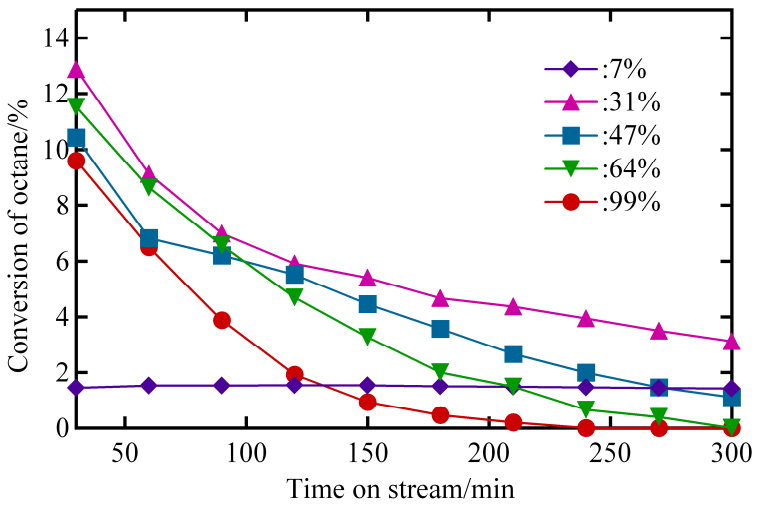

Figure 2-1-16. Change of catalytic activity with time-on-stream on various NH_4Na-mordenites with the exchange degree of NH_4^+ shown in the inset.

DFT Calculation of the Adsorption of Ammonia

Generally, adsorption energies are overestimated, when a local density approximation (LDA) such as VWN functional is used. However, in this study, VWN functional was used for all calculations to reduce the computational cost because the aim of the calculation in this study is to evaluate the difference in acid strengths qualitatively. The geometry of the structure of H-mordenite was first optimized. The ammonia adsorption energy on the Brønsted acid site was then calculated using a DMol^3 program. Calculations were made for NH_4^+ adsorbed on four kinds of Brønsted acid sites (Figure 2-1-17) because four different T sites exist in mordenite. Thus, the calculated NH_3 adsorption energy depended on the location of Al in the mordenite structure, and it was larger on the T_3 site in 8-MR than on the T_1, T_2, and T_4 sites in 12-MR, as shown in Table 2-1-2. Therefore, the DFT calculation supported the difference in strengths of acid sites, measured in the present study.

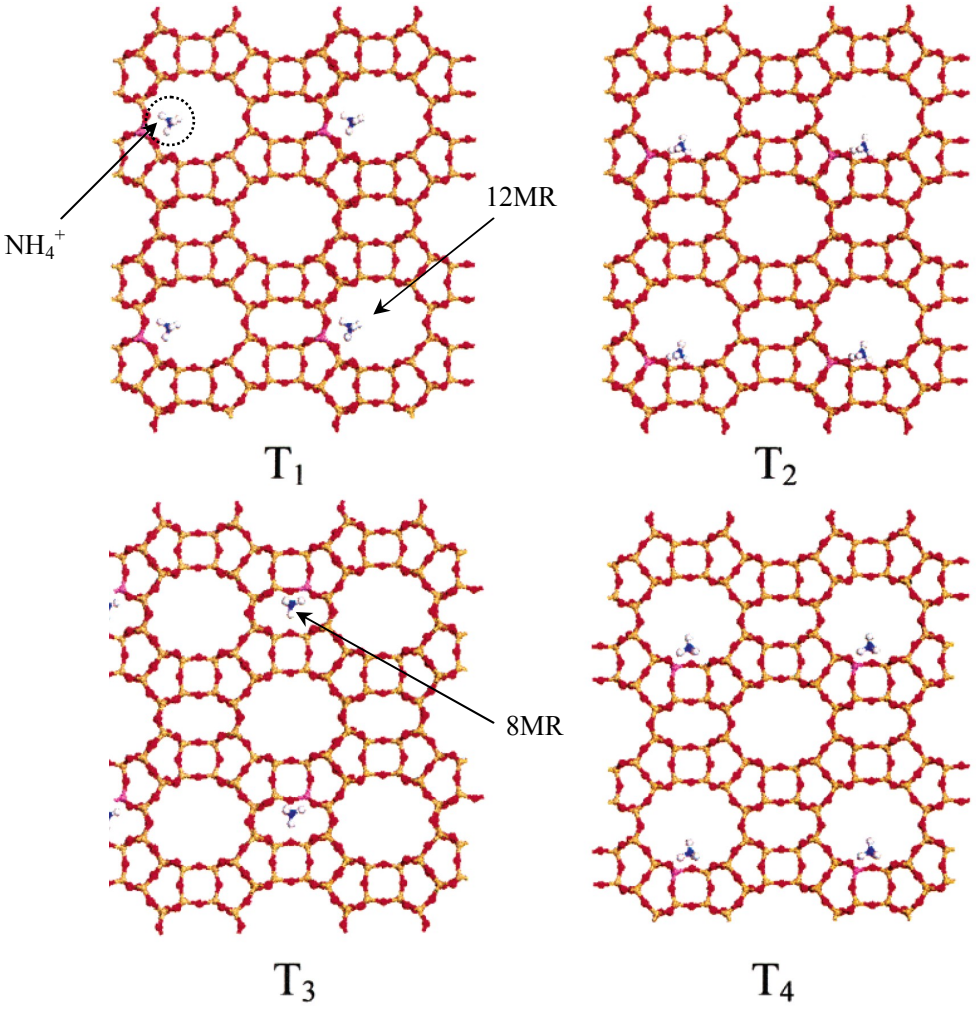

Figure 2-1-17. Fragments of optimized periodic structures of NH_4^+ bonded to T1－T4 sites (1 Al/ u.c.).

Table 2-1-2. Energy of ammonia adsorption obtained by VWN/DNP calculation.

T site	T_1	T_2	T_3	T_4
Adsorption energy of ammonia / kJ mol^{-1}	215	213	235	220

Discussion

Distribution of Acid Strength

In the present study, the acidity of mordenite was studied by a method of IRMS-TPD of ammonia. By utilizing a unique and useful property of the method, the Brønsted acid sites were measured quantitatively. Because there were two kinds of Brønsted acid sites, which depended on the structure of mordenite, the strengths and amounts were measured individually on each crystallographically specific site. Such a precise analysis on the distribution of acid sites has not been reported previously. Therefore, interesting findings about the acidity of zeolite were obtained in the present investigation.

The assignment of OH bands at high and low wavenumbers for those on 12-MR and 8-MR, respectively, was deduced from adsorption experiments of ammonia and pyridine probes[10-12]. Ammonia interacted with both hydroxyls, whereas pyridine adsorption diminished the intensity of the OH band located at a high wavenumber only. Therefore, the assignment of the OH band location is widely accepted. OH bands in the 4- or 5-MR (side pocket) of the mordenite structure, however, neither exist nor are detectable in the IR spectra. Although a recent study by Marie *et al.*[14] suggested the presence of a third Brønsted OH, the present study could not find any evidence to prove it.

However, distribution of the strengths of acidity is a matter of controversy. Zholobenko *et al.* reported that the acidity of Brønsted OH situated on 8-MR was stronger than that on 12-MR on the basis of a study using an ammonia probe[10]. However, Wakabayashi *et al.* drew a contradictory conclusion[12] because adsorption of the N_2 probe decreased the intensity of the OH band on 12-MR only; therefore, they concluded that, because of its stronger acidity, N_2 interacted with OH on the 12-MR only. Datka *et al.* measured the extinction coefficient of OH bands[11] and found a larger value for the OH of 12-MR; because the stronger OH was reported to have a larger value of extinction coefficient, they identified the stronger acidity of hydroxyl in the large pore.

In the present study, ammonia was used as a probe and the stronger acidity of OH on 8-MR was derived, in consistent with Zholobenko *et al*[10]. Contradictory conclusions seem to have derived largely because of the selected probe molecule. The adsorption of nitrogen by Wakabayashi *et al.* was performed at a low temperature such as *ca.* 100 K,[12] and this may be a reason for the different conclusion. However, here we point out the following priority of findings in the present investigation.

(1) IRMS-TPD of ammonia is a method to follow the thermal behavior of adsorbed NH_4^+ and hydroxyl bands directly, and therefore, with this method, information of the strength of each acid site is obtained precisely.

(2) Ammonia is a small molecule; therefore, ammonia can enter into small pores with relatively low steric hindrance. All of the acid sites responsible for the catalytic reaction were counted in the experiment of ammonia TPD, as shown by the agreement between the numbers of acid sites and Al atoms in the framework[2]. Steric hindrance for adsorption can therefore be disregarded.

(3) The OH group shows the IR absorption band at the position that reflects the strength of acidity[23]. Particularly in the region of a high wavenumber above 3600 cm^{-1}, the weaker OH band is located at the higher wavenumber. Therefore, the general trend observed in the band position of OH supports the present conclusion.

(4) The DFT calculation supports the conclusion of the stronger acidity of the OH located on 8-MR.

Location of Acid Sites

Distribution of the Brønsted OH depended on the degree of NH_4^+ exchange. At the low ion exchange degree (NH_4^+/Na^+ ratio), the acid sites were preferentially located on the 12-MR. The Na cation on the site of 12-MR may be easily accessible with NH_4^+ in the solution because of less-steric hindrance. The cation at the 8-MR site was exchanged by increasing the ion-exchange degree. A high preference of Brønsted OH on the 8-MR was observed in the almost 100% NH_4^+-exchanged mordenite. This should show the preferential distribution of Al on the 8-MR.

According to an X-ray study by Alberti[9] on the position of Al in a natural mordenite sample with a Si/Al ratio, *ca.* 5, T_3 and T_4 sites in the 4-MR were the richest in Al. The position of Brønsted OH was not determined directly, because four oxygen atoms bonded to one Al cation, and the neighboring OH was directed toward one of the attached member rings. The population of Brønsted OH was therefore estimated from a comparison with spectroscopic data reported previously, and about the same probability of the OH population in the 12- and 8-MR was proposed on the basis of the spectroscopic data.

Datka *et al.*[11] measured IR bands of OH on the *in situ* prepared H-mordenite calcined at 830 K after adsorption of pyridine, accessible only to OH in the large pore, to discriminate between OH groups situated on two member rings. They reported populations of OH on 12- and 8-MR were almost the same, that is, 3.0 and 3.5 H^+/unit cell, respectively.

Wakabayashi *et al.*[12] made a peak deconvolution of OH bands of H-mordenite; the relative ratio of the integrated absorbances of OH bands was 32:25 for bands at 3616 and 3590 cm^{-1}, as seen in their experimental data. The extinction coefficients of OH bands at 12- and 8-MR were reported to be 3.50 and 1.55 cm μmol^{-1}, respectively, according to Datka *et al*,[11] and we also used similar corresponding parameters for the curve fitting, as mentioned above (Figures 2-1-7 and 2-1-9). Concentrations of OH situated on 12- and 8-MR are therefore in a ratio of approximately 9:16, the reported values of ε being taken as parameters. The relative ratio thus estimated is almost in agreement with that measured in the present study on 99% NH_4-mordenite. The relative concentration of hydroxyls can be measured correctly from IR spectroscopy, when extinction coefficients are provided. One does not become aware of the shoulder-like OH at a lower wavenumber because of the large width of the absorption.

Recently, Kato *et al.*[24] reported that mordenite synthesized in the presence of a fluoride ion had a unique distribution of Al cation in the framework; based on the experiment observation and theoretical considerations, aluminum was located only on the T site in the 12-MR. As found in the present study, the location of the Brønsted OH depended strongly on the concentration of an Na cation. Therefore, various conditions of the synthetic procedure and included cation may have an influence on the final position of OH in mordenite.

Catalysis on Acid Site on Mordenite

Mordenite is known as the zeolite with a large pore channel of 12-MR, and the presence of the strong acid site is remarkable as well. However, the Brønsted acid sites with a strength of 153 kJ mol^{-1} are located on the 8-MR, a smaller pore of the mordenite structure, as mentioned above. The conclusion has a big impact on the understanding of the catalysis in mordenite.

As found in the present study, the catalytic activity of octane cracking declined rapidly on the mordenite with

a high concentration of stronger acid sites located at the position of 8-MR, whereas only the mordenite with weaker acid sites on the 12-MR showed a slow deactivation behavior. The correlation between the acid strength and the catalytic life could be explained easily because coking occurs easily on the strong acid sites, leading to the deactivation. The strong acidity and small steric capacity of 8-MR may cause the rapid deactivation of the acid sites because plugging by polymerized species occurs easily in the small pore. The stable activity on the 7% NH_4Na-mordenite observed in the present study suggests a possible way of modifying the catalyst life.

References and Notes

1. M. Niwa, N. Katada, M. Sawa and Y. Murakami, *J. Phys. Chem.,* **99**, 8812 (1995).
2. N. Katada, H. Igi, J.H. Kim and M. Niwa, *J. Phys. Chem.* B, **101**, 5969 (1997).
3. N. Katada, Y. Kageyama and M. Niwa, *J. Phys. Chem.* B, **104**, 7561 (2000).
4. N. Katada, T. Takeguchi, T. Suzuki, T. Fukushima, K. Inagaki, S. Tokunaga, H. Shimada, K. Sato, Y. Oumi, T. Sano, K. Segawa, K. Nakai, H. Shouji, P. Wu, T. Tatsumi, T. Komatsu, T. Masuda, K. Domen, E. Yoda, J. N. Kondo, T. Okuhara, Y. Kageyama, M. Niwa, M. Ogura, M. Matsutaka, E. Kikuchi, N. Okazaki, M. Takahashi, A. Toda, S. Tawada, Y. Kubota, Y. Sugi, Y. Higashio, M. Kamada, Y. Kioka, K. Yamamoto, T. Shouji, Y Arima, Y. Okamoto and H. Matsumoto, *Appl. Catal. A: Gen*., **283**, 63 (2005).
5. J. Sauer, P. Ugliengo, E. Garrone and V.R. Saunders, *Chem. Rev.,* **94**, 2095 (1994).
6. A. Simperler, R.G. Bell, M.D. Foster, A.E. Gray, D.W. Lewis and M.W. Anderson, *J. Phys. Chem.* B, **108**, 7152 (2004).
7. M. Elanany, M. Kotama, M. Kubo, P. Selvam and A. Miyamoto, *Micropor.. Mesopor. Mater.,* **71**, 51 (2004).
8. A. Alberti, P. Davoli and G. Vezzalini, *Z. Kristallogr*, **175**, 249 (1986).
9. A. Alberti, *Zeolites*, **19**, 411 (1997).
10. V.L. Zholobenko, M.A. Makarova and J. Dwyer, *J. Phys. Chem*., **97**, 5962 (1993).
11. J. Datka, B. Gil and A. Kubacka, *Zeolites*, **17**, 428 (1996).
12. F. Wakabayashi, J. Kondo, A. Wada, K. Domen and C. Hirose, *J. Phys. Chem.,* **97**, 10761 (1993).
13. F. Geobaldo, C. Lamberti, G. Ricchiardi, S. Bordiga, A. Zecchina, G.T. Palomino and C.O. Arean, *J. Phys. Chem.,* **99**, 11167 (1995).
14. O. Marie, P. Massiani, F.T. Starzyk, *J. Phys. Chem.* B, **108**, 5073 (2004).
15. M. Niwa, S. Nishikawa and N. Katada, *Micropor. Mesopor. Mater.,* **82**, 105 (2005).
16. W. Kohn and L.J. Sham, *J. Phys. Rev.* A, **140**, 1133 (1965).
17. B. Delly, *J. Chem. Phys.,* **113**, 7756 (2000).
18. S.H. Vosko, L. Wilk and M. Nusair, *Can. J. Phys.*, **58**, 1200 (1980).
19. M. Sawa, M. Niwa and Y. Murakami, *Zeolites,* **10**, 307 (1990).
20. A. Zecchina, L. Marchese, S. Bordiga, C. Paze and E. Gianotti, *J. Phys. Chem.* B, **101**, 10128 (1997).
21. J. Datka, B. Gil and A. Kubacka, *Zeolites*, **15**, 501 (1995).
22. D.B. Lukyanov, T. Vazhnova, J.L. Cascib and J.J. Birtill, 13th International Congress on Catalysis, Paris, P1-457 (2004).
23. P. Jacobs, *Catal. Rev. Sci. Eng*., **24**, 415 (1982).
24. M. Kato, K. Itabashi, A. Matsumoto and K. Tsutsumi, *J. Phys. Chem.* B, **107**, 1788 (2003).

2-2. Identification and Measurements of Strong Brønsted Acid Site in Ultrastable Y (USY) Zeolite

Synopsis

By using the IRMS-TPD method in which IR (infrared) and MS (mass spectroscopy) worked together, acid sites of USY (ultrastable Y) zeolite were studied. A new band of OH playing a role of Brønsted acid was clearly detected on Na_2H_2-ethylenediaminetetraacetic acid (EDTA)-treated USY at 3595 cm^{-1} during an elevation in temperature after the adsorption of ammonia. MS-measured TPD (temperature-programmed desorption) of NH_3 and IR-measured TPD of the NH_4^+ cation coincided well to show that this zeolite consisted of the Brønsted acid sites. The MS-TPD profile at higher temperatures corresponded to the IR-TPD of the 3595-cm^{-1} band, and therefore, this OH was identified as a strong acid site. From comparison between IR-TPD of OH and MS-TPD, numbers of three kinds of Brønsted OH (*i.e.*, those in super and sodalite cages of a Y zeolite structure) and created strong Brønsted acid site were quantified. On the other hand, strength of the Brønsted acid site ΔH was determined individually by a simulation method, where the corrected IR-TPD of OH was simulated based on the proposed equation. Thus, a new strong Brønsted acid site was identified in the EDTA-treated USY, and the amount and strength was measured quantitatively.

Introduction

USY zeolite is a catalyst used for catalytic cracking in the petroleum refinery process, and industrially very important. This catalyst is prepared from ammonium Y zeolite by steaming at a high temperature above 773 K. Aluminum cations are dislodged from the framework of Y zeolite; not only the activity of catalytic cracking is created, but also the structure of Y zeolite is stabilized. Because of the potential importance of the USY in the industry, many kinds of studies have been performed so far, as reviewed in the literature[1-3].

The activity of parent HY zeolite for catalytic cracking of alkanes is very small, but the USY thus prepared has high catalytic properties[4,5]. It has been previously reported that the creation of active sites and mesopores due to the steaming process could enhance the catalytic activity. However, the complex profile of the USY makes it difficult to completely identify the nature of USY and its contribution to high catalytic activity. During the steaming, aluminum cations in the framework of zeolite are dislodged, and then stabilized as the extraframework aluminum (Al_{EF}). Although some of them are removed from the USY, the remaining Al_{EF} seemed to have an important role in the catalytic activity. Much effort has been already made in order to identify the active acid sites by using IR[6-8] and NMR[9,10] techniques; however, these studies were performed only qualitatively. To develop a more active catalyst, the structure of USY as well as the catalytically active site must be fully clarified. We have clarified[5] that the acid site due to Al in the FAU framework of HY zeolite is weak and its activity for octane cracking was negligible. The acid strength was enhanced by steaming, but there were both Brønsted and Lewis acid sites on USY zeolite after steaming. The catalytic activity of USY was enhanced by the treatment by using an ethylenediaminetetraacetic acid (EDTA)

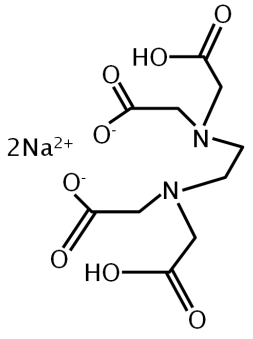

Scheme 2-2-1. Na_2H_2-EDTA

reagent, *e.g.*, Na_2H_2-EDTA (Scheme 2-2-1). Characterization of the catalyst revealed that, after the EDTA treatment, the distribution of Al changed, the acid sites became predominantly Brønsted type, and the acid strength was obviously higher than that on the HY and comparable to that on HZSM-5. The EDTA treatment is considered to thus create the high activity of octane cracking. This catalyst is studied in the present investigation in detail because the concentration of active sites is so high that it is easy to study the structure.

As shown in the previous section, we have performed the close analysis of Brønsted acidity of mordenite by using the IRMS-TPD method[11-13]. In this method, IR and MS work together in order to follow the thermal behavior of ammonia adsorbed and desorbed, respectively. Not only the amount and strength of acid sites, but also their structure, is studied simultaneously. The nature of the Brønsted acidity can be studied in detail because changes of OH bands could be correlated with those of the NH_4^+ band, and from the observation, the distribution of Brønsted acid sites can be studied.

IR measurements of ammonia adsorbed on zeolites during the programmed elevation of temperature have been reported previously[14-16]. In particular, an investigation by IR-TPD on a USY that contains a large amount of extraframework has been carried out[15]. In these studies, the IR bands of NH_4^+ and OH were studied qualitatively or quantitatively to characterize the acidity. On the other hand, the present study was carried out to measure the thermal behavior of adsorbed species of ammonia as well as its correlation with the desorbed ammonia. Therefore, we will get an insight into the nature of acid sites on zeolites precisely. Furthermore, this method allows us to study the structure of Brønsted acid sites in detail because IR bands of NH_4^+ and OH are measured together, and the correlation of these IR bands is precisely examined. In this subchapter, the Brønsted acid site in the EDTA-treated USY is studied by using this method, and evidence of the really important active Brønsted acid site is revealed. The number and strength of the sites are measured quantitatively.

Experimental Section

EDTA-treated USY Zeolite

An ammonium Y zeolite was prepared from a sodium Y (Si/Al_2, 5.1, kindly supplied by Catalysts and Chemicals Ind., Co. Ltd.), as described previously[17], and steamed at 823 K for 1 h in a mixture of 40 mol % of water vapor and nitrogen. The obtained USY (3 g) was stirred in an aqueous solution of Na_2H_2-EDTA (0.1 mol dm^{-3}) under refluxing, followed by cooling, filtration, washing with 1 dm^3 of water, ion-exchange in an ammonium nitrate solution, filtration, washing again with 1 dm^3 of water, and drying at 373 K for 10 h in atmosphere. The zeolite sample was the same one as used previously[5] and named 2E-U823, meaning the USY steamed at 823 K, followed by the treatment with Na_2H_2-EDTA. Details of the characterization data were listed in ref 5.

IRMS-TPD of Ammonia

IR (Perkin-Elmer Spectrum-One) and MS (Pfeiffer QME200) were connected with a vacuum line kept at 25 Torr (1 Torr = 0.133 kPa) to which Helium was allowed to flow as the carrier (flow rate, 125 ml min^{-1}) at the standard conditions. The carrier gas was fed in the rapid flow rate, which was 100 times faster than before (vide infra). An IR beam was transmitted to the self-compressed disk (about 8 mg and 10 mm in diameter). After

evacuation of the sample at 773 K, IR spectra were recorded before the ammonia adsorption at every 10 K from 373 to 773 K during the elevation of temperature in a ramp rate of 10 K min^{-1} (*N(T)*, recorded). The bed temperature was then lowered to 373 K, where ammonia was adsorbed at 100 Torr, and then gas-phase ammonia was evacuated for 30 min. IR spectra were measured again at every 10 K from 373 to 773 K during the elevation of temperature (*A(T)*, recorded). The difference spectrum, *i.e.*, *A(T)* - *N(T)*, was calculated at each temperature, from which changes of IR absorptions were observed to identify the absorptions of NH_4^+ and NH_3 adsorbed on the surface. Changes of hydroxyl bands were also detected in the difference spectra as negative peaks. A differential change of difference spectra with respect to temperature, *i.e.,* $-d\{A(T) - N(T)\}/dT$, was calculated at the selected band positions (hereafter, called IR-TPD). In the present study, the area of IR absorption was quantified in the range of absorption. The IR-TPD was compared with the MS-measured TPD of ammonia (m/e, 16) to identify the nature of adsorption site for the desorbed ammonia, Lewis, or Brønsted acid site.

Results

Conditions for Measurement of IRMS-TPD

We have previously studied the profile of ammonia TPD on zeolites and concluded that it was measured under the conditions of equilibrium between ammonia molecules adsorbed on the surface and mixed in the carrier gas[18]. A theoretical equation of TPD (described in Chapter 2-1) was derived on the basis of the conditions, and ΔH enthalpy change by ammonia adsorption could be determined as the strength of acid sites, as mentioned above. However, a rapid flow rate of helium carrier gas was selected in the present experiment because the experimental apparatus was complex, and at usual conditions that were previously selected, a portion of ammonia gas arrived at the MS detector as a tail-like broad desorption. Therefore, the experimental conditions for the IRMS-TPD were examined in order to know whether the equilibrium was achieved or not.

Figure 2-2-1 (a) shows plots of peak temperature of ammonia desorption against the experimental conditions *W/F* (*W*, weight of sample; *F*, flow rate of carrier). The temperature shifted to high with increase of the *W/F, i.e.*, contact time of the carrier gas with the sample. From these data, a theoretical relationship due to theoretical equation of TPD was examined in Figure 2-2-1 (b). A linear relationship should be observed for the plots when the equilibrium between ammonia molecules was fully achieved. However, the linear relation was observed only partly and not realized at the conditions of 120 ml min^{-1} of the flow rate and 25 Torr inside the cell. Actually, these conditions were selected in the present study because the rapid flow rate was necessary. Therefore, it was found that the equilibrium between ammonia molecules was achieved incompletely under the present experimental conditions.

ΔH 128 kJ mol^{-1} was determined from the linear portion in Figure 2-2-1 (b); this was in agreement with the value we have previously reported on this zeolite by using the conventional ammonia TPD (126 kJ mol^{-1}, for h_2-peak)[5]. ΔS consists of ΔS upon desorption of ammonia and ΔS upon physical mixing of ammonia with a carrier gas. ΔS upon desorption of ammonia under the equilibrium conditions was previously determined as a parameter required for determination of ΔH from the TPD experiment. However, the thus-determined parameter of ΔS was not appropriate because of the incomplete equilibrium conditions. ΔS 51 J K^{-1} mol^{-1} was, therefore,

calculated under the present conditions and used in a following measurement. This value is in reasonable agreement with the value obtained in the previous section (47 J K^{-1} mol^{-1}).

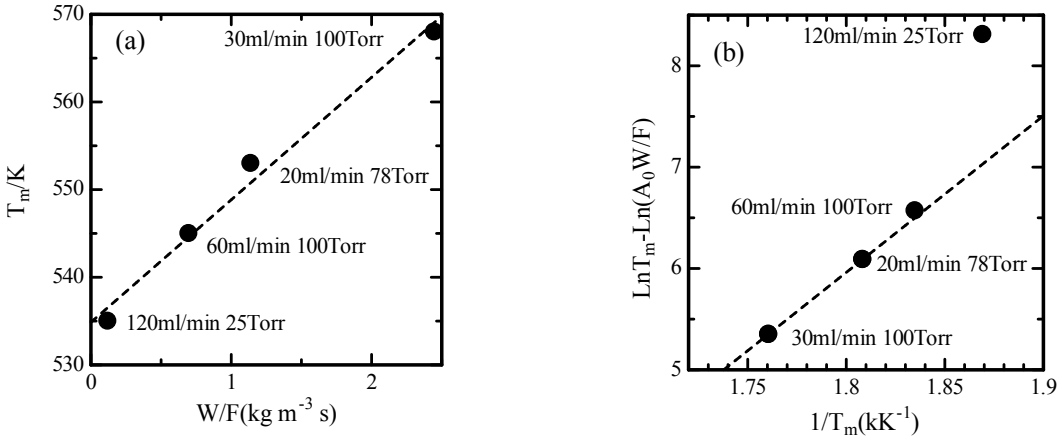

Figure 2-2-1. (a) Plots of peak temperature of desorbed ammonia against *W/F* and (b) the derived plots due to theoretical equation of TPD (described in chapter 2-1).

Effect of Measurement Temperature on Frequency of OH Stretching Vibration

As mentioned below, a shift of the OH band was observed with increasing the measurement temperature. Preceding the measurements, the temperature effect of the OH band was examined by using NH_4Y zeolite, *i.e., in situ* prepared HY zeolite, without adsorption of ammonia. The band of OH changed reversibly with increasing and decreasing the temperature, as shown in Figure 2-2-2. It was deduced into a following differential equation, which was used for correction of IR bands, where Δv and ΔT denoted changes in wave number and temperature, respectively.

$$\Delta v/\Delta T = -0.034 \text{ cm}^{-1} \text{ K}^{-1} \qquad (1)$$

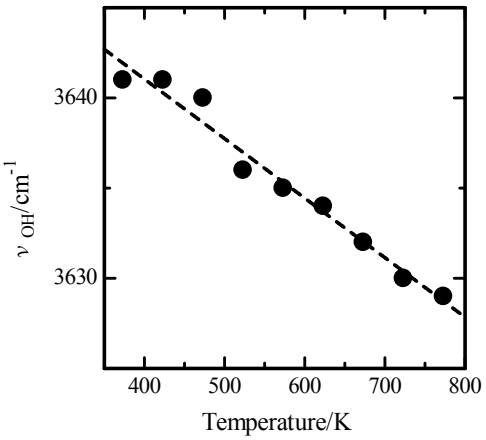

Figure 2-2-2. Change of the frequency of OH on NH_4Y with increasing of the temperature for measurement.

Detection of Strong Brønsted Acid Site in EDTA-treated USY

Figure 2-2-3 shows the difference spectra of adsorbed ammonia, which were measured at temperatures from 373 to 773 K in the TPD experiment. The largest intensity of difference spectra was observed at 373 K due to adsorbed ammonia, and it decreased gradually with increasing the temperature. The difference spectra became invisible at *ca.* 773 K because all the adsorbed ammonia was desorbed.

A sharp absorption at 1432 cm^{-1}, ascribable to the bending vibration of NH_4^+, was observed clearly. Furthermore, a small absorption was observed at 1665 cm^{-1}, and this band was identified as NH_3 weakly adsorbed.

NH stretching vibration also appeared at the broad region of 3400-2500 cm^{-1}. A reference spectrum measured at 373 K showed two OH bands at 3623 and 3550 cm^{-1}, which were identified as hydroxyls in the super and sodalite cages of the Y zeolite, respectively. Upon adsorption of ammonia, these OH bands almost disappeared; however, OH remained at 3600 cm^{-1} after the adsorption of ammonia, as shown in Figure 2-2-3. This means the presence of the hydroxyl band without the acidity or without the accessibility to ammonia.

During the TPD experiment, intensities of the OH bands were recovered gradually, as shown in Figure 2-2-4. Simultaneously, there was a small position shift to the low wave number (Figure 2-2-4 (a)). However, the shift of wave number was not observable after the wave number was corrected into that of 373 K by using eq (3) (Figure 2-2-4 (b)). Therefore, the shift of band with increasing the temperature was only due to a temperature effect on the band position.

At high temperatures, a new negative band was noticeable at 3595 cm^{-1} in the region of the broad OH band, as shown in Figure 2-2-4 (b). The detected OH band at 3595 cm^{-1} was neither observed in the unmodified HY zeolite nor in the USY zeolite (IR absorption band of HY zeolite assigned the OH stretching vibration is shown in next subchapter). This OH band was hardly detected in the reference spectrum of the EDTA-treated USY, but was easily detectable during the elevation of temperature. Therefore, this band is created on the USY zeolite, and its intensity seems to be enhanced by the treatment with the EDTA reagent. In addition, two other small bands were observed at 3603 and 3666 cm^{-1}. In this study, the shoulder band at 3603 cm^{-1} was identified as one of the created strong OH bands and treated as an additional band to the strong acid site. On the other hand, the small one at 3666 cm^{-1} was regarded as Al-OH in the extraframework and disregarded in the following measurement of Brønsted acidity.

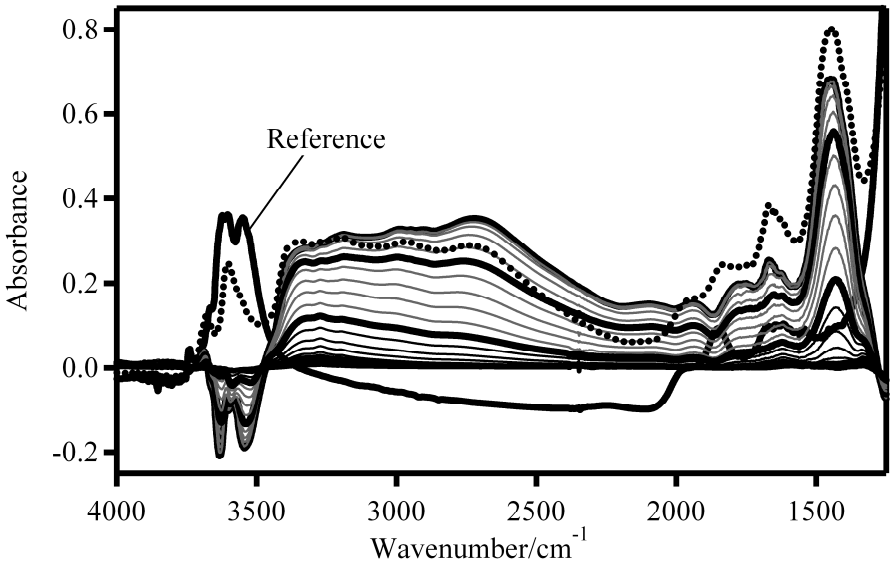

Figure 2-2-3. Difference spectra measured on Na_2H_2EDTA-treated USY with adsorbed ammonia during the elevation of temperature from 373 to 773 K. Spectra were taken every 10 K, but shown at every 20 K; bold lines show the spectra measured at 373, 473 and 573 K. Spectra of the OH bands before (solid line, marked reference) and after (dotted line) the ammonia adsorption at 373 K are shown for a comparison.

Thus, at least four kinds of OH bands were observable in difference spectra of Figure 2-2-4 (b). For quantification, OH bands of which intensity decreased by adsorption of ammonia were divided into four kinds of OH by using Gaussian distribution functions, as shown in Figure 2-2-5 (a) and (b) for difference spectra of OH measured at 373 and 523 K, respectively. The simulated spectrum, which was a sum of band intensities, agreed well with the experimentally observed difference spectrum of OH. It should be noted that only the hydroxyls on which ammonia was adsorbed was measured in the present experiment.

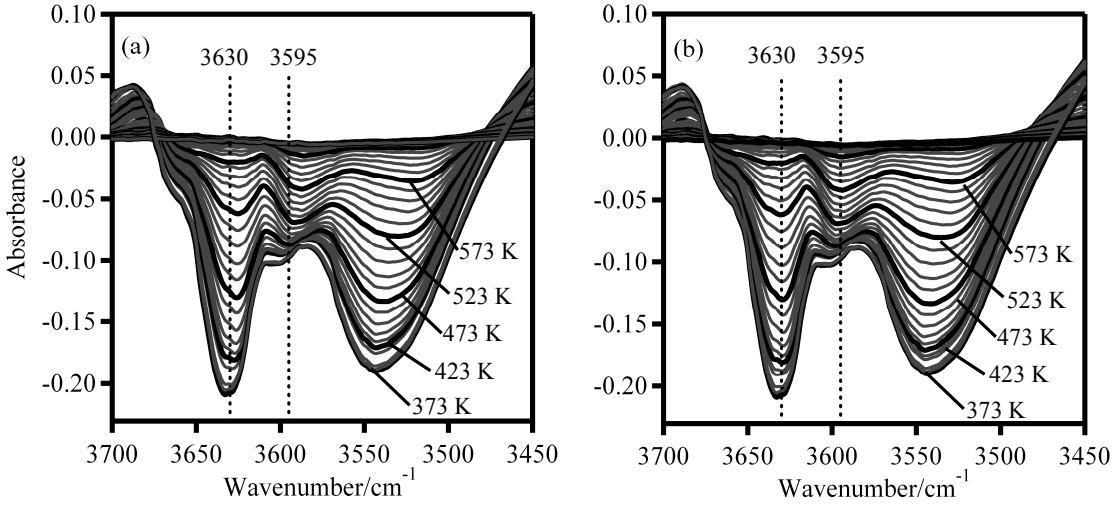

Figure 2-2-4. Magnified portion of OH band of Figure 2-2-3 (a), and the spectra after the wavenumber was corrected into that of 373 K by using eq (1) (b). Bold lines show the spectra measured at every 50 K from 373 to 573 K.

IRMS-TPD of Ammonia

IR-TPD profiles were then calculated for OH bands and adsorbed ammonia species, as shown in Figure 2-2-6; MS-measured TPD was also shown for a comparison. In the calculation of IR-TPD, the absorbance areas due to NH_4^+ and NH_3 at 1432 and 1665 cm^{-1}, respectively, were used for the quantification of adsorbed ammonia. On the other hand, the deconvolution of OH bands was made, as shown in Figure 2-2-5, and the area of the OH band was quantified.

MS-measured TPD of ammonia in Figure 2-2-6 was found to consist of two desorptions at *ca.* 430 and 520 K as so-called *l*- and *h*-peaks, respectively. Because the IR-TPD of NH_3 at 1665 cm^{-1} and of NH_4^+ at 1432 cm^{-1} showed their desorptions at these temperatures, respectively, two peaks, *i.e.*, *l*- and *h*-peaks, were found to be due to these adsorbed ammonia species, respectively. The *l*-peak was expected to be caused by ammonia species weakly adsorbed on the NH_4^+ cation. The suspect is thereby confirmed in the present study, and the species was identified to show the IR absorption band at 1665 cm^{-1}. On the other hand, the *h*-peak was identified as NH_3 desorbed from the Brønsted acid site.

The Brønsted OH bands should show a mirror-image correlation with that of NH_4^+. It was, therefore, found from Figure 2-2-6 that ammonia was desorbed at different temperatures from the OH species, *i.e.*, at *ca.* 480 K from OH in the super cage, at *ca.* 500 K from OH in the sodalite cage, and at *ca.* 580 K from OH in the newly created site. Thus, the distribution of Brønsted OH in the USY was clearly observed by utilization of the

IRMS-TPD technique. Figure 2-2-6 provides us evidence to show the OH band at 3595 cm^{-1} as the strong Brønsted acid site.

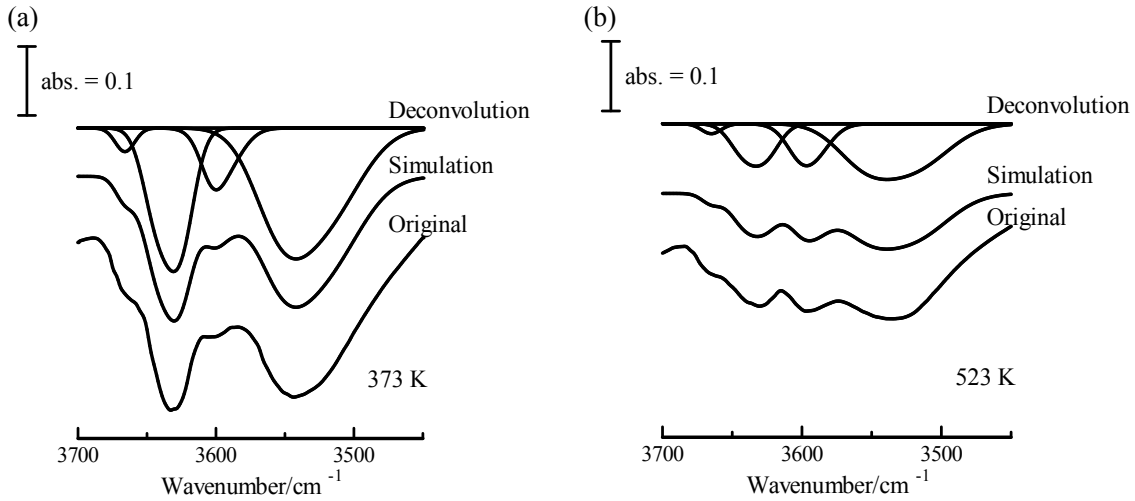

Figure 2-2-5. Deconvolution of OH bands measured 373 (a) and 523 K (b) into four components. Sum of them (simulation) was fitted well to the original drawn OH band in the difference spectrum. The wave number in (b) was corrected into that 373 K by using eq (1).

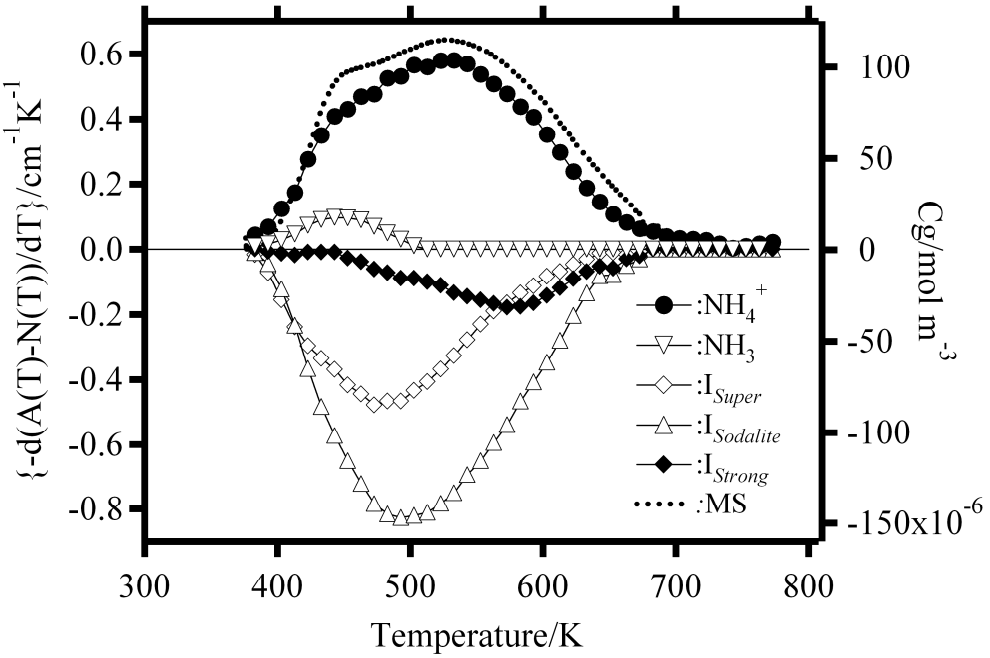

Figure 2-2-6. IR-TPD of NH_4^+, NH_3 and hydroxyl bands in the super and sodalite cages, and in the strong acid sites at 3630, 3545 and 3595 cm^{-1}, respectively, with MS-TPD as a comparison.

Quantitative Measurements of the Brønsted Acid Site in Na_2H_2-EDTA treated USY

We measured acid sites quantitatively based on these experimental findings. The number and strength of the OH could be individually determined. First, parameters *a*, as defined by eq (2), were determined from the comparison of the IR-TPD of OH with MS-measured TPD of ammonia

$$I_0 = a_1 I_1 + a_2 I_2 + a_3 I_3 \qquad (2)$$

where I_1, I_2, and I_3 mean the intensity of IR-TPD of the OH band at super and sodalite cages and the strong acid site, respectively, and I_0 should agree with MS-TPD in size and shape. IR-TPD and MS-TPD have different units, but these are convertible because of the coincidence between IR-TPD of NH_4^+ and MS-TPD of NH_3 shown in Figure 2-2-6. The number of total Brønsted acid sites was calculated from the desorbed amount of NH_3, but a small portion of the *l*-peak was disregarded. The parameter a is a negative value and corresponds to the reciprocal of an extinction coefficient of the OH band. In other words, a is a parameter to cancel the difference in extinction coefficients in IR bands. By taking parameters as a_1 = -0.53, a_2 = -0.2, and a_3 = -1.8, I_0 could be compared with MS-TPD, as shown in Figure 2-2-7. The ratio of reciprocals of the parameters, $1/a_1$ to $1/a_2$, is in agreement with that of reported extinction coefficients[19], 3.2 and 8.5 cm μmol^{-1} for OH in super and sodalite cages, respectively, thus supporting the validity of parameters selection. The number of the Brønsted hydroxyls was thus determined, as summarized in Table 2-2-1.

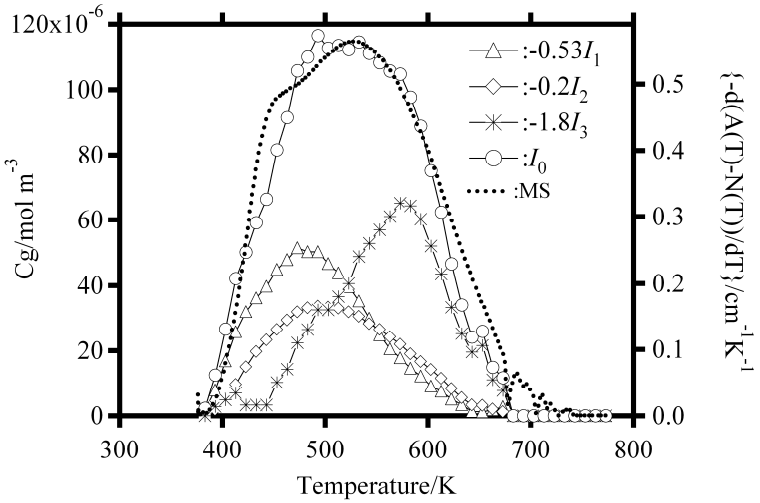

Figure 2-2-7. Corrected IR-TPD of three kinds of OH, sum of them (I_0), and MS-TPD of ammonia to measure the amounts of Brønsted OH.

In our previous paper[5], we identified that a portion of TPD of ammonia observed at *ca.* 600 K, named the h_2-peak, was responsible for the catalytic activity. However, the h_2-peak corresponds to the sum of amounts of three OH bands measured in the present study, and therefore, C_w in Table 1 is almost equal to the amount of h_2-peak previously reported (1.29-1.48 mol kg^{-1}).

On the other hand, ΔH was determined by a simulation method by using theoretical equation of TPD. Corrected IR-TPD ($a_n I_n$: n = 1, 2, and 3) was compared with simulated TPD profiles S_n with a parameter of ΔH, respectively, as shown in Figure 2-2-8. ΔH was thus determined by the simulation individually, as summarized in Table 2-2-l.

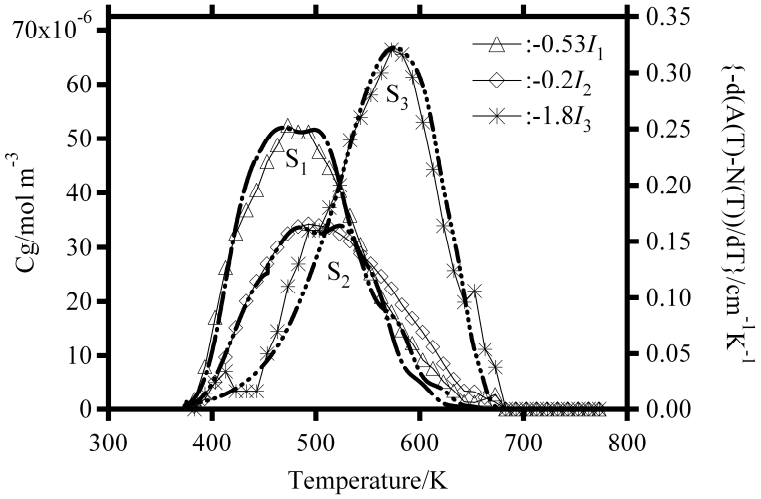

Figure 2-2-8. Comparison between corrected IR-TPD of OH ($a_n I_n$) and simulated one (S_n) based on theoretical equation of TPD.

Table 2-2-1. Strength (ΔH) and amount (A_0) of Brønsted hydroxyl bands in Na_2H_2EDTA-treated USY

		ν_{OH} / cm^{-1}	A_0 / mol kg^{-1}	ΔH / kJ mol^{-1}	C_w [a] / mol kg^{-1}	included element [b] / mol kg^{-1}	Al_F [c] / mol kg^{-1}
OH	in supercage	3635	0.39	116 (10) [d]			
	in sodalite cage	3540	0.27	122 (11)	1.1.3	Al, 5.01; Na, 0.26	2.2
	created	3595	0.47	137 (9)			

[a] Weight-based concentration of acid site, sum of A_0. [b] Concentrations of Al and Na measured by ICP. [c] Measured from ^{29}Si MAS NMR and XRD[5]. [d] Distribution parameter, *e.g.*, 116 ± 10.

The determined strength of the acid site ΔH 116 kJ mol^{-1} for OH in the super cage is similar to that of the unmodified HY zeolite (110 kJ mol^{-1}), as reported previously[17], and shows the unmodified property of the structural OH of Y zeolite. The value of 122 kJ mol^{-1} for the OH in the sodalite cage seems to indicate an enhanced strength of the site, although the reason is uncertain. On the other hand, ΔH 137 kJ mol^{-1} for the created Brønsted acid site is not observed in the usual HY, and the strength is as high as on an HZSM-5 zeolite (*ca.* 135 kJ mol^{-1} [18]). The Brønsted acid sites having this strength of an acid site, most probably, caused the high activity of the USY for the cracking of hydrocarbons. Thus, we identified the active and strong Brønsted acid sites in USY zeolite and determined their amount and strength quantitatively.

The extinction coefficient in the Lambert-Beer equation for the NH_4^+ bending vibration can be determined from the absorbance at 1432 cm^{-1} and the desorbed amount of NH_3 from the Brønsted acid sites (C_w in Table 2-2-1). This was 6.0 m^2 mol^{-1}, which was similar to that in β-zeolite (5.3-8.4 m^2 mol^{-1})[12], but smaller than those in mordenite reported (14.7 m^2 mol^{-1})[20] and measured by us (13.7 m^2 mol^{-1})[13]. It would imply a difference in the structure of the ammonium cation in zeolites

Discussion

Identification of Strong Brønsted Acid Site

Various IR studies have been already performed with a purpose of identification of the active acid sites in USY. Fritz and Lunsford detected a shoulder-like IR band at 3602 cm^{-1} on the dealuminated Y zeolite treated with $SiCl_4$ and found a strong relation between the band intensity and the catalytic activity of hexane cracking[7]. Although the intensity of the band is small and not clearly observable, the OH they detected seems to be similar or almost the same as the species detected here. Corma *et al.* also reported the appearance of the shoulder band at 3600 cm^{-1} in USY[6,21,22]. They reported a small band at 3525 cm^{-1} also, which had an acidic character. The enhanced strength of the OH band at 3525 cm^{-1} was observed also in the present study. However, its strength was lower than that of the band at 3595 cm^{-1}. Datka *et al*. also detected two strongly acidic OH at 3605 and 3525 cm^{-1} on the industrially available USY, which was prepared by steaming at 920 K, followed by EDTA treatment[23]. We also found the band at 3595 cm^{-1} as the active strong acid sites, which were similar to those previously reported. Difference in band positions by 5-10 cm^{-1} is, most probably, due to the shift of the band depending on the temperature because the wave number of OH detected in the present study was adjusted to that

observed at 373 K, and a small shift of the wave number was included.

Therefore, the OH band at 3595 cm^{-1} is clearly confirmed to be a species with the strong enough acidity to play the active site for catalytic cracking. By utilizing the unique property of IRMS-TPD, the profile of the OH was made clear in more detail than those previously reported, and therefore, a quantitative measurement was possible. The treatment with Na_2H_2-EDTA reagent also is a possible reason to make the detection possible because the strong Brønsted acidity was enhanced by changing the distribution of Al. The presence of a strong Brønsted acid site has been proposed to explain the high cracking activity of USY, but is not completely identified yet. Other models for the high catalytic activity were, therefore, discussed[24], for example, a participation of Lewis acid sites to the reaction or creations of mesopores in USY. The present study, however, adds a strong support for the presence of a strong Brønsted acid site.

The band position of 3595 cm^{-1} may imply the *ca.* 30 cm^{-1} shift toward a lower frequency of the OH band in the super cage (3628 cm^{-1}), as suggested previously[21,23]. Therefore, the strong Brønsted acid site maybe locates in the super cage.

Determination of Aluminum in EDTA-treated USY as Estimated from the Quantitative Measurements

NH_4Y contained 4.9 mol kg^{-1} of Al in the zeolite framework, and after the steaming, 2.0 mol kg^{-1} of Al remained in the framework. The treatment by Na_2H_2-EDTA increased a small amount of the framework Al and may be due to reinsertion of Al in the framework. The reinsertion in a basic medium has been reported[25]. It should be noted that the treatment by Na_2H_2-EDTA did not decrease the aluminum content in USY, but only changed the distribution of Al. ^{27}Al NMR showed that alumina-like species was removed after the treatment by Na_2H_2-EDTA, although the total content of Al showed a small decreased[5]. Approximately 0.7 mol kg^{-1} of Al_F (Al in the framework tetrahedral position), therefore, remains uncounted from concentrations of Al_F, Na, and C_w in Table 2-2-1. As pointed out previously[5], the active site for cracking in USY consists of an extraframework Al (Al_{EF}) close to the framework Al, *i.e.*, a pair of two aluminums. Some cluster or cation containing the Al_{EF}, *e.g.*, $Al^+(OH)O^-$, $Al(OH)^{2+}$, or $Al^-(OH)^3$, has the electron withdrawing property and interacts with the Brønsted acid site, thus lengthening the OH bond to shift the IR band and enhancing the acidity. Al_{EF} (0.45 mol kg^{-1}) is therefore used for the strong acid site at 3595 cm^{-1}; thus, *ca.* 2 mol kg^{-1} Al_{EF} remains uncounted.

In the previous investigation on USY with a large amount of extraframework Al, an absorption band at 1296-1306 cm^{-1} was identified as NH_3 strongly adsorbed on the Lewis acid site[15]. However, the EDTA-treated USY does not have alumina-like species because the octahedral Al was not observed in the MAS NMR of ^{27}Al[5]. This was in agreement with a study by Gola *et al.*[26] and, further, was precisely confirmed in our recent study by using MAS and MQMAS NMR at 16 T because Al with the octahedral configuration was not detected[27]. Figure 2-2-9 shows ^{27}Al MQMAS spectra of NaY (a), USY (b) and Na_2H_2-EDTA-treated USY (c). ^{27}Al MQMAS NMR spectra of parent NaY shows a narrow peak assigned to the framework tetra-coordinated Al species (IV). On the other hand, in the spectra of USY, multiple signals assigned to the extraframework tetra- (IV_b), penta- (V) and hexa- (VI) coordinated Al species were observed. As shown in Figure 2-2-9 (c), the NMR spectra of USY were drastically changed by means of Na_2H_2-EDTA treatment, and the V and VI species were almost completely disappeared. Therefore, the large portion of Al_{EF} still remains in the zeolite as a highly dispersed tetra-coordinated extraframework Al species. Maybe a portion of Al_{EF} and Al_F contributes to the formation of an

unidentified OH band at 3600 cm^{-1}, which remained after the adsorption of ammonia. When the site is located in the sodalite cage, its interaction with the ammonia molecule may be difficult. Because of the complex property of USY zeolite, no quantitative study on the strong acid site using spectroscopy has been reported so far. Exceptionally, a previous study with ^{31}P MAS NMR using trimethylphosphine oxide identified the strong acid site at 63 ppm and quantified it at *ca.* 0.3 mol kg^{-1}, which was a portion of 0.68 mol kg^{-1} of the total Brønsted acid sites[28]. These values correspond to 0.45 and 1.2 mol kg^{-1} in the present study, respectively. Concentration of strong Brønsted acid sites is higher in the present study, which suggests the effective treatment by Na_2H_2-EDTA. Catalytic activity for hydrocarbon cracking will be analyzed by using these characterized parameters.

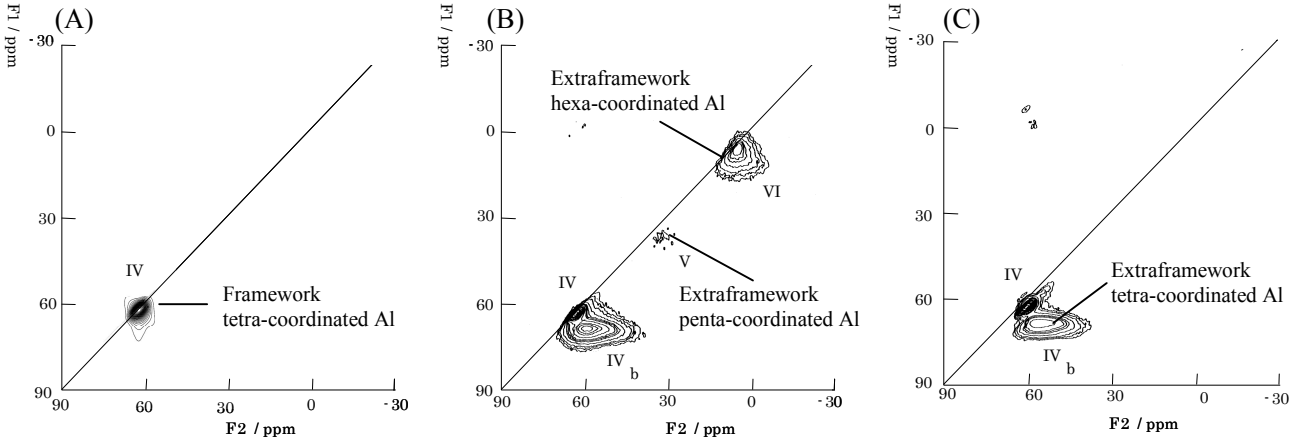

Figure 2-2-9. ^{27}Al MQMAS NMR spactra (16 T) of NaY (A), USY (B) and Na_2H_2-EDTA-treated USY (C)[27]. Reproduced from ref. 27.

Conclusion

By using an advanced new technique of IRMS-TPD, we made a clear investigation on the USY zeolite to identify and measure the strong acid site.

1. EDTA-treated USY zeolite has a strong Brønsted acid site, which is detected at 3595 cm^{-1} of the IR band at the measurement temperature of 373 K.

2. Number and strength of the strong acid site are measured to be 0.47 mol kg^{-1} and 137 kJ mol^{-1}, respectively.

The structural, thermodynamic and spectral properties of Brønsted acid site in USY will be additionally discussed in Chapter 5.

References and notes

1. J.H. Lunsford, In Fluid Catalytic Cracking II: Concepts in Catalyst Design; Occelli, M. L., Ed.; American Chemical Society: Washington, DC, p 1 (1991).
2. R.A. Beyerlein, C,-C. Feng, J.B. Hall, B.J. Huggins and G.J. Ray, *Top. Catal.*, **4**, 27 (1997).
3. B.A. Williams, S.M. Babitz, J.T. Miller, R.Q. and H.H. Kung, *Appl. Catal.,* A, **177**, 161 (1999).
4. S.J. DeCanio, J.R. Sohn, P.O. Fritz and J.H. Lunsford, *J. Catal.*, **101**, 132 (1986).
5. N. Katada, Y. Kagetama, K. Takahara, T. Kanai, H.A. Begum and M. Niwa, *J. Mol. Catal.,* A, **211**, 119 (2004).

6. A. Garralon, A. Corma and V. Formes, *Zeolites,* **9**, 84 (1989).
7. P.O. Fritz and J.H. Lunsford, *J. Catal*., **118**, 85 (1989).
8. O. Cairon, T. Chevreau and J.-C. Lavalley, *J. Phys. Soc. Taraday Trans*., **94**, 3039 (1998).
9. J.H. Lunsford, P.N. Tutunjian, P.-J. Chu, E.B. Yeh and D. Zalewski, *J. Phys. Chem.*, **93**, 2590 (1989).
10. J.A. van Bokhoven, A.K. Roset, D.C. Koningsberger, J.T. Miller, G.H. Nachtegaal, A.P.M. Kentgens, *J. Phys. Chem*. B, **104**, 6743 (2000).
11. K. Suzuki, N. Katada and M. Niwa, *Chem. Lett.*, **34**, 398 (2005).
12. M. Niwa, S. Nishikawa and N. Katada, *Micropor. Mesopor. Mater.,* **82**, 105 (2005).
13. M. Niwa, K. Suzuki, N. Katada, T. Kanougi and T. Atoguchi, *J. Phys. Chem.* B, **109**, 18749 (2005).
14. X. Zhiyuan, Z. Leiming, L. Quanzhi, Z. Ruiming, *Stud. Surf. Sci. Catal*., **49**, 651 (1989).
15. H. Miessner, H. Kosslick, U. Lohse, B. Parlitz, V.-A. Tuan, *J. Phys. Chem*., **97**, 9741 (1993).
16. A. Trunschke and B. Hunger, *Top. Catal*., **3-4**, 215 (2002).
17. N. Katada, Y. Kageyama and M. Niwa, *J. Phys. Chem.* B, **104**, 7561 (2000).
18. M. Niwa, N. Katada, M. Sawa and Y. Murakami, *J. Phys. Chem*., **99**, 8812 (1995).
19. M.A. Makarova, A.F. Ojo, K. Karim, M. Hunger and J. Dwyer, *J. Phys. Chem.,* **98**, 3619 (1994).
20. J. Datka, B. Gil and A. Kubacka, *Zeolites*, **15**, 501 (1995).
21. A. Corma, V. Fornes and F. Rey, *Appl. Catal.,* **59**, 267 (1990).
22. A. Corma, A. Martinez and C. Martinez, *Appl. Catal.* A*,* **134**, 169 (1996).
23. J. Datka, B. Gil, J. Zlamanied, P. Batamack, J. Fraissard and P. Massiani, *Pol. J. Cham*., **73**, 1535 (1999).
24. H.H. Kung, B.A. Williams, S.M. Babitz, J.T. Miller and R.Q. Snurr, *Catal. Today,* **91**. 52 (1999).
25. D.-S. Liu, S.-L. Bao and Q.-H. Xu, *Zeolites*, **18**, 162 (1997).
26. A. Gola, B. Rebours, E. Milazzo, J. Lynch, E. Benazzi, S. Lacombe, L. Delevoye and C. Fernandez, *Micropor. Mesopor. Mater.,* **40**, 73 (2000).
27. N. Katada, S. Nakata, S. Kato, K. Kanehashi, K. Saito and M. Niwa, *J. Mol. Catal.* A, **236**, 239 (2005).
28. K.J. Sutovich, A.W. Peters, E.F. Rakiewics, R.F. Wormsbecher, S.M. Mattingly and K.T. Mueller, *J. Catal*., **183**, 155 (1999).

2-3. Detection and Quantitative Measurements of Four Kinds of OH in HY Zeolite

Synopsis

Acidity of *in situ* prepared HNaY zeolite was studied by a method of infrared mass spectrometry/temperature-programmed desorption (IRMS-TPD) of ammonia. Two kinds of energetically different acid sites were detected in the TPD experiment. Adsorption of ammonia on the HNaY revealed the IR bending vibration bands at *ca.* 1430 and 1665 cm^{-1}, and these bands corresponded to ammonia molecules desorbed at high and low temperatures, respectively. By using the IR-TPD, four kinds of OH bands were detected, although the evacuated HY showed usually only two OH bands. Two OHs in the super cage and two in the sodalite cage and hexagonal prism were identified. From the comparison of IR-TPD of adsorbed ammonia and OH, it was found that the NH_4^+ cation was formed on three of four OHs located in super and sodalite cages. An interaction of ammonia on the OH located in the hexagonal prism was, however, different. By using a curve fitting method, the number of these OHs as the acid site was quantified, and the strength was measured on the basis of the theoretical equation on in situ prepared HNaY with a 96% proton exchange degree. A dependence of the OH concentration on the exchange degree 14-96% was measured. Extinction coefficients of OH stretching vibrations were also determined.

Introduction

Zeolites are aluminosilicate crystals and catalytically active due to the strong solid acidity. Among them, Y-zeolite is particularly important because it has been used in the petroleum refinery process. To fully understand the generation of the catalytically active sites in the Y-zeolite, the acidity and its dependence on the structure have to be studied in detail.

Y-type zeolite has only one kind of T (Si or Al) site. Four oxygens bond to the T-site in the tetrahedral configuration; therefore, four kinds of oxygen exist and four kinds of Brønsted acid site are structurally possible (O1 to O4), numbered as shown in Figure 2-3-1). It has been well-known that the evacuated HY zeolite shows two distinguishable OH IR bands at 3635 (high frequency, HF) and 3548 (low frequency, LF) cm^{-1}.[1] However, a recent study by Sarria *et al.* reported the presence of one more OH bands at the tail of the absorption (3501 cm^{-1})[2], and they identified it as O(3)H. Thus, three of four possible OH bands have been identified using IR spectroscopy. A study by neutron powder diffraction[3] reported the presence of O(1)H, O(2)H, and O(3)H

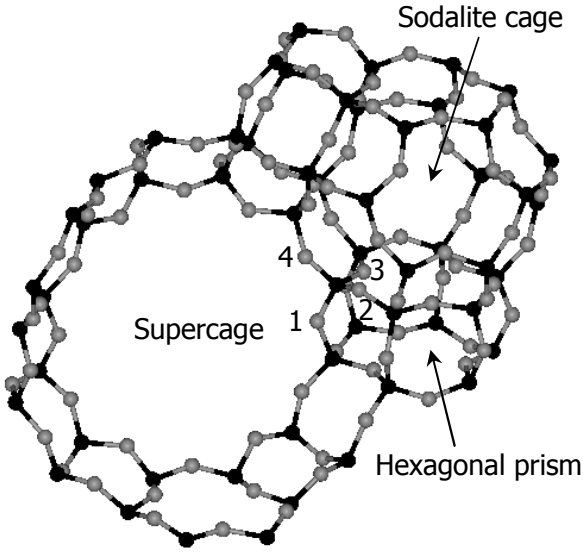

Figure 2-3-1. Position of four kinds of nonequivalent oxygen sites in the FAU-type framework structure. 1 ― 4 show the position of oxygen named O1 to O4.

located in the super cage, sodalite cage, and hexagonal prism, respectively, but did not detect O(4)H. To our knowledge, there is no experimental confirmation for the presence of the O(4)H. However, a theoretical study using DFT calculation concluded four kinds of Brønsted acid site were energetically possible[4-7].

By means of ammonia IRMS-TPD method[8-10], two kinds of Brønsted acid sites are found and the distribution depends on the structure of mordenite (Chapter 2-1). Such a precise study for dependence of the acid site on the structure of zeolite is important to understand the generation of the acid site in the zeolite. In particular, our interest is directed to understanding the dependence of acid site strength on the structure of zeolite. To arrive at the conclusion, Y-zeolite is a zeolite unavoidable to study because it is not only structurally simple as mentioned above, but the most important catalytic material[11-13].

Experimental Section

Materials

A NaY zeolite (Catalysts & Chemicals Ind. Co.; $Si/Al_2 = 5.1$) was put into a solution of NH_4NO_3 to exchange Na^+ with the NH_4^+ cation. To fully exchange with the NH_4^+ cation, an extremely high concentration of NH_4NO_3 (2.25 mol dm^{-3}) was used, and the molar ratio of NH_4^+ in the solution to Na^+ in zeolite was adjusted to 100. The ion exchange was performed three times[14]. The degree of ion exchange was measured by ICP after digestion in HF. Thus prepared NH_4-NaY (96%, NH_4^+) zeolite was used in the present study because the NH_4 type zeolite retains a clear structure of acid sites, and thereby it is less affected by the extra framework cations[14,15]. $NaNH_4Y$ zeolites with 14, 32, 44, and 77% of NH_4^+ exchange degrees were also prepared and used for the measurements. A reference catalyst HY zeolite supplied by the Catalysis Society of Japan, JRC-Z-HY5.3, was used without any treatment as an *ex situ* prepared sample.

IRMS-TPD of Ammonia

An IR spectrometer (Perkin-Elmer Spectrum-One) and a mass spectrometer (Pfeiffer Vacuum QME200), connected with a vacuum line, worked simultaneously, and adsorbed and desorbed ammonia probes were measured altogether. A self-supporting disk of zeolite (5-10 mg) was set in an *in situ* IR cell and evacuated at 773 K for 1 h prior to the measurement. IR spectra were then measured at every 10 K from 373 to 773 K during the elevation of temperature (ramp rate 10 K min^{-1}) in a flow of helium at 0.082 mmol s^{-1} and 25 Torr (1 Torr = 133.3 Pa) before the adsorption of ammonia. After the adsorption of ammonia at 373 K by admitting 100 Torr of ammonia into the cell, followed by evacuation, IR spectra were again measured during the TPD experiment in a flow of helium at 0.082 mmol s^{-1} and 25 Torr, and simultaneously, the mass spectrometer followed the change of concentration of desorbed ammonia in the gas phase at m/e = 16. A difference spectrum was calculated from the IR spectra before and after the ammonia adsorption at each temperature. The differential change of the calculated difference in intensity with respect to the temperature provides us the change of concentration of adsorbed ammonia species during the TPD experiment (hereafter called IR-TPD). It was observed on zeolites[9] that OH bands shifted to the low wave number with increasing the temperature; the wave number (ν) changed linearly with the temperature (T), i.e., $\Delta\nu/\Delta T = -0.034$ cm^{-1} K^{-1}, where $\Delta\nu$ and ΔT were changes of band position

and temperature. The OH band position was therefore corrected using this equation to the wave number observed at 373 K. Heat of ammonia adsorption (ΔH) as a parameter to show the strength of the Brønsted OH acid site was determined based on the theoretical equation previously derived by us for the ammonia TPD experiment[16], which was controlled by the equilibrium between ammonia molecules in the gas phase and adsorbed on the zeolite.

Results

Effect of the Water Vapor Treatment on the TPD Spectrum

The TPD of ammonia on an acidic zeolite usually shows two desorption peaks of ammonia in conventional conditions at such a high *W/F* (weight of sample/volumetric flow rate of carrier) ratio as 10 kg m^{-3} s. Among them, only the h-peak (high temperature peak) was ascribable to ammonia, which had been adsorbed directly on the acid site[17]. The *l*-peak (low temperature peak) was ascribable to ammonia weakly adsorbed on the NH_4^+ cation. Therefore, the *l*-peak should be removed to measure the acidity. This is especially important on Y-zeolite because the *l*-peak seriously overlaps the *h*-peak[18].

It has been known that a water vapor treatment after the adsorption of ammonia removes the *l*-peak[18]. After the treatment with water vapor, only ammonia adsorbed directly on the acid site was detected, from which the number of the acid site was precisely measured. In the present study, the effect of the water vapor treatment was measured using the IRMS-TPD equipment in the experimental conditions at a relatively low *W/F* ratio, 0.1 kg m^{-3} s, which had been adopted to observe the IR spectrum clearly.

Figure 2-3-2 shows MS-TPD on the NH_4Y (96% NH_4^+ exchanged) with and without the water vapor treatment; to clearly show the spectrum in a low-temperature region, the adsorption of ammonia and the water vapor treatment were carried out at 298 K and the TPD was measured from 298 K. Three desorption peaks of ammonia appeared at about 360 (shoulder), 450, and 530 K. The water vapor treatment decreased the intensity of desorption peak at 360 K only but did not affect two others. This means that the ammonia desorbed at 360 K was ascribable to the so-called *l*-peak, which was adsorbed so weakly and removable easily by the water vapor treatment. However, in contrast to the experiments at high *W/F* ratios, the *l*-peak in the present conditions was small even when the water vapor treatment was not carried out, probably because the ammonia weakly adsorbed on the NH_4^+ cation was removed by feeding the carrier gas at such a low *W/F* ratio.

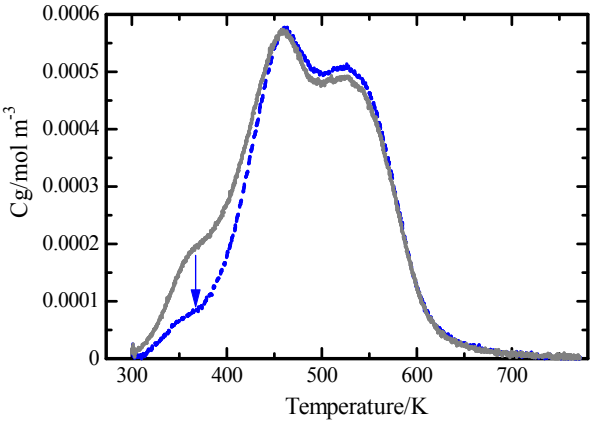

Figure 2-3-2. MS-TPD with (dotted line) and without (solid line) the water vapor treatment.

In other words, it was confirmed that the Y-zeolite possessed the two kinds of energetically different acid sites (450 and 530 K). Two latter desorptions of ammonia at 450 and 530 K will be studied in the present study. Because it was evidenced that the amount of weakly held ammonia was negligible, and in order to avoid possible

disturbance to IR spectrum by the presence of water, the water vapor treatment was not performed in the following experiments.

Assignment of Ammonia and OH Species Based on IR Spectrum on the 96 % NH_4Y

Figure 2-3-3 shows the difference spectra of ammonia on the $NaNH_4Y$ (96% NH_4^+/4% Na^+) measured at 373-773 K in the TPD experiment: a reference spectrum measured at 373 K before adsorption of ammonia was added for a comparison. Stretching vibration of ammonia was seen broadly at 3300-1800 cm^{-1}, and the bending vibration was noticeable at the region of 1700-1400 cm^{-1}.[19] The bending vibration of NH_4^+ appeared at 1430 cm^{-1}, and weak bands overlapped at the higher (1496 cm^{-1}) and lower (1369 cm^{-1}) wave numbers at the low temperatures from 450 to 550 K. All these bands are ascribable to asymmetric deformation of NH_4^+. It has been explained that this feature is generated by the difference in NH_4^+ symmetry resulting from different hydrogen bond with the neighboring oxygen atom[20,21]. In addition, a sharp band was observed at 1665 cm^{-1} and diminished at relatively low temperature. From the band position, it is ascribable to the symmetric deformation of NH_4^+ or asymmetric deformation of NH_3. On the other hand, a small band at 1320 cm^{-1} shows the presence of ammonia adsorbed on the dislodged Al[10] with Lewis acidity.

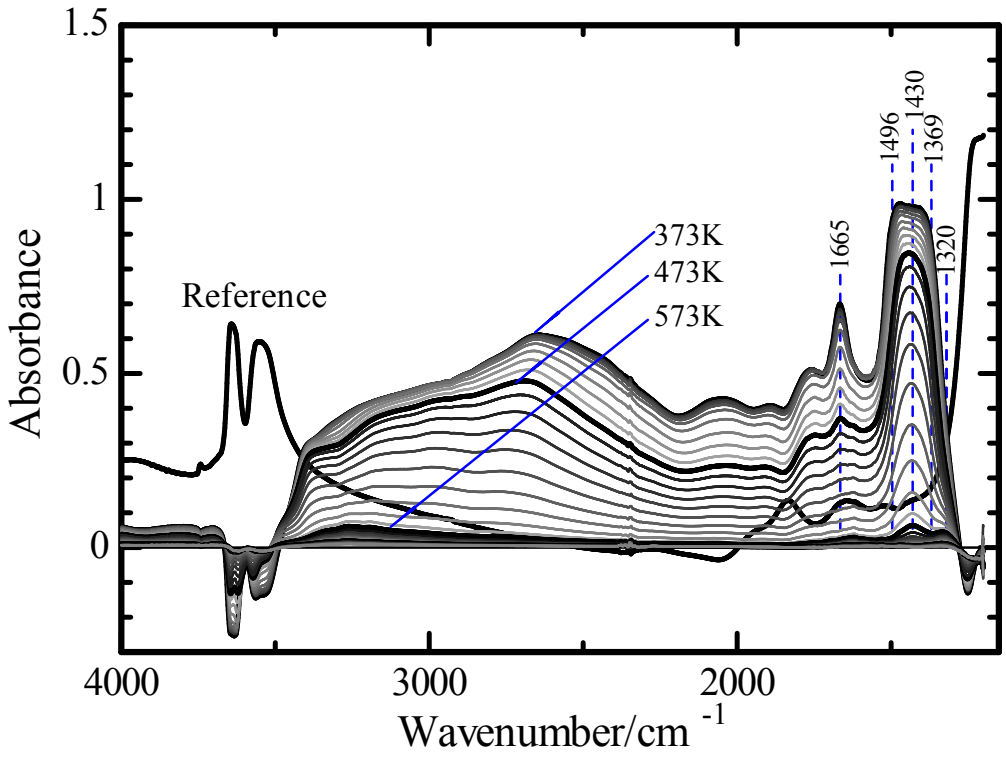

Figure 2-3-3. Difference spectra of adsorbed ammonia measured at the indicated temperatures during ammonia TPD on the NaNH4Y (96 %NH_4^+) reference spectrum measured at 373 K after the evacuation was shown as a comparison.

Figure 2-3-4 shows the enlarged difference spectra of OH bands at 3700-3450 cm^{-1} during the TPD. It should be noted that the band position was corrected to that observed at 373 K using a linear equation as mentioned

above. The reference spectrum (dotted line) shows two large bands at ca. 3640 and 3550 cm^{-1}, usually called HF and LF bands (high- and low-frequencybands), respectively. The former is attributed to O1H and/or O4H in a super cage, while the latter is attributed to O2H in a sodalite cage and/or a O3H in hexagonal prism. The decreased intensity of OH recovered gradually upon desorption of ammonia. Interestingly, four kinds of OH bands were clearly observable at 3648, 3625, 3571, and 3526 cm^{-1}. The overlapping two OH bands in the reference spectrum were therefore able to be divided furthermore into two OH groups, respectively, using the present technique of IR-TPD experiment. On the other hand, it is noteworthy that the difference spectrum in the OH stretching region seems to be disturbed by the generation of NH stretching vibration at below 3550 cm^{-1}.

Because the LF band consists of O2H and O3H and the O3H has been reported to appear at the lower wave number, 3526 cm^{-1},[2] the band at 3571 cm^{-1} is ascribable to O2H. As mentioned below, the OH band at 3648 cm^{-1} appeared preferentially by the exchange with NH_4^+ cation, and it is assigned to the most preferential site (most stable site), O1H. The band at 3625 cm^{-1} is ascribable either to the O1H with one or two aluminums in the nearest next neighbor site or to the O4H, as discussed below. Therefore, this OH is named the O1' or 4H hereafter. Table 2-3-1 summarizes the band position and assignment of four kinds OH.

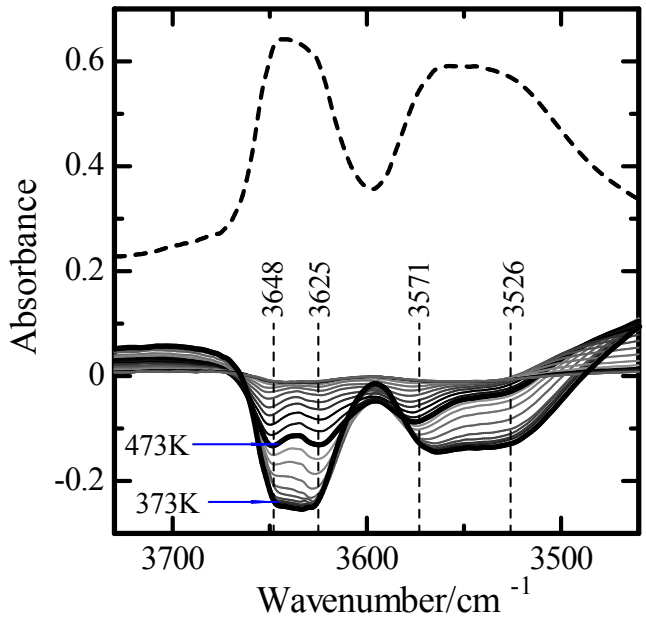

Figure 2-3-4. Enlarged portion of the change of OH intensity shown in Figure 2-3-3. Dotted line shows the OH stretching band measured at 373 K before ammonia adsorption.

Table 2-3-1. Assignment, number, strength, and extinction coefficient of OH on NH_4NaY (96 % NH_4^+)

Band position / cm^{-1}	Assignment	Location	A_0 / mol kg^{-1}	ΔH / kJ mol^{-1}	ε / cm μmol^{-1}
3648	O1H	Supercage	0.58	108	1.4
3625	O1' or 4H		0.57	110	1.3
3571	O2H	Sodalite cage	1.10	119	0.52
3526	O3H	Hexagonal prism	0.80	105	1.3

Assignment of Ammonia and OH Species Based on Thermal Behavior Shown in IR-TPD

Intensities (or decreased absorbances) of IR bands were measured quantitatively by deconvolution. Figure 2-3-5 shows examples of deconvolution, where the IR bands of ammonia and OH were divided into five and four Gaussian portions of ammonia adsorbed and OH, respectively. A small intensity observed at 1320 cm^{-1}, maybe ascribable to ammonia adsorbed on the dislodged Al[10], was disregarded. The peak positions 1496, 1430, and 1369 cm^{-1} were assumed according to Earl *et al*[20].

The band positions of OH were assumed based on the difference spectrum at 373 K and its second derivative. The peak width was assumed to increase linearly with decrease of the wave number according to the finding by Onida *et al*[22]. Parameters in this line ar relationship were determined based on the observed curves as σ_ν (cm^{-1}) = $-0.12\ \nu$ (cm^{-1}) + 441, where σ_ν was the standard deviation of the OH band at a wave number ν.

Figure 2-3-6 shows the IR-TPD (decrease rate of peak intensity) of the bending vibration of ammonia species and the stretching vibration of OH based on the calculated intensities, and MS-TPD of ammonia was added to for a comparison. IR-TPD of the NH_4^+ band at 1430 cm^{-1} showed a peak at a high temperature, *ca.* 540 K, and those shoulders observed at 1496 and 1369 cm^{-1} showed peaks at *ca.* 500 K. In addition, the band with a small intensity at 1665 cm^{-1} showed a peak at a low temperature, *ca.* 440 K; these peaks show that the corresponding species were desorbed around these temperatures. Thus different thermal behaviors of these ammonia species were identified.

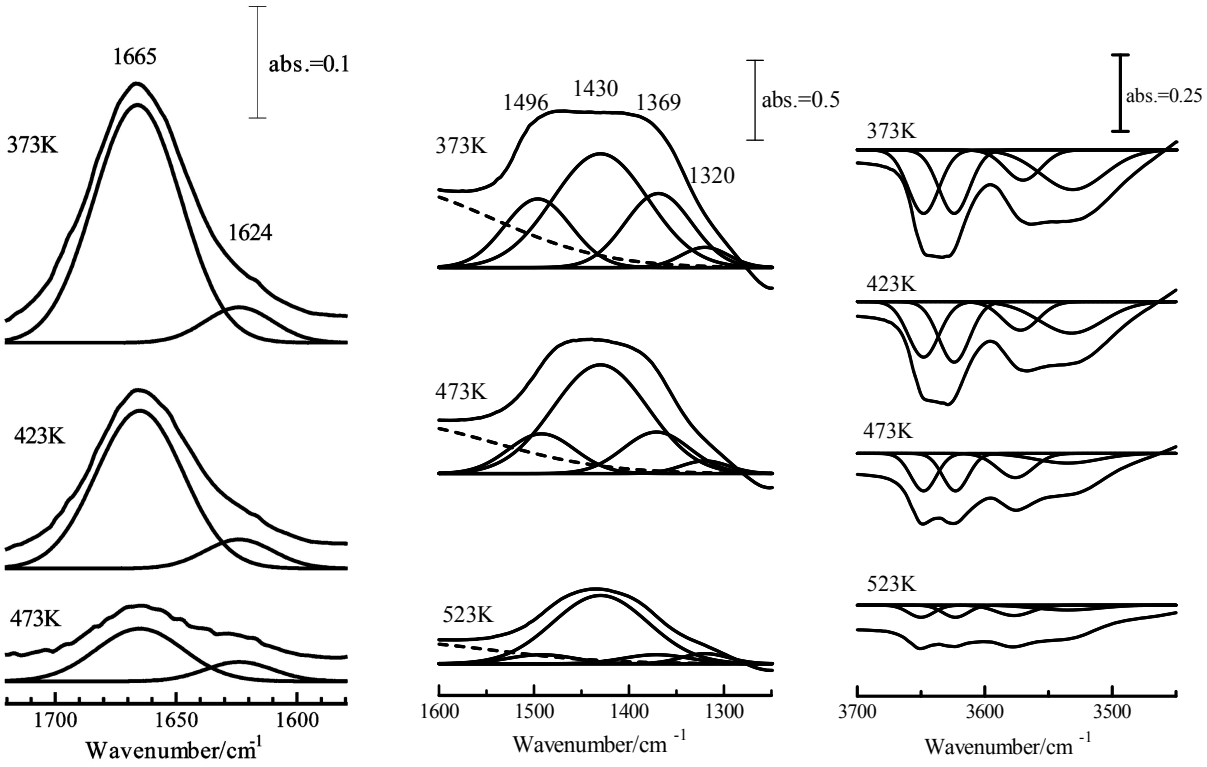

Figure 2-3-5. Deconvolution of difference spectra for NH_4^+ bending vibration and OH stretching vibration.

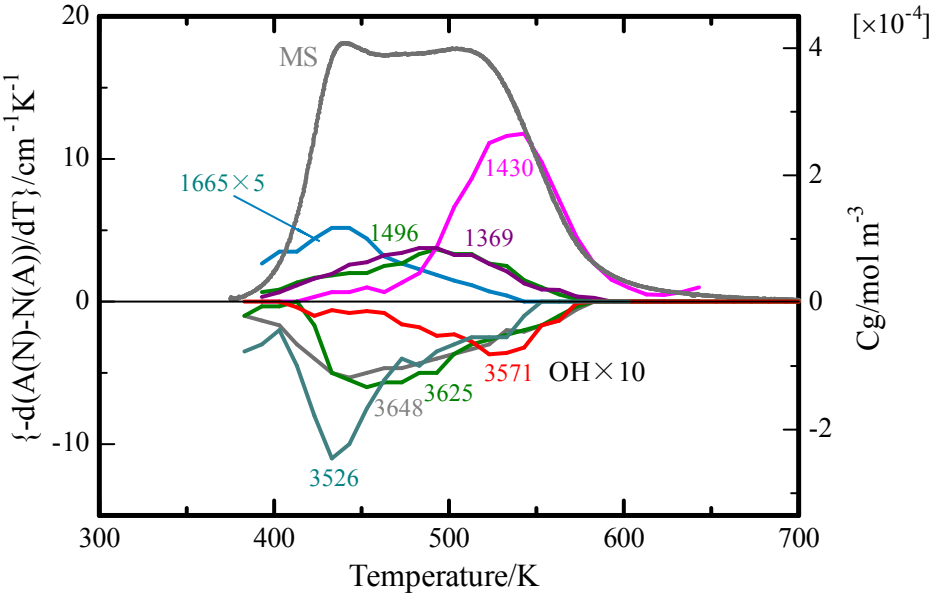

Figure 2-3-6. IR-TPD of ammonium cation at 1496, 1430 and 1369 cm^{-1}, ammonia species at 1665 cm^{-1}, and OH bands at 3526, 3648, 3625 and 3571 cm^{-1}. For OH, 10 times of the values was shown. MS-TPD was added for a comparison.

IR-TPD of OH also showed different thermal changes of intensities. The O2H band at 3571 cm^{-1} showed a negative peak at the highest temperature, *ca.* 530 K, whereas the O1' or 4H and O1H at 3625 and 3648 cm^{-1}, respectively, showed negative peaks at moderate temperatures, and the O3H at 3526 cm^{-1} showed a negative peak at the lowest temperature, *ca.* 440 K. These negative peaks indicate that the adsorbed ammonia was desorbed from the corresponding OH groups at these temperatures. We can therefore find that the acid strength of OH group is in the order of O2H > O1H ≒ O1' or 4H > O3 H.

Recovery of O1H, O1' or 4H, and O2H was observed in the temperature range 450-600 K, where disappearing of 1496, 1369, and 1430 cm^{-1} bands was observed. It seems that the sum of recovery of these OH groups corresponded to the sum of diminishing of these asymmetric deformation bands of NH_4^+, but there was no clear correspondence among individual peak temperatures. Therefore, we can assume that O1H, O1'or 4H, and O2H formed NH_4^+ species, giving a large asymmetric deformation band at 1496-1369 cm^{-1}, as observed commonly on zeolites. It is proposed that the coordination environment affects the position and intensity of the asymmetric deformation band of NH_4^+.[19] Probably such an environment was varied with a change in density of NH_4^+, and this caused the different thermal behaviors of 1496, 1369, and 1430 cm^{-1} bands.

On the other hand, the peak temperatures of the 1665 and 3526 cm^{-1} bands were similar and obviously lower than those of other bands, *ca.* 440 K. We can assume that the ammonia species showing the 1665 cm^{-1} band is adsorbed on O3H.

In conclusion, we can divide bridging OH groups on Y-zeolite into four portions. O3H formed an ammonia species, giving a band at 1665 cm^{-1} by the reaction with ammonia. The other three, O1H, O1' or 4, and O2H, yielded a NH_4^+ cation, giving a broad band at around 1430 cm^{-1}. Although the attribution of the 1665 cm^{-1} band and O(1' or 4) needs discussion as stated in the following section, it is noteworthy that the analysis of thermal behavior of IR bands with a newly developed technique of IRMS-TPD of ammonia clarified the four kinds of OH groups with different acid strengths on Y-zeolite.

Quantitative Measurements of Ammonia Species and OH

Sum of the amounts of desorbed ammonia species thus shown by the four IR-TPD curves must be equal to the MS-TPD of ammonia. Curve fitting of the IR-TPD to MS-TPD was attempted, as shown in Figure 2-3-7. To do so, parameters to cancel the difference in extinction coefficients of the ammonia species are required, and sum of the corrected IR-TPD of ammonia species is fitted to the MS-TPD, i.e.,

$$I\text{ (MS-TPD)} = I\text{ (corrected IR-TPD of ammonia)} = \sum a_n I_n \ (n = 1\text{-}4)$$

where I means intensity of MS or IR-TPD, a is a parameter that corresponds to the reciprocal of the extinction coefficient, and I_n (n = 1-4) are the intensities of IR-TPD of 1430, 1369, 1496, and 1665 cm^{-1}. As shown in Figure 2-3-7a, the sum of IR-TPD of ammonia species corrected by parameters a_n, 1 (for 1430 cm^{-1}), 3.3 (for 1369 and 1496 cm^{-1}), and 19 (for 1665 cm^{-1}), was fitted well to the MS-TPD where two broad desorptions were observed.

As mentioned above, the sum of 1496, 1430, and 1369 cm^{-1} bands should show the asymmetric deformation of NH_4^+ cation due to O1H, O1' or 4, and O2H. Therefore, the IR-TPD of O1H, O1' or 4, and O2H is fitted to the IR-TPD of the asymmetric deformation of NH_4^+ according to the equation

$$(\text{IR-TPD of asymmetric deformation of } NH_4^+) = \sum a_{O(n)H} I_{O(n)H} \ (n = 1, 1' \text{ or } 4, \text{ and } 2)$$

As a result, $a_{O(n)H}$ was found to be -1.44 and -1.5 for OH at 3648 and 3625 cm^{-1}, respectively, -6 for OH at 3571 cm^{-1}, and the sum of these corrected IR-TPD was fitted to IR-TPD of asymmetric deformation of NH_4^+ (Figure 2-3-7b). On the other hand, IR-TPD for O(3)H was fitted to that of ammonia species, giving a 1665 cm^{-1} band, with $a_{O(n)H}$ = -1.6 for OH at 3526 cm^{-1}. Amounts of four kinds of OH were thus determined from the integrated area and desorbed ammonia, as shown in Table 2-3-1.

Heat of ammonia adsorption (ΔH) to show acid strength was determined using the one-point method previously derived by us. As mentioned previously, change of entropy upon desorption was determined experimentally as ΔS, 51 J K^{-1} mol^{-1}.[10] Thus, the determined ΔH was shown in Table 2-3-1. The ΔH for HY zeolite previously reported[14,18], 110 kJ mol^{-1}, corresponds to an averaged value of these parameters. From the MS-TPD of ammonia, the acid sites are roughly divided into three portions, and these correspond to the OH groups in a hexagonal prism [O3H] with 105 kJ mol^{-1} of ΔH, the OH groups in a supercage [O1H and O1' or 4H] with 110 kJ mol^{-1}, and the OH group in a sodalite cage [O2H] with 119 kJ mol^{-1}.

In addition, from the parameters measured at 373 K, extinction coefficients of four kinds of OH were calculated, as shown in Table 2-3-1. Datka reported[23] ε_{HF}, *ca.* 1.2 cm ímol^{-1} for NaHY (40%, H) which was similar to the value in the present study. However, the reported data (ε_{HF} = 3.2 cm μmol^{-1} and ε_{LF} = 8.5 cm μmol^{-1}) by Makarova *et al.*[24] were fairly inconsistent.

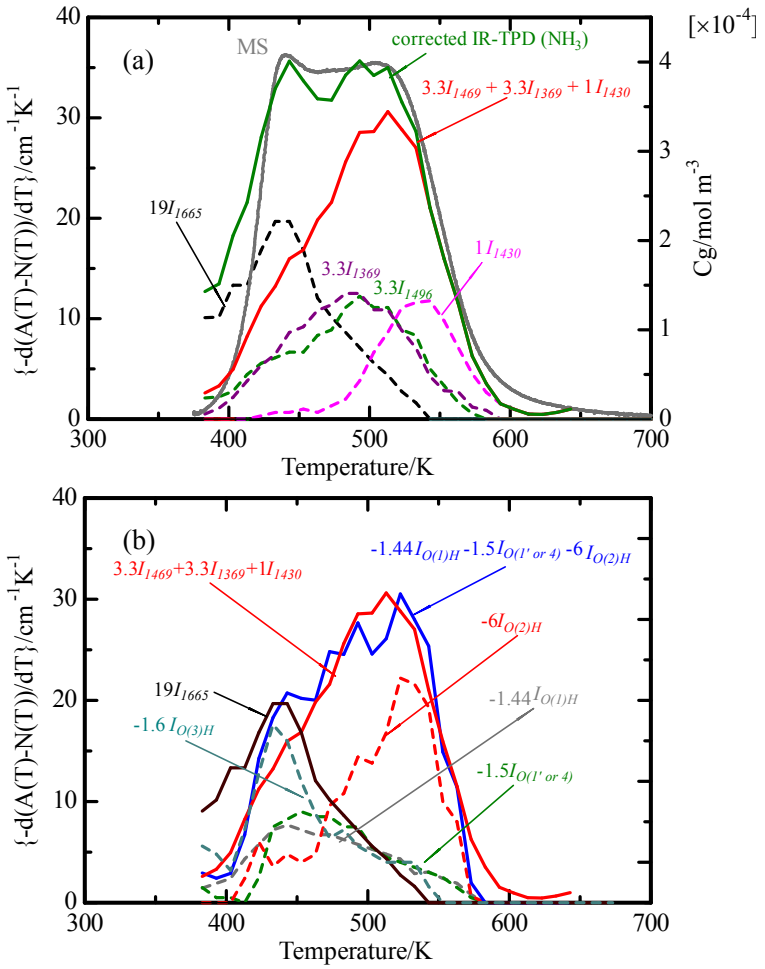

Figure 2-3-7 Curve fitting corrected IR-TPD for OH and ammonia bands to MS-TPD: (a) fitting of sum of IR-TPD for NH_4^+ and ammonia bands (corrected IR-TPD) to MS-TPD; (b) fitting of IR-TPD profiles of OH and NH_4^+ and ammonia bands.

IRMS-TPD of NH_4NaY (NH_4^+, 77-14 %).

IRMS-TPD of ammonia was measured on the NH_4NaY with smaller degrees of exchange of NH_4^+, 77-14%. Figure 2-3-8 and 2-3-9 show difference spectra caused by adsorption and desorption of ammonia on NH_4NaY (exchange degree of NH_4^+: 14, 33, 44 and 77 %). In the ammonia bending region (Figure 2-3-8, 1750-1250 cm^{-1}), the band at 1665 cm^{-1} was observed on the NH_4^+ exchange degrees of 77% and 44%, but not on those of 33% and 14%.

Consistently, the O3H was observed only on the 77% and 44% of exchange degrees (Figure 2-3-8 (b)). Therefore, the interaction between ammonia species at 1665 cm^{-1} and O3H was confirmed also in these measurements.

Quantitative analysis of OH groups was made by the same method applied to the NH_4NaY with 96% NH_4^+ shown above. Figure 2-3-10 shows the relationship between the amount of OH groups and ion exchange degree thus obtained. It was found that the O(1)H in a super cage was formed preferentially on the exchange with NH_4^+. Above 40 % of the exchange, two kinds of OH, O2H in the sodalite cage, and O3H in the hexagonal prism,

increased. One more OH in the super cage, the O1' or 4H, also increased in the similar region of exchange.

In addition, we confirmed the validity of the present analysis as follows. By using the extinction coefficients of OH groups shown in Table 2-3-1, the amount of OH was directly determined from the intensity of the negative peak in the difference spectrum at 373 K. The amounts of four kinds of OH groups and their changes with varying the ion exchange degree were in agreement with those determined by the curve fitting of IR-TPD shown above. Moreover, extinction coefficients of OH in Table 2-3-1 were confirmed to be almost constant on the samples with different exchange degrees.

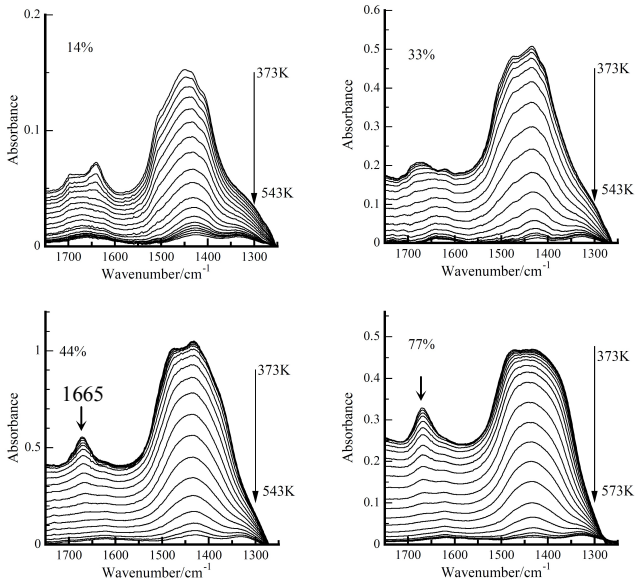

Figure 2-3-8. Difference spectra in the region on 1750 to 1250 cm^{-1}, which were obtained by the adsorption and desorption of ammonia on 14 to 77 % NH_4^+ exchanged Y zeolites.

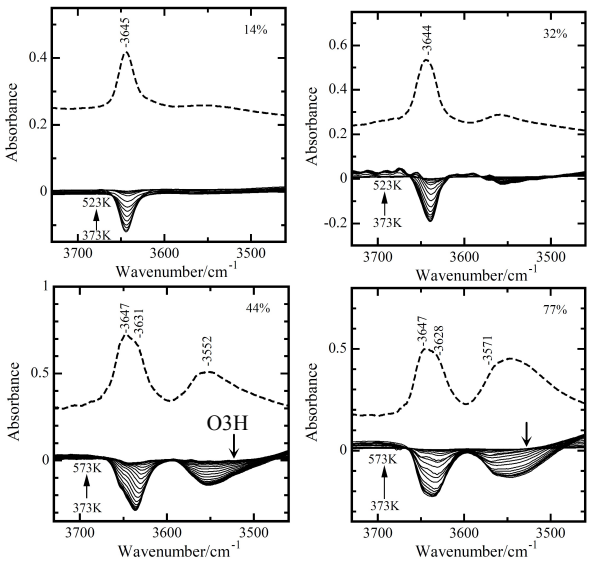

Figure 2-3-9. Difference spectra in the OH stretching region, which were obtained due to the adsorption and desorption of ammonia on 14 to 77 % NH_4^+ exchanged Y zeolites.

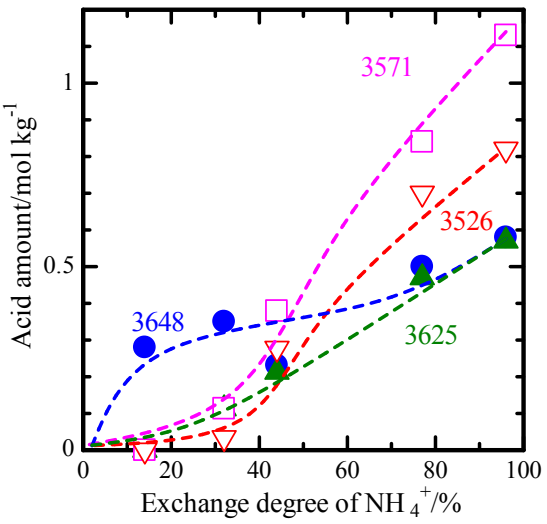

Figure 2-3-10. Amounts of four kinds of OH observed at 3648, 3625, 3571 and 3526 cm^{-1} plotted against the exchange degree of NH_4^+.

Discussion

Two Kinds of Ammonia on the Y-zeoliote

Two kinds of desorption of ammonia were identified to come from ammonia species, which showed the IR bands at *ca.* 1430 and 1665 cm^{-1}, respectively. Obviously, these are not assignable to a single adsorbed ammonia species, because different thermal changes are observed. The acid sites to contact with the ammonia species are then identified; *i.e.*, ammonia molecules that show the bands at 1665 and *ca.* 1430 cm^{-1} are adsorbed on the O(3)H and other three kinds of OH, respectively.

Formation of the NH_4^+ cation on the OH to show the band at *ca.* 1430 cm^{-1} is a usual observation, while the interaction between ammonia and O3H, which locates in the hexagonal prism, needs a detailed discussion. The band position of 1665 cm^{-1} is ascribable to symmetric deformation of NH_4^+ or asymmetric deformation of NH_3. The extinction coefficient of the band is small, and only 1/19 of that for the NH_4^+ cation at 1430 cm^{-1}, supporting that the 1665 cm^{-1} band is due to a different vibration mode or different species from those of 1430 cm^{-1} band. These mean that ammonia interacts with the O3H differently from NH_4^+ with usual OH. Zecchina *et al.*[19] reported the same observation of ammonia adsorbed on the Y-zeolite, and explained by the formation of the triply bridged NH_4^+, which had a bending mode at *ca.* 1665 cm^{-1} (symmetric deformation) as well as at 1450 cm^{-1} (asymmetric deformation). Yin *et al.*[25] also reported a similar assignment. However, the present study showed that these bands were not caused by two vibration modes of a common species. Either a different adsorbed ammonia species or a different vibration mode will explain the present observation, however, it is not yet decided which is the correct explanation. Further study will be needed to fully understand the interaction.

Lonyi and Valyon discussed the assignment of this band[21], but they did not draw a conclusive remark. Sarria *et al.* pointed out[26] that ammonia adsorbed on the O3H gave absorptions of NH_4^+ at 1510, 1434, and 1395 cm^{-1}. However, the bands at 1496 and 1369 cm^{-1} observed in the present study are removed at the temperatures higher than that of the O3H, which does not support their explanation.

Distribution of OH in Y-zeolite

Among previous studies, only a study using neutron powder diffraction reported a precise analysis of the distribution of OH in Y-zeolite[3]. Three kinds of OH existed in nature, and O4H was not detected; *i.e.*, for the distribution, O1H/O2H/O3H/O4H = 3 (54%)/1 (18%)/1.6 (29%)/0 unit $cell^{-1}$. The distribution measured in the present study, O1H/O2H/O3H/l' or 4H = 0.6 (19%)/1.1 (35%)/0.8 (25%)/0.6 mol kg^{-1} (19%) (Table 2-3-1) looks inconsistent with the reported value, but the difference between them becomes small when the distribution of O1' or 4H is counted in O1H. The distribution of the O2H increased sharply with the exchange degree of NH_4^+ above 80%, as shown in Figure 2-3-10. Therefore, a higher exchange degree of the present study than in the neutron diffraction could be indicated as a possible difference in the samples.

The neutron diffraction was measured at the temperature of 5 K, while the present study was done at 373-873 K; therefore, a difference in the temperature could affect the distribution of OH. Because the O1H and O4H does not have a large difference in the relative energies, it is possible that some portions of OH in the super cage could move to the position of O4 at the higher temperature. Therefore, the identification of the O4H could not be totally denied. Daturi most recently[27] reported that the O4H could be observed using IR spectroscopy.

Datka *et al*. reported that the distribution of Brønsted OH depends on the number of Al in the nearest next

neighbor (NNN) to the OH site[28-30]. They understood that the HF and LF bands mainly consisted of O1H and O3H, respectively, and the splitting of these bands was caused by the chemical composition. Therefore, it may be reasonable to say that the O1H at the HF band is ascribable to OH with one Al and the O1' or 4H band to the O1H with two neighbored Al atoms.

Alternatively, it may be referred to that the O1' or 4H band was formed due to the influence by extra framework Al. The effect caused by the extra framework Al, thereby, has been studied using the ex situ prepared HY, *i.e.*, a usually prepared Y-zeolite that contained the extra framework Al. When the IRMS-TPD experiment was applied to the *ex situ* HY, two kinds of OH ascribable to HF and LF were observed (Figure 2-3-11), and further splitting into four kinds of OH as shown in Figure 2-3-4 was not observed. Maybe both in the HF and LF bands, two components were overlapped strongly and the intensity of O1' or 4H was not enhanced. This means that the O1' or 4H was not related to the presence of extra framework Al. In our previous study on USY (ultrastable Y) with a large amount of extra framework Al[10], one more OH was clearly observed at 3595 cm^{-1}, not detected on HY zeolite. Therefore, an interaction of the Brønsted OH with the extra framework Al creates one more OH that does not exist in the HY.

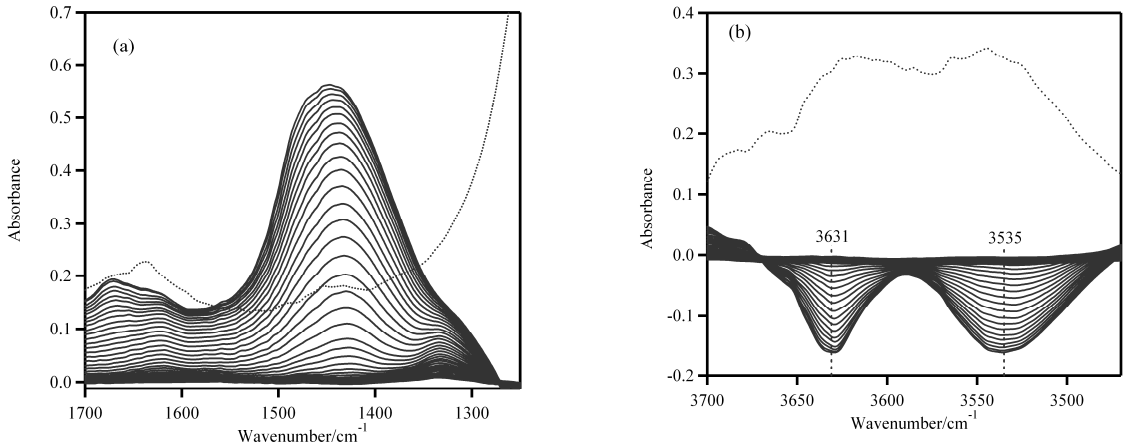

Figure 2-3-10. Difference spectra on *ex situ* prepared HY zeolite in the regions of bending vibration of ammonia (a) and stretching vibration of OH (b) during TPD on ammonia.

Sarria[2] *et al.* detected the O3H at 3501 cm^{-1}, which was lower than that of the present study by *ca.* 25 cm^{-1}. As shown in Figure 2-3-4, this band showed the broad spectrum, thus suggesting an interaction with a neighbored oxygen atom. Such an interaction may affect the band position depending on the experimental conditions and makes it difficult to precisely determine the band position.

Among four kinds of OH, the strength as the Brønsted acidity is ordered as O1H ≒ O1' or 4H < O2H, which is the decreasing order of the wave number. The strongest Brønsted acid site locates in the sodalite cage, but because of the steric reason, it may be catalytically inactive in most reactions. From the viewpoint of the band position, the O3H site seems to be the strongest. However, the hydrogen bonding to the wall of Y-zeolite may shift the band position.

Conclusion

(1) Y-zeolite has four kinds of structurally different of acid sites and shows two kinds of desorption of

ammonia in the TPD experiment. Interaction of ammonia with the sites forms NH_4^+ on three of four OHs, but does not usually on the OH in the hexagonal prism.

(2) The strongest Brønsted OH with 119 kJ mol^{-1} of ΔH is found in the sodalite cage. The previously reported value of 110 kJ mol^{-1} of Δ*H* for Y-zeolite is an averaged one of these OHs.

(3) Distribution of the acid site depends on the exchange degree of NH_4^+.

References and Notes

1. D.H. Olson and E. Dempsey, *J. Catal*., **13**, 221 (1967).
2. F.R. Sarria, O. Marie, J. Saussey and M. Datsuri, *J. Phys. Chem.* B, **109**, 1660 (2005).
3. M. Czjzek, H. Jobic, A.N. Fitch and T. Vogt, *J. Phys. Chem.,* **96**, 1535 (1992).
4. M. Brandle and J. Sauer, *J. Mol. Catal. A: Chem.,* **119**, 19 (1997).
5. U. Eichler, M. Brandle and J. Sauer, *J. Phys. Chem.* B, **101**, 10035 (1997).
6. J.-R. Hill, C.M. Freeman and B. Delley, *J. Phys. Chem.* A, **103**, 3772 (1999).
7. R.A. van Santen and G.J. Kramer, *Chem. Rev*., **95**, 637 (1995).
8. M. Niwa, S. Nishikawa and N. Katada, *Micropor. Mesopor. Mater.,* **82**, 105 (2005).
9. M. Niwa, K. Suzuki, N. Katada, T. Kanougi and T. Atoguchi, *J. Phys. Chem.* B, **109**, 18749 (2005).
10. M. Niwa, K. Suzuki, K. Isamoto and N. Katada, *J. Phys. Chem.* B, **110**, 264 (2006).
11. S. Kotrel, M.P. Rosynek and J.H. Lunsford, *J. Phys. Chem.* B, **103**, 818 (1999).
12. B.A. Williams, S.M. Babitz, J.T. Miller, R.Q. Snurr and H.H. Kung, *Appl. Catal.* A*,* **177**, 161 (1999).
13. C.A. Martinez and C. Martinez, *Appl. Catal.* A, **134**, 169 (1996).
14. N. Katada, Y. Kageyama and M. Niwa, *J. Phys. Chem.* B, **104**, 7561 (2000).
15. N. Katada, T. Kanai and M. Niwa. *Micropor. Mesopor. Mater.,* **75**, 61 (2004).
16. M. Niwa, N. Katada, M. Sawa and Y. Murakami, *J. Phys. Chem.* B, **99**, 8812 (1995).
17. M. Niwa, M Iwamoto and K. Segawa, *Bull. Chem. Soc. Jpn*., **59**, 3735 (1986).
18. H. Igi, N. Katada and M. Niwa, In Proceedings of the 12th International Zeolite Conference; Treacy, M. M. J., Markus, B. K., Bisher, M. E., Higgins, J. B., Eds.; Materials Research Society: Warrendale, PA, 2643 (1999).
19. A. Zecchina, L. Marchese, S. Bordiga, C. Paze and E. Gianotti, *J. Phys. Chem.* B, **101**, 10128 (1997).
20. W.L. Earl, P.O. Fritz, A.A.V. Gibson and J.H. Lunsford, *J. Phys. Chem.*, **91**, 2091 (1987).
21. F. Lonyi and J. Valyon, Micropor. Mesopor. Mater., **47**, 293 (2001).
22. B. Onida, Z. Gabelica, J. Lourencüo and E. Garrone, *J. Phys. Chem.* B, **100**, 11072 (1996).
23. J. Datka, *J. Chem. Soc., Faraday Trans.,* **77**, 2877 (1981).
24. M.A. Makarova, A.F. Ojo, K. Karim, M. Hunger and J. Dwyer, *J. Phys. Chem,*. **98**, 3619 (1994).
25. F. Yin, A.L. Blumenbeld, V. Gruver and J.J. Fripiat, *J. Phys. Chem.* B, **101**, 1824 (1997).
26. F.R. Sarria, J. Saussey, J.-P. Gallas, O. Marie and M. Daturi, *Stud. Surf. Sci. Catal*., **158**, 821 (2005).
27. M. Daturi, Abstract for Zeolite and Microporous Crystals 2006 (ZMPC2006), Yonago, Japan; KA203 (2006).
28. J. Datka and B.J. Gil, *J. Catal*., **145**, 372 (1994).
29. M. Sierka, U. Eichler, J. Datka and J. Sauer, *J. Phys. Chem.* B, **102**, 6397 (1998).
30. J. Datka, B. Gil and P. Baran, *J. Mol. Struct.,* **645**, 45 (2003).

2-4. IRMS-TPD of Ammonia: Direct and Individual Measurement of Brønsted Acidity in Zeolites and Its Relationship with the Catalytic Cracking Activity

Synopsis

By using an improved method of infrared mass spectrometry/temperature-programmed desorption (IRMS-TPD) of ammonia, the number and strength of Brønsted acid sites on various zeolites were precisely measured. Using this method, it is possible to measure the property of acid site directly and individually when the multiply overlapped acid sites exist. Thus, measured ΔH (enthalpy change of ammonia adsorption) as a parameter of strength was roughly correlated with the IR band position of hydroxide, as long as the OH was located in a large pore consisting of an 8- to 12-member ring; that is, the lower the wave number of the OH band position, the stronger the ΔH. Under the conditions of monomolecular reaction, the rate of octane cracking was measured on these zeolites, and the turnover frequency (TOF) was calculated from the reaction rate and number of Brønsted acid sites. Among the distributed acid sites, the Brønsted acid site with the stronger acidity located in a large pore was considered the active site. Thus measured TOF was related strongly with the ΔH of the Brønsted acid sites. Therefore, it is concluded that the Brønsted acid sites play a predominant role in the cracking of hydrocarbons.

Introduction

Strong acid sites created in a framework of zeolite play a role as active sites for various organic reactions. In particular, zeolite-based catalysts have been used in the industrial processes of petroleum refinery, which has a great impact on human society. Therefore, zeolite acidity and the cracking of hydrocarbons are fundamental and important chemical subjects, and both should be comprehensively understood. A great deal of study related to these subjects has already been carried out[1–6].

As described in the previous sections, ammonia IRMS-TPD studies on mordenite (MOR)[7], ultra-stable Y (USY) zeolite[8] and HY zeolites[9] have revealed another important advantage of this method. The distribution of Brønsted acid sites was measured quantitatively. Two kinds of OH in MOR located in different member rings were observed, and their number and strength were measured individually. In the study of USY, it was possible to detect the OH responsible for the enhanced Brønsted acidity among the multiple overlapped hydroxides. The detection of four kinds of OH in Y-zeolite was possible, and their positions and acid site strengths were studied. In other words, the present method has a powerful advantage in characterizing the Brønsted acidity.

In this subchapter, our attention is thereby directed to investigating the acid sites on various zeolites to summarize the overall features of Brønsted acidity. Because the Brønsted acidity in zeolites has already been studied by means of NMR spectroscopy[10] and computational calculation[11,12], conclusions are drawn carefully from a comparison with previous findings based on these investigations. Moreover, octane cracking is studied as a test reaction on these zeolites. To study the relationship between Brønsted acidity and catalytic activity, reaction conditions are selected for those of monomolecular reactions, because under these conditions, correlating between them is relatively easy. Williams *et al.* also found that monomolecular reaction conditions are the most suitable for studying the dependence of Brønsted acid sites on catalytic cracking[13]. An overall view of the Brønsted acidity is provided not only from the ammonia TPD, but also from the catalytic activity of the test

reaction. To do this, zeolites ZSM-5 (MFI), ferrierite (FER), β-zeolite (BEA) and MCM-22 (MWW), prepared in the NH_4^+ form and converted *in situ* or *ex situ* in the IR cell and catalytic reactor to the proton form, are measured by IRMS-TPD. La and Ca ion-exchanged Y and commercially available HY zeolites are also studied, because the enhanced catalytic activities are reported on these Y zeolites.

Experimental Section

Zeolite Samples

Zeolite MFI with a Si/Al_2 ratio of 23.8 was kindly provided by Tosoh Corporation. In addition, two kinds of zeolite MFI were prepared under hydrothermal conditions; the Si/Al_2 ratios obtained were 46 and 58. Zeolite FER with a Si/Al_2 ratio of 17.6, also provided by Tosoh Corporation, was converted into the NH_4^+ form before the measurements. Zeolite MWW was prepared as described previously[14]. Ludox HS40 (Du Pont) as the silica source, $NaAlO_2$, and hexamethylenimine (Aldrich) as the template were used and synthesized in an autoclave rotating vertically at 15 rpm at 423 K for 84 h. Synthesized Na-form MWW was ion-exchanged into the NH_4^+. Na-form zeolite BEA was prepared by a dry gel conversion method[15], and it was converted into the NH_4^+ form. *Ex situ* H-form zeolite BEA supplied from PQ Corporation. Y-zeolite with a Si/Al_2 ratio of 5.1 was kindly provided by Catalysts & Chemicals Industries Co. After being converting to the NH_4-form, it was treated in a $La(NO_3)_3$ solution to prepare an NH_4LaY zeolite with 28% La^{3+} exchanged. Ca ions also were exchanged in a $Ca(NO_3)^2$ solution to prepare an NH_4CaY with 37% Ca^{2+} exchanged. Reference catalyst HY with a Si/Al_2 of ratio 5.3, JRC-Z-HY5.3, was supplied by the Catalysis Society of Japan and used without further treatment. For the *in situ* study, before the measurements, zeolite samples were treated in an NH_4NO_3 solution at 353 K for 24 h to exchange Na^+ with NH_4^+.

IRMS-TPD of Ammonia

The IRMS-TPD method has been described previously in detail. The testing apparatus consisted of a glass vacuum line to which an infrared spectroscope (Perkin Elmer Spectrum one) and a mass spectroscope (Pfeiffer QME200) were connected. Carrier gas helium was fed into the IR cell and pumped from the exit to keep the line pressure at 25 Torr (1 Torr = 0.133 k Pa). A thin, self-compressed wafer of <10 mg and 1 cm in diameter was used for the measurements. Before adsorption of ammonia, IR spectra were taken on the evacuated sample at every 10 K from 373 to 773 K during TPD to measure the reference $N(T)$, with the temperature raised at a ramp rate of 10 K min^{-1}. Adsorption of ammonia was followed by evacuation at 373 K, and IR spectra were repeatedly obtained every 10 K during TPD to measure the IR absorption due to the adsorbed ammonia $A(T)$. Difference spectra were calculated as $A(T) - N(T)$, in which IR bands ascribable to ammonia species and hydroxide were observed. Differential change of the IR absorption (*i.e.*, $-d[A(T) - N(T)]/dT$) was calculated at the selected wave number to be compared with MS-measured TPD. Through comparison between IR- and MS-TPD, nature of the acid site for adsorbed ammonia (*i.e.*, Brønsted or Lewis acid site) was identified, and the number and strength of the acid site were quantitatively measured, because the amount of desorbed ammonia can be measured by MS, and the strength was obtained by a curve-fitting method on the basis of a theoretically derived equation[16]. Simultaneously, the band position of the Brønsted OH was determined. The OH band position (ν), however, changed with the temperature (T) linearly in a slope $\Delta\nu/\Delta T = -0.03 - 0.05$ cm^{-1} K^{-1}, where

Δv and ΔT were changes in band position and temperature. Thus, the band position of OH was corrected using the afore-measured parameter to the wave number observed at 373 K.

The curve-fitting method for determining ΔH has been described previously in detail[16]. To do this, the value of ΔS change of entropy on desorption of ammonia must be determined before the measurements are taken. ΔS determined in a previous study[8] coincided well with ΔS for phase transformation (vaporization) from liquid to gas ammonia; therefore, it was theoretically supported. However, the present IRMS-TPD experiments were not performed under full-equilibrium conditions, because a very fast flow of helium was fed into the IR cell to avoid the tailing of ammonia due to the complex structure of the apparatus, and only a small amount of sample was used as an IR wafer. Therefore, ΔS 51 J K^{-1} mol^{-1} was used. This was corrected experimentally in the present study.

An extinction coefficient ε (m^2 mol^{-1}) of NH_4^+ bending vibration in the region of 1450 cm^{-1} was measured from the number of Brønsted acid sites and IR absorption intensity A (area in cm^{-1}) at 373 K based on the Lambert–Beer equation,

$$A = \varepsilon \frac{W}{S} C_W$$

where W (kg), C_W (mol kg^{-1}), and S (m^2) denote sample weight, weight-based concentration of NH_4^+, and sample disk area, respectively.

Catalytic Reaction

Cracking of octane was measured under atmospheric pressure by a continuous-flow method using a Pyrex glass reactor. Here 30 mg of the NH_4-form catalyst was converted into the H form (*in situ* prepared H zeolite) or the *ex situ* catalyst was preheated in a flow of nitrogen carrier at 773 K for 1 h. Octane of 14 Torr was fed into the reactor in nitrogen carrier gas at a flow rate of 40 ml min^{-1} of at 773 K, and products were analyzed by Gas Chromatography with a silicone capillary column. Because the conversion of octane was often >10%, an integrated equation was used to measure the reaction rate r,

$$r = \frac{F}{W} \ln \frac{1}{1 - x/100} \frac{p}{RT}$$

where F, W, and R denote the flow rate of the carrier gas, the weight of the catalyst, and the gas constant (0.0831 bar K^{-1} mol^{-1}), respectively. Here p and T were kept constant at 0.019 bar (14 Torr) and room temperature (298 K), respectively, because it was confirmed that the monomolecular reaction proceeded under these conditions[17]. The degree of conversion, x (in %), was measured at 15 min after the start of the reaction.

Results

MFI Zeolite

Figure 2-4-1 shows framework structure of MFI. MFI structure is built from three dimensional channel system included straight and sinusoidal 10MR channels, and it has 12 kinds of nonequivalent T sites. Datka *et al.* studied the heterogeneity of acidic OH groups in H-ZSM-5 by IR measurements; and then, they have assumed that this property depend on the difference of local crystal structures (T-O length and/or T-O-T angle)[18]. Zholobenko *et al*. reported that the broad absorption band at *ca.* 3250 cm^{-1} was assigned to the acidic OH groups H-bonded to the neighbored oxygen atoms[19]. Additionally, Pinto *et al.* have carried out the quantitative measurements of the

acid strength distributions caused by difference of pore size in ZSM-5 by combined technique of ammonia TPD and ^{1}H MAS NMR measurements[20].

Difference spectra obtained on MFI (23.8) at 373–773 K during the TPD experiment, along with a reference spectrum measured at 373 K, are shown in Figure 2-4-2. A broad spectrum at 3400–1500 cm^{-1} was ascribed to stretching vibration of N–H, and a sharp band at *ca.* 1450 cm^{-1} was ascribed to bending vibration of NH_4^+ adsorbed on the Brønsted acid sites. Simultaneously, a decrease in OH intensity was observed at *ca.* 3600 cm^{-1}, and the intensity recovered gradually with an increase in temperature. Figure 2-4-3 (a) and (b) show enlarged portions of difference spectra of NH_4^+ bending vibration and OH stretching vibration, respectively. As shown in Figure 2-4-4, the bending vibration of NH_4^+ seemed to consist of three components at 1484, 1430, and 1380 cm^{-1}, and the sum of the intensity was used to show the thermal behavior. Differential changes of the intensity with respect to temperature are plotted against the temperature (hereafter called IR-TPD) in Figure 2-4-5, where MS-measured ammonia TPD is also shown as a comparison. Good agreement between IR-TPD for NH_4^+ and MS-TPD at high-temperature desorption indicates that desorbed ammonia at the high temperature came mainly from NH_4^+ adsorbed on the Brønsted acid site.

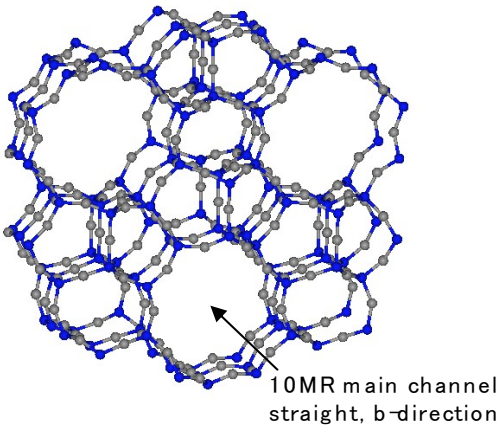

Figure 2-4-1. MFI-type framework structure.

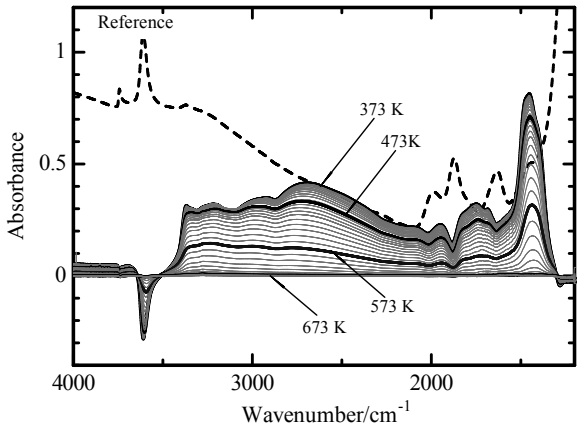

Figure 2-4-2. Difference spectra during TPD of ammonia on ZSM-5 (Si/Al_2 = 23.8) at 373-773 K. A reference spectrum before adsorption of ammonia measured at 373 K was included as a comparison.

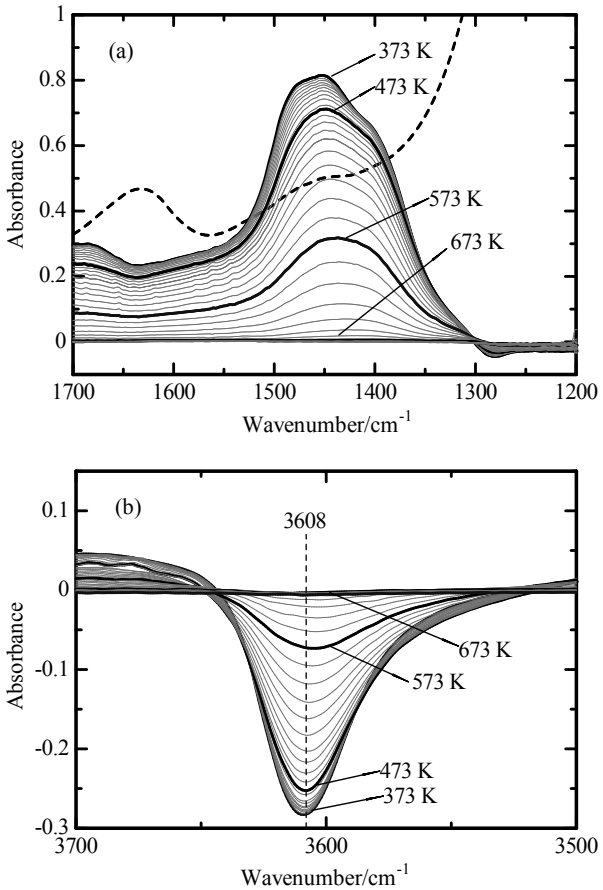

Figure 2-4-3. Enlarged portion of NH_4^+ (a) and OH (b) vibrations in Figure 2-4-1.

On the other hand, IR-TPD of OH centered at 3608 cm^{-1} showed a mirror-image relationship with the IR-TPD of NH_4^+, as expected. By multiplying by a parameter −9, which corresponded to the reciprocal of the extinction coefficient, the corrected IR-TPD of OH agreed well with MS-TPD. Thus, it was found that the MFI zeolite had only one kind of the Brønsted acid site observed at 3608 cm^{-1}, which could be identified as OH located in a 10-member ring, and the number and strength were calculated based on the theoretical equation, as shown in Table 2-4-1. The desorption peak observed at 430 K in MS-TPD was not fully identified in the IR observation. MFI (46) prepared *ex situ* and MFI (58) prepared in situ also were measured by the present method, as shown in Table 2-4-1. IR band position of the Brønsted OH and ΔH measured on these zeolites were almost the same as on the MFI (23.8).

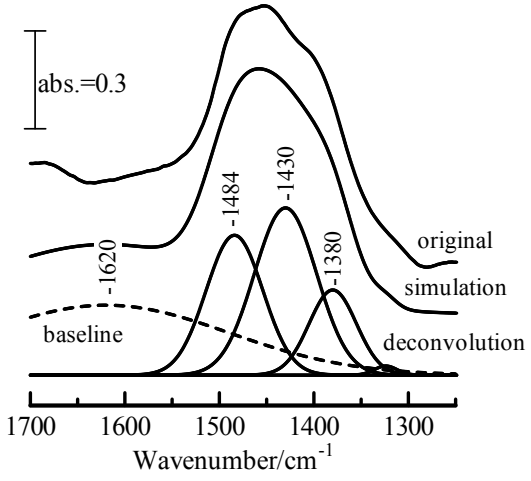

Figure 2-4-4. Deconvolution of difference spectrum for NH_4^+ bending vibration on ZSM-5.

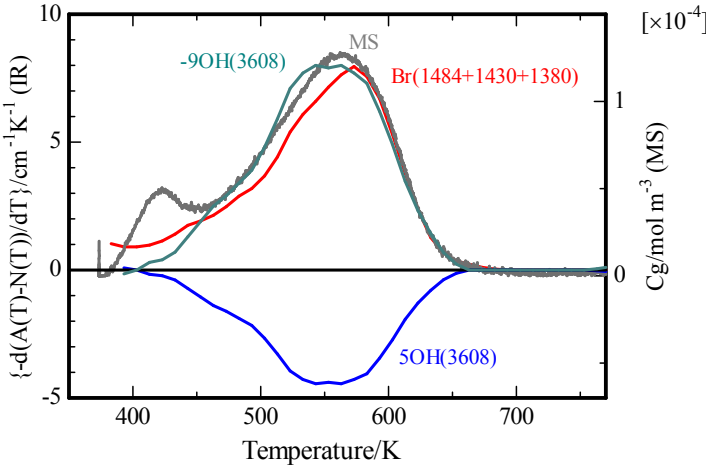

Figure 2-4-5. Comparison between MS-TPD and IR-TPD for the bending vibration of NH_4^+ (Br) on ZSM-5. IR-TPD of stretching vibration of acidic OH is magnified by 5, and corrected by multiplying by -9 for the fitting.

FER Zeolite

Figure 2-4-6 shows FER-type framework structure. FER zeolite has four kinds of nonequivalent T sites. This structure is built from two-dimensional straight 10MR channel systems which are bridged by intersections via 8MR windows. The protonated oxygen sites have been determined by neutron diffraction studies[21], and the specified T(3)-O(4)H-T(1) and T(4)-O(6)H-T(4) groups were located in 8-/6- (ferrierite cage) MRs and 10MR, respectively

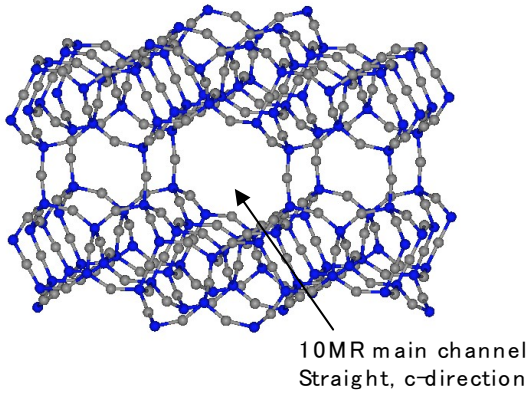

Figure 2-4-6. FER-type framework structure.

Figure 2-4-7 (a) and (b) show enlarged portions of NH_4^+ bending vibration and OH stretching vibration in the difference spectra, respectively. Unlike for in the MFI shown above, the OH band could not be ascribed to a single IR band. Therefore, a deconvolution and fitting treatment was carried out, as shown in Figure 2-4-8.

Namely, the stretching vibration of OH could be divided into two components. The OH stretching vibrations at 3599 and 3550 cm^{-1} was most likely ascribable to OH located in ferrierite cage member rings of FER structure, respectively.

Figure 2-4-8 compares MS-TPD and IR-TPD for NH_4^+ and OH on FER. The number and strength of the Brønsted OH observed at 3599 and 3550 cm^{-1} were measured individually from the curve fitting (Table 2-4-1). Thus, FER has a Brønsted acid site distribution based on the structure.

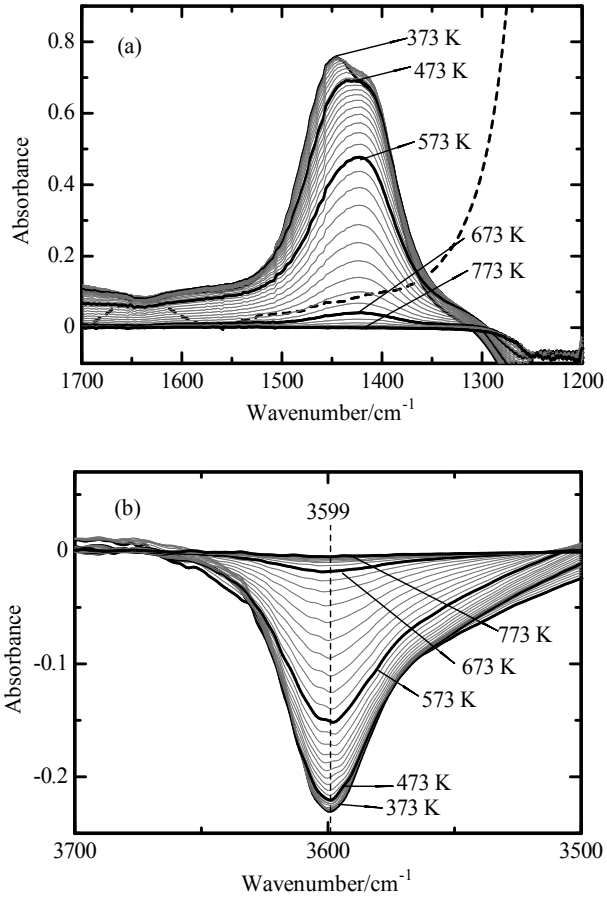

Figure 2-4-7. Enlarged portion of NH_4^+ (a) and OH (b) vibrations in the difference spectra obtained during TPD of ammonia at 373-773 K on FER zeolite

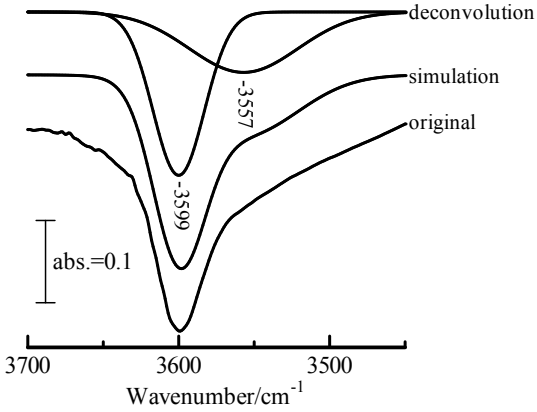

Figure 2-4-8. Deconvolution of OH band into two components by curve-fitting.

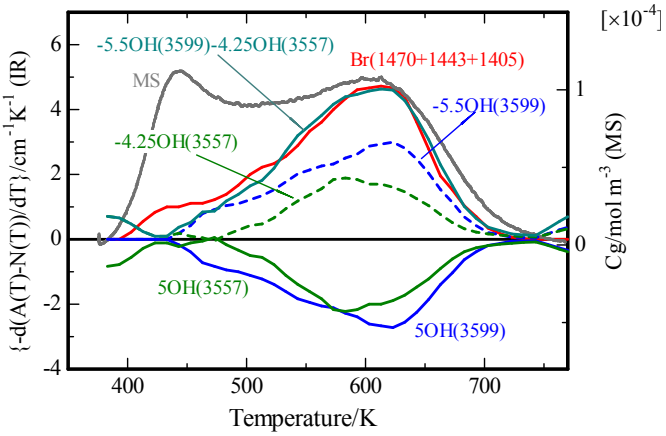

Figure 2-4-9. Comparison between MS-TPD and IR-TPD of NH_4^+ (Br) and OH on FER zeolite. IR-TPD of OH was magnified by 5, and corrected by multiplying by appropriate parameters for the fitting.

MWW Zeolite

Figure 2-4-10 shows MWW-type framework structure. MWW structure has eight kinds of nonequivalent T sites, and it has two kinds of different independent 10MR pore systems. One of them is two-dimensional 10MR sinusoidal channels, and the other is the three-dimensional12MR super cages which interconnected through perpendicular 10MR windows.

Figure 2-4-11 (a) and (b) show enlarged portions of NH_4^+ bending vibrations and OH stretching vibrations in the difference spectra on the MWW (35) prepared *in situ*, respectively. Figure 2-4-12 compares the thus-measured MS-TPD and IR-TPD for NH_4^+ and OH. As shown in the cases of MFI and FER, the IR-TPD of NH_4^+ agreed well with MS-TPD at the high-temperature desorption. The IR-TPD of OH is plotted in Figure 2-4-12, showing a similar mirror-image relation with IR-TPD of NH_4^+. Onida *et al.* have divided the OH bands into three components located in supercages, sinusoidal 10MRs and double six rings between two super cages at 3628, 3610 and 3585 cm^{-1}, respectively[22]. The stretching vibration of OH in MWW seems to consist of a single component, although distribution of OH bands has been estimated because of the complex structure of MWW by Onida's work. In the present study, therefore, it was not precisely analyzed, and the integrated area of the OH band region was measured to calculate the IR-TPD of OH. Based on Figure 2-4-12, the number and strength of Brønsted acid sites in MWW was calculated, as shown in Table 2-4-1. The sample MWW (35) prepared *ex situ* was also measured, as shown in Table 2-4-1; almost the same characterization data are observed as for the MWW prepared *in situ*.

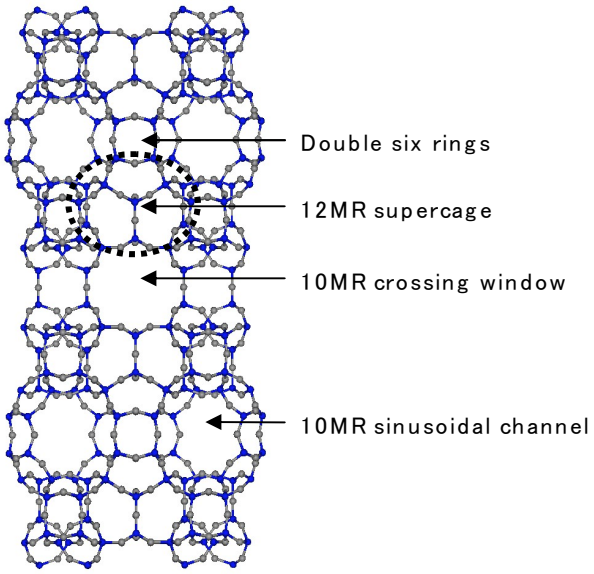

Figure 2-4-10. MWW-type framework structure.

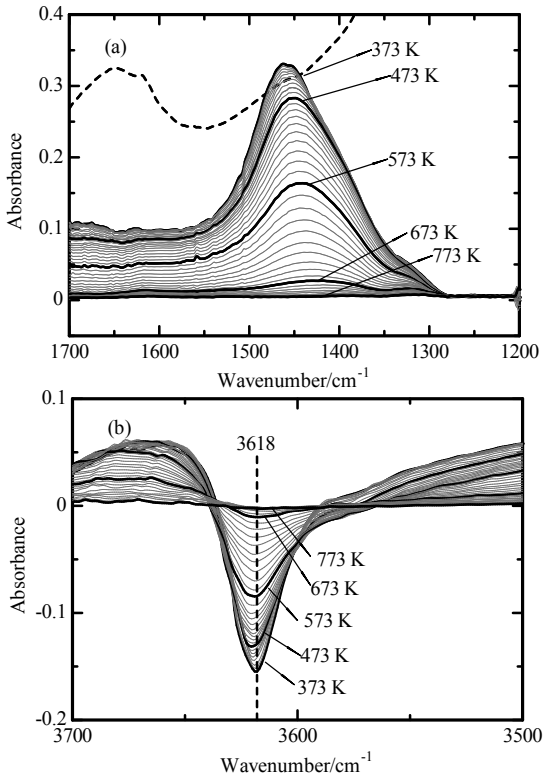

Figure 2-4-11. Enlarged portion of NH_4^+ (a) and OH (b) vibrations in the difference spectra obtained during TPD of ammonia at 373 to 773 K on MCM-22.

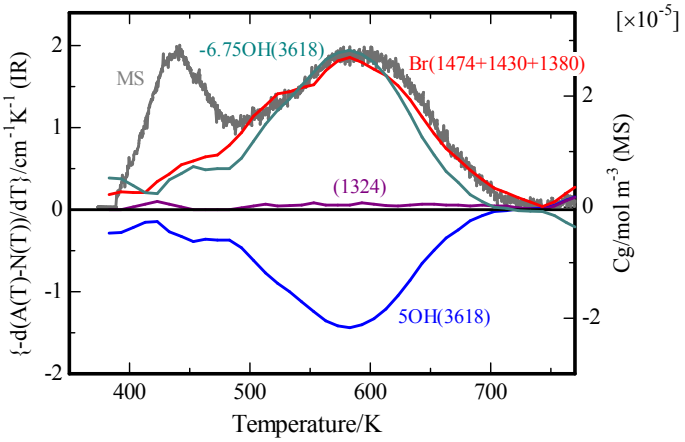

Figure 2-4-12. Comparison between MS-TPD and IR-TPD of NH_4^+ (Br) and OH on MCM-22. IR-TPD of OH was magnified by 5, and corrected by multiplying by -6.75 for the fitting.

BEA Zeolite

Figure 2-4-13 shows BEA-type framework structure. BEA structure has three dimensional networks, and those are built from straight and sinusoidal 12MR channels. There are nine kinds of T sites, and those are classified into three groups. T1, T2 sites are associated with one 4MR, and T3, T4, T5, T6 sites are associated with two 4MRs. Then, residual T7, T8, T9 sites are not associated with 4MR.

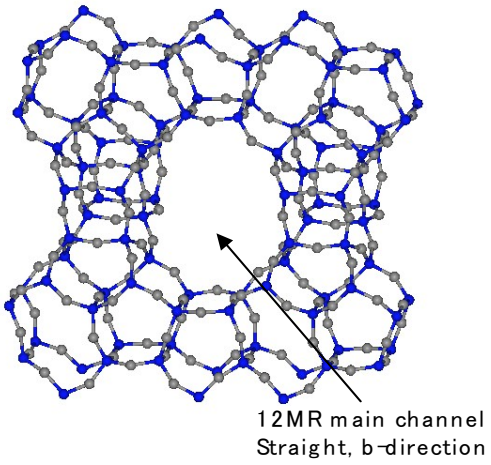

Figure 2-4-13. BEA-type framework structure.

Already, we have performed ammonia IRMS-TPD measurements on the solid acidities of *in situ* and *ex situ* prepared H-BEA zeolites[23]. However, those measurements have not been carried out under the appropriate experimental conditions optimized by recent study (see Chapter 2-1). Thus, we re-measured the solid acidities of H-BEA zeolites at the optimized conditions. Figure 2-4-14 (a) and (b) show enlarged portions of NH_4^+ bending vibration and OH stretching vibration in the difference spectra on *in situ* prepared H-BEA, respectively. In the OH stretching region (Figure 2-4-14 (b)), the absorption intensities assigned to the internal Si-OH groups (3733 cm^{-1}) and the acidic SiO(H)Al groups (3606 cm^{-1}) were diminished by adsorption of ammonia.

IR-TPD of bridged OH band and NH_4^+ bending band showed the similar TPD behavior, and those behaviors and MS-TPD were almost same. On the other hand, IR-TPD of internal Si-OH band and NH_3 bending band corresponded to the tail-like MS-TPD peak at high temperature. In our previous work[23], a small shoulder band at *ca.* 1320 cm^{-1} was assigned to strongly adsorbed NH_3 species on the dislodged Al with Lewis acidity and/or interacted with Si-OH near the defective domain (Figure 2-4-14 (a)). Thus, these IR-TPD and MS-TPD behaviors were in reasonable agreement with this assignment.

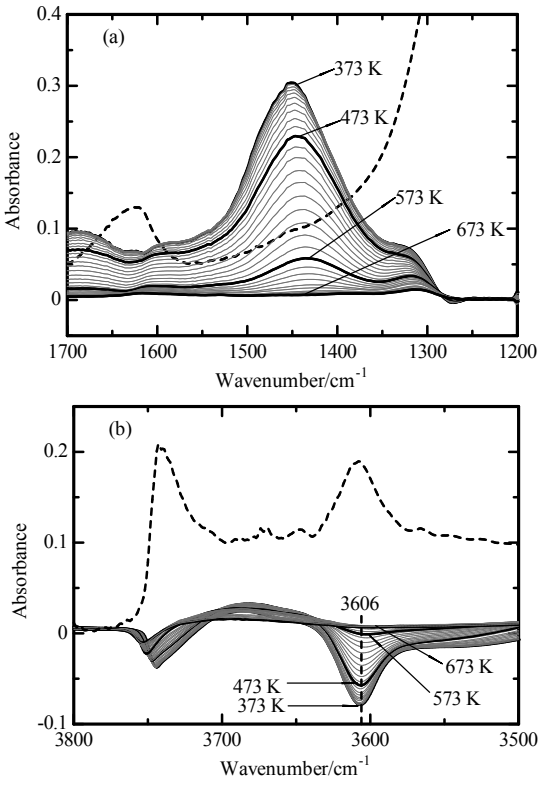

Figure 2-4-14. Enlarged portion of NH_4^+ (a) and OH (b) vibrations in the difference spectra obtained during TPD of ammonia at 373 to 773 K on *in situ* H-BEA.

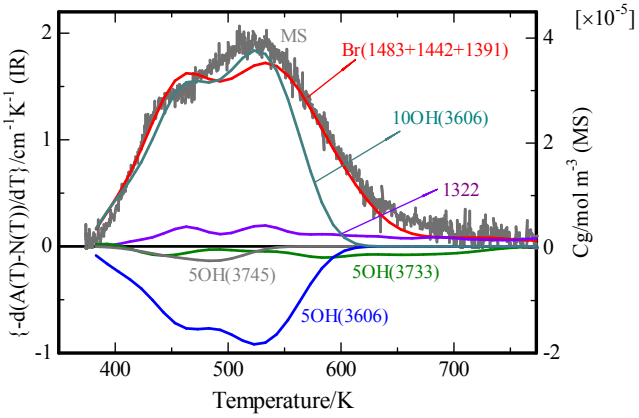

Figure 2-4-15. Comparison between MS-TPD and IR-TPD of NH_4^+ (Br) and OH on *in situ* H-BEA. IR-TPD of OH was magnified by 5, and corrected by multiplying by -10 for the fitting.

Figure 2-4-16 (a) and (b) show enlarged portions of NH_4^+ bending vibration and OH stretching vibration in the difference spectra on *ex situ* prepared H-BEA, respectively. In a comparison between *ex-* and *in-situ* prepared H-BEA, absorption intensity at 1319 cm^{-1} increased and additional small absorption peak was observed at 1625 cm^{-1} (Figure 2-4-16 (a)). Additionally, in the OH stretching region, a newly absorption peak appeared at 3780 cm^{-1}. The absorption at 3780 cm^{-1} has been identified as the OH attached on the dislodged Al (Al-OH or $AlOOH^+$)[24]:

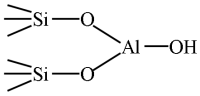

For the calculation of IR-TPDs, difference spectra in the OH stretching region was divided into five components at 3608 (bridged acidic OH), 3655 (hydrolyzed aluminum species), 3732 (internal Si-OH groups), 3748 (external Si-OH groups) and 3780 (dislodged Al species) cm^{-1}, respectively (Figure 2-4-17). Figure 2-4-18 shows the MS-TPD and IR-TPDs of adsorbed ammonia species and OH groups. The IR-TPDs of bridged acidic OH (3608 cm^{-1}) and NH_4^+ showed the almost similar TPD behavior, and it corresponded to the main desorption peak of the MS-TPD. The bands at 1625 and 1319 cm^{-1} showed the different TPD behavior with respect to the temperature, and the IR-TPD of 1319 cm^{-1} showed the desorption peak at the relatively higher temperature. The absorption band at 1625 cm^{-1} would be assigned to the weakly adsorbed NH_3 species on the Lewis acid sites. IR-TPDs of the internal Si-OH (3732) and Al-OH or $AlOOH^+$ (3780) showed desorption peak at the broad temperature region.

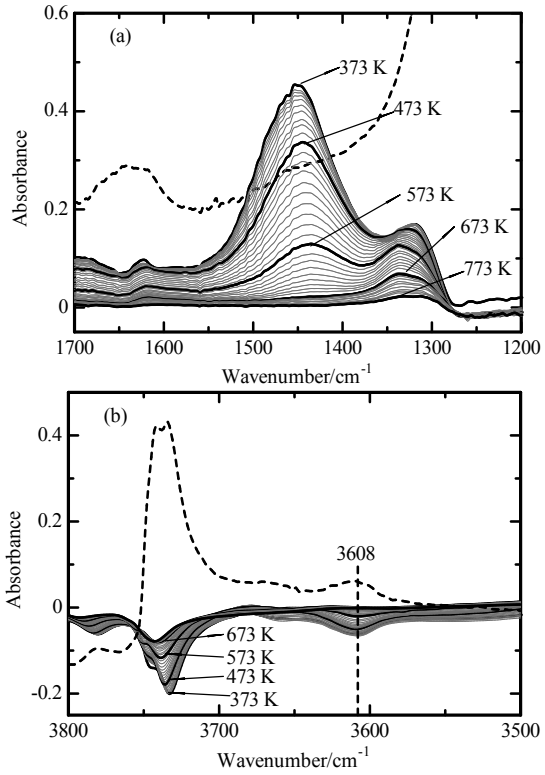

Figure 2-4-14. Enlarged portion of NH_4^+ (a) and OH (b) vibrations in the difference spectra obtained during TPD of ammonia at 373 to 773 K on *ex situ* H-BEA.

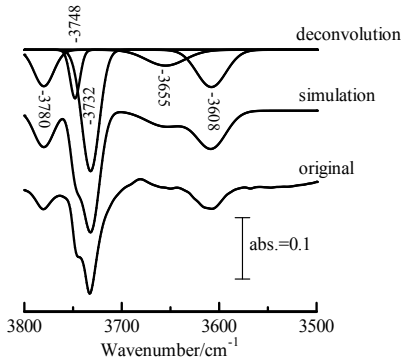

Figure 2-4-15. Deconvolution of OH band into five components by curve-fitting.

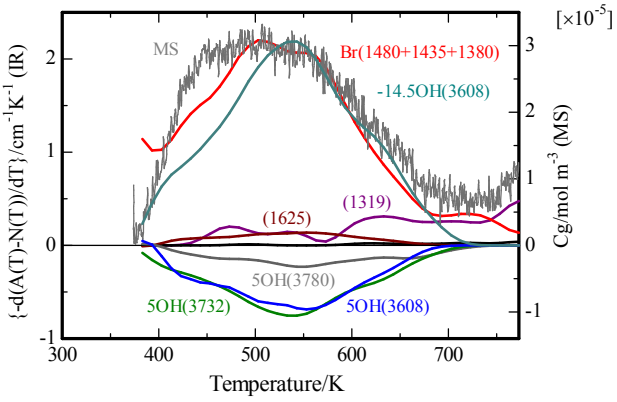

Figure 2-4-16. Comparison between MS-TPD and IR-TPD of NH_4^+ (Br) and OH on *ex situ* H-BEA. IR-TPD of OH was magnified by 5, and corrected by multiplying by -14.5 for the fitting.

La and Ca Ions Exchanged HY Zeolite

La and Ca cation-exchanged HY zeolites have been known to catalyze the cracking of hydrocarbons, whereas the inherent HY has shown very little activity. Figure 2-4-17 shows the enlarged portions of NH_4^+ and OH in the difference spectra measured on LaHY during the TPD experiment. In the reference spectrum before adsorption of ammonia, two kinds of OH were observed at 3634 cm^{-1} (HF [high-frequency]) and 3555 cm^{-1} (LF [low-frequency]), ascribable to OH on super cages and sodalite cages, respectively. These OH intensities diminished on adsorption of ammonia and recovered by desorption, with an increase in the measurement temperature. In the bending vibration region, the NH_4^+ band was observed at 1450 cm^{-1}, and small bands identified as NH_3 were observed at 1670 and 1607 cm^{-1}. Therefore, IR-TPD was calculated for each of two kinds of OH and NH_3, and NH_4^+; these are summarized in Figure 2-4-18 in comparison with MS-TPD. Fig. 2-4-18 shows that NH_3 desorbed at a higher temperature was due to NH_4^+ on the Brønsted acid sites at 3555 and 3634 cm^{-1}, whereas NH_3 desorbed at a lower temperature was due to NH_3 on the Lewis acid sites at 1670 and 1607 cm^{-1}. Thus, a simple desorption peak of MS-TPD was divided into four kinds of acid sites. The number and strength of two kinds of Brønsted OH were individually calculated, as shown in Table 2-4-1. The Brønsted acidity strength of OH in the supercage was enhanced by the ion exchange with La cations, because the ΔH for the OH in the supercage became larger than that on *in situ* prepared HY.

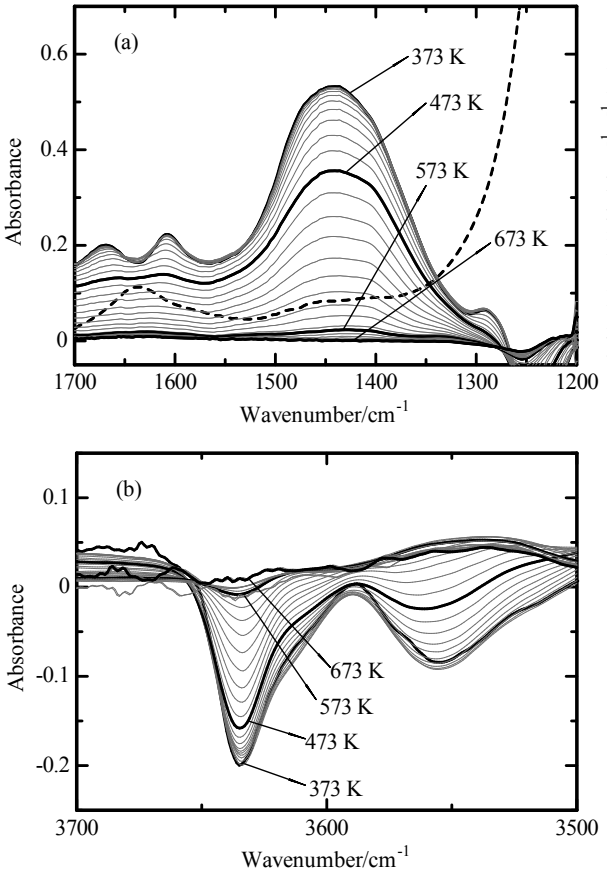

Figure 2-4-17. Enlarged portion of NH_4^+ (a) and OH (b) vibrations in the difference spectra obtained during TPD of ammonia at 373 to 773 K on LaHY.

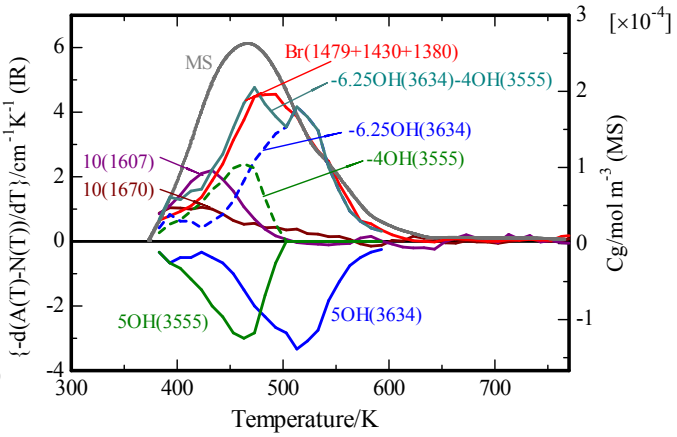

Figure 2-4-18. Comparison between MS-TPD and IR-TPD of NH_4^+ (Br) and OH on LaHY. IR-TPD of OH was magnified by 5.

On a Ca ion-exchanged zeolite, OH in the supercage only was observed (Figure 2-4-19), and NH_4^+ and two kinds of NH_3 were observed in the difference spectra. However, the absorption due to the Fermi resonance[25] at 1630 cm^{-1} disturbed the difference spectrum in the region of 1620–1670 cm^{-1}, as shown in Figure 2-4-20 (a). The Fermi resonance was observed strongly only in the reference spectra measured at temperatures below 450 K, but was not observed in the spectra after adsorption of ammonia. Therefore, we calculated the difference spectra, $A(T)-A(373)$, shown in Figure 2-4-20 (b), from which we calculated the change in intensity of NH_3.

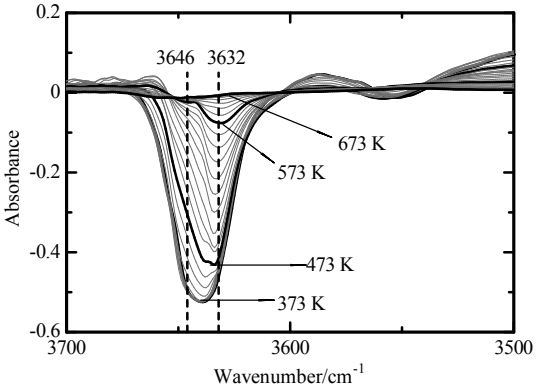

Figure 2-4-19. Enlarged portion of OH vibrations in the difference spectra obtained during TPD of ammonia at 373 to 773 K on CaHY.

IR-TPD of NH_4^+ and OH was measured from Figure 2-4-20 (a). Figure 2-4-21 shows the IR-TPD findings of NH_4^+ (at 1433, 1480, and 1389 cm^{-1}) and NH_3 (at 1664 and 1606 cm^{-1}), and the IR-TPD findings of two kinds of OH (at 3632 and 3646 cm^{-1}). Based on these observations, we calculated the number and strength of the Brønsted OH on the super cage (Table 2-4-1). The Brønsted OH at 3632 cm^{-1} exhibited increased ΔH compared with *in situ* HY zeolite; therefore, this site is considered an active site for cracking.

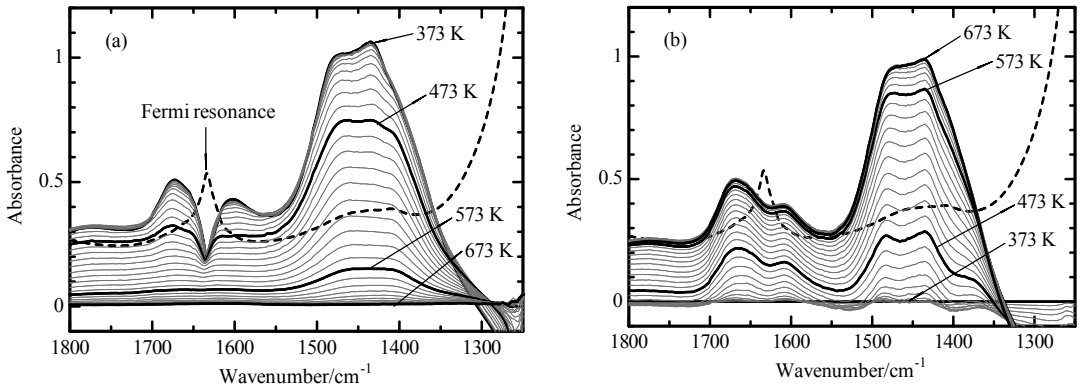

Figure 2-4-20. Bending vibration of NH_4^+ and NH_3: (a) difference spectra $A(T) - N(T)$; (b) difference spectra $A(373) - A(T)$ obtained during TPD of ammonia at 373 to 773 K on CaHY zeolite. Be aware that the intensity of the difference spectra decreases and increases with an increase in the temperature at (a) and (b), respectively.

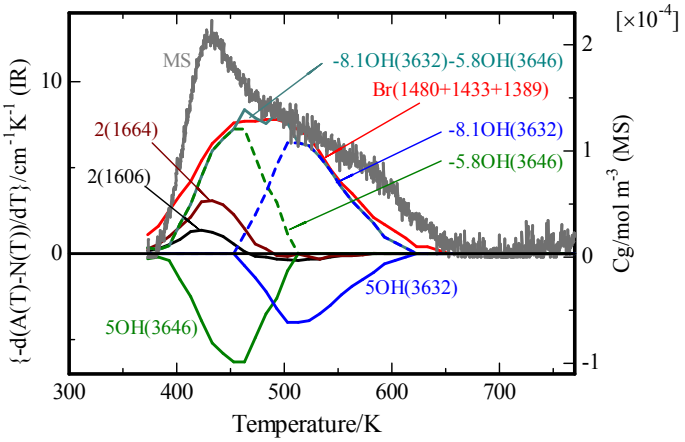

Figure 2-4-21. Comparison between MS- and IR-TPD of NH_4^+ (Br) and OH on CaHY zeolite. IR-TPD of OH was magnified by 5, and corrected by multiplying by −5.8 and −8.1 for the fitting.

Ex situ prepared HY zeolite

Ex situ prepared HY zeolite usually contains extra-framework aluminum, which is a required element for stabilization and catalytic activity. Therefore, commercially available HY does not contain a pure, unmodified structure of Y-zeolite. To compare *in situ* HY and metal cation-exchanged Y zeolite, *ex situ* HY, a reference catalyst supplied by the Catalysis Society of Japan was measured using IRMS-TPD of ammonia.

Enlarged portions of NH_4^+ and OH in the difference spectra measured on *ex situ* HY during the TPD experiment have been shown in Figure 2-3-10 (Chapter 2-3). Difference spectra have shown absorptions ascribable to NH_4^+, NH_3 (at 1672, 1630, and 1330 cm^{-1}), and two kinds of OH (at 3631 and 3535 cm^{-1}). Figure 2-4-22 shows the IR-TPD findings of NH_4^+ and NH_3, and the IR-TPD findings of two kinds of OH. Two desorptions of ammonia in MS-TPD came from NH_4^+ and NH_3 at 1450 and 1670 cm^{-1}, respectively, and NH_4^+ was adsorbed on the OH at 3631 and 3535 cm^{-1}. Thus, the number and strength of the two kinds of Brønsted acid sites were calculated individually from the high-temperature desorption of ammonia (Table 2-4-1). The thus-calculated ΔH was larger than that of the Brønsted acid sites of *in situ* HY.

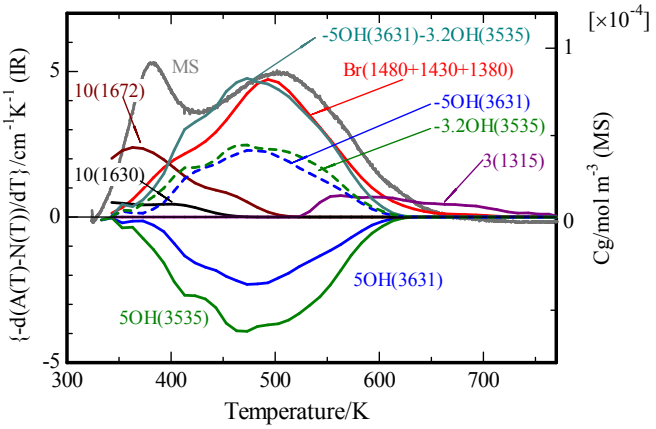

Figure 2-4-22. Comparison between MS- and IR-TPD of NH_4^+ (Br) and OH on *ex situ* HY zeolite. IR-TPD of OH was magnified by 5, and corrected by multiplying by −5 and −3.2 for the fitting.

Summary of Brønsted Acidity on Various Zeolites

Table 2-4-1 summarizes the IR band positions and number and strength of Brønsted acid sites on various zeolites. Data on MOR[7], USY[26], EDTA-treated USY[8], and *in situ* prepared HY[9] have been reported previously.

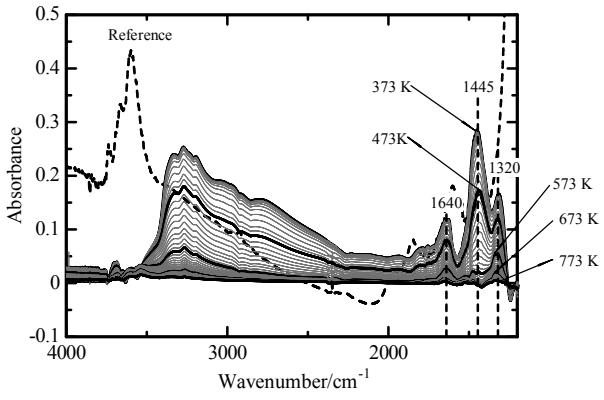

Figure 2-4-23. Difference spectra during TPD of ammonia on USY at 373-773 K. A reference spectrum before adsorption of ammonia measured at 373 K was included as a comparison.

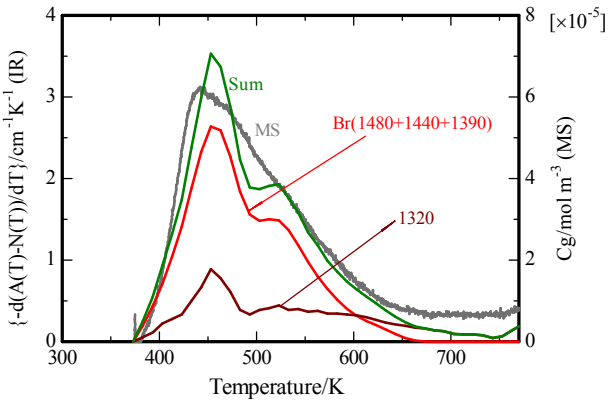

Figure 2-4-24. Comparison between MS- and IR-TPD of NH_4^+ (Br) and NH_3 (1320) on USY zeolite. Sum of calculated ones (Sum) are fitted to the MS-TPD.

Figure 2-4-23 shows difference spectra obtained on USY during the TPD experiment. Absorption bands assigned to the bending vibrations of NH_4^+ (1445 cm^{-1}) and two kinds of NH_3 (1320 and 1640 cm^{-1}) were remarkably observed. On the other hand, the IR band of OH was not clearly observed; the number and strength of the Brønsted acid sites were measured from the bending vibration of NH_4^+ centered at *ca* 1450 cm^{-1} using the extinction coefficient, 9.4 cm μmol^{-1}, as shown below. Figure 2-4-24 shows the MS-TPD and IR-TPDs of adsorbed ammonia species. Based on the extinction coefficient and the IR-TPD of NH_4^+ (denoted as Br(1480+1440+1390)), number and strength of the Brønsted acid sites were determined as 0.51 mol kg^{-1} and 118 kJ mol^{-1}, respectively.

Figure 2-4-25 shows plots of NH_4^+ band absorption intensity (area) measured at 373 K against WC_WS^{-1}. An averaged extinction coefficient obtained from the Lambert–Beer equation was measured experimentally as 9.4 ± 0.7 cm μmol^{-1} in these zeolite samples. The averaged extinction coefficient is a useful parameter for the quantitative measurement of Brønsted acid sites. In our previous study, a difference in extinction coefficients in BEA[23] and MOR[7] was reported. However, these extinction coefficients were measured based on the absorbance intensity in height.

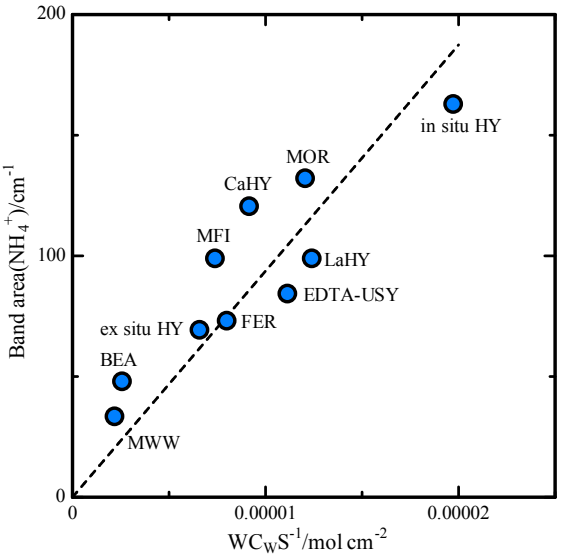

Figure 2-4-25. Determination of an averaged extinction coefficient of NH_4^+ on various Zeolites.

Octane Cracking

Catalytic activity of octane cracking was measured on these zeolites. In a previous study on the cracking on HZSM-5, Haag and Dessau reported that the monomolecular reaction proceeded under conditions of high temperature and low partial pressure of paraffin[26]. We confirmed that the temperature of 773 K and the partial pressure of octane of 14 Torr were sufficient to consider the reaction as proceeding through the mechanism; because under these conditions, the rate of cracking was proportional not only to partial pressure of octane, but also to the amount of Brønsted acid sites[17]. Therefore, the rate of octane cracking was measured under the experimental conditions.

The rates of octane cracking thus measured are summarized in Table 2-4-1. Under the monomolecular reaction conditions, Haag and Dessau proposed that paraffin adsorption occurred on the Brønsted acid site to form the penta-coordinate carbonium ion as the reaction intermediate (Scheme 2-4-1). Therefore, the TOF was calculated from the number of Brønsted acid sites, which can be considered active sites. The following considerations were required to assign the Brønsted acid sites to the active site. On FER, LaHY, *ex situ* and *in situ* prepared HY with more than 2 kinds of OH identified, the Brønsted acid sites located in the larger pore were considered active sites, because the reaction on the OH located in such a small pore as a 6 member ring could be severely hindered. On Na_2H_2-EDTA treated USY, only the strongest created Brønsted OH, observed at 3595 cm^{-1}, was assigned as an active site. Likewise, one of two OHs in the super cage of CaHY was considered as an

active site because of the higher ΔH. MOR contains two kinds of OH in 12- and 8-member rings, and the distribution depends on the degree of exchange with NH_4^+ cation[7]. On the NaHMOR with 93% Na and 7% H, OH was identified only in the 12-member ring, on which a constant cracking activity was observed. Thus, the TOF on the OH in the 12-member ring was determined based on the constant reaction rate and the number of Brønsted acid sites. On other MOR samples containing between 31 and 97% H, the rate of cracking dropped significantly with increasing time on stream. Therefore, precise determination of TOF on the OH in the 8-member ring of MOR was impossible. The TOF thus calculated for octane cracking is summarized in Table 2-4-1.

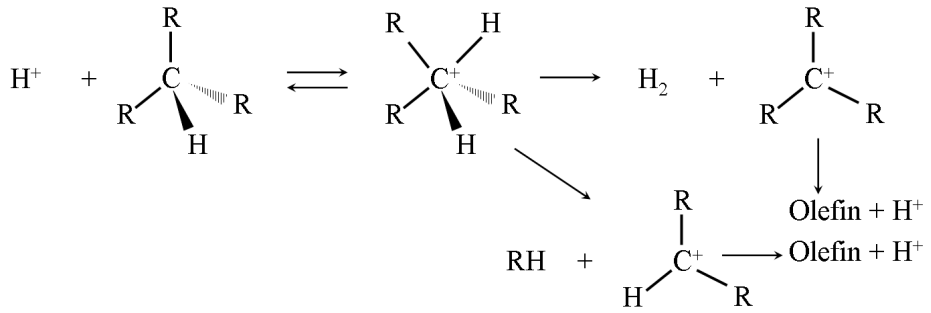

Scheme 2-4-1. Monomolecular mechanism of cracking of hydrocarbon through penta-coordinate carbonium ion.

Discussion

Measured ΔH of Brønsted Acid in Zeolites

In the present study, ΔH values in zeolite as the strengths of Brønsted acid sites were measured precisely. To date, no data on the ΔH as the strength of Brønsted acid sites have been reported, because previous studies could not measure the Brønsted acid sites directly and independently. Various methods for characterizing these sites have been proposed, but these provide qualitative or comparative information. Gorte and co-workers proposed propyl amine probe for the TPD experiment as a method of characterizing Brønsted acidity[27,28]. They reported advantages of the method in counting the number of Brønsted acid sites; however, the strength parameter was not provided. IRMS-TPD has the advantage of combining IR spectroscopy with MS, making both qualitative and quantitative measurements possible. Therefore, the strengths measured by the present method provide valuable information on the Brønsted acidity in zeolites. In addition, when more than two kinds of acid sites were observed, such as on FER and Y zeolites, the Brønsted acid sites were measured individually by a curve-fitting method. On the cation-exchanged HY and *ex situ* HY, both Brønsted and Lewis acid sites were observed. On these zeolites with complex profiles, the Brønsted acid sites on which the reaction should predominately proceed were measured. The present method has the advantage of providing quantitative measurements of the divided sites.

Table 2-4-1. IR band position, number and strength ΔH of the Brønsted acid site and catalytic cracking activity on various zeolites.

Zeolite sample (Si/Al_2 ratio)	*in situ* or *ex situ*	Brønsted acid site			Octane cracking	
		IR ν OH / cm^{-1} (member ring)	Number / mol kg^{-1}	ΔH / kJ mol^{-1}	Reaction rate / 10^{-3} mol s^{-1} kg^{-1}	TOF 10^{-3} s^{-1}
MFI (23.8)	*in situ*	3608 (10)	0.7	137	22	31
MFI (46)	*ex situ*	3604 (10)	0.42	134	12.6	30
MFI (58)	*in situ*	3606 (10)	0.54	134	-	-
FER (16.7)	*in situ*	3599 (10)	1	142	1.1	1.1
		3550 (8/6)	0.6	141	-	-
MWW (35)	*in situ*	3618 (12)	0.25	140	5.1	20
MWW (35)	*ex situ*	3618 (12)	0.24	137	8	33
LaHY (5.1)	*in situ*	3634 (12)	0.93	116	5.3	5.7
		3555 (6)	0.55	106	-	-
CaHY (5.1)	*in situ*	3646 (12)	0.55	104	-	-
		3632 (12)	0.5	122	6.6	13
HY (5.3)[a]	*ex situ*	3631 (12)	0.4	119	5.8	15
		3535 (6)	0.4	119	-	-
USY (5.1)[b]	*ex situ*		0.51	118	4.4	8.6
MOR (15)[c]	*in situ*	3616 (12)	0.42	142	4.4	11[d]
		3585 (8)	0.77	153	-	-
Na_2H_2-EDTA treated USY (4.9)[e]	*in situ*	3635 (12)	0.39	116	-	-
		3595 (12)	0.47	137	13.1	28
		3540 (6)	0.27	122	-	-
HY (5.1)[f]	*in situ*	3648 (12)	0.58	108	1.6	1.4
		3625 (12)	0.57	110		
		3571 (6)	1.1	119	-	-
		3526 (6)	0.8	105	-	-
BEA (22)[g]	*in situ*	3606 (12)	0.37	128	10.8	29
BEA (27)[g]	*ex situ*	3608 (12)	0.35	129	9.3	27

[a] JRC-Z-HY 5.3, a reference catalyst supplied by Catalysis Society of Japan. [b] Measured from the NH_4^+ bending vibration using extinction coefficient (9.4 cm μ mol^{-1}), see text. [c] see Chapter 2-1, [d] Measured on the NaHMOR (7% H), see text. [e] see Chapter 2-2. [f] see Chapter 2-3. [g] ref. 23.

The values of ΔH are plotted against the IR wave numbers of νOH in Figure 2-4-26. Experimental errors included in the measured values of ΔH are estimated ± 5 kJ mol^{-1}, but these are small for the IR band position. When the experimental errors are taken into consideration, a weak correlation is observed between the ΔH and IR band positions of OH located in the 12-to 8-member rings, as shown in Figure 2-4-26. The band position of OH is related not only to the force constant of stretching vibration, but also to the structure of oxide[29]. Therefore, as long as similar structures of oxide are concerned, a lower wave number indicates a weaker chemical bond. Under these conditions, the bond length of OH and thus the partial charge of H^+ increases, thereby enhancing the acid strength. Therefore, IR band position is a fundamental parameter, as is the strength of Brønsted acid site on oxides with the similar structures. The straight lines in Figure 2-4-26 show this relationship in the large pores of 12- to 8-member rings of zeolites.

In contrast, the significant deviation from this relationship observed in the small pores may be explained based on the steric effect. In small pores such as in a 6-member ring, the OH could interact with the oxygen wall, and the hydrogen bond thus formed may shift the band position. In other words, interaction of ammonia with the small-pore OH could be suppressed to decrease the value of ΔH. These two explanations may validate the large deviation.

Ammonium cation is usually stabilized on the framework of zeolites as bidentate or tridentate, as reported by Zecchina *et al.*[25]. In particular, these authors reported the tetradentate structure of NH_4^+ on mordenite; this means that ammonia is stabilized on a zeolite species as NH_4^+, depending on the zeolite structure. Based on these considerations, the dependence of the ΔH on the band position should be theoretically true, as long as the same species of zeolite are studied. In Figure 2-4-26, therefore, a relationship observed in various Y zeolites is supported theoretically. The enhancement effect on Brønsted acid strength of Y zeolite by ion-exchanging of polyvalent metal cation will be studied by theoretical methodology in the Chapter 5.

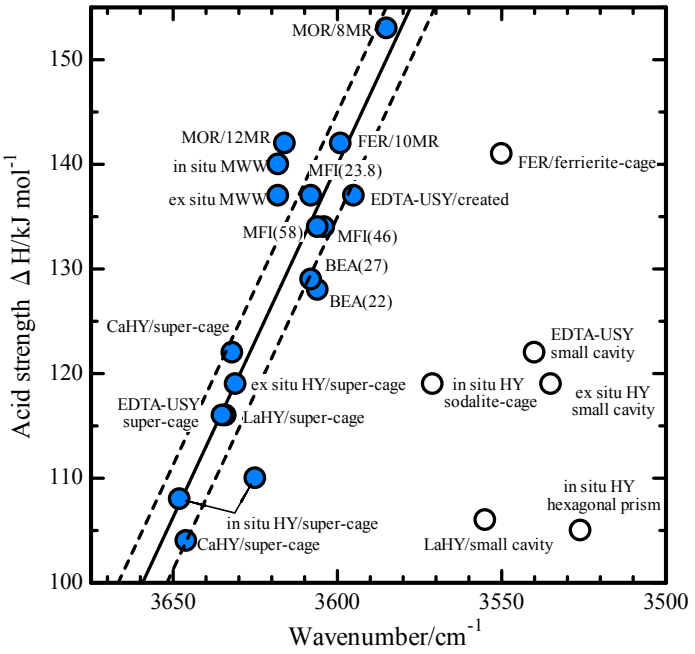

Figure 2-4-26. Plots of acid strength ΔH with band position of OH located in 12-, 10-, and 8-member rings (●), and 6-member ring (○). Lines are drawn in order to show the extent of experimental errors.

Catalytic Activity for Cracking

Plots of the logarithm of TOF of octane cracking against the ΔH are shown in Figure 2-4-27. A strong dependence of the TOF on the ΔH is observed; on many zeolites, the larger the ΔH, the higher the TOF. This means that the cracking activity is closely related to the strength of the Brønsted acid site. Because we selected the reaction conditions for monomolecular catalytic cracking, the reaction is believed to proceed through the pentacoordinated carbonium ion as the reaction intermediate. Under these conditions, it may be postulated that the equilibrium constant of formation of the reaction intermediate is

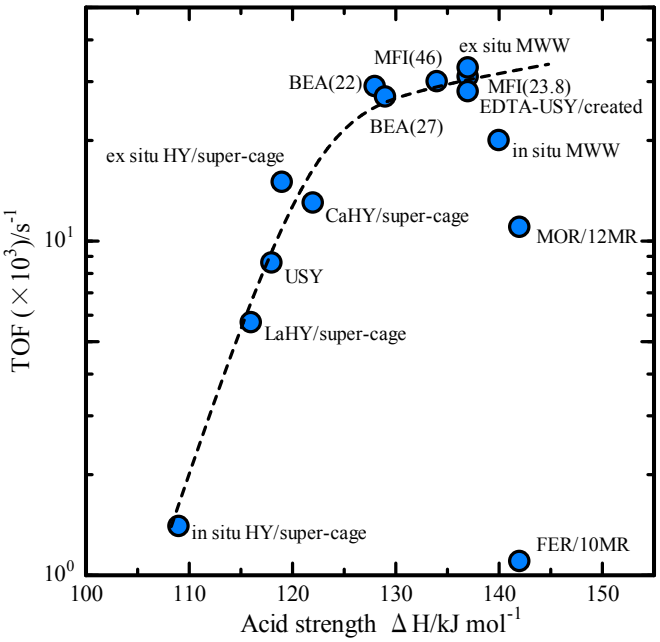

Figure 2-4-27. Dependence of TOF for octane cracking at 773 K upon the acid strength ΔH.

proportional to the strength of the Brønsted acid site, ΔH. Therefore, this relationship suggests that the Brønsted acid sites on these zeolites are the active sites in the cracking of octane, and that carbonium ions are produced on the Brønsted acid sites as the rate-determining step. Significant deviations from this relationship are observed on MOR and FER, however. Steric inhibition of the reaction or deactivation of the site may be postulated to explain these deviations. On the small pore size of FER, the reaction seems to be hindered. A rapid deactivation was observed on the sites of 8-member rings of MOR, and it may affect the reaction on the sites of 12-member ring as well.

When more than two kinds of Brønsted OH are observed, and the contribution of the weaker acid site to the reaction cannot be disregarded, the TOF should decrease as the number of active sites increases. In this case, the value of ΔH is also decreased by averaging the ΔH; therefore, the relationship in Figure 2-4-27 does not change much. For example, when two OH sites in the supercage are assumed to be active sites, the CaHY has 6.3×10^{-3} s^{-1} of TOF at 113 kJ mol^{-1} of ΔH. Similar arguments can be applied to *in situ* HY and EDTA-USY.

Kotrel *et al.*[4] measured the intrinsic monomolecular and bimolecular rate constant for n-hexane cracking. They measured the adsorption of hexane on Na-type zeolites and, by considering the equilibrium constant K and concentration Al, derived the rate constant. The resulting intrinsic rate constants were in the order MFI > BEA > USY > HY; this sequence is not different from ours in the present study (*i.e.*, MFI > BEA > USY > *in situ* HY). Kotrel *et al.*[30] also measured the strength of the acidity using the hydrogen bonding of CO, N_2, and H_2 to the acid sites with IR spectroscopy, and correlated it with the intrinsic rate constant. Their study is based on the concept that the cracking occurs on the active acid site and that the difference in the activity on zeolites is due to the difference in the strengths of acid sites; therefore, their concept is in agreement with ours.

On the other hand, recent studies by van Bokhoven and co-workers[31,32] arrived at a different conclusion, that the cracking activity is primarily controlled not by the strength of acid sites, but rather by the differences in the adsorption of the reactant in the pores of the zeolites. Preceding that study, Miller and Kung and co-workers[13, 33-35] studied the cracking mechanism and active sites on zeolites. They measured the solid acidity of zeolites, particularly on the USY; however, they did not find enhanced active sites, and the enhanced catalytic activity was correlated with the formation of mesopores. However, the presence of enhanced Brønsted acid sites in USY was clearly observed in our previous investigation[8], and detection of the active sites may be one cause of the large difference between their findings and ours. Ramachandran *et al.*[31] measured adsorption of hydrocarbon at 423 K, obviously lower than the reaction temperature; thus, the measured parameters of adsorption do not seem to be directly related to those of the reaction intermediate.

Our present study directly measured the strengths of Brønsted acid sites on various zeolites with an ammonia probe. However, no information on the contact of the reactant on the acid site is available. Further investigation into this matter may be needed.

Conclusion

Using IRMS-TPD of ammonia, we measured the number and strength of the Brønsted acid sites on various zeolites directly and individually. Combined with the catalytic cracking activity, the measured Brønsted acidity is summarized as follows:

(1) The strength of Brønsted acid sites in zeolites is roughly correlated with the IR band position of OH, as

long as it is located in a large pore consisting of a 12- to 8-member ring.

(2) The TOF of catalytic cracking of octane under the conditions of monomolecular reaction is correlated with the strength of Brønsted acid sites, thus implying the predominant role of the Brønsted acid sites in catalytic cracking.

(3) Extinction coefficients of the bending vibration of NH_4^+ on various zeolites are averaged to obtain 9.4± 0.7 cm μmol^{-1}. This will be available as a useful parameter to do the quantitative measurement of Brønsted acid sites from IR observation.

References and Notes

1. P.V. Shertukdte, W.K. Hall, J.-M. Dereppe and G. Marcelin, *J. Catal*., **139**, 468 (1993).
2. Y. Hong, V. Gruver and J.J. Fripiat, *J. Catal*., **161**, 766 (1996).
3. T. Baba, Y. Inoue and Y. Ono, *J. Catal*., **159**, 230 (1996).
4. S. Kotrel, M.P. Rosynek and J.H. Lunsford, *J. Phys. Chem.* B, **103**, 818 (1999).
5. A. Corma, *J. Catal*., **216**, 298 (2003).
6. H. Liu, G.H. Kuehl, I. Halasz and D.H. Olson, *J. Catal*., **218**, 155 (2003).
7. M. Niwa, K. Suzuki, N. Katada, T. Kanougi and T. Atoguchi, *J. Phys. Chem.* B, **109**, 18749 (2005).
8. M. Niwa, K. Suzuki, K. Isamoto and N. Katada, *J. Phys. Chem.* B, **110**, 264 (2006).
9. K. Suzuki, N. Katada and M. Niwa, *J. Phys. Chem. C*, **111**, 894 (2007).
10. M. Hunger, *Catal. Rev. Sci. Eng.*, **39**, 345 (1997).
11. J. Sauer, P. Ugliengo, E. Garrone and V.R. Saunders, *Chem. Rev.*, **94**, 2095 (1994).
12. R.A. van Santen and G.J. Kramer, *Chem. Rev.*, **95**, 345 (1997).
13. B.A. Williams, S.M. Babitz, J.T. Miller, R.Q. Snurr and H.H. Kung, *Appl. Catal. A: Gen.*, **177**, 161 (1999).
14. A. Corma, C. Corell and J. Pérez-Pariente, *Zeolites*, **15**, 2 (1995).
15. Y. Miyamoto, N. Katada, M. Niwa, *Micropor. Mesopor. Mater*., **40**, 271 (2000).
16. N. Katada, H. Igi, J.H. Kim, M. Niwa, *J. Phys. Chem.* B, **101**, 5969 (1997).
17. T. Hashiba, D. Hayashi, N. Katada and M. Niwa, *Catal. Today*, **97**, 35 (2004).
18. J. Datka, B. Gil and P. Baran, *Micropor. Mesopor. Mater*., ***58***, 291 (2001).
19. V.L. Zholobenko, L.M. Kustov, V. Yu. Borovkov and V.B. Kazansky, *Zeolites*, **8**, 175 (1988).
20. R.R. Pinto, P. Borges, M.A.N.D.A. Lemos, F. Lemos, J.C. Vedrine, E.G. Derouane and F.R. Riberio, *Appl. Catal., A: Gen*., **39**, 284 (2005).
21. A. Martucci, A. Alberti, G. Cruciani, P. Radaelli, P. Ciambelli and M.Rapacciulo, *Micropor. Mesopor. Mater.*, **30**, 95 (1999).
22. B. Onida, F. Geobaldo, F. Testa, F. Crea and E. Garrone, *Micropor. Mesopor. Mater.*, **30**, 119 (1999).
23. M. Niwa, S. Nishikawa and N. Katada, *Micropor. Mesopor. Mater*., **82**, 105 (2005).
24. I. Kiricsi, C. Flego, G. Pazzuconi, W.O. Parker, J.R. Millini, C. Perego and G. Bellussi, *J. Phys. Chem*., **98**, 4627 (1994).
25. A. Zecchina, L. Marchese, S. Bordiga, C. Paze and E. Gianotti, *J. Phys. Chem.* B, **101**, 10128 (1997).
26. W.O. Haag and R.M. Dessau, 8th International Congress on Catalysis, Proceedings, vol. II, Verlag Chemie,

Weinheim, 1984, p. 305.

27. W.E. Farneth and R.J. Gorte, *J. Chem. Rev.*, **95**, 615 (1995).
28. A.I. Biaglow, D.J. Parrillo and J.R. Gorte, *J. Catal.*, **144**, 193 (1993).
29. J.A. Lercher, C. Grundling and G. Eder-Mirth, *Catal. Today*, **27**, 353 (1996).
30. S. Kotrel, J.H. Lunsford and H. Knözinger, *J. Phys. Chem.* B, **105**, 3917 (2001).
31. J.A. van Bokhoven, B.A.Williams,W. Ji, D.C. Koningsberger, H.H. Kung and J.T. Miller, *J. Catal.,* **224**, 50 (2004).
32. C.E. Ramachandran, B.A. Williams, J.A. van Bokhoven and J.T. Miller, *J. Catal.*, **233**, 100 (2005).
33. M.A. Kuehne, H.H. Kung, J.T. Miller, J. Catal. 171 (1997) 293.
34. H.H. Kung, B.A. Williams, S.M. Babitz, J.T. Miller and R.Q. Snurr, *Catal. Today*, **52**, 91 (1999).
35. B.A. Williams, J.T. Miller, R.Q. Snurr and H.H. Kung, *Micropor. Mesopor. Mater*., **35–36**, 61 (2000).

Chapter 3.

Combined Study of Ammonia IRMS-TPD Method and Density Functional Calculation on Brønsted Acidity of Zeolite

3-1. Quantitative Measurements of Brønsted Acidity of Zeolites by Ammonia IRMS-TPD Method and DFT Embedded Cluster Calculation

The accurate measurement of solid acidities of zeolites is one of the important subjects in order to analyze those catalytic performances. For this reason, many experimental and theoretical studies of solid acidity of zeolites have been carried out. In the experimental methodologies, the infrared spectroscopy[1, 2], ^{1}H MAS NMR[3], temperature-programmed desorption (TPD) technique[4], microcalorimetry technique[5], Raman spectroscopy[6] and neutron diffraction[7] have been utilized well. On the other hand, first-principle calculations based on the density functional theory (DFT) have developed in recent years, and those have been considered as effective methodology for physicochemical analysis of zeolites[8]. In accordance with the development of theoretical and experimental methodologies, several interesting studies by combined of both techniques have been reported [9, 10].

A combined study of experimental and theoretical methodology is recently becoming a mainstream approach for analyzing of physicochemical property of catalysts. A quantum chemical calculation should be performed on a parallel with an experiment; thus, the theoretical methodology with a low computational cost is more desirable. Therein, DFT has been known as flexible methodology which has a high accuracy and a low cost, and the DFT calculation has been frequently performed by many researchers.

As described in the Chapter 2, IRMS-TPD of ammonia allows to directly determining the OH frequency and the heat of ammonia adsorption on the OH Brønsted acid site. On the other hand, the adsorption energy of base molecule and the frequency of stretching vibration can be calculated based on DFT. Therefore, combined technique of IRMS-TPD and DFT will be established as one of the useful methodology for analysis of Brønsted acidity of zeolites. In this subchapter, our initial attempt for a direct comparison between the experimental and theoretical values of adsorption energies of ammonia on various zeolites will be summarized.

Embedded 8T cluster calculations were carried out with a Dmol^{3} software developed by Accelrys Inc. The geometrical parameters for initial structures of MFI, FER, MWW, MOR, FAU, and BEA were obtained from the Material studio 4.0 library. Embedded 8T cluster models consisting of 8T (Si or Al) sites were cut off from

those structures, and terminated by H atom to keep the neutrality. The position of proton on zeolite was selected according to previous investigations of quantum chemical calculation or neutron diffraction. The Si(OH)Al groups selected as typical acid center were shown in Table 3-1-1, and Figure 3-1-1 shows all calculated cluster models.

Selected acid centers of MFI are Al(11)–O(11)–Si(2) and Al(7)–O(17)–Si(4); and those bridged OH groups locate in straight and sinusoidal 10MR (member-ring) channels, respectively[11]. Acid centers of FER selected are Al(4)–O(6)–Si(4) and Al(3)–O(4)–Si(1). In the neutron diffraction[12], T(4)–O(6)D–T(4) and T(3)–O(4)D–T(1) groups were identified, and those OD groups were reported to locate in the 10MR channel and ferrierite-cage, respectively. Location of the Al atom was decided also from the quantum chemical calculation[11]. MWW has three kinds of acidic OH groups in the super-cage, sinusoidal 10 MR channel and hexagonal prism, and these sites have been attributed to Al(4)–O(3)H–Si(1), Al(3)–O(11)H–Si(2) and Al(2)–O(9)H–Si(5), respectively[13]. Out of 32 OH groups, 17 of them are located in the supercage and 12 MR[14]. Many of the active centers locate in the large cavity, therefore we selected the Al(4)–O(3)H–Si(1) as typical active center. Acid centers of MOR are selected from our previous study[15]; and Al(1)–O(3)H–Si(2), Al(2)–O(2)H–Si(4), and Al(4)–O(2)H–Si(2) in 12 MR and Al(3)–O(1)H–Si(1) in 8 MR are selected. Acid centers of BEA are Al(1)–O(4)H–Si(8) and Al(9)–O(12)H–Si(4) which locate in the 6 MR and 12 MR, respectively[16]. T site of FAU is only one kind, therefore nonequivalent oxygen sites are four kinds. Experimental identification of O(1 – 3)H groups in FAU has been carried out, while O(4)H has not been detected[17]. In this study, we calculated the acidities of O(1 – 3)H groups as active sites.

Table 3-1-1. Adsorption energy of ammonia and geometry parameters for all calculated cluster models and experimental thermodynamics parameters obtained by ammonia IRMS-TPD measurements.

		DFT				Ammonia IRMS-TPD		
	Acid site / position	Composition	∠Si(OH)Al /deg	d(OH) /Å	E_{ads} /kJ mol^{-1}	ΔH /kJ mol^{-1}	Tm /K	ΔU /kJ mol^{-1}
MFI	Al(11)-O(11)-Si(2)/straight 10MR	$AlSi_{37}O_{53}H_{47}$	137.4	0.984	129	137	563	132
	Al(7)-O(17)-Si(4)/sinusoidal 10MR	$AlSi_{40}O_{61}H_{43}$	136.6	0.981	146			
FER	Al(4)-O(6)-Si(4)/10 MR	$AlSi_{43}O_{63}H_{51}$	140.4	0.985	134	142	623	137
	Al(3)-O(4)-Si(1)/ferrierite cage	$AlSi_{34}O_{51}H_{39}$	143.7	0.983	145	141	583	136
MWW	Al(4)-O(3)-Si(1)/super cage	$AlSi_{37}O_{61}H_{31}$	134.4	0.979	133	140	583	135
MOR	Al(1)-O(3)-Si(2)/12MR	$AlSi_{48}O_{70}H_{57}$	129.7	0.980	133	145	603	140
	Al(2)-O(2)-Si(4)/12MR	$AlSi_{47}O_{72}H_{49}$	135.2	0.978	146			
	Al(4)-O(2)-Si(2)/12MR	$AlSi_{47}O_{72}H_{49}$	139.3	0.982	136			
	Al(3)-O(1)-Si(1)/8MR	$AlSi_{48}O_{70}H_{57}$	140.6	0.982	143	153	673	147
BEA	Al(9)-O(12)-Si(4)/12MR	$AlSi_{43}O_{67}H_{43}$	130.6	0.979	133	129	533	125
	Al(1)-O(4)-Si(8)/6MR	$AlSi_{40}O_{64}H_{37}$	137.0	0.984	119			
FAU	Al(1)-O(1)-Si(1)/super cage	$AlSi_{47}O_{78}H_{37}$	130.4	0.976	100	108	443	104
	Al(1)-O(2)-Si(1)/sodalite cage	$AlSi_{47}O_{78}H_{37}$	139.0	0.981	110	119	523	115
	Al(1)-O(3)-Si(1)/D6R	$AlSi_{47}O_{78}H_{37}$	132.2	0.981	93	105	433	101

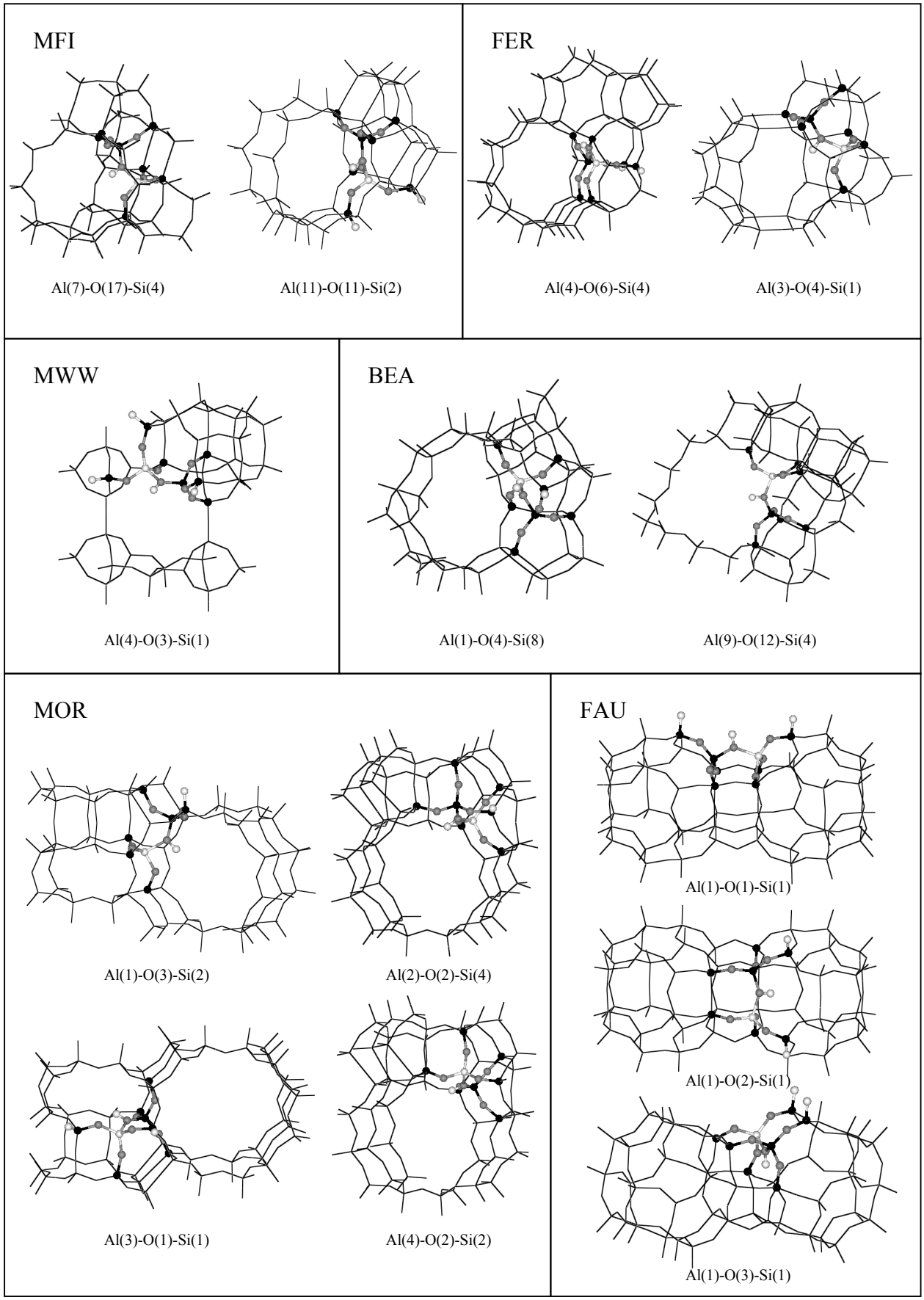

Figure 3-1-1. Embedded 8T clusters. Fixed atoms are drawn as line style, and relaxed atoms are drawn as ball and stick style.

The structure of NH_3, H-Zeolite (H-Z), and NH_3-H-Z were optimized by generalized gradient approximation (GGA) level using Becke−Lee−Yang−Parr (BLYP) exchange and correlation functional. All calculations were performed using the double numerical with polarization (DNP) basis set. The convergence criteria (energy, force, and displacement) were set as 2×10^{-5} Ha, 4×10^{-3} Ha/Å , and 0.005 Å , respectively. The adsorption energy (E_{ads}) was calculated by following equation: $E_{ads} = E_{NH4\text{-}Z} - (E_{H\text{-}Z} + E_{NH3})$, where $E_{NH4\text{-}Z}$, $E_{H\text{-}Z}$, and E_{NH3} are total energy of each structure. E_{ads} from this equation is calculated as negative parameter.

Table 3-1-1 shows parameters of optimized structures of H−Z, E_{ads} of typical acid centers, and experimental parameters obtained by ammonia IRMS−TPD measurements (described in Chapter 2). E_{ads} depended on the structural position of acid site, and those were in a range of 93 to 146 kJ/mol. E_{ads} corresponds to ΔU, and this parameter is equal to $\Delta H - RT_m$, where ΔH is experimentally determined parameter, and R and T_m are gas constant (8.314 JK^{-1} mol^{-1}) and peak maximum temperature of the TPD experiment, respectively.

For example, ΔU in the 12 MR of MOR was 140 kJ mol^{-1}, because ΔH was 145 kJ mol^{-1}. Figure 3-1-2 shows the correlation between the E_{ads} thus calculated and the ΔU experimentally measured. It is extremely interesting that an agreement between E_{ads} and ΔU was found in the various studied zeolites.

It should be aware that E_{ads} obtained by the quantum chemical calculation is influenced by a calculation method (size of cluster model and/or functional). For example, we reported that E_{ads} of acid sites of 12 MR in MOR was 213−220 kJ mol^{-1} (from periodic calculation using LDA[15]), whereas these were reported 142.2−147.9 kJ mol^{-1} (from periodic cluster calculation using GGA[18]) and 119 kJ mol^{-1} (from embedded cluster calculation[19]), respectively. Therefore, the embedded 8T cluster models using GGA approximation is a good method to show accurate values for ammonia adsorption energies on zeolite structures.

In conclusion, the E_{ads}'s calculated by DFT were in good agreement with ΔU of ammonia adsorption on acid sites in various H-form zeolites. This agreement indicates that both methods provide us the acid strength of the zeolite correctly. Therefore, Brønsted acidity, *i.e.*, number, strength, and structure, will be studied more profoundly by combining these advantages of the experiment and the theory. The relationship between the Brønsted acidity and the crystal structure will be discussed in a forthcoming study. Advantage of the embedded 8T cluster method for the Brønsted acidity also will be studied furthermore.

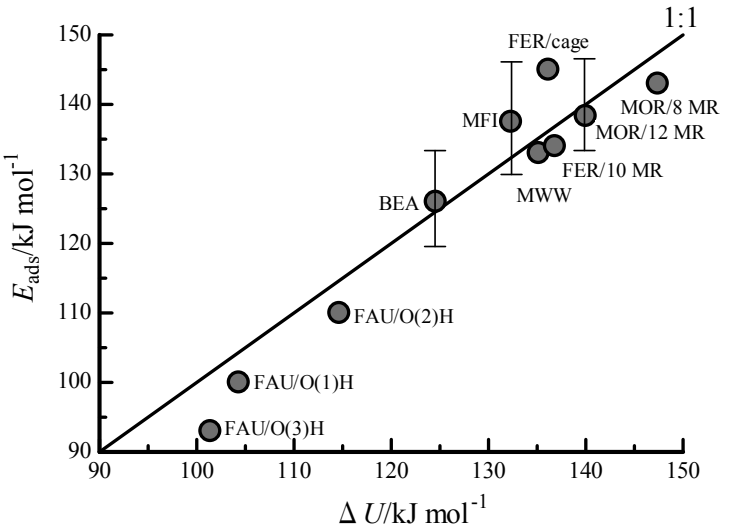

Figure 3-1-2. Correlation between ΔU and E_{ads}.

References and Notes

1. P. A. Jacobs and W. J. Mortier, *Zeolites*, **2**, 226 (1982).
2. J. A. Lercher, C. Grundling and G. Eder-Mirth, *Catal. Today*, **27**, 353 (1996).

3. H. Pfeifer, D. Freude and M. Hunger, *Zeolites*, **5**, 274 (1985).
4. M. Niwa, N. Katada, M. Sawa and Y. Murakami, *J. Phys. Chem*., **99**, 8812 (1995).
5. A. Auroux, *Topic in Catal.*, **19**, 205 (2002).
6. A. H. Hardin, M. Klemes, B. A. Morrow, *J. Catal.*, **62**, 316 (1980).
7. M. Czjzek, H. Jobic, A. N. Fitch, T. Vogt, *J. Phys. Chem*., **96**, 1535 (1992).
8. J. B. Nicholas, *Topic in Catal*., **4**, 157 (1997).
9. M. Boronat, P. Concepción, A. Corma, M. Renz and S. Valencia, *J. Catal.* **234**, 111 (2005).
10. S. Li, A. Zheng, Y. Su, H. Zhang, L. Chen, J. Yang, C. Ye and F. Deng, *J. Am. Chem. Soc*., **129**, 11161 (2007).
11. A. Simperler, R.G. Bell, M.D. Foster, A.E. Gray, D.W. Lewis and M.W. Anderson, *J. Phys. Chem.* B, **108**, 7152 (2004).
12. A. Martucci, A. Alberti, G. Cruciani, P. Radaelli, P. Ciambelli and M. Rapacciulo, *Micropor. Mesopor. Mater.,* **30**, 95 (1999).
13. D. Zhou, Y. Bao, M. Yang, N. He and G. Yang, *J. Mol. Catal. A: Chem*., **244**, 11 (2006).
14. G. Sastre, V. Fornes and A. Corma, *J. Phys. Chem.* B, 104, 4349 (2000).
15. M. Niwa, K. Suzuki, N. Katada, T. Kanougi and T. Atoguchi, *J. Phys. Chem.* B, **109**, 18749 (2005).
16. H. Fujita, T. Kanougi and T. Atoguchi, *Appl. Catal. A: Gen*. **313**, 160 (2006).
17. K. Suzuki, N. Katada and M. Niwa, *J. Phys. Chem.* C, 111, 894 (2007).
18. M. Elanany, D. P. Vercauteren, M. Koyama, M. Kubo, P. Selvam, E. Broclawik and A. Miyamoto, *J. Mol. Catal. A: Chem.* **243**, 1 (2006).
19. M. Braöndle and J. Sauer, *J. Am. Chem. Soc.*, **120**, 1556 (1998).

3-2. Ammonia IRMS-TPD measurements and DFT calculation on acidic hydroxyl groups in CHA-type zeolite

Synopsis

Brønsted acidity of H-CHA zeolite (Si/Al_2 = 4.2) was investigated by means of ammonia infrared-mass spectrometry/temperature-programmed desorption (IRMS-TPD) method and density functional calculations. Four IR bands were observed at 3644, 3616, 3575 and 3538 cm^{-1}, and they were ascribable to the acidic OH groups on four nonequivalent oxygen sites in the CHA structure. The absorption band at 3538 cm^{-1} was attributed to the O4H in the 6MR (6 membered-ring), and ammonia adsorption energy (ΔU) of this OH group was the lowest among the 4 kinds of OH groups. The other 3 bands were assigned to the acidic OH groups in 8MR. It was observed that the ΔU in 8 and 6 MR were 131 (± 3) and 101 kJ mol^{-1}, respectively. On the other hand, the density functional calculations within periodic boundary conditions yielded the adsorption energies on these OH groups in 8 and 6 MR to be ca. 130 and 110 kJ mol^{-1}, respectively, in good agreement with the experimentally observed values.

Introduction

Quantum chemical calculations have been frequently applied for analyzing chemical property of zeolites, and supporting the experimental findings. For example, deprotonation energy (or proton affinity)[1], adsorption energy of base molecule[2], frequency of stretching vibration of OH groups[3] have been calculated to understand the solid acidity.

CHA structure consists of D6Rs (double six-rings) which are connected with tilted 4MRs, and its main channel is 8MR. All tetrahedral (T) sites are equivalent; therefore four kinds of nonequivalent oxygen sites exist. Those oxygen sites were labeled as O1 – 4 according to literature[13], as shown in Figure 3-2-1. Nature of the structurally different four acid sites in CHA-type zeolite has been studied by quantum chemical calculations[3,14-16, 27, 30-34]; the number of atoms in the unit cell of CHA is very small (36 atoms), which enables a rapid and easy calculation. However, experimental measurements of solid acidity of CHA-type zeolite have not been carried out sufficiently; therefore no comparison between experimental and theoretical values has been performed. In this study, we will study the Brønsted acidity of high-aluminum H-CHA by means of the ammonia IRMS-TPD method, and compare it with the density functional calculation within periodic boundary conditions.

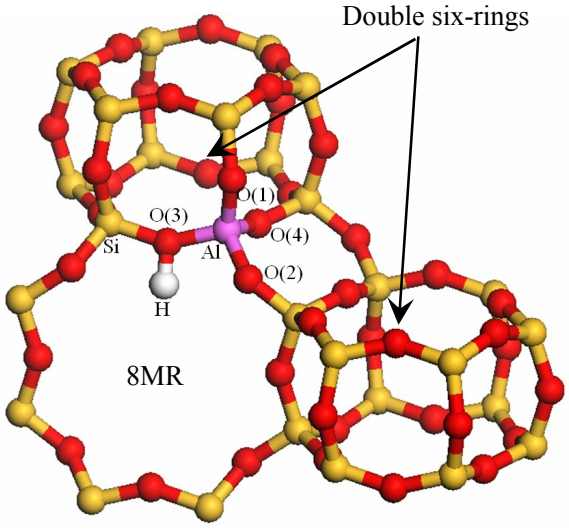

Figure 3-2-1. Four kinds of structurally-non-equivalent Brønsted acid sites (O1 – 4H) in CHA structure. O3H is shown as an example.

Experimental and Calculation Methods

Materials

A CHA-type zeolite was synthesized from HY zeolite (Si/Al_2=5.3, JRC-Z-HY5.3, a reference catalyst supplied by Catalysis Society of Japan) as parent material[17]. The HY was treated with a 2 mol dm^{-3} KOH solution at 368 K for 96 h in a polypropylene bottle; the product was filtered and twice washed with de-ionized water. The thus synthesized K-CHA zeolite was ion-exchanged in a solution of NH_4NO_3 at 353 K for 4 h. The chemical composition was measured by an inductively coupled plasma emission spectrometer (ICP-ES, Rigaku CIROS CCD). The K-CHA had 5.14 and 4.61 mol kg^{-1}, and the ion-exchanged NH_4K-CHA had 5.80 and 0.36 mol kg^{-1} of Al and K, respectively. The exchange degree (NH_4^+/Al calculated from 1-K/Al) of NH_4K-CHA was 94 %, and this sample was named 94NH_4K-CHA.

The crystal structure of ion-exchanged sample was analyzed by a Rigaku Miniflex plus X-ray diffractometer (XRD) with 0.45kW CuKα X-ray source (30 kV, 15 mv).

^{29}Si and ^{27}Al magic-angle spinning (MAS) NMR spectra were recorded by a JEOL ECP300 spectrometer with a spinning speed 5.0 kHz. The chemical shift is shown with an aqueous solution saturated with $Al_2(SO_4)_3$ as a standard material for ^{27}Al, and polydimethylsilane was used as a standard of chemical shift at -34 ppm for ^{29}Si.

IRMS-TPD of Ammonia

IR (Perkin-Elmer Spectrum-One with a mercury cadmium telluride (MCT) detector kept at 77 K by liquid N_2 during measurements) and MS (Pfeifer QME200) spectrometers were connected with a vacuum line. NH_4K-CHA wafer (about 10 mg and 10 mm in diameter) was mounted on a holder in an in situ IR cell, and evacuated at 773 K for 1h. IR spectra were recorded before and after ammonia adsorption during the elevation of temperature from 373 to 773 K at a ramp rate of 10 K min^{-1}. Flow rate of helium carrier gas was 82 μmol s^{-1}, the inside of IR cell was kept 25 Torr (1 Torr = 133 Pa), and desorbed ammonia was monitored by MS based on a signal at m/e = 16. After the measurements, the difference IR spectra were calculated, and the differential change of the IR band area with respect to measurement temperature (hereafter called IR-TPD) was compared with MS-TPD (conventional TPD) to quantify the ammonia species adsorbed on Brønsted or Lewis acid site. It has been known that the wave number of acidic OH band on zeolites shifts to lower frequency with increasing the temperature[9]. This temperature effect on frequency of OH band (νOH) is estimated as $\Delta\nu/\Delta T$ = - 0.052 $cm^{-1}K^{-1}$ where $\Delta\nu$ is the shift of νOH and ΔT is the difference of temperature. Difference spectra of ammonia in the OH stretching region were corrected using this equation. Heat of ammonia adsorption (ΔH) as a parameter to show the strength of the acid site was determined based on the theoretical equation of TPD[18]. In this study, change of entropy upon desorption was determined experimentally as ΔS, 40 J K^{-1} mol^{-1}.

DFT Calculation

Density functional calculations within periodic boundary conditions were performed by using Dmol^3 software[19] (Accelrys Inc.). Geometry optimization and energy calculation were based on a generalized gradient approximation (GGA) level using Hamprecht-Cohen-Tozer-Handy (HCTH) exchange and correlation functional[20]. All calculations were performed using a double numerical polarization (DNP) basis set. The convergence

criteria (energy, force and displacement) were set as 2×10^{-5} Ha, 4×10^{-3} Ha/Å, and 0.005 Å, respectively. The adsorption energy (E_{ads}) was calculated on the basis of the following equation: $E_{ads} = (E_{H\text{-}Z} + E_{NH3}) - E_{NH4\text{-}Z}$, where $E_{NH4\text{-}Z}$, $E_{H\text{-}Z}$, and E_{NH3} were total energies of NH_4-zeolite, H-zeolite and gaseous ammonia, respectively.

The initial structure of CHA was obtained from the Material studio 4.0 library. This unit cell had the lattice parameters a = b = c = 9.421 Å, $\alpha = \beta = \gamma = 94.20$ °. Composition of the unit cell of the acidic structure was assumed to be $HAlSi_{11}O_{24}$; therefore Si/Al_2 ratio in the model was 22.

Results and Discussion

Characterization of Materials

Figure 3-2-2 shows that the XRD pattern of $94NH_4K$-CHA was in agreement with that of CHA structure, and no additional peak was detected.

^{29}Si MAS NMR spectrum (Figure 3-2-3 (a)) showed Si(0Al), Si(1Al), Si(2Al), Si(3Al) and Si(4Al) at -109.8, -104.1, -98.5, -93.3 and -90.3 ppm, respectively[21]. The strongest signal was that of Si(2Al). Figure 3-2-3 (b) shows ^{27}Al MAS NMR spectrum. A strong resonance ascribed to tetrahedral Al was observed at 60 ppm, while almost no signal was observed at 0 ppm. Thus, it was found that the $94NH_4K$-CHA was almost free from extra-framework aluminum.

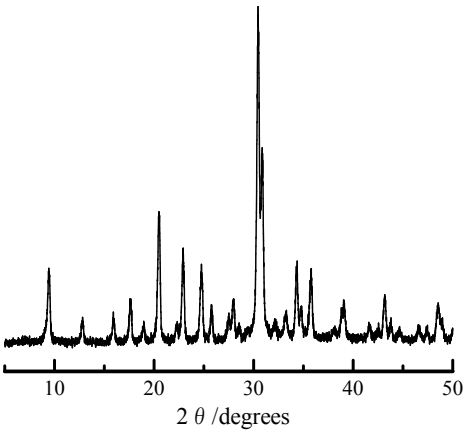

Figure 3-2-2. XRD pattern of ion-exchanged $94NH_4K$-CHA.

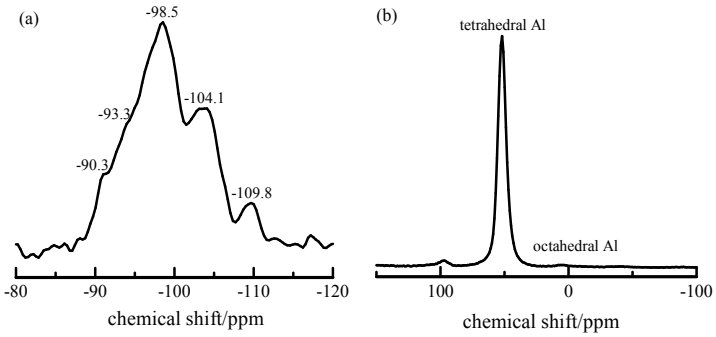

Figure 3-2-3. MAS NMR spectrum of ion-exchanged $94NH_4K$-CHA. (a) ^{29}Si MAS NMR spectrum, (b) ^{27}Al MAS NMR spectrum.

IRMS-TPD: Quantitative Analysis

Figure 3-2-4 shows the difference IR spectra of adsorbed ammonia in the range of 4000 to 1250 cm^{-1} on in situ prepared 94HK-CHA, namely, $94NH_4K$-CHA evacuated at 773 K in the IR cell and measured without exposing atmosphpere. These spectra were observed at temperatures from 373 to 773 K in the TPD experiment, and the reference spectrum taken at 373 K was shown altogether. Observed positive peaks were assigned to adsorbed ammonia species, and these intensities decreased accompanied by the thermal decomposition of NH_4^+ species. In contrast, negative peaks were assigned to the acidic OH bands, and these intensities were restored with desorption of NH_3.

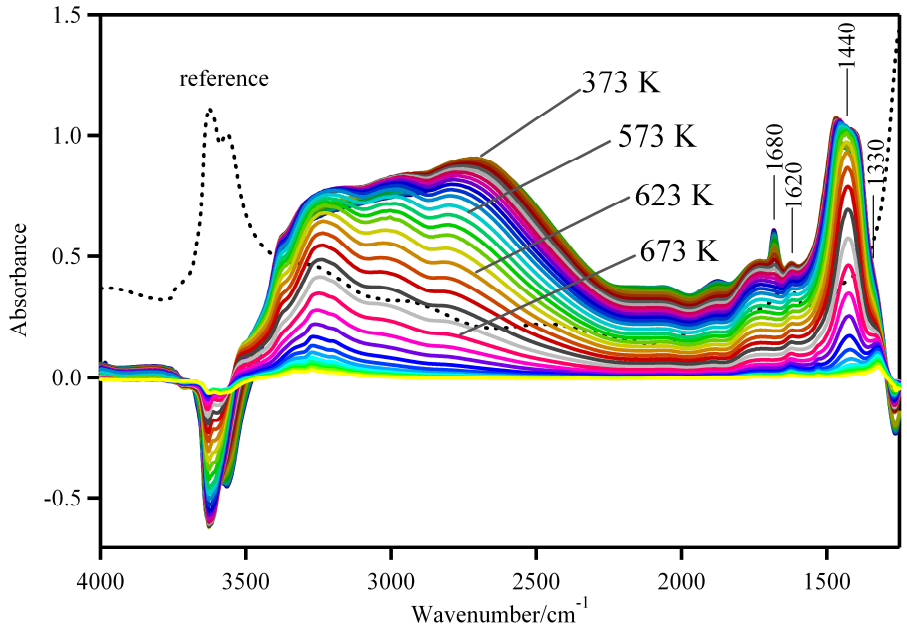

Figure 3-2-4. Difference spectra obtained during TPD of ammonia at 373 to 773 K on *in situ* prepared 94HK-CHA. A reference spectrum before adsorption of ammonia measured at 373 K was included as a comparison.

A broad absorption observed in the range of 3400 to 2000 cm^{-1} is attributed to the NH stretching vibration[22]. A sharp band at *ca.* 1440 cm^{-1} was assigned to the bending vibration of NH_4^+ on Brønsted acid site, and a small absorption at 1620 cm^{-1} was assigned to NH_3 coordinated on Lewis acid site[5]. A small absorption at 1330 cm^{-1} showed the presence of strongly adsorbed NH_3 species on the dislodged Al with Lewis acidity[5]. However, the attribution of 1680 cm^{-1}-band has not been made clear. This absorption was observed also on the HY zeolite, and we tentatively assign it to a weak adsorption of ammonia (NH_3 and/or NH_4^+) perturbed by a steric hindrance due to small window of D6Rs[8]. In order to quantitatively analyze the band intensity, a deconvolution was performed as shown in Figure 3-2-6. The absorption bands at 1495, 1450 and 1390 cm^{-1} due to bending vibrations of NH_4^+ were assumed, and the IR-TPD of those species were calculated to show the TPD behavior of adsorbed ammonia on the Brønsted acid sites.

Figure 3-3-5 shows an enlarged portion of the difference spectra of OH bands in the range of 3750 to 3450 cm^{-1}. Two kinds of acidic OH (Si(OH)Al) groups were observed at 3622 and 3564 cm^{-1} in the reference spectrum (dotted line). On the other hand, the negative absorption due to adsorption of ammonia indicates the presence of a new OH band at 3644 cm^{-1}. Two kinds of acidic OH bands at high (OH_{HF}) and low frequencies (OH_{LF}) have been assigned to OH groups located in 8 and 6 member rings, respectively, in a previous study[2]. Therefore, this new OH band at 3644 cm^{-1} would be assigned to the acidic OH group in 8MR.

Figure 3-2-6 shows examples of deconvolution of difference spectra of NH_4^+ and OH. In our recent study[8], we assumed that the width of OH band increased linearly with a decrease in the peak frequency according to the findings by Onida *et al.*[23] The assumed width (standard deviation, σ) of those bands were 14, 17, 21, 26 cm^{-1}, and the correlation between the ν(OH) and σ was described with the following equation; $\sigma = -0.11\nu(OH) + 423$.

This equation is almost the same as previously applied to the HY (σ = -0.12ν(OH) + 441)[8]. The difference spectra were divided into the four kinds of acidic OH bands at 3644, 3616, 3575 and 3538 cm^{-1}. The IR band at the lowest frequency (3538 cm^{-1}) was fully recovered even at the low temperature (*ca.* 473 K), while the OH bands at 3644, 3616 and 3575 cm^{-1} showed the negative peaks up to the temperatures higher than 643 K.

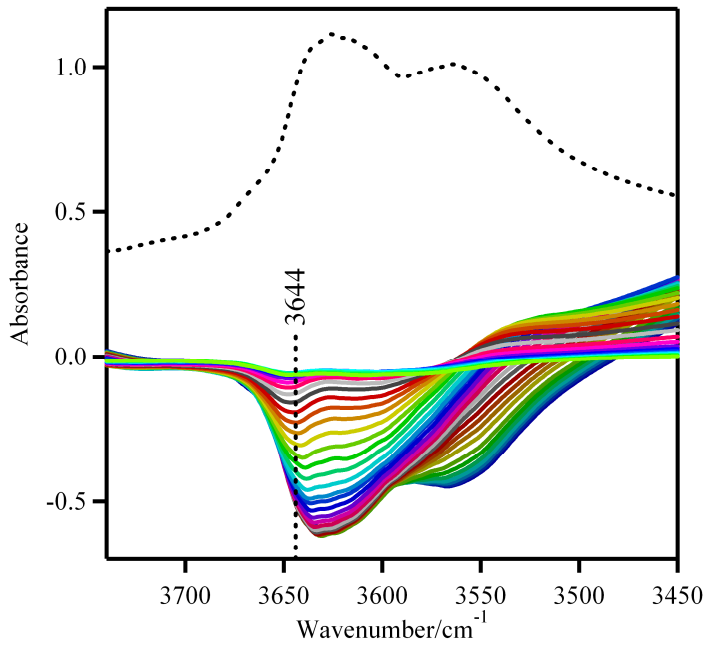

Figure 3-2-5. Enlarged portion of OH stretching region in Figure 3-2-4.

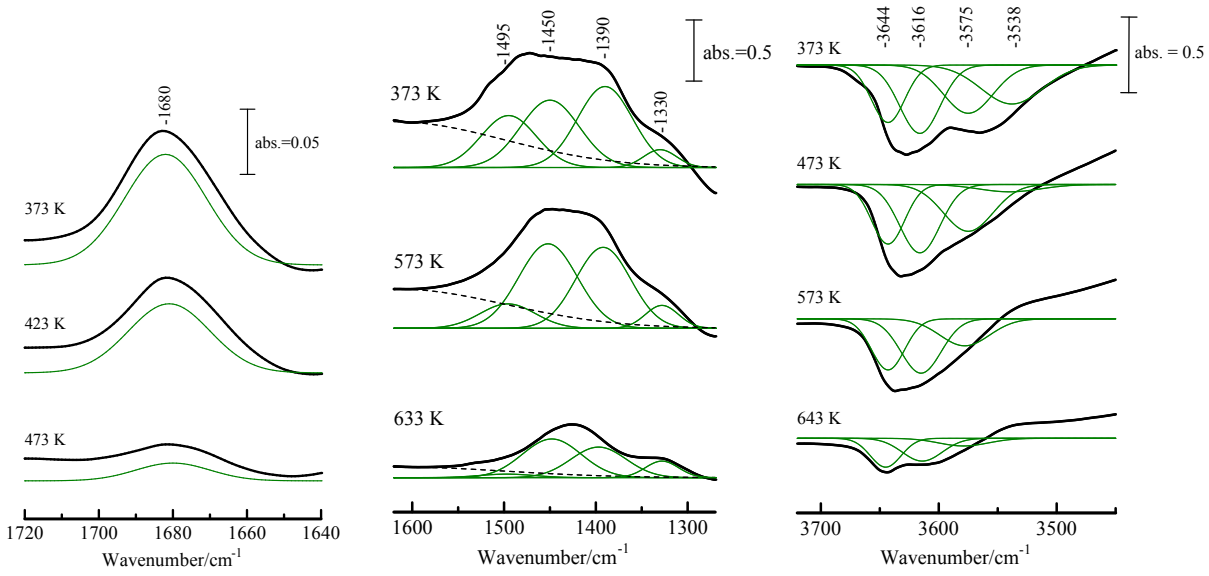

Figure 3-2-6. Deconvolution of difference spectra of NH_4^+ bending vibration and OH stretching vibration.

There are four kinds of crystallographically different bridging oxygen sites in the CHA structure; *i.e*., the O1 – 3H located in the 8MR, and the O4H in the 6MR, as shown in Figure 3-2-1. The IR bands at 3616 and 3575 cm^{-1} are probably assigned to the O1H and the O3H, because those frequencies are similar to the reported frequencies of O1H (3603 cm^{-1}) and O3H (3579 cm^{-1}) on a high-silica H-CHA (H-SSZ-13)[24]. Thus, the additional peaks at 3644 and 3538 cm^{-1} can be assigned to other sites. Spoto *et al.*[25] recently assigned the OH_{HF} and OH_{LF} bands to the O1 – 3H and O4H, respectively. On the other hand, Smith *et al.*[26] assigned three kinds of OH on H-SAPO-34 at 3630, 3625 and 3601 cm^{-1} to O2H, O1H, and O3H, respectively. In addition, an IR band at 3526 cm^{-1} was attributed to the O3H located in D6Rs in HY[8], whose structure should be strongly related with CHA. Taking into account these findings, the OH bands at 3644 and 3538 cm^{-1} are considered to be O2H and O4H, respectively.

Assignments of OH bands previously reported from neutron diffraction and quantum chemical calculations were summarized in Table 3-2-1. With an exception[27], the four OH bands can be divided into OH_{HF} (O1H and O2H) and OH_{LF} (O3H and O4H)bands; and this supports the present assignment. Torres *et al*.[27] reported that O4H and the surrounding oxygen atoms interacted weakly to form a hydrogen bond, and hence the wave number of O4H was the smallest among the four kinds, also supporting our attribution.

Table 3-2-1. IR frequencies of stretching vibration of four non-equivalent acidic OH groups in CHA.

	ν(OH)/cm^{-1}			
	O1H	O2H	O3H	O4H
Experiment				
Ammonia IRMS-TPD	3616	3644	3575	3538
Neutron diffraction[a]	3603	-	3579	-
Calculation				
Periodic[b]	3578	3541	3514	3532
Periodic[c]	3816	3791	3803	3776
Periodic[d]	3875	3920	3820	3815
Periodic[e]	3590.1	3596.7	3572.8	3577.8
Embedded[f]	3601		3574	

[a] ref. 24. [b] ref. 16. [c] ref. 27. [d] ref. 31. [e] ref. 34. [f] ref. 15.

IR-TPD of the adsorbed ammonia species and acidic OH groups are shown in Figure 3-2-7, altogether with MS-TPD of ammonia. MS-TPD showed two kinds of desorption peaks at *ca.* 450 and *ca.* 610 K. IR-TPD of adsorbed ammonia species and acidic OH groups showed complex profiles. From the comparison of IR-TPD of NH_4^+ (1495, 1450 and 1390 cm^{-1}) with MS-TPD, the main desorption peak at *ca.* 610 K was assigned to the desorption of ammonia from NH_4^+ adsorbed on Brønsted acid site. On the other hand, IR-TPD of NH_3 (1330 cm^{-1}) showed a broad desorption profile, and the desorption temperature was in the range of 593 to 773 K. On the other hand, the desorption peak at *ca.* 450 K almost resembled the behavior of IR-TPD of NH_4^+ (1680 cm^{-1}).

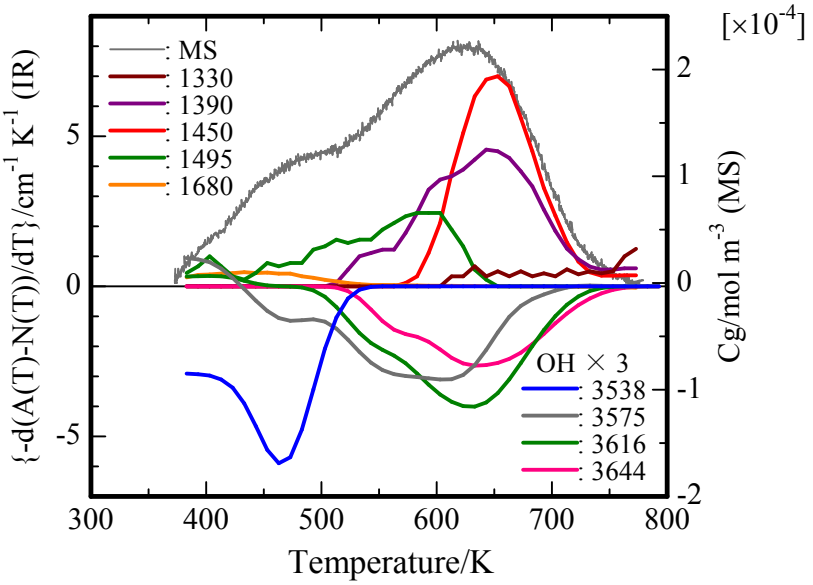

Figure 3-2-7. Comparison between MS-TPD and IR-TPD of adsorbed ammonia species (NH_4^+ = 1495, 1450 and 1390, NH_3 = 1330, NH_4^+ and/or NH_3 = 1680) and acidic OH groups (3644, 3616, 3575 and 3538). IR-TPD of OH was magnified by 3.

Four kinds of IR-TPD of acidic OH bands showed different temperature profiles. IR-TPD of the O2H (3644 cm^{-1}) showed a peak at the highest temperature, *ca.* 633 K, and temperature of other desorptions were in the order; O1H (3616 cm^{-1}) (623 K) > O3H (3575 cm^{-1}) (593) > O4H (3538 cm^{-1}) (463). From the comparison of IR-TPD of NH_4^+ (1495, 1450 and 1390 cm^{-1}) with IR-TPD of the latter three OH (3644, 3616 and 3575 cm^{-1}), a negative relation was observed between the wave number and desorption temperature. At the low temperature of about 480 K, the lowest frequency component *i.e.*, (O4H/3538) was restored and, simultaneously, the band due to NH_4^+ or NH_3 (1680 cm^{-1}) decreased, thus showing their correlation.

Quantitative Measurements of Brønsted OH Bands

Next, we calculated the Brønsted acid amount and strength by means of a curve fitting method. Sum of IR-TPD curves must be equal to MS-TPD, *i.e*, change of gaseous concentration of ammonia with temperature. Therefore, a curve fitting was attempted to obtain parameters A – D, in an equation $AI_{1680}+BI_{1495}+CI_{1450}+DI_{1390}$ where I ν meant the IR-TPD at ν cm^{-1}. The parameters A – D correspond to reciprocal of the extinction coefficients of these bands. As shown in Figure 3-2-8 (a), the calculated curve $19I_{1680}+5I_{1495}+1I_{1450}+2.5I_{1390}$, had a similar shape to MS-TPD. These parameters were selected analogous to those on HY zeolite (A: 19, B: 3.3, C: 1 and D: 3.3)[8]. The thus corrected IR-TPD profile shows the rate of desorption of ammonia from each type of acid sites, and the sum of the corrected IR-TPDs of 1495, 1450 and 1390 must show the property of Brønsted acid sites.

At 480 K, IR-TPDs of O4H (3538 cm^{-1}) and NH_3 (1680 cm^{-1}) showed the peaks. As shown in Figure 3-2-8 (b), $-4.2I_{3538}$ could be fitted to the corrected IR-TPD of 1680 cm^{-1}-band. Thus, it is postulated that the species showing the band at 1680 cm^{-1} is an NH_4^+ species adsorbed on the O4H. Then, a curve fitting was attempted to get the parameters L – N giving the best fitted curve between $LI_{3644}+MI_{3616}+NI_{3575}$ and the corrected IR-TPD of

Brønsted acid site determined as above. Bordiga *et al.*[28] reported that the OH_{LF} groups have a larger extinction coefficient than OH_{HF} groups. Therefore, reciprocal number of the extinction coefficients of the OH_{LF} groups must be smaller than OH_{HF} groups. As shown in Figure 3-2-8 (b), L - N were -8.3, -7.6 and -6.2, respectively. Thus, the coefficient of O4H (3538 cm^{-1}) was -4.2, and the number was the lowest among the four OH bands.

Amounts and strengths of the four kinds of OH were then calculated on the basis of the equation which we derived theoretically for ammonia TPD[29], as summarized in Table 3-2-2. Adsorption heats of ammonia (ΔH, an index of acid strength) on the four kinds of OH groups at 3644, 3616, 3575 and 3538 cm^{-1} were 139, 136, 133 and 105 kJ mol^{-1}, respectively. Extinction coefficients of four kinds OH bands calculated from the parameters at 373 K were shown in Table 3-2-2. In addition, the extinction coefficient of the NH_4^+ (at *ca.* 1440 cm^{-1}) was 9.1 cm μmol^{-1}, and this value is almost the same as reported in our previous study for NH_4^+ adsorbed on various zeolites (9.4 cm μmol^{-1})[9].

In the study of HY[8], a mirror-image relation was observed between IR-TPD of NH_4^+ (1496, 1430 and 1369 cm^{-1}) and IR-TPD of OH located in super cage and sodalite cage (3648, 3625 and 3571 cm^{-1}). In addition, IR-TPDs of NH_4^+ (1665 cm^{-1}) and OH located in D6Rs (3525 cm^{-1}) showed a similar positive-negative profile, and an ammonia desorption peak was observed at the low-temperature. As shown above, these profiles of IR-TPD in the HY zeolite resembled the observation of H-CHA. Thus, the assignment of the absorption peak at 1680 cm^{-1} in H-CHA would be similar to the absorbed species observed at 1665 cm^{-1} in H-Y.

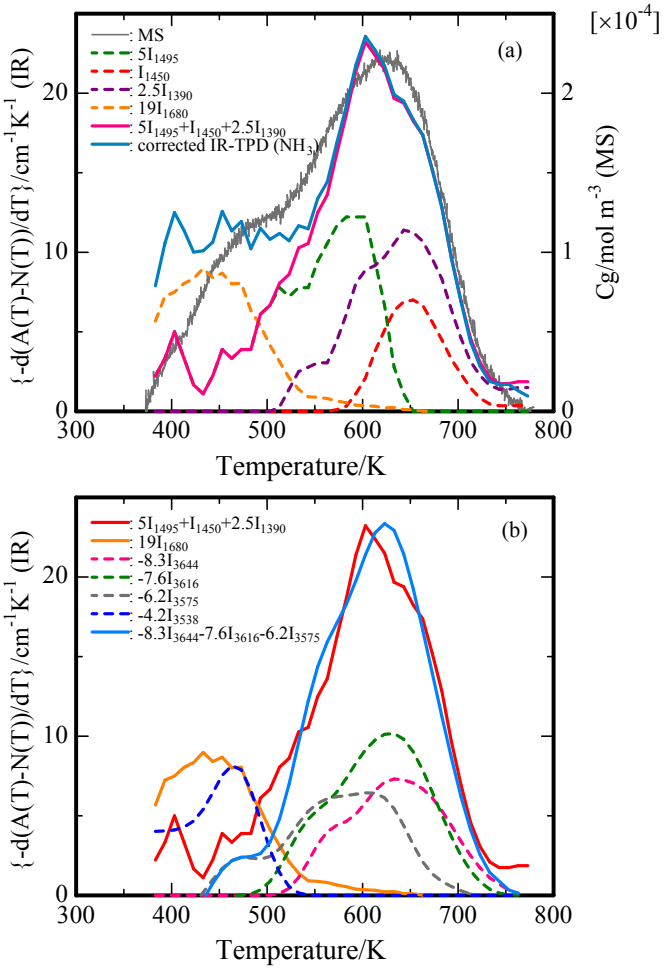

Figure 3-2-8. Curve fitting of corrected IR-TPD for OH and ammonia bands to MS-TPD: (a) fitting of sum of IR-TPD for adsorbed ammonia species to MS-TPD; (b) fitting of IR-TPD profiles of OH and adsorbed ammonia; at the low temperature, OH (3538 cm^{-1}) and NH_4^+ (1680 cm^{-1}); at the high temperature, OH (3644, 3616, and 3575 cm^{-1}) and NH_4^+ (1495, 1450, and 1390 cm^{-1}).

Table 3-2-2. Assignment, number, strength, and extinction coefficient of OH on $94NH_4K$-CHA obtained from IRMS-TPD.

ν(OH) /cm^{-1}	Assignment	A_0 /mol kg^{-1}	ΔH /kJ mol^{-1}	T_m /K	ΔU /kJ mol^{-1}	ε(OH) /cm μmol^{-1}
3644	O2H	0.50	139	633	134	2.9
3616	O1H	0.65	136	623	131	3.2
3575	O3H	0.52	133	593	128	3.6
3538	O4H	0.40	105	463	101	4.7

DFT Calculations

Finally, we calculated the adsorption energy of ammonia by a DFT calculation using periodic boundary condition. First, we performed the geometry optimization of pure siliceous CHA, and compared it with experimental structure of H-SSZ-13 ($Si/Al_2 = 32$). The calculated geometrical parameters for the pure siliceous CHA and the experimental values[24] of H-SSZ-13 are compared in Table 3-2-3. The theoretical calculated values of Si-O bond length (1.626 to 1.639 Å) almost agreed with the experimental values (1.599 to 1.617 Å). The calculated values of SiOSi angle assigned to the O1 – 4 (146.8, 151.0, 150.0, 147.6°) also were in good agreement with the experimental values (144.8, 150.0, 149.4 and 147.8°). It was therefore confirmed that good geometric parameters were given by the present calculation method.

Next, we calculated the geometrical parameters of the H-form CHA ($Si/Al_2 = 22$) which was studied in the present paper, as shown in Table 3-2-4. The Si-O bond lengths in the SiO(H)Al linkages were 1.710 – 1.729 Å, and those were slightly longer than values of Si-O in SiOSi calculated in the pure siliceous CHA (Table 3-2-3). This observation is supported by the previous finding, because it is widely known that Si-O bond lengths in Si(OH)Al linkages are longer than those in SiOSi linkages[32]. The Si-O and Al-O bond lengths obtained from the present study were in good agreement with those parameters from *ab initio* calculations[33] (1.697 – 1.714 Å, and 1.876 – 1.938 Å), respectively.

Table 3-2-3. Geometrical parameters of the optimized structures of siliceous CHA structure and experimental parameters of SSZ-13[a].

	Si-O/Å		SiOSi/deg.	
	Calc.	Exp.	Calc.	Exp.
O1	1.626	1.617	146.8	144.8
O2	1.630	1.613	151.0	150.0
O3	1.631	1.599	150.0	149.4
O4	1.639	1.615	147.6	147.8

[a] Experimental values are taken from the neutron diffraction study of the H-SSZ-13 ($Si/Al_2 = 32$) in ref. 23.

On the other hand, the calculated Si(OH)Al angles assigned to the O1 – 4 in Table 3-2-4 were smaller than the corresponding SiOSi angles in Table 3-2-3, and the difference between those parameters was almost the same (*ca.* 12.1 °). On the other hand, the theoretical values of Si(OH)Al angle obtained in this study (132.3, 138.1, 137.1 and 136.1 °) in Table 3-2-4 were in agreement with those by *ab initio* calculation[33] (132.9, 135.2, 136.8 and 135.2 °). Thus, geometrical parameters of bond length Si-O and bond angle Si(OH)Al optimized for the H-CHA structure by the present calculation were confirmed.

Table 3-2-4. Geometrical parameters of the optimized structures of H-form CHA (1 Al/u. c.) and the adsorption energies of ammonia.

	E_{rel} /kJ mol^{-1}	E_{ads} /kJ mol^{-1}	AlO(H)Si /deg.	d(Si-O) /Å	d(Al-O) /Å	d(O-H) /Å
O(1)	0	127.9	132.3	1.711	1.955	0.964
O(2)	11.0	129.3	138.0	1.712	1.912	0.967
O(3)	2.7	131.3	137.1	1.710	1.928	0.966
O(4)	6.7	110.1	136.1	1.729	1.966	0.966

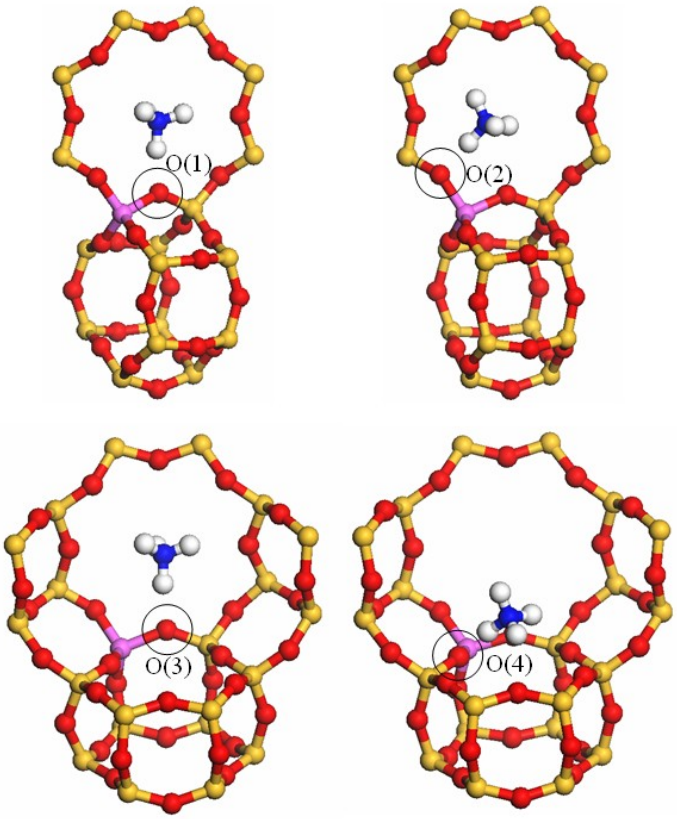

Figure 3-2-9. Optimized structures of NH_4^+ on O1 – O4 of CHA

The optimized NH_4-form CHA structures are shown in Figure 3-2-9, and E_{ads} are summarized in Table 3-2-4. Ammonium cation on the O 1 – 3 were stabilized in 8MR, while NH_4^+ on O4 was stabilized in 6MR. No significant difference was observed in the E_{ads} on O1 – 3H, while that on O4H only was obviously weak (110.1 kJ mol^{-1}).

It is noteworthy that E_{ads} obtained from the quantum calculation corresponds to $\Delta U = \Delta H - RT_m$, where T_m is the peak maximum temperature of the TPD measurement, and R is gas constant (8.314 J K^{-1} mol^{-1}). ΔU of acid sites located in 8MR (O1 – 3H) and 6MR (O4H) were thus 131 ± 3 and 101 kJ mol^{-1}, respectively. E_{ads} obtained in the present study using GGA of HCTH calculations are therefore in good agreement with those experimental parameters.

Additionally, the E_{ads} on acid sites in H-CHA calculated by several kinds of methods are compared. For example, reported E_{ads} of O1 – 4 from periodic boundary calculation using GGA of Perdew-Wang 91 (PW91) were 149.3, 142.9, 144.5 and 135.7 kJ mol^{-1}, respectively[16]. Absolute values are larger than in the present study; however those are roughly divided into three larger and one smaller OH, which is in agreement with our values. The value of O1 from periodic boundary calculation using GGA of Becke3-Lee-Yang-Parr (B3LYP)[30] was 134 kJ mol^{-1} in good agreement with the present experimental parameter (131 kJ mol^{-1}). The adsorption energies of ammonia (ΔU) obtained from the IRMS-TPD measurement are therefore supported by the DFT calculations; in other words, the assumed assignments of the acidic OH bands are also supported.

Stabilities of acid sites (E_{rel}) were in the order: O1H (0 kJ mol^{-1}) > O3H (2.7) > O4H (6.7) > O2H (11.0). The stable OH sites determined from the calculation were therefore O1H and O3H, and this agrees with the neutron diffraction study[24]. Furthermore, most researchers indicated that the O1H was the most stable acid site[30-33]. Amounts of acid sites assigned to O1H, O2H, O3H and O4H were 0.65, 0.50, 0.52 and 0.40 mol kg^{-1}, respectively. The highly occupied site determined by ammonia IRMS-TPD method was the O1H; and this is in good agreement with the theoretical calculation.

Conclusions

We investigated the Brønsted acidity of H-CHA by ammonia IRMS-TPD measurement and density functional calculation. This study is a first attempt for a direct comparison between the experimental and theoretical values of adsorption energies of ammonia on Brønsted acid sites in H-CHA. The findings in the present study are summarized.

(1) High-aluminum H-CHA has four kinds of acidic OH groups assigned to the structurally different oxygen atoms. The O1 – 3H were located in the 8MR, and those absorption bands were observed at 3644 – 3575 cm^{-1}. On the other hand, the absorption band of O4H which was located in the 6 MR was observed at 3538 cm^{-1}.

(2) The energies of ammonia adsorption (ΔU) on OH groups in the 8 and 6 MR were *ca.* 131 and 101 kJ mol^{-1}, respectively. Those values were in good agreement with *ca.* 130 and 110 kJ mol^{-1} obtained by the density functional calculation within periodic boundary conditions, respectively.

As shown in previous section, Ammonia IRMS-TPD method and density functional calculation were useful methods for quantitative measurement of solid acidity of zeolites. Combined utilization of both methods is a powerful methodology to understand the solid acidity[35].

References and Notes

1. A. Corma, *Chem. Rev*., **95**, 559 (1995).
2. P. A. Jacobs and W. J. Mortier, *Zeolites*, **2**, 226 (1982).
3. M. Brändle and J. Sauer, *J. Am. Chem. Soc*., **120**, 1556 (1998).
4. M. Niwa and N. Katada, *Catal. Surveys Jpn.*, **1**, 215 (1997).
5. M. Niwa, S. Nishikawa and N. Katada, *Micropor.. Mesopor. Mater*., **82**, 105 (2005).
6. M. Niwa, K. Suzuki, N. Katada, T. Kanougi and T. Atoguchi, *J. Phys. Chem.* B, **109**, 18749 (2005).
7. M. Niwa, K. Suzuki, K. Isamoto and N. Katada, *J. Phys. Chem.* B, **110**, 264 (2006).
8. K. Suzuki, M. Niwa and N. Katada, *J. Phys. Chem.* C, **111**, 894 (2007).
9. K. Suzuki, T. Noda, N. Katada and M. Niwa, *J. Catal*., **250**, 151 (2007).
10. G. J. Kramer and R. A. van Santen, *J. Am. Chem. Soc.*, **115**, 2887 (1993).
11. A. Simperler, R. G. Bell, M. D. Foster, A. E. Gray, D. W. Lewis and M. W. Anderson, *J. Phys. Chem.* B, **108**, 7152 (2004).
12. G. Sastre, V. Fornes and A. Corma, *J. Phys. Chem.* B, **104**, 4349 (2000).
13. M. Calligaris, G. Nardin, L. Randaccio and P.C. Chiaramonti, *Acta Crystallogr*. B, **38**, 602 (1982).
14. E. H. Teunissen, A. P. J. Jansen and R. A. van Santen, *J. Phys. Chem.*, **99**, 1873 (1995).
15. V. V. Mihaleva, R. A. van Santen and A. P. J. Janaen, *J. Chem. Phys.*, **119**, 13053 (2003).
16. C. Lo and B. L. Trout, *J. Catal*., **227**, 77 (2004).
17. M. Bourgogne, J. L. Guth and R. Wey, *US Pat*., 4503024 (1985).
18. M. Niwa, N. Katada, M. Sawa and Y. Murakami, *J. Phys. Chem*., **99**, 8812 (1995).
19. B. Delly, D.E. Ellis, A.J. Freeman, E.J. Baerends and D. Post, *Phys. Rev*. B, **27**, 2132 (1983).
20. A.D. Boese and N.C. Handy, *J. Chem. Phys*., **114**, 5497 (2001).
21. D.E. Akporiaye, I.M. Dahl, H.B. Mostad and R. Wendelbo, *J. Phys. Chem*., **100**, 4148 (1996).
22. A. Zecchina, L. Marchese, S. Bordiga, C. Paze and E. Gianotti, *J. Phys. Chem.* B, **101**, 10128 (1997).
23. B. Onida, Z. Gabelica, J. Lourencüo and E. Garrone, *J. Phys. Chem*., **100**, 11072 (1996).
24. L.J. Smith, A. Davidson and A. K. Cheetham, *Catal. Lett.,* **49**, 143 (1997).
25. G. Spoto, S. Bordiga, A. Zecchina, D. Cocina, E.N. Gribov, L. Regli, E. Groppo and C. Lamberti, *Catal. Today,* **113**, 65 (2006).
26. L. Smith, A. K. Cheetham, L. Marchese, J. M. Thomas, P. A. Wright and J. Chen, *Catal. Lett*., **41**, 13 (1996).
27. F. J. Torres, B. Civalleri, C. Pisani and P. Ugliengo, *J. Phys. Chem.* B, **110**, 10467 (2006),.
28. S. Bordiga, L. Regli, D. Cocina, C. Lamberti, M. Bjorgen and K. P. Lillerud, *J. Phys. Chem.* B, **109**, 2779 (2005).
29. N. Katada, H. Igi, J.H. Kim, and M. Niwa, *J. Phys. Chem.* B, **101**, 5969 (1997).
30. X.S-. Monfort, M. Sodupe, V. Branchadell, J. Sauer, R. Orlando and P. Ugliengo, *J. Phys. Chem.* B, **109**, 3539 (2005).
31. R. Shah, M.C. Payne and J.D. Gale, *J. Phys. Chem*., **100**, 11688 (1996).
32. P. Treesukol, J.P. Lewis, J. Limtrakul and T.N. Truong, *Chem. Phys. Lett*., **350**, 128 (2001).
33. Y. Jeanvoine, J.G. Àngyán, G. Kresse and J. Hafner, *J. Phys. Chem.* B, **102**, 5573 (1998).
34. G. Sastre and D. W. Lewis, *J. Chem. Soc., Faraday Trans*., **94**, 3049 (1998).

35. K. Suzuki, G. Sastre, N. Katada and M. Niwa, *Chem. Lett*., **36**, 1034 (2007).

Chapter 4.

Acidity and Catalytic Activity of Mesoporous ZSM-5 in Comparison with Zeolite ZSM-5, Al-MCM-41 and Silica-alumina

Synopsis

Acidity of mesoporous HZSM-5 prepared using amphiphilic organosilane template molecules was measured. Brønsted acid sites were observed in the prepared sample, and the number and the strength of Brønsted acid sites were determined quantitatively by a method of infrared-mass spectroscopy/temperature-programmed desorption (IRMS-TPD) of ammonia. ΔH for ammonia adsorption as an index of the strength was *ca.* 150 kJ mol^{-1} that was almost the same as on usual HZSM-5, but the number was smaller than that of HZSM-5. From the measured acidity, it was concluded that the mesoporous materials contained a smaller concentration of Brønsted acid site notable on the structure of HZSM-5. Measurements of turnover frequency (TOF) in the catalytic cracking of octane supported the conclusion. Density functional calculations showed that the defect sites Al–OH and Si–OH attached to the Brønsted acid site changed the strength of the acid sites to show some possible structures of the weak and strong Brønsted acid sites included in the mesoporous HZSM-5. Acidities of Al-MCM-41 and silica–alumina were also measured, and the difference in the solid acidities of these materials was discussed.

Introduction

Inventions of mesoporous materials by Kresge *et al*[1], Yanagisawa *et al*[2] and Inagaki *et al*[3] belonging to Mobil, Waseda and Toyota research groups, respectively, have led us to intensive studies for developing highly active catalytic materials. Addition of the strong acidity to these materials is anticipated, because when the strong acidity is created on the mesoporous materials, catalytic reactions of large molecules can proceed. Important studies have already been reported, in which highly active catalytic reactions have been reported over the developed catalysts[4–18].

Addition of Al atom into the MCM-41 and FSM-16, however, usually produces catalysts with relatively weak activity irrespective of the preparation methods, for example, a direct insertion of Al during the synthesis procedure or an impregnation in the post-synthesis. Some strategies[19-21] for the improvement of the solid acidity

are therefore definitely required. Recently, Ryoo and coworkers reported a new method for the preparation of mesoporous material having the strong acidity[22]. They proposed to use an amphiphilic organosilane template molecule, [3-(trimethoxysilyl)propyl]-hexadecyldimethylammonium (TPHAC), and reported a successful preparation of mesoporous HZSM-5. They reported that zeolite ZSM-5 was created on the wall of the materials. Because this method is so interesting to produce the new meso- and microporous materials which have the strong acidity, in the present study, the solid acidity of synthesized mesoporous HZSM-5 is measured using an infrared-mass spectroscopy/temperature-programmed desorption (IRMS-TPD) of ammonia. This method has been recently proposed by us to overcome the difficulty of the ammonia TPD[23,24]. The Brønsted and Lewis acid sites are measured quantitatively to compare with those on usual HZSM-5, Al-MCM-41 and silica–alumina. The number and strength of the Brønsted acid sites are used as parameters to judge the presence of the ZSM-5 structure in the materials. Density functional theory (DFT) calculations will be performed in order to confirm the experimental findings, because the DFT calculation supported the experimentally measured ΔH (enthalpy change of ammonia adsorption) on broad kinds of zeolite species.

Experimental methods

Preparation of Catalytic Materials

Highly controlled mesoporous HZSM-5 was synthesized by adding TPHAC into a conventional synthesis composition of HZSM-5. The recipe to obtain a parent solution was improved in this study as follows.

Method 1, Already Reported[22]

Sodium aluminate (53 wt% Al_2O_3, 43 wt% Na_2O, RiedeldeHaën), tetra propyl ammonium bromide (TPABr) and NaOH were dissolved in distilled water. To the resultant solution, tetra ethoxy silane (TEOS or Ludox) and TPHAC (55.5 wt% methanol solution) were simultaneously added under vigorous stirring.

Method 2, Improved to Obtain Higher Acidity

TPHAC, TPABr and NaOH were homogeneously dissolved in H_2O, followed by mixing water glass solution (6.83 wt% SiO2). Into the resultant homogeneous solution, a sodium aluminate solution was slowly added under stirring. Subsequently, the synthesis mixture was added with H_2SO_4 solution in drop wise manner under vigorous stirring conditions. The final molar composition of the gel was 2.5 Al_2O_3/40 Na_2O/95 SiO_2/10 TPABr/26 H_2SO_4/9000 H_2O/5 TPHAC. The flowchart for synthesis procedure of mesoporous HZSM-5 materials is presented in Figure 4-1.

Hydrothermal Synthesis and Calcination

The synthesis mixture thus prepared (Method 1 or 2) was heated with stirring at 423 K for 4 days, in a Teflon-coated stainless steel autoclave. The precipitated product was filtered by suction, and washed with distilled water. The product was dried in an oven at 373 K and subsequently calcined in air at 823 K. A sample of HZSM-5 (KAIST) was prepared by Method 1 except for the use of TPHAC, in order to study the influence of preparation conditions on the solid acidity. One more sample of zeolite ZSM-5 (Tosoh) was kindly provided by Tosoh Co., and the molar ratio Si/Al_2 was 23.8.

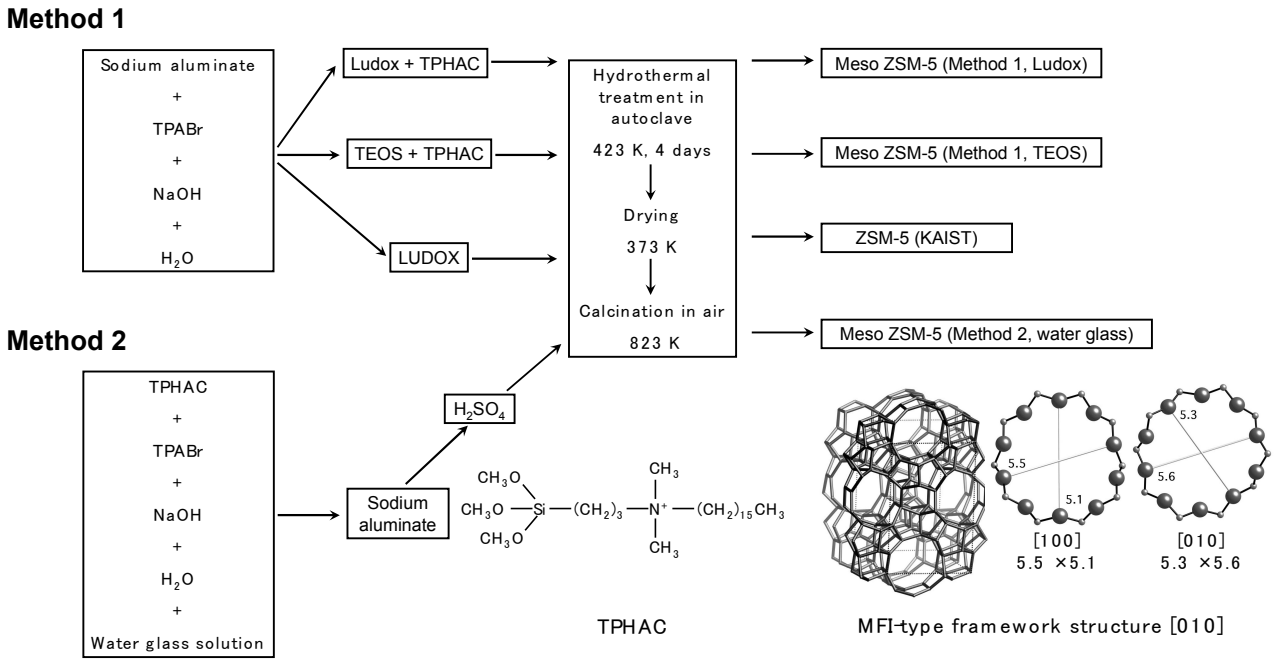

Figure 4-1. Flowchart for synthesis of mesoporous HZSM-5 materials.

MCM-41 (Figure 4-2) was prepared according to the method reported by Ryoo and Kim[26] using $[C_{16}H_{33}N(CH_3)_3]Br$ and colloidal silica Ludox HS-40. The silica source was pre-dissolved with NaOH into an aqueous solution, prior to mixing with surfactant. The resultant gel was heated at 373 K for 24 h in a polypropylene bottle. After 24 h, pH value of the prepared gel was adjusted to 11 using a 30 wt% acetic acid solution, followed by heating again at 373 K for 24 h. The pH adjustment was repeated four times to obtain the highly synthesized mesoporous material MCM-41. After calcination at 813 K, Al was loaded from aluminum chloride on the MCM-41 by an impregnation method. The Al-loaded MCM-41 was calcined again in air at 813 K.

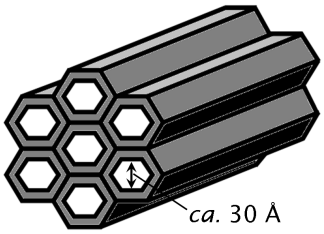

Figure 4-2. Structure of MCM-41.

A commercially available catalyst (Nikki N631L) was used as a silica–alumina catalyst. The sample contained 12.5 wt% Al_2O_3.

IRMS-TPD of Ammonia and Catalytic Cracking

Infrared spectroscopy and mass spectroscopy, connected with the glass-made vacuum apparatus, were measured simultaneously in order to follow the thermal behaviors of adsorbed and desorbed ammonia in the TPD experiment, respectively. Ammonia was adsorbed on the evacuated sample at 373 K, from which the sample temperature was elevated to 773 K. After the experiment, the difference IR spectra were calculated, and the differential change of the IR intensity with measurement temperature (hereafter called IRTPD) was compared with MS-TPD (usual TPD) to assign the ammonia species adsorbed on Brønsted or Lewis acid site. Number of the desorbed ammonia was measured from the desorbed ammonia, and the ΔH for the adsorbed species was determined as the strength of acid site based on the theoretically derived equation for the equilibrium-controlled conditions.

Cracking of octanewas measured in a Pyrex glass reactor after the pretreatment of catalyst at 773 K for 1 h. Reaction conditions were following: temperature, 773 K; partial pressure of reactant, 14 Torr (1 Torr = 133 Pa); flow rate of carrier nitrogen, 40 ml min^{-1}; weight of the catalyst, 30 mg. Conversion of octane was measured at 15 min after the reaction, and the reaction rate was measured under the integrated equation because the conversion often exceeded to 10%.

Density Functional Calculation for Ammonia Adsorption

Energy required for ammonia adsorption on the acid sites consisting of ZSM-5 framework and those modified was calculated using a software program Materials Studio DMol^3 developed by Accelrys Co. The geometry for initial structure of MFI zeolite was obtained from the Materials studio 4.0 library. Geometry optimizations and energy calculations of a cluster consisting of acid center in the MFI structure were carried out at generalized gradient approximations (GGA) with BLYP functional. The adsorption energy of ammonia was calculated according to the equation, $E_{ads} = E_{AS\text{-}NH3} - E_{AS} - E_{NH3}$, where E_{ads} is the energy of ammonia adsorption on an acid site and $E_{AS\text{-}NH3}$, E_{AS} and E_{NH3} are the corresponding total energies (AS; acid site). Detail of the assumed structure is shown later.

Results

Measurements of Acidity on Mesoporous HZSM-5

Figure 4-3 shows the change of IR difference spectra on the mesoporous ZSM-5 prepared by Method 1 from TEOS, which was measured during the TPD experiment; for a comparison, a reference IR spectrum measured after the evacuation is also shown. On adsorption of ammonia, both the stretching vibration of ammonia and the bending vibration of NH_4^+ and NH_3 were observed, while the intensities of OH bands decreased partially, showing its interaction with adsorbed ammonia species. As shown in Figure 4-4(a), the bending vibration of ammonia consisted of three absorptions. A strong absorption at *ca.* 1450 cm^{-1} was assigned to the bending vibration of NH_4^+ adsorbed species, while the bands at 1620 and 1320 cm^{-1} seem to be adsorbed NH_3 species weakly and/or strongly adsorbed. To quantitatively measure the intensity of the absorption, a deconvolution and fitting treatment was performed, as shown in Figure 4-4(b). Four portions of the absorption were assumed, and sum of the divided

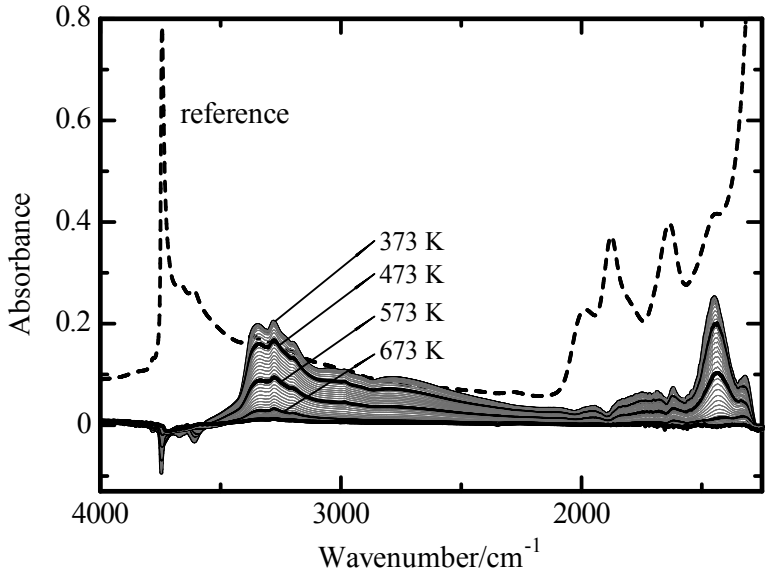

Figure 4-3. Difference spectra observed upon adsorption and desorption of ammonia on the mesoporous HZSM-5 prepared by Method 1 from TEOS during the TPD experiment. Reference spectrum after the evacuation was added as a comparison.

peaks were fitted to the experimental observation. Three of four at 1475, 1430 and 1380 cm^{-1} were due to the bending vibration of NH_4^+, and sum of the intensities was used to calculate the change in intensity of adsorbed NH_4^+ with respect to the measurement temperature. Figure 4-5 shows the decreased intensity of OH bands simultaneously measured during the TPD experiment. The OH absorptions that changed the intensity upon adsorption and desorption of ammonia were the IR bands observed at 3781, 3746, 3670 and 3607 cm^{-1}. From the band positions, these were assigned to OH on dislodged Al [27,28], isolated Si–OH, Al–OH, and the Si–O(H)–Al Brønsted acid site, respectively. The 3781-cm^{-1} band of OH on the dislodged Al (Al–OH or AlOOH+) was often identified in the study of β-zeolite[29], but not usually found on other species of zeolite. The difference spectra of the OH were also divided into five portions, as shown in Figure 4-5 (b), and the changes of these OH were calculated as mentioned above.

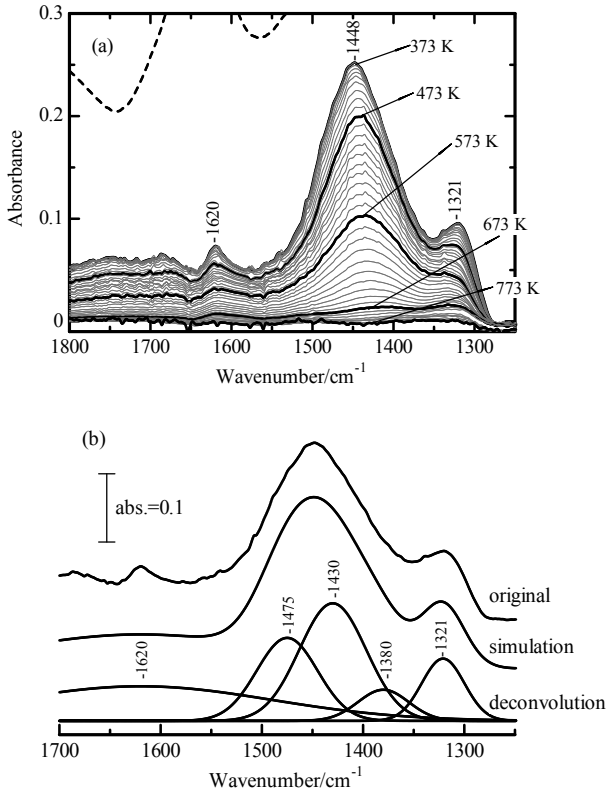

Figure 4-4. (a) Magnified portion of NH_4^+ and NH_3 bending vibrations shown in Figure 4-3, (b) an example of the deconvolution.

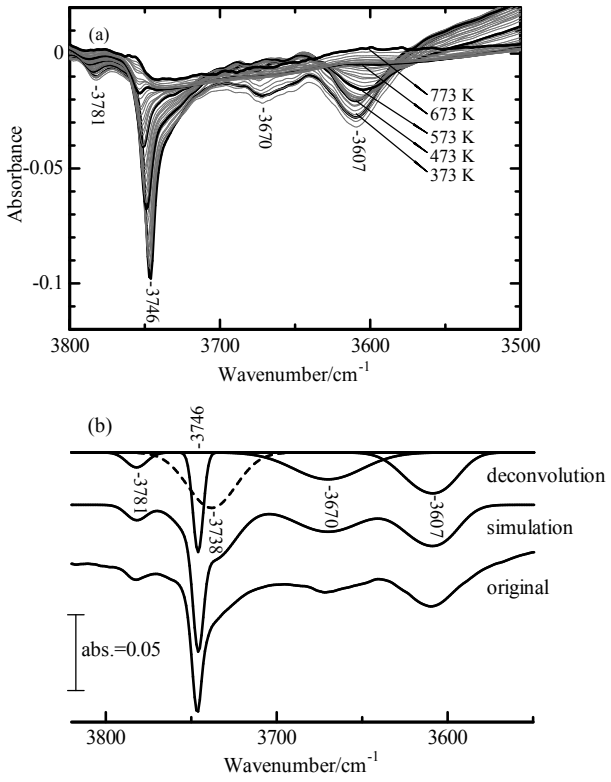

Figure 4-5. (a) Magnified portion of OH stretching vibrations in Figure 4-3, (b) an example of the deconvolution.

Changes of IR intensities against the measurement temperature, *i.e.*, called IR-TPD, are shown in Figure 4-6, in which MS-TPD of ammonia is shown together. MS-TPD showed two desorption peaks, while IR-TPD for ammonia and OH gave us complex profiles. From the comparison between IR- and MS-TPD profiles, following remarks were observed. From the comparison of IR-TPD for desorbed ammonia with MS-TPD, it was identified that desorption of ammonia at about 570 K mainly came from NH_4^+ adsorbed on the Brønsted OH. On the other hand, ammonia adsorbed as NH_3 was desorbed in the broad temperature ranges from 400 to 700 K. In addition, it was found that the NH_4^+ band and the OH at 3607 cm^{-1} changed at the same temperature regions, thus proving

the Brønsted acid site. Because the NH_4^+ intensity changed at low temperature *ca.* 450 K also, and the Brønsted OH at 3607 cm^{-1} changed its intensity at the same temperature, a small portion of ammonia was desorbed from NH_4^+ at the low temperature *ca.* 450 K. It was possible to identify the interaction of NH_4^+ with the OH at 3670 cm^{-1}, because the band changed the intensity at the same temperature.

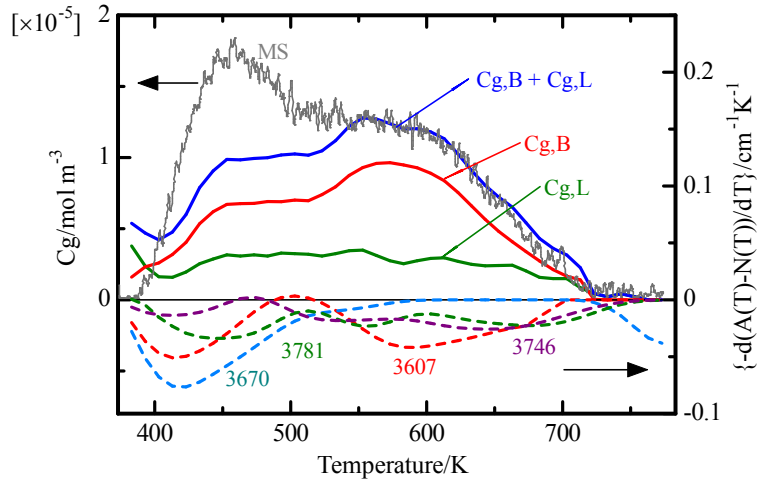

Figure 4-6. IR-TPD for NH_4^+ and NH_3, and OH to be compared with MS-TPD on the mesoporous HZSM-5 prepared by Method 1 from TEOS.

The deconvolution of the TPD profile into the Brønsted and Lewis acid sites was not justified easily from the experimental finding, because both profiles strongly overlapped. Therefore, following assumptions were made for the quantitative measurements of these acid sites. Because IR bands of ammonia molecules on Brønsted and Lewis acid sites have the different extinction coefficients, the amount of desorbed ammonia is simply described as

$$\text{Amount (ammonia)} = a_1 \times I(NH_4^+) + a_2 \times I(NH_3)$$

where a_n means a parameter corresponding to reciprocal of extinction coefficient for the species and I means its IR intensity. The parameters should be constants throughout the present measurements. However, in fact, constant values were not available due to the included experimental error. Therefore, in the present study, only the ratio a_1/a_2 was taken as nearly a constant, *ca.* 15/40. The parameter ratio being provided, number and strength of Brønsted sites were able to be calculated using a curve fitting method based on the derived theoretical equation, as shown in Table 4-1. However, only the number was measured for the Lewis acid site; because of the too broad profile, a distinct value of ΔH for the Lewis acid site was not determined.

Acidities on other samples of mesoporous ZSM-5 were measured using IRMS-TPD of ammonia experiments. As shown in Table 4-1, a sample prepared at the same synthesis conditions (Method 1) from different silica source (Ludox) had almost the same properties of number and strength of the Brønsted acid site. A sample prepared from water glass by Method 2 at the modified synthesis conditions, however, had different properties of the acidity. The NH_4^+ bending vibration showed the fine absorption at 1453 cm^{-1}, and intensities of shoulder bands at 1620 and 1320 cm^{-1} were weak, as shown in Figure 4-7. The Si–O(H)–Al Brønsted acid site at 3607 cm^{-1} was

observed distinctively in the reference spectrum, and this band decreased the intensity upon adsorption of ammonia. IRMS-TPD profiles were calculated as shown in Figure 4-8 from which the number and strength of acid sites were calculated. Because the IR-TPD of the 3607-cm^{-1} band had a mirror image relation with that of NH_4^+ bending vibration, fine Brønsted acidity was noteworthy on the mesoporous ZSM-5 (Method 2). Concentration of Brønsted acid site increased to about double as much as on meso HZSM-5 (Method 1) prepared at the initial stage of the investigation.

We speculate that the observed difference in the acidity among the mesoporous ZSM-5 samples were due to the difference in the synthesis methods. In Method 1, the aluminum source was mixed into the parent solution in vigorous conditions, while in Method 2, the aluminum source was completely dissolved into a homogeneous solution. It is speculated that the latter recipe had an advantage to disperse more Al atoms into the silicate framework to generate the Brønsted acidity.

Micro-pore volumes of the samples prepared from TEOS, Ludox, and water glass were 0.16, 0.17 and 0.17 ml g^{-1}, respectively. No difference in the zeolite crystal formations was therefore observed from the viewpoint of physical texture. BJH pore diameters on these meso-pores were 11.2, 5.4 and 5.1 nm, respectively.

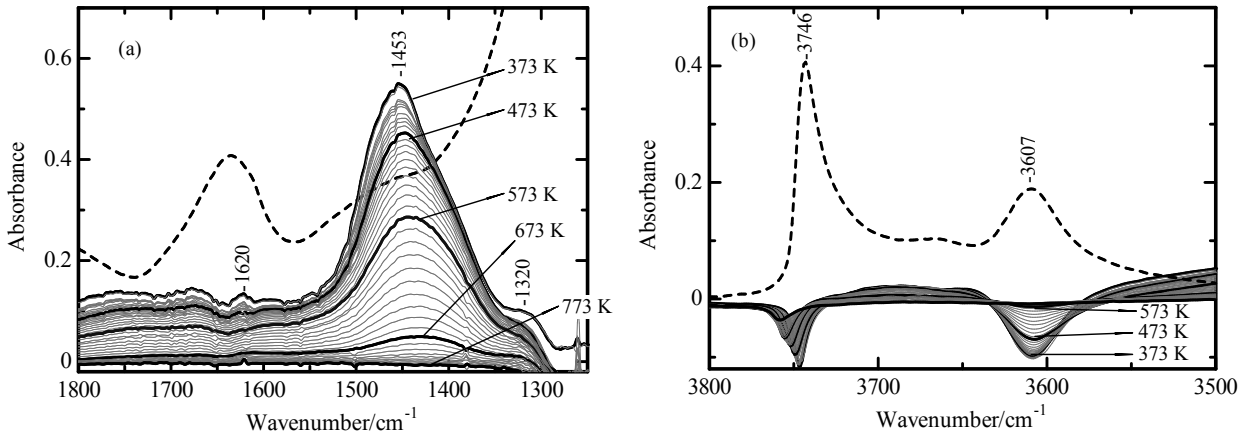

Figure 4-7. Changes of difference spectra in the band position of NH4+ (a) and OH (b) on the mesoporous HZSM-5 prepared by Method 2 from water glass.

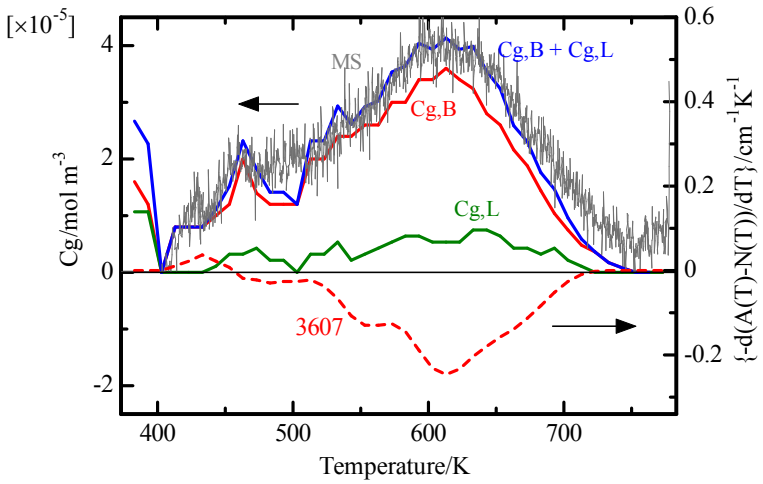

Figure 4-8. IR-TPD for NH_4^+ (Cg, B) and NH_3 (Cg, L) and OH (3607) to be compared with MS-TPD on the mesoporous HZSM-5 prepared by Method 2 from water glass.

Table 4-1. Solid acidity and catalytic cracking activity on mesoporous ZSM-5, usual ZSM-5, AlMCM-41 and silica-alumina catalyst.

Sample (silica source, institution or company)	Si/Al_2 ratio	Brønsted acid		Lewis acid		
		Number / mol kg^{-1}	Strength, ΔH / kJ mol^{-1}	Number / mol kg^{-1}	Cracking rate / $\times 10^{-3}$ mol s^{-1} kg^{-1}	Turn-over Frequency / 10^{-3} s^{-1}
Meso ZSM-5 (Method 1, TEOS)	26	0.11	148(18)	0.04	2.4	22
Meso ZSM-5 (Method 1, Ludox)	36	0.13	148(15)	0.03	2.6	20
Meso ZSM-5 (Method 2, water glass)	35	0.3	151(14)	0.04	6	20
ZSM-5 (KAIST)	36	0.25	143(6)	0.01	8.3	33
ZSM-5 (Tosoh)	24	0.7	137(6)	0	22	31
Al-MCM-41	26	0.14	130-157	0.15	0.34	2.4
Silica-alumina (Nikki N631L)		0.47	120-155	0.17	0.41	0.87

[a] 12.5 wt% Al_2O_3 contained. [b] Standard deviation in the parenthesis.

Measurement of Acidity on ZSM-5, Al-MCM-41 and Silica-alumina

An ordinary ZSM-5 prepared at almost the same conditions in which only the template TPHAC was excluded was measured using a method of IRMS-TPD of ammonia. As shown in Figure 4-9, IR-TPD for the NH_4^+ adsorbed species coincided well with the MS-TPD, thus showing the predominant Brønsted acidity. Because the Brønsted OH on the sample was not clearly observed, IR-TPD for the OH was not calculated. The concentration of Brønsted acid site was larger than those of mesoporous ZSM-5 prepared at the similar conditions, meso ZSM-5 (Method 1, TEOS) and (Method 1, Ludox), as shown in Table 4-1. Profile of the HZSM-5 was similar to on the HZSM-5 provided by Tosoh Co. (Chapter 2.4); however, the latter sample had the larger concentration of Brønsted acid site.

Adsorption of ammonia on both Al-MCM-41 and silica–alumina showed both the bending vibrations of NH_4^+ and NH_3 clearly at 1437 and 1321 cm^{-1}, respectively. However, the Brønsted OH was not observed distinctively on these samples. IRMS-TPD for Brønsted and Lewis acid sites were calculated, as shown in Figures 4-10 and 4-11. Both samples were characterized to be similar in the acidity as found from the IRMS-TPD, and not only the Lewis but also the Brønsted acid sites had the broad distribution of the strengths. Because of the broad distribution of the strength of the Brønsted acid sites, only the width of the ΔH was derived, as shown in Table 4-1.

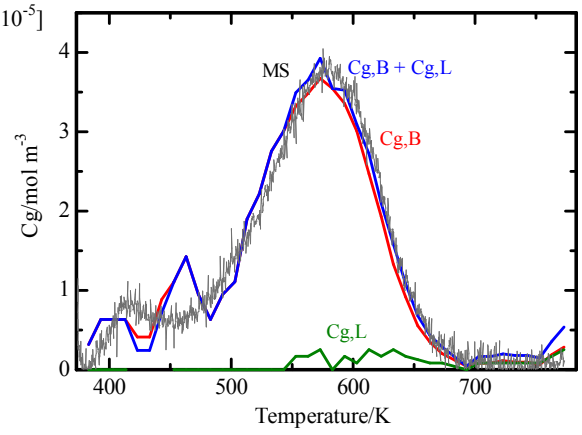

Figure 4-9. IR-TPD for NH_4^+ (Cg, B) and NH_3 (Cg, L) compared with MS-TPD on the ordinary HZSM-5 (KAIST).

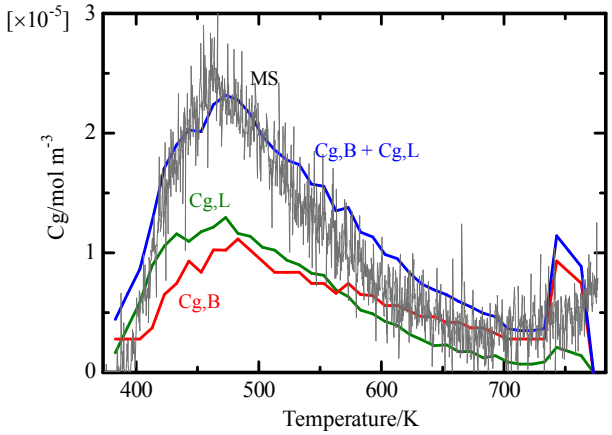

Figure 4-10. IR-TPD for NH_4^+ (Cg, B) and NH_3 (Cg, L) compared with MS-TPD on the Al-MCM-41.

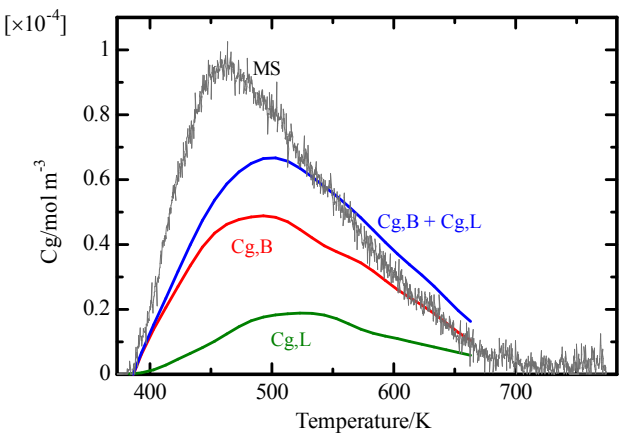

Figure 4-11. IR-TPD for NH_4^+ (Cg, B) and NH_3 (Cg, L) compared with MS-TPD on the silica-alumina.

Catalytic Cracking of Octane

To understand the catalytic property of these materials, cracking of octane was studied. The first-order reaction proceeds under the conditions of high temperature and low partial pressure, as described in the previous study by Haag and Dessau[30]. We confirmed that the reaction conditions of temperature 773 K and partial pressure of octane 14 Torr were enough to regard the reaction as proceeding under the first order reaction mechanism[31]. In this mechanism, the pentacoordinate carbonium cation adsorbed on the Brønsted acid sites is regarded as the reaction intermediate. Therefore, the turnover frequency (TOF) was determined from the rate of the reaction and the number of the Brønsted acid site. As shown in Table 4-1, the highest value of TOF was observed in two samples of ordinary HZSM-5. Compared with that on the HZSM-5, the mesoporous HZSM-5 samples showed similar values of TOF. Therefore, also from the viewpoint of catalytic cracking activity, the mesoporous HZSM-5 had the property similar to the usual HZSM-5. On the other hand, Al-MCM-41 and silica–alumina showed the very small values of the TOF of the octane cracking, and it was about one tenth to one thirties of the TOF on the micro- and meso-HZSM-5.

Density Functional Calculation

Structure models of the Brønsted acid site included in the mesoporous HZSM-5 were assumed, and the Brønsted acidities were studied using a DMol^3 software. Table 4-2(a) shows the assumed structure of NH_4^+ from MFI zeolite. The geometry optimization was carried out for a region containing 8 T sites shown by ball and stick model, in which the T(7) site was replaced by Al, while atoms shown by wire frame were fixed at the crystallographic coordinates. The dangling silicone atom was neutralized by hydrogen, and thereby the treated cluster had a composition $NH_4AlSi_{40}O_{61}H_{42}$. Calculation for corresponding proton from cluster ($AlSi_{40}O_{61}H_{43}$) was also carried out in the same method, and the adsorption energy of ammonia was calculated. As shown in Table 4-2 (b) and (c), adsorption energies were also calculated for other two kinds of embedded cluster models. Energy of the adsorption of ammonia on the usual HZSM-5 (model a) was 146 kJ mol^{-1}, and well agreed with the experimentally observed value. In the model b, NH_4^+ species interacts with the Si–O(H)Al–OH to show the ΔH

value of 119 kJ mol^{-1}. In the model c, NH_4^+ species is stabilized on the HO–Si–O(H)–Al to show the energy of 156 kJ mol^{-1}. These calculated values show that the strength of ammonia adsorption changes on the acid sites attached to defect sites Al–OH or Si–OH. These are consistent with the experimental findings of IRMS-TPD, because IR-TPD for Al–OH and Si–OH changed at low and high temperatures, respectively, as shown in Figure 4-6. Therefore, it is possible to estimate that these structures are included in the mesoporous HZSM-5.

Table 4-2. Calculated energy of ammonia adsorption on possible structure models of Brønsted acid site (Al(7)-O(17)H-Si(4)/ sinusoidal 10 member ring channel) contained in mesoporous HZSM-5.

Model	Structure of the Brønsted acid site with adsorbed ammonium cation. In these drawings, the atoms shown by wire frame model were fixed, and those shown by ball-stick model were geometrically optimized	E_{ads} / kJ mol^{-1}
(a) Usual site	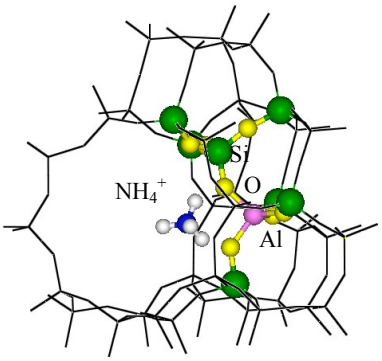	146
(b) Site with Al-OH	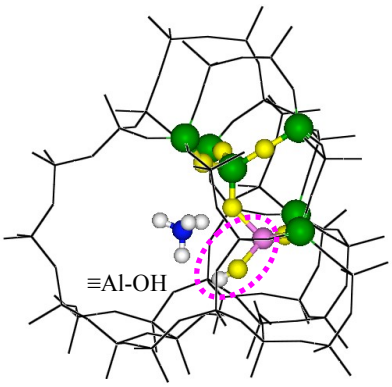	119
(c) Site with Si-OH	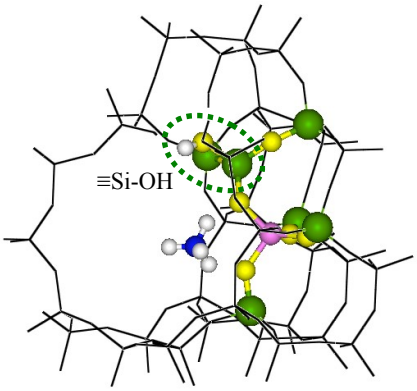	156

Discussion

HZSM-5 zeolite has the fine Brønsted acidity, *i.e.*, number of the site is equal or close to number of Al located in the framework, and the strength ΔH is about 135–140 kJ mol^{-1}. The strength of acid site depends on the structure of zeolite as reported previously[32]; therefore, the value of the ΔH is a parameter to identify the presence of structure in the studied material. In other words, we can identify the quantity and quality of the zeolitic structure from the number and strength of the Brønsted acidity, respectively. IRMS-TPD of ammonia is a method to measure the Brønsted acid sites directly and individually. Using this method, therefore, the solid acidity of the mesoporous HZSM-5 can be studied quantitatively.

The mesoporous HZSM-5 prepared by Ryoo and coworkers has the Brønsted acidity with the ΔH of about 150 kJ mol^{-1}, which is a little larger than that of HZSM-5. Number of the Brønsted acid site is however less than that of the usual HZSM-5. Therefore, a simple conclusion that we can draw from the observation is a partial formation of the structure of HZSM-5 in the mesoporous materials. Presence of the structure depended on the synthesis procedure, and at most optimized preparation (Method 2), the mesoporous material includes the zeolite HZSM-5 by *ca.* 50% in compared with HZSM-5 (Tosoh).

A distribution of the Brønsted acidity was observed in the less improved samples of the mesoporous HZSM-5 (Method 1). From the profile of the TPD, a small amount of the weak Brønsted acid site was notified in addition to the usual strong Brønsted acid site. Because the Al–OH bands at 3670 and 3781 cm^{-1} changed the intensity at the low temperature, it was suspected that the NH_4^+ species adsorbed on the Brønsted acid site interacted with these Al–OH species.

TOF for octane cracking, which was measured under the conditions of the first-order reaction, is a useful parameter to characterize the Brønsted acidity. Because of the similar values of TOF, the Brønsted acidities of the mesoporous and usual HZSM-5 resembled well. From this point of view, the presence of the HZSM-5 structure in the mesoporous HZSM-5 is clearly confirmed.

Al-MCM-41 has shown the acidity, which is similar to that on the silica–alumina catalyst. Not only the Brønsted but also the Lewis acid site is formed on the material to some degree. The IR Brønsted OH bands were not seen clearly both on silica–alumina and Al-MCM-41; however, these materials had Brønsted acidity as measured by ammonia adsorption. Numbers of these acid sites are not small compared with that on the mesoporous HZSM-5. The most striking property of the material is not the small concentration but the broad strength distribution of the acid sites. The characterized acidity implied the complex profile of the acid sites with Brønsted and Lewis characters. In other words, complex profiles of the surface structure are estimated.

Density functional calculation suggests some possible structures of Brønsted acid sites. In the present DFT study, the Al–OH in the neighbor of the Brønsted acid site decreases the strength, while the Si–OH defect site increases the strength. These calculations agree with the experimental findings, and propose a possible model of the distribution of the strength of Brønsted acid sites. The mesoporous HZSM-5 contains defects as well as the Brønsted acid site, thus showing a small distribution of the acid sites.

Conclusion

From the characterization study using IRMS-TPD of ammonia, measurements of TOF of catalytic cracking, and DFT calculation, following conclusions were obtained.

(1) From the IRMS-TPD of ammonia and TOF of catalytic cracking, it was found that the mesoporous

HZSM-5 prepared using amphiphilic organosilane template molecules had the strong Brønsted acid sites notable in the HZSM-5 zeolite; but the concentration was smaller than that of HZSM-5.

(2) DFT study showed that the defect sites Al–OH and Si–OH attached to the Brønsted acid site changed the strength of the acid sites to show some possible structures of the weak and strong Brønsted acid sites included in the mesoporous materials.

(3) The Al-MCM-41 and silica–alumina were characterized to have the large distribution of acid sites and large amounts of defect sites, which differed greatly from the zeolite and mesoporous HZSM-5.

References and Notes

1. C.T. Kresge, M.E. Leonowicz, W.J. Roth, J.C. Varutuli and J.S. Beck, *Nature*, **359**, 710 (1992).
2. T. Yanagisawa, T. Shimizu, K. Kuroda and C. Kato, *Bull. Chem. Soc. Jpn*. **63**, 988 (1990).
3. S. Inagaki, Y. Fukushima and K. Kuroda, *J. Chem. Soc., Chem. Commun*., 680 (1993).
4. M. Busio, J. Janchen and J.H.C. van Hooff, *Micropor. Mater.* **5**, 211 (1995).
5. R. Mokaya, W. Jones, Z. Luan, M.D. Alba and J. Klinowski, *Catal. Lett*., **37**, 113 (1996).
6. J.H. Kim, M. Tanabe and M. Niwa, *Micropor. Mater*., **10**, 85 (1997).
7. Y. Yue, Y. Sun, Q. Xu and Z. Gao, *Appl. Catal. A: Gen*., **175**, 131 (1998).
8. H.H.P. Yiu and D.R. Brown, *Catal. Lett*., **56**, 57 (1998).
9. J. Wang, L. Huang, H. Chen and Q. Li, *Catal. Lett*., **55**, 157 (1998).
10. M.J. Climent, A. Corma, R. Guil-Lopez, S. Iborra and J. Primo, *J. Catal*., **175**, 70 (1998).
11. A. Tuel, Micropor. *Mesopor. Mater.*, **27**, 151 (1999).
12. Y. Yue, A. Gedeon, J.-L. Bonardet, N. Melosh, J.-B. D'Espinose and J. Fraissard, *Chem. Commun*., 1967 (1999).
13. L.Y. Chen, Z. Ping, G.K. Chuah, S. Jaenicke, G. Simon, *Micropor. Mesopor. Mater.* **27**, 231 (1999).
14. H. Kosslick, G. Lischke, B. Parlitz, W. Storek and R. Fricke, *Appl. Catal. A: Gen*., **184**, 49 (1999).
15. K. Chaudhari, T.K. Das, A.J. Chandwandkar and S. Sivasanker, *J. Catal*., **186**, 81 (1999).
16. M. Cheng, Z. Wang, K. Sakurai, F. Kumata, T. Saito, T. Komatsu and T. Yashima, *Chem. Lett*., 131 (1999).
17. K. Okumura, K. Nishigaki and M. *Niwa, Micropor. Mesopor. Mater*., **44–45**, 509 (2001).
18. Z. Zhang, Y. Han, F.-S. Xiao, S. Qiu, L. Zhu, R.Wang, Y. Yu, Z. Zhang, B. Zou, Y. Wang, H. Sun, D. Zhao and Y. Wei, *J. Am. Chem. Soc.*, **123**, 5014 (2001).
19. Y. Liu, W. Zhang and T. Pinnavaia, *Angew. Chem. Int. Ed*., **40**, 1255 (2001).
20. C.H. Christensen, K. Johannsen, I. Schmidt and C.H. Christensen, *J. Am. Chem. Soc.*, **125**, 13370 (2003).
21. A. Ungureanu, S. Royer, T.V. Hoang, D.T. On, E. Dumitriu and S. Kaliaguine, *Micropor. Mesopor. Mater*., **84**, 283 (2005).
22. M. Choi, H.S. Cho, R. Srivastava, C. Venkatesan, D.-H. Choi and R. Ryoo, *Nat. Mater.*, **5**, 718 (2006).
23. M. Niwa, K. Suzuki, N. Katada, T. Kanougi and T. Atoguchi, *J. Phys. Chem.* B, **109**, 18749 (2005).
24. K. Suzuki, T. Noda, N. Katada and M. Niwa, *J. Catal*., **250**, 151 (2007).
25. K. Suzuki, G. Sastre, N. Katada and M. Niwa, *Chem. Lett*., **36**, 1034 (2007).
26. R. Ryoo and J.M. Kim, *J. Chem. Soc., Chem. Commun*., 711 (1995).
27. E. Bourgeat-Lami, P. Massiani, F.D. Renzo, P. Espiau and F. Fajula, *Appl. Catal*., **72**, 139 (1991).

28. I. Kiricsi, C. Flego, G. Pazzuconi, W.O. Parker Jr., R. Millini, C. Perego and G. Bellussi, *J. Phys. Chem*., **98**, 4627 (1994).
29. M. Niwa, S. Nishikawa and N. Katada, *Micropor. Mesopor. Mater*., **82**, 105 (2005).
30. W.O. Haag, R.M. Dessau, in: Proceedings of the Eighth International Congress on Catalysis, vol. 2, Verlag Chemie, Weinheim, 1984, p. 305.
31. T. Hashiba, D. Hayashi, N. Katada and M. Niwa, *Catal. Today*, **97**, 35 (2004).
32. N. Katada, H. Igi, J.-H. Kim and M. Niwa, *J. Phys. Chem.* B, **101**, 5969 (1997).

Chapter 5.

Periodic Density Functional Calculation on Brønsted Acidity of Modified Y-type Zeolite

Synopsis

Periodic density functional calculations on Brønsted acidities of Ca^{2+}, Ba^{2+} and $Al(OH)^{2+}$ exchanged Y-type zeolites was performed. When a divalent cation was stabilized in the sodalite cage, the vibrational frequency of acidic O1H group (ν_{OH}) located in the supercage was decreased, and the adsorption energy of ammonia (E_{ads}) were enhanced. Those calculated values agreed with the corresponding experimental values obtained by ammonia infrared spectroscopy/ mass spectroscopy-temperature programmed desorption (IRMS-TPD) method. The calculated ν_{OH} and E_{ads} of periodic FAU systems containing $Al(OH)^{2+}$ at the sites I' and II' were 3603 cm^{-1}/ 144 kJ mol^{-1} and 3605 cm^{-1}/ 135 kJ mol^{-1}, respectively; and those values were in agreement with the experimental values of the strong Brønsted acid site in Na_2H_2-EDTA treated USY (3595 cm^{-1}/ 133 kJ mol^{-1}). Al in $Al(OH)^{2+}$ located in the sites I' and II' coordinated to surrounding three oxygen atoms in the 6 member ring, and those were stabilized as tetra-coordinated extra-framework Al (EFAL) species. This configuration of EFAL species has been supported by ^{27}Al MQ MAS NMR measurement at a high magnetic field (16T). High electron withdrawing potentials of cations at the sodalite cage enhanced the strength of the acidic O1H group located in supercage, and thus the catalytic activity of paraffin cracking was improved.

Introduction

Ultra-stable Y zeolite (USY) is one of the zeolites most widely used as industrial catalysts in fluid catalytic cracking (FCC) process.[1] High catalytic activities of divalent or trivalent metal cation-exchanged FAU-type zeolites have been recognized from the beginning of their commercialization.[2,3] Not only from the catalytic viewpoint but also from the physicochemical properties, the modification mechanism in Y-type zeolite has been an important and interesting subject.

USY is generally obtained from NH_4-Y zeolite by steaming at a high temperature above 773 K. By the hydrothermal steaming, the tetrahedral Al atoms are released from the framework, and the generated defective domain shows meso-porosity.[4] In contrast, the dislodged Al atoms, so-called extra-framework Al (EFAL) species, are stabilized inside the cavities as cationic and/or neutral species, and they play the role of a Lewis acid

site.[5] Corma *et al* proposed that the polarizability of acidic OH group was increased by an electron-withdrawing effect of neighboring EFAL species.[6] Additionally, the nature and location of EFAL species in FAU structure have been analyzed in detail by advanced experimental and theoretical methodologies.[7-9] The enhancement of the Brønsted acid strength by charge compensating metal cations has been analyzed.[10-13]

Recently, we have proposed the ammonia infrared spectroscopy/ mass spectroscopy-temperature-programmed desorption (IRMS-TPD) method.[14] Direct measurements of spectral properties of acidic SiO(H)Al groups by *in situ* IR measurements (IR-TPD) during the conventional ammonia TPD measurements (MS-TPD) provide us with information of the amount, adsorption heat of NH_3 (ΔH, an index of acid strength[15, 16]) and proton locations.[17, 18]

Additionally, in accordance with the development of theoretical methodologies, quantum chemical calculation is recently becoming a useful tool for analyzing physicochemical property of zeolite. Embedded cluster[19, 20] or quantum mechanical/ molecular mechanical (QM/MM) approaches are developed for calculation of large molecular system with sufficient-accuracy ad low-computational cost. ONIOM approach developed by Morokuma and co-workers[21] and Qm/Pot approach developed by Sauer and co-workers[22] have been successfully applied to investigation of physicochemical property of zeolite.[23-29] Moreover, Kohn-Sham density functional theory (DFT)[30] has been developed as a flexible approach requiring low-computational cost giving high accuracy comparable to the *ab initio* calculation. The periodic DFT calculations were recently performed for several zeolite systems.[18, 31-35] We have calculated the frequencies of stretching mode of acidic OH groups in FAU-type periodic system which has the realistic Al distribution, and those theoretical values were in good agreement with our experimental values. The detail of computational methodologies and conditions are described in ref. 40.

We have already performed quantitative measurements of the Brønsted acidity of unmodified and divalent metal cation-exchanged Y-type zeolites (H-Y, CaH-Y and BaH-Y) by ammonia IRMS-TPD measurements; in the study, the improvement of catalytic activity for paraffin cracking has been observed.[36] Divalent metal cation (Ca^{2+} and Ba^{2+}) were preferentially exchanged with NH_4^+ in the sodalite cage and double six rings (D6Rs). At about 35 % of the exchange degree of the divalent cation, NH_4^+ on the narrow pore systems was almost completely exchanged (see Figure 2-4-19 in Chapter 2-4). In that case, the strength of the Brønsted OH group located in the supercage was enhanced and the catalytic activity was improved. This enhanced Brønsted acidity was confirmed theoretically by means of density functional theory (DFT) embedded cluster calculations. Lunsford *et al.* assigned the origin of enhancement of Brønsted acid strength to an electron withdrawing effect by the divalent metal cations located in the sodalite cage, [37, 38] in agreement with our calculations[36]. Based on systematic studies on Brønsted acidity of divalent metal cation exchanged Y-type zeolites, it was considered that the Brønsted acidity of USY was enhanced by the EFAL species according to the same mechanism.

In the present study, the enhancement of Brønsted acid strength in divalent metal cation exchanged Y-type zeolites will be investigated in detail by the density functional theory (DFT) calculations within periodic boundary conditions which will be compared with experimental values obtained from the IRMS-TPD method. The aims of this study are to gain insight into the Brønsted/Lewis acid synergy from structural and physicochemical viewpoints, and to clarify the relationship between the enhanced Brønsted acid strength and the property of the added metal cation, which may induce the high catalytic activity of such an industrially important material as USY zeolite.

Computational Details

The periodic DFT calculations were performed as follows by using the Dmol^3 software.[39] Rhombohedral unit cells of acidic FAU structure were considered with lattice parameters a=b=c= 17.343 Å, α=β=γ= 60.0°.[40] The chemical compositions considered were $HAlSi_{47}O_{96}$ and $M_aHAl_{(a\times b+1)}Si_{(47-a\times b)}O_{96}$, with M being a divalent cation (M^{b+}). Geometry optimizations and energy calculations were made based on the generalized gradient approximation (GGA) level using the Hamprecht-Cohen-Tozer-Handy (HCTH) exchange and correlation functional.[41] Relativistic effects were taken into account with an all-electron scalar relativistic method based on the DKH transformation.[42, 43] All calculations were performed using a double numerical polarization (DNP) basis set. The adsorption energy of ammonia (E_{ads}) was calculated on the basis of the following equation: $E_{ads} = (E_{H\text{-}Z} + E_{NH3}) - E_{NH4\text{-}Z}$, where $E_{NH4\text{-}Z}$, $E_{H\text{-}Z}$, and E_{NH3} are the total energies of NH_4-zeolite, H-zeolite and gaseous ammonia, respectively. The harmonic vibrational frequency of the acidic OH group -ν_{OH}- was obtained from the calculation of the partial Hessian matrix[44] including the SiO(H)Al group, six O atoms in the first coordination sphere, and six tetrahedral (T = Si or Al) atoms in the second neighborhood of the OH site. To account for the anharmonicity effects, a scaling factor was determined by comparing the theoretical and experimental frequencies of OH stretching modes of gaseous H_2O molecule[45]. The theoretical frequencies of symmetric and asymmetric OH stretching modes of H_2O molecule were 3800 and 3918 cm^{-1}, and the corresponding experimental values were 3657 and 3756 cm^{-1}, respectively. Thus, the scaling factor was determined as 0.961.

Results and Discussion

Geometrical Parameters of Purely Siliceous FAU Structure

FAU structure consists of sodalite cages which are connected with double six rings (D6Rs), and the large pore system (supercage) is built from the combination of those units (Figure 5-1). All T sites in this structure are equivalent, thus it has only four kinds of oxygen sites which are linked to the T site labeled as O(1 - 4). O1 and O4 sites face to the supercage, O2 site is located in the 6 member ring (6MR) window between the supercage and sodalite cage, and O3 site is located in the double 6 rings (D6Rs). First, the geometric optimization of purely siliceous FAU structure was performed in order to confirm the validity of optimized structure. The calculated geometrical parameters for the purely siliceous FAU and the experimental values of siliceous Y-type zeolite[46] are compared in Table 5-1. The theoretically calculated values of Si-O bond length (1.621 to 1.634 Å) were slightly overestimated compared with the experimental values (1.597 to 1.614 Å). On the other hand, the calculated values of Si-O-Si and O-Si-O bond angles were in good agreement with the experimental values.

Table 5-1. Optimized geometries of purely siliceous FAU-type zeolite ($Si_{48}O_{96}$/ u.c.) and experimental values.

	Calc.	Exp.[a]
Bond distances/ Å		
Si-O1	1.632	1.607
Si-O2	1.622	1.597
Si-O3	1.634	1.604
Si-O4	1.621	1.614
Bond angles/ deg.		
Si-O1-Si	137.7	138.4
Si-O2-Si	149.2	149.3
Si-O3-Si	144.7	145.8
Si-O4-Si	141.6	141.4
O2-Si-O4	109.3	108.7
O2-Si-O1	110.7	110.7
O2-Si-O3	108.4	108.7
O4-Si-O1	108.0	108.2
O4-Si-O3	110.7	111.5
O1-Si-O3	109.6	109.1

a) Experimental values are taken from the neutron diffraction study of siliceous faujasite in ref. 46.

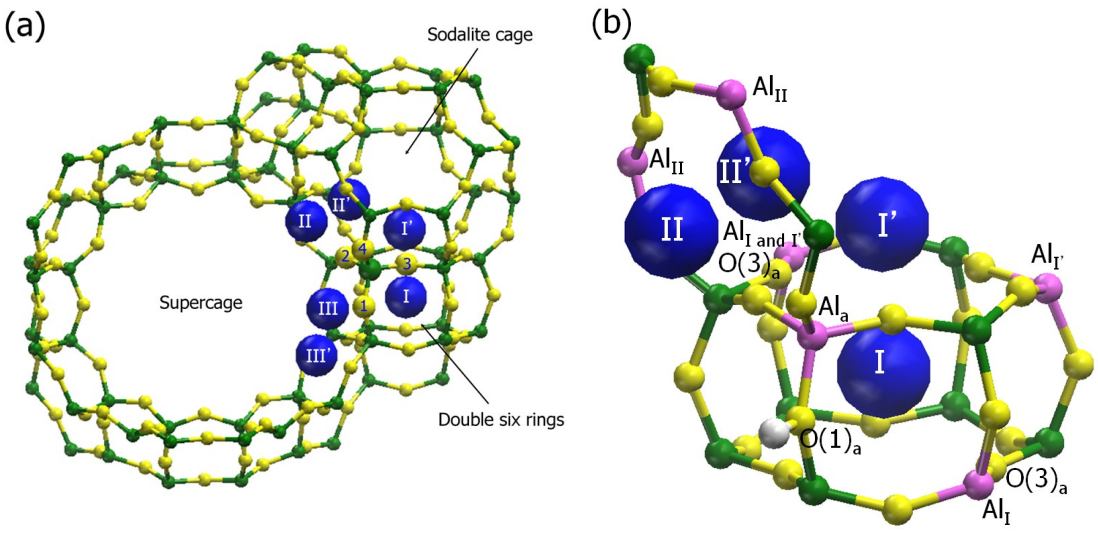

Figure 5-1. FAU-type framework structure (a) and schematic illustration of positions of divalent metal cations and lattice Al atoms in FAU structure (b). Arabic and Roman numbers show nonequivalent oxygen sites and cation sites, respectively. The location of two Al atoms depends on the divalent cation location as follows: Al_I when cation is in I, Al_{II} when cation is in II, $Al_{I'}$ when cation is in I'.

Geometric and Energetic Parameters of Isolated Nonequivalent Four SiO(H)Al Groups

Next, we performed the calculations of four kinds of nonequivalent Si(O)HAl groups. Among them, only O(1 – 3) sites can be bonded to proton.[47] From ammonia IRMS-TPD measurements on *in situ* prepared HY ($Si/Al_2 = 5.5$),[17] four kinds of OH stretching modes were observed at 3648, 3625, 3571 and 3526 cm^{-1}. We have identified those as O1H, O(1' or 4)H, O2H and O3H groups, respectively. The assignments of two OH stretching modes at high frequency (3648 and 3625 cm^{-1}) have not been clarified yet. Datka *et al.* reported that the heterogeneity of OH groups depended on the number of Al atoms in the next nearest neighbor to OH groups.[48] Optimized geometries and energetic parameters of four kinds of nonequivalent SiO(H)Al groups obtained from HCTH/DNP (this work) and VWN/DNP[49] periodic DFT calculations are summarized in Table 5-2. Relative energies of SiO(H)Al groups obtained from HCTH/DNP calculations were in agreement with the values obtained from VWN/DNP calculations. The T-O bond lengths obtained from HCTH/DNP calculations were slightly longer than those of VWN/DNP calculations. On the other hand, the O-H bond lengths were slightly shorter than those of VWN/DNP calculations. The optimized geometries were slightly different depending on the computational conditions (GGA or LDA approximations); however, the optimized geometries of the H-form FAU in the present calculations is in reasonable agreement with reported geometries. The relative stabilities of the four OH groups from the periodic DFT calculations were: O1H (0 kJ mol^{-1}) > O3H (1.6) > O4H (6.7) > O2H (8.3). The most stable OH group is O1H (located in the supercage), in agreement with several theoretical studies.[27, 40] The high accessibility of reactants to O1H and its larger population are the reasons why we have selected O1H site as the active centre for studying paraffin cracking.

By means of ammonia IRMS-TPD method, the enhancement of Brønsted acid strength by ion-exchanging of divalent cation has been measured.[36] The spectral (ν_{OH}) and thermodynamic (ΔU) parameters obtained from ammonia IRMS-TPD measurements (Exp.) are summarized in Table 5-3. Experiments show an inverse

relationship between ΔU and ν_{OH}; *i.e.,* the higher ΔU, the lower ν_{OH}. Further, turnover frequencies (TOF) of octane cracking in the monomolecular reaction conditions closely relate to ΔU. This relationship strongly suggests that the octane cracking was catalyzed by Brønsted acid sites. These relationships have been observed on zeolites having different structures such as MFI, BEA and MWW.[14] In the following section, we will calculate spectral (ν_{OH}) and thermodynamic (E_{ads}) parameters of the modified Y-type zeolites by means of DFT calculations in order to clarify the improvement of the strength of Brønsted acid site caused by the addition of divalent metal cations.

Table 5-2. Optimized geometries of isolated SiO(H)Al groups ($HAlSi_{47}O_{96}$/ u.c.).

	Acid site	E_{rel} / kJ mol^{-1}	d(AlO) / Å	d(SiO) / Å	d(OH) / Å	d(AlH) / Å	∠Si(O)HAl /deg.
HCTH/DNP	1	0	1.927	1.711	0.965	2.484	129.8
	2	8.3	1.934	1.708	0.966	2.431	136.6
	3	1.6	1.972	1.718	0.965	2.495	133.5
	4	6.7	1.918	1.703	0.965	2.455	132.1
VWN/DNP[a]	1	0	1.909	1.705	0.980	2.490	128.7
	2	10.8	1.905	1.699	0.985	2.372	140.4
	3	3.4	1.921	1.705	0.984	2.421	136.1
	4	8.6	1.906	1.701	0.982	2.436	134.2

[a] Optimized geometries for nonequivalent bridged OH groups (O1-O4) in ref. 49.

Table 5-3. Summary for the frequencies of OH stretching vibration and adsorption energies of ammonia obtained from periodic DFT calculations (Calc.), ammonia IRMS-TPD measurements (Exp.) and turn-over frequencies of octane cracking.

	Cation site	Electronegativity of added elements[a]	ν_{OH} /cm^{-1}		E_{ads} /kJ mol^{-1}		TOF of octane cracking[d] /10^{-3} s^{-1}
			Calc. × 0.961	Exp.[b]	Calc.	Exp. (ΔU)[c]	
H^+(1Al)	-	-	3649	3648	122	105	1.4
$3H^+$ (3Al)			3649		119		
H^+Ba^{2+} (3Al)	I	0.78	3643	3632	118	114	6.1
	I'		3629		135		
	II		3640		122		
H^+Ca^{2+} (3Al)	I	1.22	3654	3632	122	118	13
	I'		3615		136		
	II		3636		128		
$H^+Al(OH)^{2+}$ (3Al)	I'	3.47	3603	3595	144	133	28
	II'		3605		135		

[a] Sanderson's electronegativity. [b] Experimental values of HY, CaHY (exchange degree of Ca^{2+} = 37 %), BaHY (exchange degree of Ba^{2+} = 35 %) and Na_2H_2-EDTA treated USY were summarized in ref. 14, 36. [c] E_{ads} obtained from the DFT calculation corresponds to $\Delta U = \Delta H - RT_m$, where T_m is the peak maximum temperature of the TPD measurement, and R is gas constant (8.314 J K^{-1} mol^{-1}). [d] Measured at 773 K.

Brønsted Acidity of Unmodified HY Zeolite

Energy of ammonia adsorption on O1H (E_{ads}) and O1H stretching frequency (ν_{OH}) were calculated, and those values were compared with the corresponding experimental values in Table 5-3. In addition, the structural parameters of all calculated H- and NH_4-formed periodic models are summarized in Table 5-4 and 5-5, respectively.

Table 5-4. Optimized geometries of the O1H Brønsted site in the different periodic models considered.

	Cation site	d(AlO) / Å	d(SiO) / Å	d(OH) / Å	d(AlH) / Å	∠Si(OH)Al / deg.
H^+(1Al)	-	1.927	1.711	0.965	2.484	129.8
$3H^+$ (3Al)	-	1.903	1.720	0.965	2.462	129.0
H^+Ba^{2+} (3Al)	I	1.893	1.728	0.964	2.466	126.7
	I’	1.875	1.726	0.966	2.444	129.9
	II	1.897	1.721	0.965	2.462	129.3
H^+Ca^{2+} (3Al)	I	1.909	1.724	0.964	2.490	126.0
	I’	1.877	1.722	0.966	2.447	129.7
	II	1.882	1.724	0.965	2.445	129.6
$H^+Al(OH)^{2+}$ (3Al)	I'	1.888	1.728	0.967	2.441	131.0
	II'	1.881	1.740	0.967	2.451	131.2

Table 5-5. Optimized geometries of O1 sites in NH_4-form periodic models.

	Cation site	d(AlO) / Å	d(SiO) / Å	∠Si(OH)Al / deg.
H^+(1Al)	-	1.795	1.611	131.3
$3H^+$ (3Al)	-	1.778	1.619	129.7
H^+Ba^{2+} (3Al)	I	1.791	1.631	126.5
	I’	1.771	1.623	130.5
	II	1.786	1.625	129.9
H^+Ca^{2+} (3Al)	I	1.801	1.632	125.1
	I’	1.773	1.622	129.3
	II	1.765	1.617	132.1
$H^+Al(OH)^{2+}$ (3Al)	I'	1.711	1.629	131.2
	II'	1.765	1.631	132.7

First, we considered the unmodified Y-type zeolite ($HAlSi_{47}O_{96}$) containing an isolated $SiO1_a(H)Al_a$ Brønsted site (as shown in Figure 5-1 (b)). The optimized geometries of NH_4-formed periodic models are shown in Figure 5-2. The NH_3 molecule adsorbed on the acidic $O1_a(H)$ group was protonated, and the formed NH_4^+ was H-bonded to the $O1_aAl_aO4$ linkage as bidentate species. The NH···$O1_a$ and NH···O4 distances were 1.761 and 1.741 Å, respectively. The Si-O and Al-O bond lengths in the $SiO1_a(H)Al_a$ linkage were shortened by the

formation of NH_4^+, and this structural change indicated the enhancement of covalent character of the $Al_a\cdots O1_aSi$ bond. The calculated values for E_{ads} and ν_{OH} were 122 kJ mol^{-1} and 3649 cm^{-1}, respectively (H^+(1Al) in Table 5-3). E_{ads} was overestimated compared to the experimental value of ΔU (105 kJ·mol^{-1}), while ν_{OH} was in excellent agreement with the experimental value (3648 cm^{-1}). E_{ads} obtained by quantum chemical calculation may be influenced by a calculation method. In our previous study,[36] for example, we calculated the E_{ads} on O1H by means of DFT embedded 8T cluster calculation (BLYP/DNP) using a basic model of X-type zeolite, and that value was 95-100 kJ·mol^{-1}.

Second, we considered three OH groups in the $H_3Al_3Si_{45}O_{96}$ unit cell (denoted as $3H^+$(3Al) in Table 5-3). In addition to the above mentioned $SiO1_a(H)Al_a$ Brønsted site, two protons were placed at $O3_a$ sites with neighbor Al at Al_I positions as shown in Figure 5-1(b). We found, based on the structure, that E_{ads} and ν_{OH} of the $O1_aH$ group (119 kJ·mol^{-1} and 3649 cm^{-1}) were practically the same to those of the isolated OH group (122 kJ·mol^{-1} and 3649 cm^{-1}). This means that in this case there is little significant affect of the neighbor Brønsted sites on the physicochemical properties of the acidic OH group. Having shown the effect of neighbor Brønsted sites on E_{ads} and ν_{OH}, we now study the effect of neighbor cations on the $SiO1_a(H)Al_a$ Brønsted site.

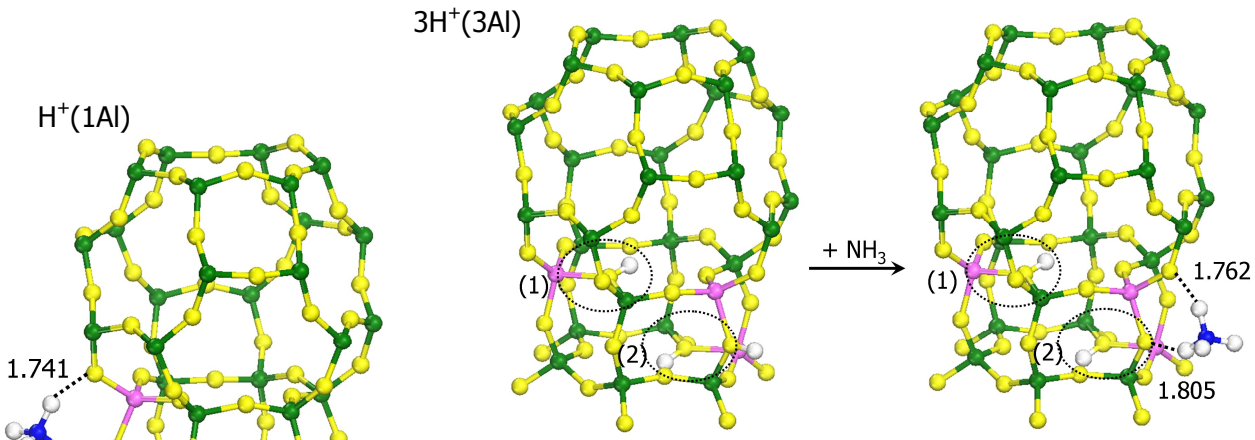

	d(AlO) /Å	d(SiO) /Å	d(OH) /Å	d(AlH) /Å	∠SiO(H)Al /deg.
Si(O3a)HAl (1)	1.935	1.745	0.968	2.509	131.2
Si(O3a)HAl (2)	1.968	1.724	0.966	2.504	132.8

Figure 5-2. Optimized geometries of NH_4-form H^+(1Al) and $3H^+$(3Al) systems. Two Si(O3H)Al groups in $3H^+$(3Al) system were labeled as (1) and (2), whose optimized geometries were summarized in the table.

Ca^{2+} and Ba^{2+} Exchanged HY Zeolites

Locations of exchanged cations in FAU structure are labeled, as shown in Figure 5-1 (b). Sites I and I' are located inside and outside of D6Rs, respectively. Sites II and II' are located near the 6MR window between the supercage and the sodalite cage, outside and inside of the sodalite cage, respectively. Sites III and III' are located in 4MRs of D6Rs, and sodalite cage facing to the supercage, respectively.[50] Among them, sites I and II are known as the predominant cation exchange sites in dehydrated Ca or Ba exchanged X-type zeolite.[51] As

shown in Figure 5-1 (b), the divalent metal cations in sites I and II were compensated by two Al atoms located in Al_I and Al_{II} positions, respectively (denoted as H^+M^{2+}(3Al) in Table 5-3).

The optimized geometries of H- and NH_4-formed H^+M^{2+}(3Al)/ site I systems are shown in Figure 5-3. The calculated Ca-O3 and Ba-O3 bond lengths (*ca.* 2.5 and 2.8 Å) are very similar to the experimental values[51] of dehydrated Ca-X and Ba-X (2.43 and 2.78 Å), respectively. On the other hand, M^{2+} on the site II (H^+M^{2+}(3Al)/ site II systems) is surrounded by three O2 in single 6MR, as shown in Figure 5-4. The calculated Ca-O2 and Ba-O2 bond lengths (*ca.* 2.3 and 2.7 Å) are in very good agreement with the experimental values[51] of dehydrated Ca-X and Ba-X (2.28 and 2.67 Å), respectively, and therefore the theoretical calculated values were supported by the experiment.

When Ba^{2+} or Ca^{2+} cations occupy the site I', the E_{ads} and ν_{OH} of the $SiO1_a(H)Al_a$ group were similar to those of H^+(1Al) and $3H^+$(3Al), as shown in Table 5-3. In contrast, when divalent metal cations locate in site II, enhanced Brønsted acid strength (with respect to the H form without metal cations) can be observed; *i.e.*, E_{ads} values are 122 and 128 kJ·mol^{-1} (Ba^{2+} and Ca^{2+} respectively), compared to 118-122 kJ·mol^{-1} in the HY; and ν_{OH} values are 3640 and 3636 cm^{-1} (Ba^{2+} and Ca^{2+} respectively), compared to 3649 cm^{-1} in the HY. The enhancement effect by Ca^{2+} is stronger than that by Ba^{2+}, in agreement with experimental results (Table 5-3).

Because Yeom *et al* reported that a small amount of Ba^{2+} existed in the site I' in dehydrated Ba exchanged X-type zeolite,[51] the structure also was studied. The divalent metal cation in site I' was compensated by two Al atoms located in $Al_{I'}$ (see Figure 5-1 (b)). Figure 5-5 shows H- and NH_4-formed H^+M^{2+}(3Al)/ site I' systems. The calculated Ba-O3 bond lengths (*ca.* 2.7 Å) were relatively longer than experimental values (2.44 Å). When Ba^{2+} located in site I', the enhancement effect on the strength of Brønsted O1H was the highest among all considered Ba^{2+} exchanged systems and the E_{ads} and ν_{OH} were 135 kJ mol^{-1} and 3629 cm^{-1}, respectively. Similarly, the E_{ads} and ν_{OH} of Ca^{2+} exchanged system on site I' showed relatively strong Brønsted acid strength (136 kJ mol^{-1} and 3615 cm^{-1}). From the disagreement of the calculated M^{2+}-O3 distances, ν_{OH}, and E_{ads} with the experimental values, we conclude that site I' is not predominant. This is in agreement with the low populations found by Yeom *et al*.[51]

Thus, we conclude that the strength of the Brønsted O1H in the supercage was enhanced by Ba^{2+} and Ca^{2+} seated in sites II and I', respectively. When the exchange degree of the divalent cation reached the *ca.* 35 % of the exchange degree, IR absorption intensities of the stretching vibrations of O3H (3525 cm^{-1}) and O2H (3571 cm^{-1}) disappeared almost completely. In those conditions, the strength of residual acidic O1H groups located in the supercage (*ca.* 3630 cm^{-1}) is enhanced and the catalytic activity was improved as well. From these observations, it can be inferred that the protons bonded to the O2 and O3 atoms are preferentially exchanged by the divalent metal cations, and thus the O1H is activated. This feature is depicted in Figures 5-3~5, where it is shown that the divalent cations located on sites I and I' interact with the O3, and that on site II with the O2, and in both cases the intensity of the low frequency OH band decreases. Thus, the enhancement effect on the Brønsted O1H caused by divalent cations located in the site I' and II is reasonably explained by our experimental and theoretical results.[36]

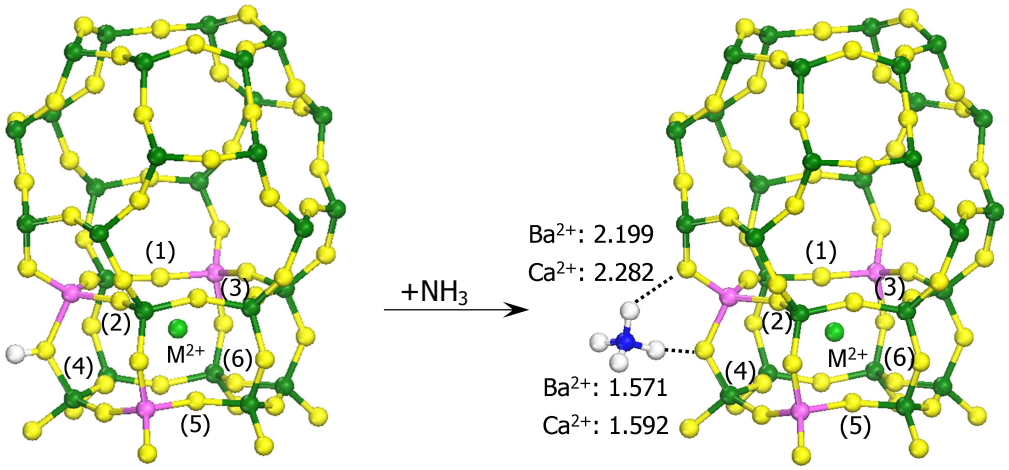

	Ca-O3 /Å	Ba-O3 /Å
(1)	2.387	2.676
(2)	2.367	2.655
(3)	2.505	2.749
(4)	2.659	2.992
(5)	2.530	2.845
(6)	2.616	2.887
Average	2.511	2.801

	Ca-O3 /Å	Ba-O3 /Å
(1)	2.408	2.694
(2)	2.364	2.649
(3)	2.541	2.787
(4)	2.607	2.880
(5)	2.510	2.797
(6)	2.625	2.873
Average	2.509	2.780

Figure 5-3. Optimized geometries of NH_4-form H^+M^{2+}(3Al)/ site I systems (M^{2+} = Ca^{2+} and Ba^{2+}). Six O3 sites coordinated to M^{2+} were numbered as (1) to (6), and those M-O3 distances were summarized in the tables.

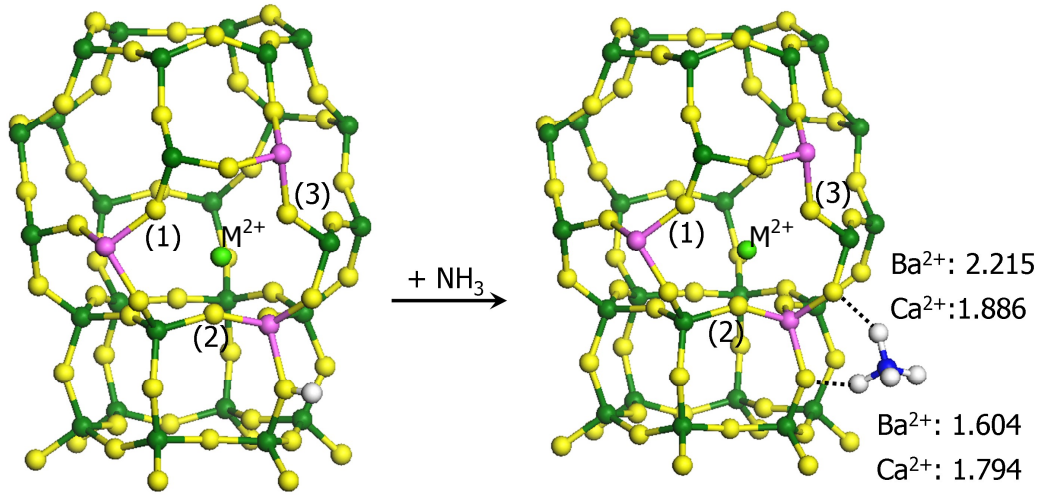

	Ca-O2/Å	Ba-O2/Å
(1)	2.245	2.601
(2)	2.394	2.769
(3)	2.317	2.676
Average	2.319	2.682

	Ca-O2/Å	Ba-O2/Å
(1)	2.24	2.585
(2)	2.35	2.745
(3)	2.33	2.698
Average	2.307	2.676

Figure 5-4. Optimized geometries of NH_4-form H^+M^{2+}(3Al)/ site II systems (M^{2+} = Ca^{2+} and Ba^{2+}). Three O2 sites coordinated to M^{2+} were numbered as (1) to (3), and those M-O2 distances were summarized in the tables.

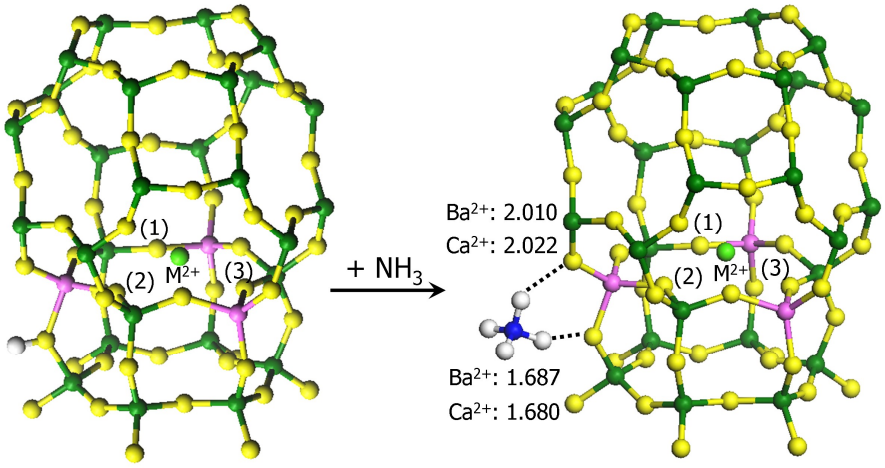

	Ca-O3/Å	Ba-O3/Å
(1)	2.340	2.674
(2)	2.389	2.778
(3)	2.279	2.627
Average	2.336	2.698

	Ca-O3/Å	Ba-O3/Å
(1)	2.320	2.684
(2)	2.352	2.709
(3)	2.290	2.647
Average	2.321	2.681

Figure 5-5. Optimized geometries of NH_4-form H^+M^{2+}(3Al)/ site I' systems (M^{2+} = Ca^{2+} and Ba^{2+}). Three O3 sites bonded to M^{2+} were numbered as (1) to (3), and those M-O3 distances were summarized in the tables.

USY Zeolite

The quantitative identification of the strong Brønsted acid site in the Na_2H_2-EDTA treated USY has already been studied by means of ammonia IRMS-TPD measurements.[52] Furthermore, the structural character of the strong Brønsted acid site was analyzed by the ^{27}Al MQ MAS NMR measurement[53] at a high magnetic field (16T) (see Chapter 2-2). By Na_2H_2-EDTA treatment, extra-framework penta- (V) and hexa- (VI) coordinated Al atoms in steamed USY were converted to tetra- (IV) coordinated EFAL species with large structural anisotropy (named $Al(IV_b)$).[53] Na_2H_2-EDTA-treated USY had a large amount of strong Brønsted acid sites and a small amount of Lewis acid sites compared to untreated USY, and the catalytic activity was highly enhanced.[14] Thus, we proposed that the $Al(IV_b)$ species was the origin of catalytic cracking activity of paraffins. Gola *et al.* reported that the cationic EFAL species in the Na_2H_2-EDTA treated USY were stabilized at the sodalite cage,[54] and several researchers suggested that Brønsted acid strength was enhanced by the cationic EFAL species stabilized in the sodalite cage.[37, 38, 55, 56] Williams *et al* assumed the $Al(OH)^{2+}$ species located within the sodalite cage and/or D6Rs as the realistic cationic EFAL species.[56] In addition, Li *et al.* reported that $Al(OH)_3$ and $Al(OH)^{2+}$ in the supercage, and $Al(OH)^{2+}$ in the sodalite cage were an effective EFAL species for enhancement of the Brønsted acid strength by means of a combined study of solid state ^{1}H and ^{13}C NMR measurements and DFT calculation.[9]

In the ion exchange of zeolites by di- and trivalent cations, the exchanged metal cation is hydrated according to the Hirschler-Plank mechanism[57]; *i.e.* $M^{2+} + H_2O + \equiv Si\text{-}O\text{-}Al\equiv \rightarrow M(OH)^+ + \equiv Si\text{-}O(H^+)\text{-}Al\equiv$. This equation takes place readily on the small cations which have high electrostatic potential (= valence/ ionic radius).[58, 59] The Ca^{2+} and Ba^{2+} have relatively low electrostatic potentials (2.01 and 1.48 $Å^{-1}$), thus the amounts of hydrated Ca^{2+} and Ba^{2+} cations may be small.[60] In contrast, the hydration of Al^{3+} which has a higher electrostatic potential (5.61 $Å^{-1}$) occurs readily.

Based on these considerations, we assumed that divalent EFAL species ($Al(OH)^{2+}$) were located in sites I' and II' within the sodalite cage. The optimized geometries of H- and NH_4-formed $H^+Al(OH)^{2+}$ (3Al)/ site I' and II' systems are illustrated in Figures 5-6 and 5-7, respectively. On the site I', the Al in $Al(OH)^{2+}$ coordinates to three O3 atoms of the D6R and its own OH, thus forming an anisotropic tetrahedral configuration. The average distance between the Al in $Al(OH)^{2+}$ and three O3 sites was 1.890 Å, which is similar to the framework Al-O distance (1.888 Å) in the $SiO1_a(H)Al_a$ group, as shown in Table 5-4. Then, the Al in $Al(OH)^{2+}$ stabilized in the Site II' coordinates to three O2 atoms, and the average distance between the Al and three O2 was 1.882 Å. This coordination distance was similar to the framework Al-O distance (1.881 Å). Those structural parameters indicate a strong interaction between the $Al(OH)^{2+}$ species and the surrounding 6MR framework.

Calculated values of E_{ads} and ν_{OH} of $H^+Al(OH)^{2+}$(3Al)/ site I' system were 144 kJ·mol^{-1} and 3603 cm^{-1} respectively, which meant that the Brønsted acid strength was drastically enhanced compared to HY zeolite, in good agreement with experimental observation[52] (see Table 5-3). Similarly, the $Al(OH)^{2+}$ stabilized in the Site II' and coordinated to three O2 atoms also showed an enhancement effect on the acid strength of $SiO1_a(H)Al$ group (E_{ads} and ν_{OH} were 135 kJ·mol^{-1} and 3605 cm^{-1} respectively, in Table 5-3). In this study, we focused on the analysis of the well characterized high frequency band of the Brønsted acid site located in the supercage. However, usually, more realistic EFAL species may have various structures and distributions[55]; but, the EFAL model proposed in this study would be one of the most probable structures.

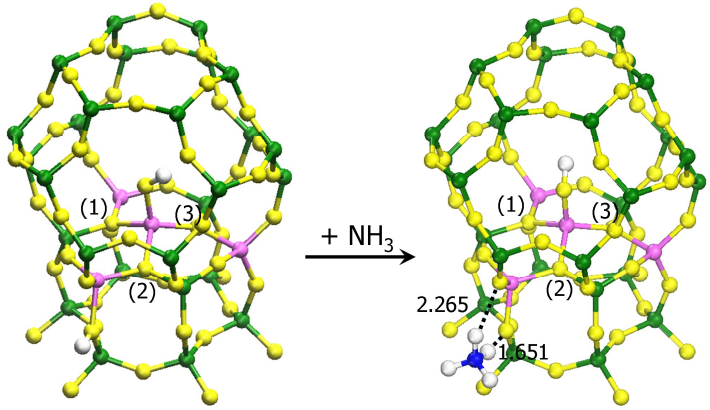

	H-form	NH_4-form
Al-O3/ Å		
(1)	1.870	1.881
(2)	1.941	1.903
(3)	1.859	1.872
Al-OH/ Å		
	1.707	1.711
AlO-H/ Å		
	0.956	0.956

Figure 5-6. Optimized geometries of NH_4-form $H^+Al(OH)^{2+}$(3Al)/ site I' system. Three O3 sites bonded to $Al(OH)^{2+}$ were numbered as (1) to (3), and those Al-O3 distances were summarized in the table.

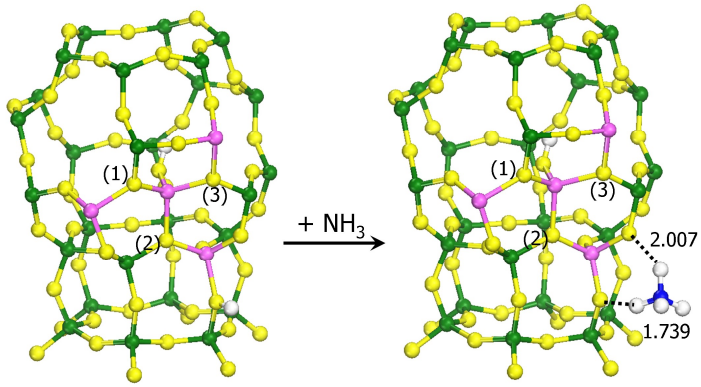

	H-form	NH_4-form
Al-O2/ Å		
(1)	1.857	1.865
(2)	1.909	1.891
(3)	1.881	1.897
Al-OH/ Å		
	1.709	1.708
AlO-H/ Å		
	0.957	0.956

Figure 5-7. Optimized geometries of NH_4-form $H^+Al(OH)^{2+}$(3Al)/ site II' system. Three O2 sites bonded to $Al(OH)^{2+}$ were numbered as (1) to (3), and those Al-O2 distances were summarized in the table.

Dependence of the Strength of Brønsted Acid Site on the Added Divalent Cation

The enhancement effect on Brønsted acid strength by divalent metal cation has been explained based on two kinds of mechanisms. One is a distortion of the zeolite framework caused by the addition of the divalent metal cations, and another is an inductive effect due to the electron-withdrawing property. Figures 5-8 (a) and (b) show the dependences of ν_{OH} and E_{ads} on the corresponding Si-O(H)-Al bond angles, respectively. The large Si-O(H)-Al bond angles tend to be related to low ν_{OH} and higher E_{ads}. In agreement with this, several theoretical studies suggested that a larger Si-O(H)-Al bond angle leads to an increase in the Brønsted acidity.[61, 62] In addition, Figures 5-9 (a) and (b) show the plots of the ν_{OH} and E_{ads} against the Al-O bond lengths in the SiO(H)Al linkages. It can be confirmed that the shorter Al-O bond length leads the stronger Brønsted acid strength.

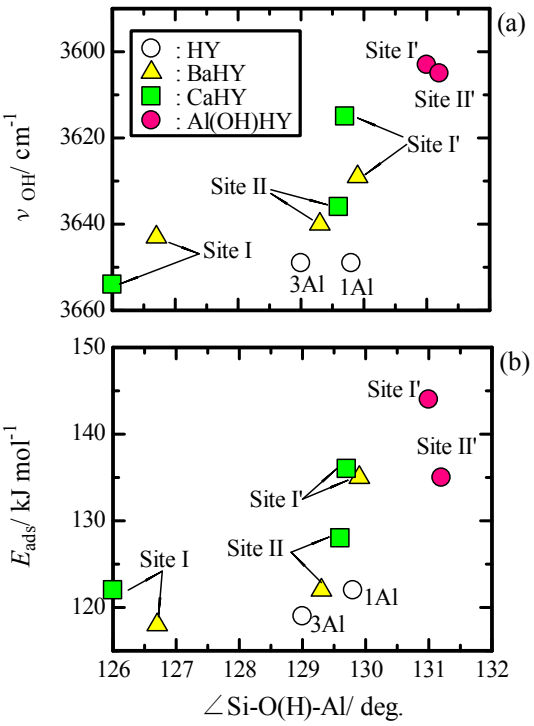

Figure 5-8. Dependence of Si-O(H)-Al bond angle on the frequency of O1H stretching vibration (a) and the adsorption energy of ammonia (b).

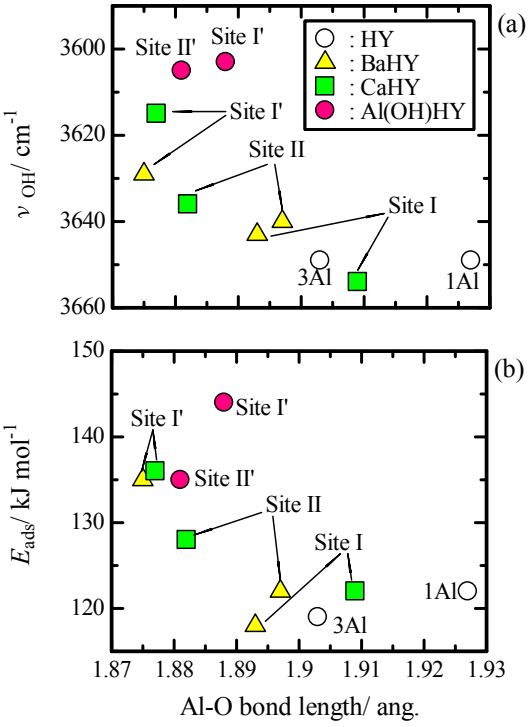

Figure 5-9. Dependence of Al-O bond length on the frequency of O1H stretching vibration (a) and the adsorption energy of ammonia (b).

These relationships between the Brønsted acid strength and the local geometric structure can be explained by changing of the oxygen hybrid orbital in the SiO(H)Al linkage. When the Si-O-Al bond angle is 180 °, the oxygen hybrid orbital is *sp* and the proton is weakly bonded to the residual *p* orbital ($2p_y$ or $2p_z$). On the other hand, when the Si-O-Al bond angle is 120 °, the oxygen hybrid orbital changes to sp^2 and the *s*-character of the OH bond is increased (O-H bond is strengthened). In other words, when the Si-O-Al bond angle is increased, the *s*-character of T-O bond is increased (T-O bond length is shortened). With those geometrical changes, the *s*-character of the acidic OH bond is decreased; *i.e.*, the proton donation becomes easier. van Santen *et al* have explained the relationship between the Brønsted acid strength and the local geometrical parameters based on above concept[63]. This concept has been supported well by the experimental results; for example, Freude *et al*[64]

have reported in their NMR study that the *s*-character of the oxygen hybrid orbital in Si-O(H)-Al linkage was increased with increasing of the Si-O-Al bond angle. van Bokhoven *et al.* [65] and Lercher *et al.*[66] have accepted this explanation for the enhancement of Brønsted acid strength of LaY and LaX zeolites.

Moreover, the polarizing and inductive effects on the acidic OH group due to the electron-withdrawing strength of the added metal cation is also a factor to consider. Electron-withdrawing effects of divalent metal cations and EFAl species promote the polarization of the acidic OH groups through the coordinated lattice oxygen atoms and Al atoms.[12, 13] Thus, larger electron-withdrawing potential of divalent metal cation could lead to a higher Brønsted acid strength. In order to explain these results, we evaluate the electron-withdrawing potentials (Lewis acidity) of divalent cations and/or hydrated metal cations based on Sanderson's electronegativity.[67] The electronegativities of Ba, Ca and Al(OH) were 0.78, 1.22, and 3.47, respectively; and those values could explain the extents of enhancement of Brønsted acid strength. This relationship means that the enhancement effect of the Brønsted acidity closely correlated with the Lewis acidity of added elements. The present result agrees with the inductive mechanism for the enhanced Brønsted acidity of divalent exchanged Y-type zeolites proposed by Lunsford.[37, 38]

From the theoretical study using periodic DFT, it was suggested that the Brønsted acid strength of acidic Y-type zeolite was drastically changed by existence of the divalent metal cation in the sodalite cage. As shown above, the role of divalent metal cation onto the enhancement of the acid strength could be explained base on two mechanisms; *i.e.*, (i) distortion of the framework, and (ii) electron-withdrawing effect. In both mechanisms, the Lewis acid strength of added divalent metal cation should be a main factor to induce the improvement.

Conclusions

In present study, we studied the Brønsted acidity of divalent cation (Ca^{2+}, Ba^{2+} and $Al(OH)^{2+}$) exchanged Y-type zeolites by periodic DFT calculation. The obtained theoretical values of adsorption energies of ammonia and stretching vibration of acidic O1H groups were in reasonable agreement with the experimental values obtained by ammonia IRMS-TPD measurements. Brønsted acid strength of SiO(H)Al group located in the supercage was enhanced by divalent metal cation located in sodalite cage, and the enhancement effect was in the sequence: $Ba^{2+} < Ca^{2+} < Al(OH)^{2+}$. This sequence agreed with the values of the electron withdrawing potential (Lewis acidity); and the higher Lewis acidity led to the higher Brønsted acidity. The assumed EFAL species ($Al(OH)^{2+}$ in the site I' and II') is, based on the systematic experimental studies, one of the most probable structures.

References and Notes

1. C.V. McDaniel and P.K. Maher, *US Patent*, 3,292,192 (1966).
2. V.J. Frilette, P.B. Weisz and R.J. Golden, *J. Catal.,* **1**, 301-306 (1962).
3. P.B. Venuto, L.A. Hamilton, P.S. Landis and J.J. Wise, *J. Catal.,* **5**, 81-98 (1966).
4. M. Kuehne, H.H. Kung and J.T. Miller, *J. Catal.,* **171**, 293-304 (1997).
5. R.A. Beyerlein, C. Choi-Feng, J.B. Hall, B.J. Huggins and G.J. Ray, *Top. Catal*., **4**, 27-42 (1997).
6. A. Corma, V. Formés and F. Rey, *Appl. Catal.,* **59** 267-274 (1990).
7. C.A. Fyfe, J.L. Bretherton, L.Y. Lam, *J. Am. Chem. Soc.,***123**, 5285-5291 (2001).

8. C.J.A. Mota, D.L. Bhering and Jr. N. Rosenbach, *Angew. Chem. Int. Ed.,* **43**, 3050-3053 (2004).
9. S. Li, A. Zheng, Y. Su, H. Zhang, L. Chen, J. Yang, C. Ye and F. Deng, *J. Am. Chem. Soc.,* **129**, 11161-11171 (2007),.
10. G.N. Vayssilov and N. Rosch, *J. Phys. Chem. B,* **105**, 4277-.4284 (2001).
11. N.O. Gonzales, A.K. Chakraborty and A.T. Bell, *Catal. Lett*., **50**, 135-139 (1998).
12. D.C. Koningsberger and J.T. Miller, *Stud. Surf. Sci. Catal.,* 97, 125-131 (1995).
13. D.C. Koningsberger and J.T. Miller, *Stud. Surf. Sci. Catal.,* 101, 841-850 (1996).
14. K. Suzuki, T. Noda, N. Katada, M. Niwa, *J. Catal.,* 250, 151-160 (2007).
15. M. Niwa, N. Katada, M. Sawa and Y. Murakami, *J. Phys. Chem.,***99**, 8812-8816 (1995).
16. The apparent desorption rate of ammonia in TPD process is related to the thermodynamic parameters according to the following equation;

$$C_g = -\frac{\beta A_0 W}{F}\frac{d\theta}{dT} = \frac{\theta}{1-\theta}\frac{P^\circ}{RT}e^{-\frac{\Delta H}{RT}}e^{\frac{\Delta S}{R}}$$

Where C_g is the concentration of ammonia in gas phase (mol m^{-3}), β is the heating rate of temperature (K s^{-1}), A_0 is the desorption amount (mol kg^{-1}), W is the amount of sample (kg), F is the flow rate of carrier gas (m^3 s^{-1}), θ is the extent of coverage of adsorption sites by ammonia, T is temperature (K), P^o is the pressure at thermodynamic standard conditions (1.013×10^5 Pa), R is the gas constant (8.314 J K^{-1} mol^{-1}), ΔH and ΔS are enthalpy (kJ mol^{-1}) and entropy (J K^{-1} mol^{-1}) change by ammonia desorption, respectively. Heat of ammonia adsorption (ΔH) as a parameter to show the strength of the acid site was determined based on the theoretical equation.[15]

17. K. Suzuki, M. Niwa, N. Katada, *J. Phys. Chem. C,* **111**, 894-900 (2007).
18. K. Suzuki, G. Sastre, N. Katada, M. Niwa, *Phys. Chem. Chem. Phys*., **9**, 5980-5987 (2007).
19. V.V. Mihaleva, R.A. van Santen, A.P.J. Janaen, *J. Chem. Phys.,* **119**, 13053-13060 (2003).
20. V.D.D-. Soria, P. Calaminici and A. Goursot, *J. Chem. Phys*., **127**, 154710-154718 (2007).
21. S. Dapprich, I. Komáromi, K.S. Byun, K. Morokuma and M.J. Frisch, *J. Mol. Struct. (THEOCHEM)* **461-462**, 1-21 (1999).
22. J. Sauer and M. Sierka, *J. Comput. Chem.,* **21**, 1470-1493 (2000).
23. X. S-. Monfort, M. Sodupe, V. Branchadell, J. Sauer, R. Orlando and P. Ugliengo, *J. Phys. Chem. B,* **109**, 3539-3545 (2005).
24. M. Boronat, P. Conceoción, A. Corma, M. Renz, S. Valencia, *J. Catal.* **234**, 111-118 (2005).
25. M. Brändle and J. Sauer, *J. Mol. Catal A: Chem.* **119**, 19-33 (1997).
26. M. Sierka, U. Eichler, J. Datka, J. Sauer, *J. Phys. Chem. B*, **102**, 6397-6404 (1998).
27. U. Eichler, M. Brändle, J. Sauer, *J. Phys. Chem. B,* **101**, 10035-10050 (1997).
28. M. Brändle and J. Sauer, *J. Am. Chem. Soc.,* **120**, 1556-1570 (1998).
29. S. Skylenak, J. Dědeček, C. Li, B. Wichterlová, V. Gábová, M. Sierka, J. Sauer, *Angew. Chem. Int. Ed.,* **119**, 7424-7427 (2007).
30. W. Kohn, J.J. Sham, *Phys. Rev.,* **140**, A1133-1138 (1965).

31. C. Lo and B.L. Trout, *J. Catal.,* **227**, 77-89 (2004).
32. P. Mignon, E.A. Pidko, R.A. van Santen, P. Geerlings and R.A. Schoonheydt, *Chem. Eur. J.,* **14**, 5168-5177 (2008).
33. J. Hafner, L. Benco and T. Bučko, *Top. Catal.,* **37**, 41-54 (2006).
34. T. Demuth, J. Hafner, L. Benco and H. Toulhoat, *J. Phys. Chem. B,* **104**, 4593-4607 (2000).
35. C. Tuma and J. Sauer, *Chem. Phys. Lett.,* **387**, 388-394 (2004).
36. T. Noda, K. Suzuki, N. Katada and M. Niwa, *J. Catal.,* **259**, 203-210 (2008).
37. R. Carvajal, P.-J. Chu and J.H. Lunsford, *J. Catal*., **125**, 123-131 (1990).
38. P.O. Fritz and J.H. Lunsford, *J. Catal.,* **118**, 85-98 (1989).
39. B. Delley, D.E. Ellis, C.M. Freeman, E.J. Baerends and D. Post, *Phys. Rev. B,* **27**, 2132-2144 (1983).
40. G. Sastre, N. Katada, K. Suzuki, M. Niwa, *J. Phys. Chem.* C, 112, 19293-19301 (2008).
41. A.D. Boese and N.C. Handy, *J. Chem. Phys*., **114**, 5497-5503 (2001).
42. D.D. Koelling and B.N. Harmon *J. Phys. C: Solid State Phys*., **10**, 31707-3114 (1977).
43. M. Douglas and N. M. Kroll, *Ann. Phys.,* **82**, 89-155 (1974).
44. H. Li and H. Jensen, *Theor. Chem. Acc.,* **107**, 211-219 (2002).
45. W.S. Benedict, N. Gailar and E.K. Plyler, *J. Chem. Phys.,* **24**, 1139-1165 (1956).
46. J.A. Hriljac, M.M. Eddy, A.K. Cheetham, J.A. Donohue and G.J. Ray, *J. Solid State Chem.,* **106**, 66-72 (1993).
47. M. Czjzek, H. Jobic, A.N. Fitch, T. Vogt, *J. Phys. Chem.,* **96**, 1535-1540 (1992).
48. J. Datka, B. Gil, T. Domagala and K.G-. Marek, *Microp. Mesop. Mater.* **47**, 61-66 (2001).
49. J.-R. Hill, C.M. Freeman and B. Delley, *J. Phys. Chem. A,* **103**, 3772-3777 (1999).
50. T. Sun, K. Seff. N.H. Heo and V.P. Petranovskii, *Science* **259**, 495-497 (1993).
51. Y.H. Yeom, S.B. Jang, Y. Kim, S.H. Song, K. Seff, *J. Phys. Chem. B,* **101**, 6914-6920 (1997).
52. M. Niwa, K. Suzuki, K. Isamoto, N. Katada, *J. Phys. Chem. B,* **110**, 264-269 (2006).
53. N. Katada, S. Nakata, S. Kato, K. Kanehashi, K. Saito and M. Niwa, *J. Mol. Catal. A: Chem.,* **236**, 239-245 (2005).
54. A. Gola, B. Rebours, E. Milazzo, J. Lynch, E. Benazzi, S. Lacombe, L. Delevoye and C. Fernandez, *Microp. Mesop. Mater.,* **40**, 73-83 (2000).
55. N. Malicki, P. Beccat, P. Bourges, C. Fernandez, A-.A. Quoineaud, L.J. Simon and F.T-. Starzyk, *Stud. Surf. Sci. Catal.,* **170**, 762-770 (2007).
56. B.A. Williams, S.M. Babitz, J.T. Miller, R.Q. Snurr, H.H. Kung, *Appl. Catal. A: Gen*., **177**, 161-175 (1999)**.**
57. A.E. Hirschler, *J. Catal.,* **2**, 428-439 (1963).
58. R.D. Shannon, *Acta Cryst*. **A32**, 751-767 (1976).
59. The electrostatic potential was calculated based on the Shannon's ionic radius[58] of the hexa-coordinated cation.
60. P. Tynjälä and T.T. Pakkanen, *J. Mol. Catal. A: Cham.,* **110**, 153-161 (1996).
61. A. Redondo, P.J. Hay, *J. Phys. Chem.,* **97**, 11754-11761 (1993).
62. J.B. Nicholas, R.E. Winans, R.J. Harrison, L.E. Iton, L.A. Curtiss and A.J. Hopfinger, *J. Phys. Chem.,* **96**, 10247-10257 (1992).

63. R.A. van Santen and G.J. Kramer, *Chem. Rev*., **95**, 637-660 (1995).
64. D. Freude, T. Loeser, D. Michel, U. Pingel and D. Prochnow, *Solid State Nucl. Magn. Reson.,* **20**, 46-60 (2001).
65. J.A. van Bokhoven, A.L. Roest, D.C. Konigsberger, J.T. Miller, G.H. Nachtegaal, A.P.M. Kentgens, *J. Phys. Chem. B,* **104**, 6743-6754 (2000).
66. C. Sievers, J.S. Liebert, M.M. Stratmann, R. Olindo and J.A. Lercher, *Appl. Catal. A: Gen.* **336**, 89-100 (2008).
67. R.T. Sanderson, *"Inorganic Chemistry", Reinhold Publishing Co, New York,* p. 136 (1967).

Chapter 6.

Conclusions and Future Prospects

Summary of Each Chapter

In this thesis, the establishment of ammonia IRMS-TPD method and the quantitative measurements of Brønsted acidity in zeolites have been carried out, and the relationship between the Brønsted acid strength and the paraffin cracking activity has been discussed. Additionally, quantum chemical approach to analysis of the physicochemical property of zeolite has been attempted using Kohn-Sham density functional theory. The important points in each chapter can be summarized as follows.

In Chapter 2-1, the author performed the optimization of the experimental conditions of ammonia IRMS-TPD measurement. The relatively small W/F ratio compared with the conventional TPD measurement was suitable for combined measurements of IR and MS, and the optimized W/F ratio was *ca.* 0.13 kg s m^{-3}. This ratio is *ca.* 1/100 of that of the conventional TPD measurement. The quantitative measurements of two kinds of acidic OH groups located in the two parallel straight 12 and 8MR channel systems of MOR structure have been successfully performed. Na cations located in the 12MR channel were preferentially exchanged with NH_4^+, and those were almost completely exchanged at *ca.* 30 % of the exchange degree of NH_4^+. The acidic OH groups located in the 8MR showed the relatively stronger adsorption heat of ammonia than that of 12MR. In addition, the catalyst life in octane cracking was improved by the partial ion exchanging of the strong acidic OH groups in the 8MR with Na cations.

In Chapter 2-2, the quantitative measurements of the catalytic active site for paraffin cracking by means of ammonia IRMS-TPD method. The stretching mode of the created strong acidic OH group in the Na_2H_2-EDTA treated USY zeolite was observed at 3595 cm^{-1}, and the acid strength was obviously higher than that on the HY (*ca.* 110 kJ mol^{-1}) and comparable to that on HZSM-5 (*ca.* 137 kJ mol^{-1}).

The quantitative measurements of four kinds of acidic OH groups in Y-type zeolite have been performed in Chapter 2-3. The acidic O2H group located in the sodalite cage showed the strongest adsorption heat of ammonia; in contrast the adsorption heat on the O3H group located in the D6Rs was the weakest among the four OH groups. At the initial stage of TPD process, the O3H absorption band (3526 cm^{-1}) was restored and, simultaneously, the band due to adsorbed ammonia species (1665 cm^{-1}) decreased. Thus, this characteristic absorption band (1665 cm^{-1}) was assigned to a weak adsorption of ammonia (NH_3 and/or NH_4^+) perturbed by a steric hindrance due to small window of the D6Rs.

In Chapter 2-4, it was showed that the adsorption energy of ammonia was correlated with the frequency of OH stretching mode, and it was larger on the smaller frequency. The smaller frequency of the stretching mode indicates the bond strength of OH is weak and proton donation is easy; thus this correlation between the spectral and the thermodynamic parameters is considered a reasonable. However, the considerable deviation from this relationship was observed on OH groups located in the small pore systems. This deviation would be explained based on the steric effect. In narrow pore systems such as in a 6MR, the OH group could interact with the oxygen site in the face-to-face position, and the hydrogen bond thus formed may shift the frequency of OH stretching mode. In other words, interaction of ammonia with the small window could be suppressed to decrease the value of adsorption heat. These two explanations may validate the large deviation. Additionally, under the conditions of monomolecular reaction, the volcano relationship was obtained from between the adsorption heat of ammonia and the TOF of octane cracking normalized by the amount of Brønsted acid site in the large pore system. This relationship shows that the paraffin cracking is activated by the Brønsted acid site. The extinction coefficient of asymmetric NH_4^+ bending vibration (*ca.* 1430 cm^{-1}) was 9.4 ± 0.7 cm μmol^{-1}.

In Chapter 3, the author performed the quantitative estimation of the Brønsted acid strength of zeolite by means of the DFT calculation. In Chapter 3-1, adsorption energies of ammonia on the typical zeolites (MOR, FAU, MFI, FER, MWW and BEA) were calculated by the DFT embedded cluster method and those obtained theoretical values were in good agreement with the corresponding experimental values. This result suggests that the Brønsted acid strength is dependent on the crystal structure.

In Chapter 3-2, the physicochemical properties of OH groups on four nonequivalent oxygen sites in CHA-type zeolite were investigated by the ammonia IRMS-TPD measurements and the periodic DFT calculations. The quantitative measurements of four acidic OH groups were successfully carried out and the experimental values of adsorption energies of ammonia were good agreement with the theoretical values. From above two works, it was suggested that the combined approach of ammonia IRMS-TPD measurement and DFT calculation is the effective method in analysis of the physicochemical property of zeolite.

In Chapter 4, the Brønsted acidities and the paraffin cracking activities of mesoporous ZSM-5 were observed. The mesoporous ZSM-5 had relatively broad distribution of the Brønsted acid strength, but averaged adsorption heat of ammonia on it was almost same to the value of usual ZSM-5 zeolite. From spectral change of OH stretching modes during the TPD process, the broad distribution of Brønsted acid strength in mesoporous ZSM-5 was assigned to the bridging OH groups located in the defective domain. In DFT calculation, the SiO(H)Al group neighbored with the ≡Si-OH group showed the relatively stronger acid strength compared with the defect-free SiO(H)Al group and this trend was in agreement with the experimental results. On the other hand, the typical mesoporous material, Al-MCM-41 had larger amounts of defective sites and large distribution of the Brønsted acid strength. The mesoporous ZSM-5 showed higher catalytic activity compared with the Al-MCM-41. From these results, the acidic OH groups generated from the regular MFI structure inside the mesoprous systems were considered as effective active sites for the paraffin cracking reaction.

In Chapter 5, the author investigated the Brønsted acid strengths of modified Y-type zeolites such as USY and divalent metal cation exchanged Y-type zeolites by periodic DFT calculations. Brønsted acid strength of SiO(H)Al group located in the supercage was enhanced by divalent metal cation located in sodalite cage, and the enhancement effect was in the sequence: $Ba^{2+} < Ca^{2+} < Al(OH)^{2+}$. The calculated frequencies of O1H groups

and adsorption energies of ammonia of periodic FAU systems containing $Al(OH)^{2+}$ at the sites I' and II' were 3603 cm^{-1}/ 144 kJ mol^{-1} and 3605 cm^{-1}/ 135 kJ mol^{-1}, respectively; and those values were in agreement with the experimental values of the strong Brønsted acid site in Na_2H_2-EDTA treated USY (3595 cm^{-1}/ 133 kJ mol^{-1}). This sequence agreed with the values of the electron withdrawing potentials (Lewis acidity); and the higher Lewis acidity led to the higher Brønsted acidity.

General Conclusions

In this work, quantitative measurements of Brønsted acidities in several kinds of zeolites were carried out by means of ammonia IRMS-TPD method in order to understand those paraffin cracking activities. Additionally, the author attempted quantum chemical approach for investigation of the physicochemical property of zeolite. The conclusions in the present study can be summarized as follows.

(i) The optimization of experimental conditions of ammonia IRMS-TPD method has been successfully carried out.

(ii) The frequencies of stretching vibration of acidic OH groups in zeolite were correlated with the adsorption heat of ammonia. From this correlation, the accuracy of adsorption heat of ammonia as scale of acid strength was confirmed.

(iii) Under the monomolecular reaction conditions, the TOFs of octane cracking reaction were strongly dependent on the Brønsted acid strengths of zeolite catalysts.

(iv) The adsorption energies of ammonia on typical zeolites (MOR, FAU, MFI, FER, MWW and BEA) obtained by ammonia IRMS-TPD measurements were supported well by the embedded cluster DFT calculations. Additionally, the enhancement mechanism of the Brønsted acid strength in modified Y-type zeolites such as USY was investigated by the periodic DFT calculations and calculated adsorption energies of ammonia and frequencies of OH stretching modes were reasonable agreement with the corresponding experimental values. The combined study of ammonia IMRS-TPD method and DFT calculation would become a powerful methodology on analysis of the solid acidity.

Future Prospects

As described in Chapter 1, several kinds of controlling factors of Brønsted acid strength have been proposed. Based on knowledge obtained from this thesis, it can be deduced that the crystal structure of zeolite is the considered factor of controlling the acid strength. This opinion is in agreement with our traditional knowledge.

In Chapter 5, the author explained the relationship between the acid strength and the local structure of acidic OH group (SiO(H)Al bond angle and AlO bond length) based on change of the hybrid orbital of oxygen atom in the SiO(H)Al linkage. At the present stage, the author is speculating that the Al-O bond length in the SiO(H)Al linkage is the main controlling factor of the Brønsted acid strength. This concept can be easily explained as follows. Shorter Al-O(H)Si bond length means higher covalent character of the Al-O bond. In that case, the ion binding property of the OH bond is enhanced; *i.e.*, the Brønsted acid strength is enhanced. This concept has been supported by theoretical analysis as shown in Chapter 5; additionally the simple relationship between the adsorption energies of ammonia and the Al-O bond lengths has been obtained from DFT embedded cluster

calculations[1].

Several geometrical factors related to T-O bond length (*e.g.* T-O-T and/or O-T-O bond angles) have been already reported[2, 3]. Naturally, the AlO bond length should also be influenced by the spatial arrangement of surrounding framework atoms of the bridged OH group. From such viewpoint, we have already found the relationship between the Al-O bond length and configuration of the nearest neighboring six oxygen sites of the acidic OH[1]. We believe that natural geometrical parameters of each zeolite structure[4] such as the framework density, pore diameter, area and ellipticity of pore entrance[5], maximum included sphere diameter[6] and lattice parameter determine the degree of distortion of the SiO(H)Al groups, and those Brønsted acid strengths. Currently, relationship between the geometrical parameter and the Brønsted acid strength is being investigated by the neural network approach developed by T. Hattori and co-workers[7].

It is widely known that the lattice parameter is increased with decreasing of the Si/Al ratio[8]. In other words, if the lattice parameter is considered as one of the controlling factors, the Brønsted acid strength should be influenced by the concentration of the framework Al atoms. The enlargement of lattice parameter means the increasing of the framework T-O bond lengths; *i.e.*, this structural change would lead the weakening of the acid strength. The negative relationship between the Al concentration and the acid strength is the traditional concept in the history of zeolite chemistry[9]. This causal relationship has been generally assigned to decrement of the framework electronegativity caused by increasing of the Al content[10]. However, because the heterogeneity of Brønsted acid sites and the distribution of Brønsted acid strength cannot be fully explained, it is difficult to consider that this concept has a sufficient generality on all zeolites. The investigation of relationship between the chemical composition and the Brønsted acid strength from the geometrical viewpoint will become an important subject in our future work. In addition, the effects of long-range Coulombic interaction between the anionic zeolite framework and proton will be also evaluated by quantum chemical approaches.

As described in Chapter 1, the intrinsic activation energy of hydrocarbon cracking is generally assumed as summation of the adsorption heat of hydrocarbon and the apparent activation energy obtained from the Arrhenius plot. Additionally, this value is always constant regardless of the difference of zeolite structures and the chain length of hydrocarbons. In other words, this experimental fact means that the adsorption heat of hydrocarbon on the framework wall and/or the acid sites is the main factor of the catalytic activity[11, 12]. Already, several relationships between the adsorption heat of hydrocarbon and the structural parameters of zeolite such as the pore diameter and the framework density have been suggested. Based on above knowledge, many researchers have suggested that the cracking activity is dependent on the zeolite structure, and is not correlated with the Brønsted acid strength. On the other hand, by means of the quantitative measurement of Brønsted acidity using the Ammonia IRMS-TPD method, the author concluded that the hydrocarbon cracking activity was closely correlated with the Brønsted acid strength (see Chapter 2-4). Additionally, in Chapter 5, the author have investigated the enhancement mechanism of Brønsted acid strength of modified Y-type zeolites by means of the combined approach of ammonia IMRS-TPD measurement and DFT calculation; and obtained results have supported well the improvement of those catalytic activities.

In order to combine the above two opinions on hydrocarbon cracking activity into one, clarification of the relationship among the Brønsted acid strength, the geometrical parameter and the catalytic activity would be important subject. The subject which should be performed in future work can be briefly summarized as follows;

quantitative evaluations of the controlling factors of the Brønsted acid strength (i) and the adsorption heat of hydrocarbon (ii). Those two subjects will be an important theme in the next stage of our study, and answers of those will give us the important hint for designing of new material with high catalytic performance.

References

1. N. Katada, K. Suzuki, T. Noda and M. Niwa, *14th Intern. Congr. Catal*., PII-13-49 (2008).
2. K.L. Geisinger, G.V. Gibbs and A. Navrotsky, *Phys. Chem. Minerals*, **11**, 266 (1985).
3. G.E. Browns, G.V. Gibbs and P.H. Ribbe, *Am. Mineral.*, **54**, 1044 (1969).
4. Ch. Baerlocher, L.B. McCusker and D.H. Olson: Atlas of Zeolite Framework Types, 6th edition, Elsevier, Amsterdam, 2007.
5. S.-H. Lee, C.-H. Shin and S. B. Hong, *J. Catal*., **223**, 200 (2004).
6. M.D. Foster, I. Rivin, M.M.J. Treacy and O. D. Friedrichs, *Micropor. Mesopor. Mater.,* **90**, 32 (2006).
7. T. Hattori and S. Kito, *Catal. Today*, **23**, 347, (1995).
8. E. Dempsey, G.H. Kuhl and O.H. Olson, *J. Phys. Chem*., **73**, 387 (1969).
9. D. Barthomeuf, *J. Phys. Chem,* **83**, 249 (1979).
10. P.A. Jacobs and W.J. Mortier, *Zeolites*, **5**, 226 (1982).
11. S.M. Babitz, B.A. Williams, J.T. Miller, R.Q. Snurr, W.O. Haag and H.H. Kung, *Appl. Catal. A; Gen.,* **179**, 71 (1999).
12. T.F. Narbeshuber, H. Vinek and J.A. Lercher, *J. Catal*., **157**, 388 (1995).

List of Publications

Chapter 2-1

1. **K. Suzuki**, N. Katada and M. Niwa
"Distribution of Acid sites in Mordenite"
Chem. Lett., **34**, 398-399 (2005).
2. M. Niwa, **K. Suzuki**, N. Katada, T. Kanougi, and T. Atoguchi
"Ammonia IRMS-TPD Study on the Distribution of Acid sites in Mordenite"
J. Phys. Chem., B, **109**, 18749-18757 (2005).

Chapter 2-2

3. M. Niwa, **K. Suzuki**, K. Isamoto, and N. Katada
"Identification and Measurement of Strong Brønsted Acid Site in Ultrastable Y (USY)"
J. Phys. Chem., B, **110**, 264-269 (2006).

Chapter 2-3

4. **K. Suzuki**, N. Katada and M.Niwa
"Detection and Quantitative Measurements of Four Kinds of OH in HY Zeolite"
J. Phys. Chem., C, **111**, 894-900 (2007).

Chapter 2-4

5. **K. Suzuki**, T. Noda, N. Katada and M. Niwa
"IRMS-TPD of Ammonia: Direct and Individual Measurement of Brønsted Acidity in Zeolites and Its Relationship with the Catalytic Cracking Activity"
J. Catal., **250**, 151-160 (2007).

Chapter 3-1

6. **K. Suzuki**, G. Sastre, N. Katada and M. Niwa
"Quantitative Measurements of Brønsted Acidity of Zeolites by Ammonia IRMS–TPD Method and Density Functional Calculation"
Chem. Lett., **36**, 1034-1035 (2007).

Chapter 3-2

7. **K. Suzuki**, G. Sastre, N. Katada and M. Niwa
"Ammonia IRMS-TPD Measurements and DFT Calculation on Acidic Hydroxyl Groups in CHA-type Zeolites"
Phys. Chem. Chem. Phys., **9**, 5980-5987 (2007).

Chapter 4

8. **K. Suzuki**, Y. Aoyagi, N. Katada, M. Choi, R. Ryoo and M. Niwa
"Acidity and Catalytic Activity of Mesoporous ZSM-5 in Comparison with zolite ZSM-5, Al-MCM-41 and Silica-alumina"
*Catal. Today***, 132**, 38-45 (2008).

Chapter 5

9. **K. Suzuki**, T. Noda, G. Sastre, N. Katada and M. Niwa
"Periodic Density Functional Calculation on Brønsted Acidity of Modified Y-type Zeolite"
J. Phys. Chem., C, in press.

Other Publications

10. K. Okumura, R. Yoshimoto, **K. Suzuki** and M. Niwa
"Selective Catalytic Reduction of NO by Methane over Pd Loaded on Heteropolyacid/SiO_2 at Low Temperature"
Bull. Chem. Soc. Jpn., 78, 361-366 (2005).
11. T. Noda, **K. Suzuki**, N. Katada and M. Niwa
"Combined Study of IRMS-TPD Measurement and DFT Calculation on Brønsted Acidity and Catalytic Cracking Activity of Cation Exchanged Y Zeolites"
J. Catal., 259, 203-210 (2008).
12. G. Sastre, N. Katada, **K. Suzuki** and M. Niwa
"Computational Study of Brønsted Acidity of Faujasite. Effect of the Al Content on the Infrared OH Stretching Frequencies"
J. Phys. Chem. C, 112, 19293-19301 (2008).
13. **K. Suzuki**, G. Sastre, N. Katada and M. Niwa
"Periodic DFT Calculation of the Energy of Ammonia Adsorption on Zeolites Brønsted Acid Sites to Support the Ammonia IRMS-TPD Experiment"
Chem. Lett., in press.

Proceedings

1. **K. Suzuki**, D. Hayashi, N. Katada and M. Niwa
"Ammonia IRMS-TPD study for Brønsted acid sites in zeolites, and relationship between the Brønsted acidity and activity of paraffin cracking"
Shokubai (Catalysts & Catalysis), **48**, 123-125 (2006).
2. **K. Suzuki**, G. Sastre, N. Katada and M. Niwa
"Quantitative measurements of Brønsted acidity of zeolites by ammonia IRMS-TPD method and density functional calculation"
Shokubai (Catalysts & Catalysis), **49**, 506-508 (2007).
3. **K. Suzuki**, T. Noda, G. Sastre, N. Katada and M. Niwa
"A combined ammonia IRMS-TPD measurement and periodic density functional calculation study on Brønsted acidities of modified Y-type zeolites"
Shokubai (Catalysts & Catalysis), **50**, 502-504 (2008).

List of Presentations

Oral presentations

1. 鈴木 克生, 奥村 和, 丹羽 幹
“水熱合成法で調製した $Pd/WO_3/ZrO_2$ による $NO-CH_4-O_2(H_2O)$反応”
第 84 回日本化学会春季年会，大阪，2004 年 3 月
2. 鈴木 克生, 片田 直伸, 丹羽 幹
“IR-TPD 法によるモルデナイト酸性質のキャラクタリゼーション”
第 34 回石油・石油化学討論会，松山，2004 年 11 月
3. 鈴木 克生, 片田 直伸, 丹羽 幹, M. Elanany, 久保 百司，宮本 明，叶木 朝則，後口 隆
“IR-TPD 法によるモルデナイト酸性質測定”
第 20 回ゼオライト研究会，東京，2004 年 12 月
4. 鈴木 克生，林 大輔，片田 直伸，丹羽 幹
“ゼオライト内ブレンステッド酸性質の一般化”
第 85 回日本化学会春季年会，東京，2005 年 3 月
5. 鈴木 克生，片田 直伸，丹羽 幹
“Ca/H-Y, La/H-Y及びEDTA-USYのブレンステッド酸性質とパラフィン分解活性との相関性”
第 96 回触媒討論会，熊本，2005 年 9 月
6. 鈴木 克生，片田 直伸，丹羽 幹
“アンモニア IRMS-TPD 法による Y 型ゼオライトの酸性質測定”
第 21 回ゼオライト研究会，豊橋，2005 年 11 月
7. 鈴木 克生，林 大輔，片田 直伸，丹羽 幹
“アンモニア IRMS-TPD 法によるゼオライト内 Brønsted 酸性質の測定と炭化水素分解活性との相関性”
第 97 回触媒討論会，東京，2006 年 3 月
8. 鈴木 克生，片田 直伸，丹羽 幹
“アンモニア IRMS-TPD 法による *in situ* HY ゼオライトの酸性質測定
第 98 回触媒討論会，富山，2006 年 10 月
9. 加藤 剛，鈴木 克生，青柳 由香里，片田 直伸，丹羽 幹
“アンモニア IRMS-TPD 法による SAPO の酸性質測定”
第 22 回ゼオライト研究会，東京，2006 年 12 月
10. 鈴木 克生，野田 敬之，片田 直伸，丹羽 幹
“アンモニア IRMS-TPD 法と DFT 計算による Y 型ゼオライトの酸性質評価”
第 87 回日本化学会春季年会，大阪，2007 年 3 月
11. 鈴木 克生，German Sastre，片田 直伸，丹羽 幹
“アンモニア IRMS-TPD 法と密度汎関数法計算によるゼオライト内ブレンステッド酸性質の定量的評価”
第 100 回触媒討論会，北海道，2007 年 9 月
12. 鈴木 克生，野田 敬之，German Sastre，片田 直伸，丹羽 幹
“周期的密度汎関数法計算とアンモニア IRMS-TPD 測定による修飾 Y ゼオライトのブレンステッド酸性質に関する研究”
第 102 回触媒討論会，名古屋，2008 年 9 月

Poster presentations

1. 鈴木 克生，片田 直伸，丹羽 幹
“アンモニア IR-TPD 法による Y ゼオライトの酸性質測定”
第 95 回触媒討論会，東京，2005 年 3 月
2. K. Suzuki, N. Katada and M. Niwa
“IRMS-TPD of Ammonia for Characterization of Acid Site in Y-type Zeolite”
2005環太平洋化学国際会議，ハワイ，2005年12月
3. K. Suzuki, N. Katada and M. Niwa
“Characterization of Brønsted Acid Sites of Y-type Zeolite by Ammonia IRMS-TPD method”
ZMPC2006, 米子，2006 年 7 月
4. 鈴木 克生，片田 直伸，丹羽 幹
“アンモニア IRMS-TPD 法による CHA と SAPO-34 の酸性質測定および計算化学的検討”
99 回触媒討論会，神戸，2007 年 3 月
5. K. Suzuki, G. Sastre, N. Katada and M. Niwa
“Quantitative Measurements of Brønsted Acidity of Zeolites by Ammonia IRMS-TPD Method and Density Functional Calculation”
15th International Zeolite Conference, 北京，2007 年 8 月
6. K. Suzuki, T. Nishio, M. Mori, N. Katada and M. Niwa
“Ammonia IRMS-TPD Measurements on Brønsted Acidities of Proton-formed SAPO-34 and Chabazite”
14th International Congress on Catalysis, ソウル，2008 年 7 月